

**Spatial memory in health and disease: Hippocampal  
stability deficits in the *Df(16)A<sup>+/−</sup>* mouse model of  
schizophrenia**

**Jeffrey D. Zaremba**

Submitted in partial fulfillment of the  
requirements for the degree  
of Doctor of Philosophy  
under the Executive Committee  
of the Graduate School of Arts and Sciences

**COLUMBIA UNIVERSITY**

2017

©2017

Jeffrey D. Zaremba

All Rights Reserved

# ABSTRACT

## Spatial memory in health and disease: Hippocampal stability deficits in the *Df(16)A<sup>+/−</sup>* mouse model of schizophrenia

Jeffrey D. Zaremba

Recognizing and understanding where and when events occurred is essential for normal learning and memory of life experiences. Disruptions in the normal processing of spatial and episodic memories can have devastating consequences; in particular, this is one component of the debilitating cognitive deficits of schizophrenia. We are just now beginning to understand the molecular changes in schizophrenia, but still very little is known about how neural circuit are disrupted that lead to behavioral and cognitive dysfunction. In my thesis I will attempt to address two primary questions; how does hippocampal circuitry support spatial-episodic memories, and what goes wrong when these circuits and memories are impaired?

First, how precisely do hippocampal circuits support spatial and episodic learning? In 1885 Hermann Ebbinghaus published the first results of a quantitative study of the psychology of memory, showing the predictable forgetting of items over time. Since then, psychologists and cognitive scientists have investigated, described, and defined the precise nature of memory and the behaviors it drives. We eventually realized that memory is not a unitary function of the brain, but that it is dissociable at its broadest level into explicit, recollectable memories and the implicit memory of learned skills and abilities. We have now identified networks of brain regions that are essential for these functions. The first functional imaging of the human brain further advanced our understanding of the particular brain regions active during memory tasks and technological advances have allowed us to generate higher resolution functional maps of the brain. Moving to rodent models, we are now getting closer to the memory engram, the set of changes that occur in the brain that store an object, event, or association for future recall. In some particular instances, such as spatial and episodic memories, we already have a very good understanding. But, which particular cells store this information and how does that memory come to be? In my primary thesis project, I will

show that the stabilization of firing patterns in principal cells in hippocampal area CA1 supports learning of a spatial reward task. More specifically, as task demands shift pyramidal cells in CA1 specifically encode the reward zone by firing when the mouse is at the correct location. Finally, by modeling the shift of pyramidal cell activity throughout learning, I show the way in which the population of cells shift their firing activity to encode the reward zone.

Second, what goes wrong in the normal processing of information that leads to disrupted memory storage and recall? Deficits in spatial and episodic memory are two of the primary cognitive dysfunctions in schizophrenia. While, hallucinations and delusions are perhaps the most widely recognized, they are in part treatable with antipsychotics, while the cognitive and memory deficits are not as well understood, untreatable, and the greatest barrier to rehabilitation. Cognitive deficits observed in schizophrenia patients are, at their core, neuronal circuit disruptions, spanning multiple brain regions and cognitive domains. What can we learn about the circuits underlying these behavioral symptoms? What goes wrong in the brain that is driving these disruptions? I focused on one particular well-characterized brain region (the hippocampus) by recording the activity of hippocampal area CA1 principal cells in an etiologically-validated mouse model of schizophrenia while the mice are actively engaged in a spatial learning task. I identified specific features of the place cell population that are disrupted and predict behavioral deficits – the day-to-day firing stability of the neuronal population and the lack of over-representation of the reward zone.

Overall, my work used head-fixed two-photon functional imaging of awake mice to chronically record the activity of distinct components of the hippocampal memory system: long-range inhibitory projections from the entorhinal cortex to hippocampal area CA1, adult-born granule cells in the dentate gyrus, and large heterogeneous populations of CA1 principal cells. I recorded activity during hippocampal-dependent learning and memory tasks in both schizophrenia-mutant and wildtype mice in order to directly probe hippocampal circuits involved in spatial learning. These experiments provided new evidence of the underlying cellular substrates of both healthy and diseased spatial memory processing.

# Table of Contents

<b>List of Figures</b>	<b>ix</b>
<b>List of Tables</b>	<b>x</b>
<b>I Introduction</b>	<b>1</b>
<b>1 Learning and Memory</b>	<b>2</b>
1.1 Memory . . . . .	3
1.1.1 Spatial memory . . . . .	4
1.1.1.1 Spatial memory as episodic memory . . . . .	5
1.1.2 Spatial reward learning . . . . .	5
1.2 Memory in the brain . . . . .	7
1.2.1 The hippocampus . . . . .	8
1.2.1.1 Circuitry of the hippocampus . . . . .	9
1.2.1.2 Local interneurons . . . . .	10
1.2.2 Functional organization of the hippocampus . . . . .	12
1.2.2.1 Pyramidal cell functional diversity . . . . .	13
1.2.2.2 Hippocampal computations . . . . .	13
1.2.3 Memory at the synapse . . . . .	14
1.2.3.1 Long-term potentiation . . . . .	14
1.2.3.2 NMDA-receptor-dependent memory . . . . .	16
1.3 Functional correlates of memory . . . . .	17
1.3.1 Spatial maps . . . . .	17

1.3.1.1	Remapping . . . . .	18
1.3.1.2	Stability . . . . .	18
1.4	Summary . . . . .	19
<b>2</b>	<b>Schizophrenia</b>	<b>21</b>
2.1	Memory deficits . . . . .	23
2.1.1	Spatial memory . . . . .	24
2.2	Schizophrenia in the brain . . . . .	26
2.2.1	The hippocampus in schizophrenia . . . . .	26
2.2.1.1	Specific role of hippocampal area CA1 . . . . .	27
2.3	Schizophrenia etiology . . . . .	27
2.3.1	Genetics . . . . .	28
2.3.1.1	Gene pathway convergence . . . . .	29
2.3.2	Schizophrenia as a neurodevelopmental disorder . . . . .	30
2.3.2.1	22q11.2 deletion syndrome . . . . .	32
2.3.2.2	<i>Df(16)A<sup>+</sup>/-</i> mouse model of 22q11.2DS . . . . .	32
2.3.2.3	Individual genes within the 22q11.2 locus . . . . .	36
2.3.3	Dopamine . . . . .	37
2.3.3.1	Dopamine in the striatum . . . . .	38
2.3.4	Excitation and inhibition . . . . .	38
2.4	Summary . . . . .	40
<b>3</b>	<b>Techniques</b>	<b>41</b>
3.1	<i>In vivo</i> two-photon Ca <sup>2+</sup> imaging . . . . .	41
3.2	Head-fixed behavior . . . . .	42
3.2.1	Random foraging . . . . .	43
3.2.2	Goal-oriented learning . . . . .	43
3.3	Data analysis pipeline . . . . .	45
3.3.1	Initial processing . . . . .	45
3.3.2	Signal processing . . . . .	46
3.3.3	Place cell identification . . . . .	47

3.3.4	Lab Analysis Bundle (LAB) . . . . .	48
3.3.5	Place cell stability . . . . .	50
<b>II</b>	<b>Projects</b>	<b>53</b>
<b>4</b>	<b>Impaired hippocampal place cell dynamics in a mouse model of the 22q11.2 deletion</b>	<b>54</b>
4.1	Introduction . . . . .	55
4.2	Results . . . . .	57
4.2.1	Head-fixed goal-oriented learning paradigm . . . . .	57
4.2.2	<i>Df(16)A<sup>+/−</sup></i> mice are impaired in GOL task following changes in both context and reward location . . . . .	60
4.2.3	Smaller, less diffuse place cell population in <i>Df(16)A<sup>+/−</sup></i> compared to WT mice	62
4.2.4	Spatial map is less stable in <i>Df(16)A<sup>+/−</sup></i> compared to WT mice . . . . .	65
4.2.5	Task performance correlates with spatial map stability . . . . .	69
4.2.6	Goal-oriented learning requires dorsal hippocampal area CA1 and relies on allocentric navigational strategies . . . . .	73
4.2.7	Disrupted sharp wave-ripple activity in <i>Df(16)A<sup>+/−</sup></i> mice . . . . .	75
4.2.8	Change in context induces disrupted place cell stability in <i>Df(16)A<sup>+/−</sup></i> mice .	76
4.2.9	Task-dependent stabilization of place cells is impaired in <i>Df(16)A<sup>+/−</sup></i> mice .	78
4.2.10	Enrichment of goal location by place cells in WT, but not <i>Df(16)A<sup>+/−</sup></i> mice .	79
4.2.11	WT place fields shift towards the new reward location . . . . .	82
4.2.12	Modeling of place cell dynamics suggests that place fields shift is the primary factor leading to reward enrichment . . . . .	85
4.2.13	Modeling of place cell dynamics corroborates the absence of enrichment in the <i>Df(16)A<sup>+/−</sup></i> mice through lack of place field shift towards reward . . . . .	87
4.3	Discussion . . . . .	91
4.3.1	Hippocampal place cell dynamics depend on both the task and the specific task parameters in goal-directed learning . . . . .	91

4.3.2	Potential mechanisms underlying impaired place cell dynamics and learning deficits in <i>Df(16)A<sup>+/−</sup></i> mice . . . . .	94
4.3.3	Relevance of <i>Df(16)A<sup>+/−</sup></i> mouse model of 22q11.2 deletion syndrome for cognitive deficits in SCZ . . . . .	96
4.4	Methods . . . . .	97
4.4.1	Mice and viruses . . . . .	98
4.4.2	Imaging window implant . . . . .	98
4.4.3	Behavioral training . . . . .	99
4.4.3.1	Run training . . . . .	99
4.4.3.2	Goal-oriented learning . . . . .	99
4.4.3.3	Random foraging . . . . .	99
4.4.4	Behavioral readout . . . . .	100
4.4.5	Comparison of GOL task to freely-moving goal-directed learning task in Dupret et al. . . . .	100
4.4.6	Stimulus presentation . . . . .	101
4.4.7	Contexts . . . . .	101
4.4.8	Hippocampal inactivation . . . . .	101
4.4.9	<i>In vivo</i> 2-photon imaging . . . . .	102
4.4.10	Data processing for Ca <sup>2+</sup> imaging . . . . .	103
4.4.10.1	Identification of calcium transients . . . . .	103
4.4.11	Data analysis . . . . .	104
4.4.11.1	Selection of spatially-tuned cells . . . . .	104
4.4.11.2	Place cell properties . . . . .	105
4.4.11.3	Remapping analysis . . . . .	106
4.4.11.4	Shuffle distributions . . . . .	106
4.4.11.5	Recurrence and stability by position . . . . .	107
4.4.11.6	LFP acquisition and sharp wave-ripple analysis . . . . .	108
4.4.11.7	Modeling goal-directed remapping . . . . .	108
4.4.11.8	Statistics . . . . .	109

<b>5 SIMA Analysis Software</b>	<b>111</b>
5.1 Abstract . . . . .	112
5.2 Introduction . . . . .	112
5.3 Functionality . . . . .	113
5.3.1 Object classes and input formats . . . . .	115
5.3.2 Motion correction . . . . .	116
5.3.3 Segmentation and ROIs . . . . .	118
5.3.4 Manual ROI Editing . . . . .	119
5.3.5 ROI Registration . . . . .	119
5.3.6 Signal extraction . . . . .	120
5.3.7 Exporting data . . . . .	121
5.4 Software details . . . . .	122
5.4.1 ROI Registration . . . . .	122
5.4.2 Signal extraction . . . . .	122
<b>6 Additional Projects</b>	<b>124</b>
6.1 Gating of hippocampal activity, plasticity, and memory by entorhinal cortex long-range inhibition . . . . .	124
6.2 Distinct contribution of adult-born hippocampal granule cells to context encoding .	125
6.3 Sublayer-specific coding dynamics during spatial navigation and learning in hippocampal area CA1 . . . . .	128
<b>III Conclusions</b>	<b>134</b>
<b>7 Conclusions</b>	<b>135</b>
7.1 Summary . . . . .	135
7.1.1 What we learned about memory . . . . .	136
7.1.2 What we learned about schizophrenia . . . . .	137
7.2 Future directions . . . . .	138
7.2.1 Context generalization . . . . .	138

7.2.2	Hippocampal GABAergic interneurons . . . . .	139
7.2.3	Functional dissection of population dynamics with <i>in vivo</i> imaging during alternate hippocampus-dependent behaviors in the <i>Df(16)A<sup>+/−</sup></i> mouse . . . . .	140
7.2.4	Sharp wave-ripples in <i>Df(16)A<sup>+/−</sup></i> during goal-oriented learning . . . . .	141
7.2.5	Reward cells . . . . .	141
7.2.6	Further exploring place field shift modeling result . . . . .	142
7.2.7	Long term stability in place cell population . . . . .	144
7.2.8	Neuromodulators in the hippocampus of <i>Df(16)A<sup>+/−</sup></i> mice . . . . .	145

## Bibliography

147

# List of Figures

1.1	Distribution of firing fields in Hollup et al. . . . .	6
1.2	Cheeseboard task and behavioral correlates from Dupret et al. . . . .	7
1.3	The neural circuitry of the rodent hippocampus . . . . .	11
1.4	Hypothesized input-output curves for the DG, CA3, and CA1 regions of the hippocampus . . . . .	15
1.5	Place cell in the HPC and grid cell in the MEC . . . . .	17
1.6	Place cell population stability over days . . . . .	20
2.1	Breakdown of non-communicable disease cost by disease type . . . . .	22
2.2	First cluster identified by the NETBAG+ approach . . . . .	31
2.3	Neurodevelopmental model of schizophrenia . . . . .	33
2.4	Genetic deletion in 22q11.2DS and <i>Df(16)A<sup>+/−</sup></i> . . . . .	34
3.1	Schematic of treadmill design for head-fixed awake two-photon Ca <sup>2+</sup> imaging . . . . .	43
3.2	Data analysis pipeline . . . . .	46
3.3	Example histogram . . . . .	50
4.1	The three conditions of the GOL task . . . . .	58
4.2	Components of the two distinct contexts used in the GOL task . . . . .	59
4.3	Example histograms of lick counts by position . . . . .	59
4.4	Learning performance of WT and <i>Df(16)A<sup>+/−</sup></i> mice based on fraction of licks in the reward zone . . . . .	61
4.5	Comparison of behavior during initial learning in GOL . . . . .	63
4.6	Laps and licks per session . . . . .	64

4.7	Learning performance for WT and <i>Df(16)A<sup>+/−</sup></i> mice on the first and last session of each day . . . . .	64
4.8	Schematic of head-fixed setup and example fields of view . . . . .	65
4.9	Example Ca <sup>2+</sup> traces and spatial tuning . . . . .	66
4.10	Comparison of place cell metrics . . . . .	66
4.11	Comparison of lifetime place coding and additional place cell metrics . . . . .	67
4.12	Comparison of recurrence probability . . . . .	68
4.13	Comparison of centroid shift . . . . .	70
4.14	Comparison of place field correlation . . . . .	71
4.15	Task performance and population stability follow similar trajectories across Conditions	72
4.16	Impaired task performance during CA1 inactivation . . . . .	74
4.17	No place cells on a cue-free belt and spatial tuning near the fabric-transition is not more stable . . . . .	75
4.18	Sharp wave-ripple spectrograms in WT and <i>Df(16)A<sup>+/−</sup></i> mice . . . . .	76
4.19	Rate and power of SWRs in WT and <i>Df(16)A<sup>+/−</sup></i> mice . . . . .	76
4.20	SWR properties at multiple thresholds . . . . .	77
4.21	Subtle contextual change induces remapping in <i>Df(16)A<sup>+/−</sup></i> mice . . . . .	78
4.22	Lack of task-dependent stability of spatial maps in <i>Df(16)A<sup>+/−</sup></i> mice . . . . .	79
4.23	Heatmaps of place cell population throughout Condition III . . . . .	80
4.24	Fraction of place cells near the goal location across all days of the experiment . . . . .	81
4.25	Correlation of place cell goal-zone enrichment with task performance during Condition III . . . . .	81
4.26	Individual place field stability examples . . . . .	82
4.27	Possible enrichment methods . . . . .	83
4.28	Recurrence probability as a function of original distance from the reward . . . . .	84
4.29	Session-to-session place field shift as a function of original distance from the reward .	84
4.30	Latent spatial tuning revealed across multiple sessions . . . . .	85
4.31	Place cell recurrence model schematic . . . . .	86
4.32	Simulated place field reward enrichment . . . . .	87
4.33	Modeled enrichment for all three Conditions . . . . .	88

4.34 Place field shift towards the reward drives reward enrichment in model . . . . .	88
4.35 Model enrichment when swapping individual parameters between WT and <i>Df(16)A<sup>+/−</sup></i> values . . . . .	89
4.36 <i>Df(16)A<sup>+/−</sup></i> mice place fields do not drift towards goal and model produces no enrichment . . . . .	90
5.1 Workflow supported by SIMA . . . . .	114
5.2 Line-by-line correction of within-frame motion artifacts . . . . .	117
5.3 Registration of ROIs across imaging sessions acquired on two different days . . . . .	120
6.1 Functional imaging of sensory coding in LEC LRIPs present in SLM of CA1 . . . . .	126
6.2 Responsive properties of LRIP boutons . . . . .	127
6.3 Contextual coding by adult-born and mature granule cells . . . . .	129
6.4 GOL task for head-fixed imaging . . . . .	131
6.5 Sublayer-specific modulation of activity by the GOL task . . . . .	132
6.6 Reward zone representation versus performance on the GOL task . . . . .	133
7.1 Mice anticipate the reward location and the anticipation is predicted by stable spatial maps . . . . .	142
7.2 <i>Df(16)A<sup>+/−</sup></i> place fields are hyper-rigid over the course of a week . . . . .	144
7.3 Place field stability in Ziv et al. . . . .	146

# List of Tables

2.1 Pathways implicated in schizophrenia . . . . .	30
--	----

# Acknowledgments

It's taken a long time to get to this point, and I truly could not have gotten here without the help and support of amazing mentors, teachers, colleagues, collaborators, friends, and family. There are so many people without whom this work would not have been possible, or at least not as enjoyable and productive. "No man is an island" could not be more true.

First, thank you to my mentors, Attila Losonczy and Joseph Gogos. They provided the opportunity to do great science and work on fascinating projects. Their guidance helped me progress as a researcher and kept me moving in the right direction, despite the occasional slowdown/interruption. There is no other place I would have rather been for my Ph.D. than Attila's lab. He showed me what it takes to do high quality research, and was supportive and understanding throughout the entire process. Thank you.

I was very fortunate to work with such an amazing group of colleagues in Attila's lab. Collaboration was central to my lab work, and having a group of colleagues who were always willing to help and progress together as a lab, was invaluable. In particular, Nathan Danielson and Patrick Kaifosh are incredibly brilliant scientists who became great friends. Whether collaborating on projects, developing shared infrastructure, discussing the issue of the moment, or just grabbing lunch, they made every day in lab fun, interesting, and fulfilling. Thank you. Special thanks to Natasha Diamantopoulou for years of wonderful collaboration on the *Df(16)A<sup>+/−</sup>* project. To the rest of Attila's lab, thanks for everything: Matthew Lovett-Barron, Gergely Turi, Thomas Reddon, Jack Bowler, Angel Castro, Mohsin Ahmed, Fraser Sparks, Max Ladow, Sebi Rolotti, Wen Li, Elizabeth Balough, Ali Kaufman, Joseph Tsai, Adrian Negrean, Andres Grosmark, Rita Nylias, and Jeff Zhang.

Thank you to my parents, grandparents, and brother for all of the support through the years that helped me get here. Most important of all, this truly would not have been possible without the

continuous support of my wife, Kate. Through the late nights working together and the long weeks working apart, the past few years have been a bit crazy. Thank you for always being there and understanding all the ups and downs. Finally, Rose, born somewhere in the middle of chapter 4, thanks for being the best baby to ever baby.

Thank you to the National Institute of Mental Health for pre-doctoral fellowship support: NIMH 1F31MH105169-01A1.

To Kate.

# **Part I**

# **Introduction**

# Chapter 1

## Learning and Memory

### Overview

Learning and memory define who we are and shape who we will become. The various components of memory – learning, adaptation, plasticity, association, conditioning – are fundamental features of nervous systems across all organisms. Indeed, humanity’s greatest adaptation is perhaps our unparalleled ability to learn from and adapt to the world around us. The study of memory in the brain spans from the level of molecular changes that occur at synapses between individual cells to the role of entire brain regions in facilitating different components of memory.

In the following sections I aim to describe an understanding of memory, the brain structures underlying it, and cellular physiological correlates of learning relevant to my later studies. In discussing learning and memory, I will first focus on spatial memory as a core component of episodic memory (section 1.1) and how we experimentally study it. While learning-related changes are fundamental to every neuron in the nervous system, I will primarily focus on the role of the hippocampus (HPC) in learning and memory, as the HPC is most relevant to the memory systems I will be studying (section 1.2). Finally, I will discuss our current understanding of cellular and circuit mechanisms by which the brain encodes and recalls memory, with a specific emphasis on hippocampal place cells underlying spatial memory (section 1.3).

## 1.1 Memory

Memory is the way in which experiences from the past can influence how we interpret the present (or the future). Memory includes explicit memories of objects, concepts, people, places, and events (DECLARATIVE MEMORY), but also skills and abilities that we cannot consciously recall, such as the ability to shoot a basketball or ride a bike (IMPLICIT MEMORY). Declarative memory can be subdivided into at least two categories: autobiographical episodic memory of events and general knowledge of facts, known as semantic memory. As Endel Tulving explained when he defined EPISODIC MEMORY, these two memory systems are not entirely independent:

Episodic memory retrieves and stores information about temporally dated episodes or events, and temporal-spatial relations among these events. A perceptual event can be stored in the episodic system solely in terms of its perceptible properties or attributes, and it is always stored in terms of its autobiographical reference to the already existing contents of the episodic memory store. The act of retrieval of information from the episodic memory store, in addition to making the retrieved contents accessible to inspection, also serves as a special type of input into episodic memory and thus changes the contents of the episodic memory store. The system is probably quite susceptible to transformation and loss of information. While the specific form in which perceptual input is registered into the episodic memory can at times be strongly influenced by information in semantic memory—we refer to the phenomenon as encoding—it is also possible for the episodic system to operate relatively independently of the semantic system.

(Tulving 1972, pgs. 385-386)

This interpretation of episodic memory encapsulates several key points that I will address going forward. The time and space at which an event occurred are essential components of the memory – they are the relationship framework that we use to categorize events in memory (subsubsection 1.1.1.1). Also, episodic memory is in effect an association of sensory inputs with previously stored memories. Perhaps the best-studied example of this are hippocampal PLACE CELLS (O’Keefe & Dostrovsky, 1971), which combine external sensory features with an internal interpretation of the world to selectively identify particular locations (subsection 1.3.1). Finally, episodic memory is

inevitably malleable. The degree of stability depends on many factors and is an inherent limit on the ability of the brain to recall memories (subsubsection 1.3.1.2).

My main thesis project investigated spatial-reward memory to inform on episodic memory impairments in a mouse model of schizophrenia, so I will focus my discussion on spatial memory and related structures.

### 1.1.1 Spatial memory

SPATIAL MEMORY is the aspect of memory that instills our sense of direction and allows us to know where we are at any given time, imagine or plan where we will be in the future, and know where we were when we recall particular memories. We use spatial memory to navigate our world. Spatial navigation consists of two primary components: location relative to an allocentric map of the world, and egocentric update cues arising from orientation and other vestibular input (Sanders et al., 2015). The dominance of allocentric or egocentric navigation depends upon the precise nature of the environment being explored; egocentric dominates in cue-rich environments, while allocentric navigation dominates when landmarks are lacking or in the dark (Knierim et al., 1998; Markus et al., 1994). Spatial memory has been studied extensively in rodents, in large part because it is a well-defined and tractable area of research. As rodents can not be asked to recall past events, we need assays that can probe for evidence of these memories (subsection 1.1.2). Not only do we have good behavioral tests for spatial memory in rodents, but we have identified what we believe to be the cognitive map of the memory itself (subsection 1.3.1).

There are two cognitively distinct forms of spatial memory: SPATIAL WORKING MEMORY and SPATIAL REFERENCE MEMORY. Spatial working memory is the short-term, on-line processing of spatial information and requires both the HPC to provide spatial maps (Morris et al., 1982) as well as the prefrontal cortex (PFC) to maintain these representations in working memory (Olton & Paras, 1979). In particular the direct HPC to PFC projection is essential during the initial encoding phase in spatial memory tasks, but not during the later maintenance or retrieval (Spellman et al., 2015). Spatial reference memory refers to the long-term storage of spatial maps of environments and is the basis of spatial navigation. These two forms of spatial memory are dissociable by the brain regions involved, but also by the underlying hippocampal synaptic and circuit mechanisms. Spatial working memory is selectively impaired, while spatial reference memory is spared, by disruption in

synaptic machinery resulting in decreased Schaffer collateral-CA1 LTD (Zeng et al., 2001) and by inactivating hippocampal area CA1 parvalbumin-positive interneurons (INs) (Murray et al., 2011). For the remainder of my discussion I will be focusing on the specifically-hippocampal components of spatial memory, and in particular, spatial reference memory.

#### **1.1.1.1 Spatial memory as episodic memory**

Experiences are innately inseparable from the time and place at which they occurred. When we think of an autobiographical memory, we remember the experience (e.g. waiting in line to get lunch) along with the location (e.g. Mike's Bagels at 168<sup>th</sup> and Broadway) and the time (e.g. last Tuesday around 2PM) they occurred. This applies to psychological memory tests as well, such as remembering words on a list, where the temporal order of items on the list (I saw ‘orange’ before ‘banana’) and the visio-spatial arrangement of the words on the paper list ('boat' was written above 'car') are core components of the stored memory. Even more than being a component of episodic memory, spatial memory may in fact *be* episodic memory. The brain structure most closely associated with episodic memory (The hippocampus) also contains cells which directly map to real world locations (Spatial maps). Indeed it has been proposed that the same neural mechanisms may underly both the ability to store the relationship amongst objects in a remembered experience, and the relationship between landmarks contributing to a map of space (Buzsáki & Moser, 2013).

#### **1.1.2 Spatial reward learning**

Tests of spatial memory are fundamental tools for rodent researchers, and a particular focus of my thesis work. The most widely used assay of spatial memory is the MORRIS WATER MAZE (Morris, 1984). While there is variability in the details of the protocol, the general structure is usually the same. Briefly, the ‘maze’ is a large water-filled tub with a single hidden platform under the surface of the water. Mice or rats are placed in the maze and over successive trials eventually learn to use distal cues around the room to locate the platform. Probe trials generally consist of removing the platform and scoring the fraction of time spent in the correct quadrant as a measure of spatial memory. More recently, virtual reality variations of the Morris water maze have been developed that allow for head-fixed spatial learning tasks in rodents (Aronov & Tank, 2014) or the ability to mirror rodent experimental paradigms in humans (Astur et al., 1998). Virtual reality water

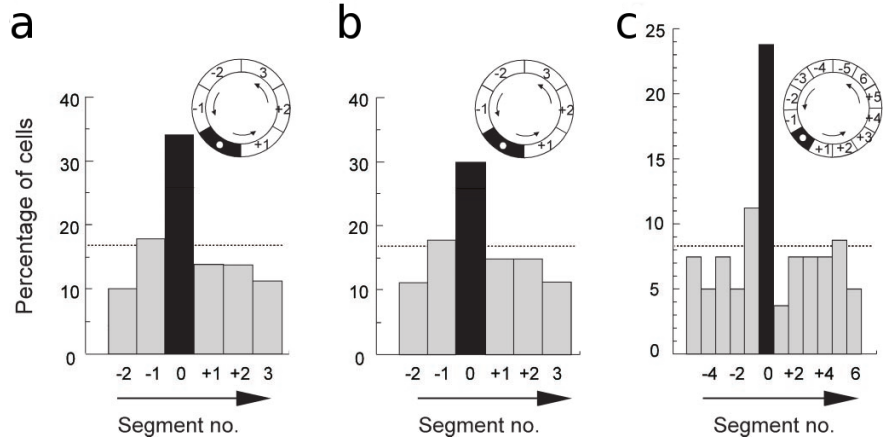


**Figure 1.1:** Distribution of firing fields in Hollup et al. after training with a constant platform location. **a.** Percentage of firing fields in each 60° segment of the corridor (80 cells; average of 3 probe tests). Field location was defined as the segment with the maximal averaged firing rate. Firing fields accumulated in the platform segment (segment 0, black). The chance level was at 16.7%. Inset, Diagram of the corridor. Arrows indicate swim direction. **b.** Percentage of firing fields in each 60° segment after directional sorting (same trials and same symbols as described in *a*). Only data sampled during swimming in the preferred direction are retained. **c.** Percentage of firing fields in segments of 30° after directional sorting. The platform was in the middle of segment 0. Reproduced from Hollup et al. (2001b).

mazes have been used to study spatial memory in schizophrenia patients, which I will discuss later (subsection 2.1.1).

One particular variation is the annular water maze used by Hollup et al., which adds an inner wall to the large circular pool creating a ‘one-dimensional’ circular track that the mice swim around (Hollup et al., 2001b). This task is similar to the goal-oriented learning (GOL) task (subsection 3.2.2) that I use throughout my primary experiments; both tasks require rodents to find hidden rewards in a simplified ‘one-dimensional’ environment while recording from hippocampal area CA1 pyramidal cells and quantify both the task performance and place cell enrichment of the reward location. In particular, the authors find an accumulation of place cells around the escape platform (Figure 1.1), a finding which I replicate and expand upon in my GOL task (subsection 4.2.10).

Conceptually similar, but drier, are the Barnes or cheeseboard maze (Barnes, 1979; Kesner et al., 1991; Dupret et al., 2010a). These mazes consist of a large platform with holes throughout. These holes can either be escapes that allow the mice/rats to avoid the exposed platform or baited/rewarded. Either way, the degree of learning can be quantified by the latency to finding the correct location or the amount of time spent near previously rewarded locations during un-

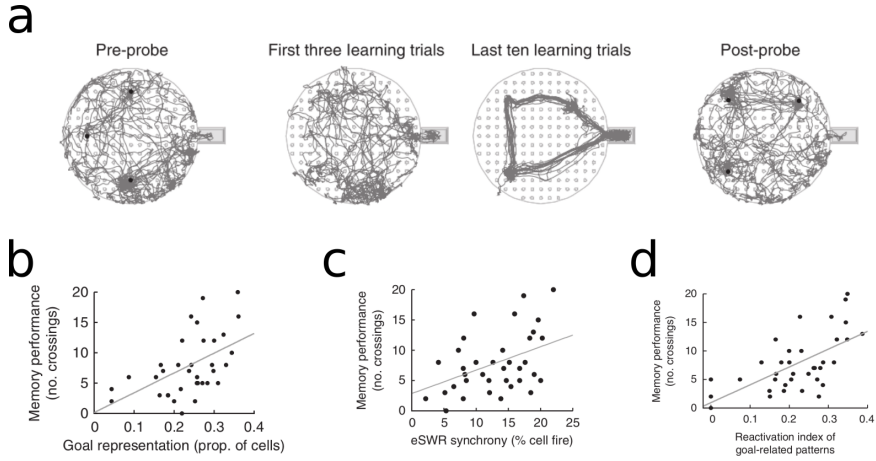


**Figure 1.2:** Cheeseboard task and behavioral correlates from Dupret et al. **a.** Representative examples of an animal’s path; for clarity, only the first 10 min of each probe session is depicted (black dots, learnt goal locations). **b.** Scatter plot showing post-probe memory performance (number of crossings) as a function of the proportion of CA1 place cells at goal location during the end of learning (gray: regression line,  $r=0.511$ ,  $P=0.0014$ ). **c.** Scatter plot showing post-probe memory performance (number of crossings) as a function of ‘eSWR synchrony’ (percentage of CA1 pyramidal cells that fire in eSWR) at the end of learning (gray: regression line,  $r=0.418$ ,  $P=0.011$ ). **d.** Scatter plot showing post-probe memory performance (number of crossings at a given goal location) as a function of the proportion of sSWRs in which assembly patterns represented the same goal location (gray: regression line,  $r=0.620$ ,  $P=0.00005$ ) Reproduced from Dupret et al. (2010a).

rewarded probe trials. In a study by Dupret et al. which partially inspired my own work, the authors used a cheeseboard maze to examine hippocampal functional correlates of learning and memory (see subsection 4.4.5; Dupret et al., 2010a). The authors identified an increase in the fraction of hippocampal area CA1 place cells that encoded the reward location, the magnitude of which correlated with task performance (Figure 1.2a,b). In addition they found properties of sharp wave-ripples (SWRs) that also correlated with task performance – the fraction of pyramidal cells that participated in SWR events during exploration (eSWRs) and the similarity of the pyramidal cell firing patterns during off-line SWRs (sSWRs) with on-line exploration of the reward locations (Figure 1.2c,d). In light of evidence pointing to a central role for SWRs in long-term memory consolidation (Buzsaki, 2015), it’s tempting to interpret these findings as task performance being aided by an increased number of pyramidal cells encoding a memory of the reward locations during exploration and increased ‘remembering’ of the rewarded locations during sleep. In my own experiments, we found dysfunctional SWR activity in mice that performed worse on our similar GOL task, which aligns with these results (subsection 4.2.7).

## 1.2 Memory in the brain

The earliest behaviorist approaches to studying memory focused solely on the behavioral responses elicited by sensory inputs – ignoring the ‘black box’ that the brain was at the time (Watson, 1913). It is now, perhaps obviously, recognized that behavioral responses intimately depend upon the organ that drives the response – the brain. The degree to which memory, and more generally cognitive functions, are localized within the brain has been widely debated. In the late 1800’s Pierre Paul Broca and Carl Wernicke identified patients with specific speech deficits related to the production and comprehension of language respectively. These deficits were later found to be associated with specific lesions in the posterior inferior frontal gyrus and posterior section of the superior temporal gyrus, providing evidence for the localization of cognitive functions within the brain. In contrast, work by Karl Lashley in the early 20<sup>th</sup> century showed that following the systematic removal of pieces of rat neocortex, performance in a previously-learned maze depended on the size of the lesion, but not the specific location (Lashley, 1929), lending support for the alternate THEORY OF MASS ACTION. Donald Hebb was one of the first to bring these two theories together, suggesting that networks of neurons could span many brain regions and collectively store memories (Hebb, 1949).

While circuits that perform many cognitive functions span the entire brain, there are also clearly cognitive functions that are localized to specific regions. For example, implicit procedural memory (e.g. driving a car) is largely localized to the striatum and cerebellum (Knowlton et al., 1996; Gerwig et al., 2007; Eichenbaum, 2000), while emotional memory (e.g. learned aversion) is largely attributed to the amygdala (LeDoux, 2000). The neocortex is important for working memory, priming effects, and eventually the long-term storage of declarative memory. While declarative memory may eventually be stored in the cortex, the HPC is central to the process of consolidating declarative memories of experiences, and building association networks, such as in the case of spatial maps (Eichenbaum, 2000). My primary research projects revolved around hippocampal-dependent spatial memory, so with no desire to minimize the important role of the rest of the brain in memory, I will focus on the HPC for the remainder of this section.

### **1.2.1 The hippocampus**

The HPC has been central to our study of memory at least since Scoville and Milner first reported in the 1950's on Henry Molaison (H.M.) who had profound anterograde amnesia following the bilateral removal of large portions of the medial temporal lobes, which includes the HPC and parahippocampal structures (Scoville & Milner, 1957). The most dramatic feature of H.M.'s memory loss was the inability to form new episodic memories, as he described it:

Every day is alone in itself, whatever enjoyment I've had, and whatever sorrow I've had.

(in Milner et al. 1968)

Despite H.M.'s near complete inability to form new memories, he still maintained the ability to recall events from childhood and showed no general cognitive or intelligence decline (Squire, 2009). Additional studies of H.M. over the next 50 years revealed that while declarative memory deficits remained severely impaired, various forms of implicit memory remained unaffected (Corkin, 2002). For example, patient H.M. was able to show day-to-day improvements in a mirror-tracing motor-learning task, despite no explicit memory of ever having performed the task before. In addition, he showed normal word-list priming effects – whereby words stems are preferentially completed by words semantically similar to recently viewed words. While the specific brain areas resectioned in the case of H.M. included structures adjacent to the HPC as well (such as the amygdala), numerous studies have since shown that the HPC in particular is essential for normal formation of long term episodic and semantic memory (reviewed in Eichenbaum, 2000; Burgess et al., 2002).

#### **1.2.1.1 Circuitry of the hippocampus**

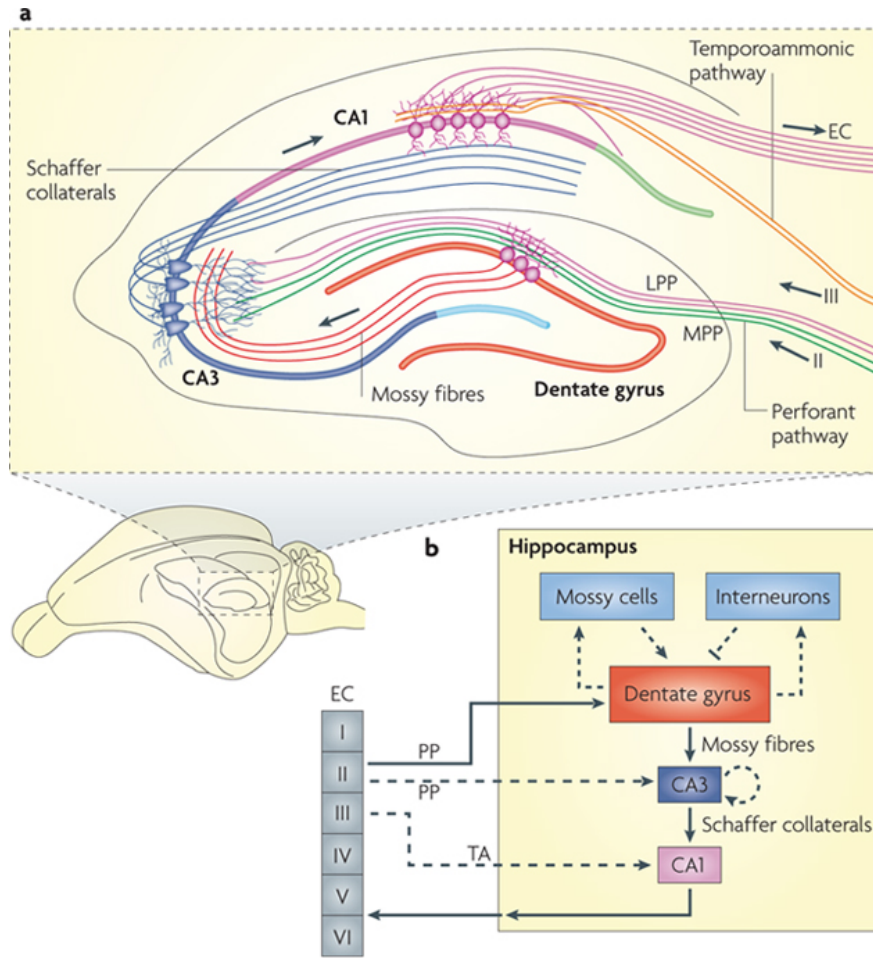
The hippocampus consists of the Ammons horn (Cornu Ammonis; CA) and dentate gyrus (DG), which make up the hippocampus proper, plus entorhinal cortex (EC), subiculum, presubiculum, and parasubiculum. The CA regions contains three sequential subregions, spanning from the subiculum to the DG; CA1, CA2, and CA3 (de Nô, 1934). The connectivity of the HPC is one of the most well-characterized neuronal circuits within the mammalian brain. Perhaps reflective of its fundamental role in memory processing, hippocampal-circuitry is also remarkably conserved across mammals (Manns & Eichenbaum, 2006). The principal neurons in the HPC communicate through the classically-defined trisynaptic loop: perforant path fibers project from layer II of the EC to

granule cells in the DG, which in turn send mossy fiber projections to CA3 that finally project along the Schaffer collateral pathway and synapse upon proximal apical and basal dendrites of CA1 pyramidal cells (CA1PCs), which are the primary output node of the HPC. Among other projections to both cortical and subcortical structures, CA1PCs also send a projection back to deep layers of the EC, completing the hippocampal loop. In addition, layer II of EC sends a direct perforant path projection to CA3 and layer III sends a direct projection through the temporoammonic pathway to distal dendrites of CA1. CA2 receives direct inputs from CA3 and layer II neurons from lateral and medial EC, and in turn send projections only within the HPC, to CA3 and CA1 (Hitti & Siegelbaum, 2014). Large excitatory cells within the hilus (MOSSY CELLS) receive excitation from DG granule cells and provide both direct feedback excitation and indirect feedback inhibition to granule cells (Danielson et al., 2017; Figure 1.3). There are also reciprocal long-range inhibitory projections (LRIPs) between the EC and CA1 that specifically target GABAergic INs (Melzer et al., 2012; Basu et al., 2016). In section 6.1, I will discuss work I did characterizing the functional properties of the LRIP from the EC to CA1.

Finally, the HPC is also targeted by afferents from neuromodulatory nuclei, including cholinergic and GABAergic projections from the medial septum (Klausberger & Somogyi, 2008), serotonergic and glutamatergic projections from the raphe nuclei (Varga et al., 2009), as well as dopaminergic and noradrenergic projections from the ventral tegmental area (Gasbarri et al., 1997) and locus coeruleus (Foote et al., 1983).

### 1.2.1.2 Local interneurons

The HPC consists not only of a dense principal cell layer of excitatory pyramidal cells, but also diverse populations of local GABAergic INs which control pyramidal cell spiking (Freund & Buzsáki, 1996). Classifications of INs are generally determined by their unique neurochemical markers, morphological structure, location of the soma within the lamina of the HPC, afferent connectivity, and target of inhibition. Within area CA1 for example, at least 21 GABAergic IN subtypes have been identified (Klausberger & Somogyi, 2008). These can be broadly segregated into three functional categories based on their target: DENDRITE-TARGETING, SOMA-TARGETING, and INTERNEURON-TARGETING. The two main classes of pyramidal cell-targeting INs – dendrite-targeting (e.g. somatostatin-positive; SST+) and soma-targeting (e.g. parvalbumin-positive: PV+)



Nature Reviews | Neuroscience

**Figure 1.3:** The neural circuitry of the rodent hippocampus. **a.** An illustration of the hippocampal circuitry. **b.** Diagram of the hippocampal neural network. The traditional excitatory trisynaptic pathway (EC–DG–CA3–CA1–EC) is depicted by solid arrows. The axons of layer II neurons in the EC project to the DG through the perforant pathway (PP), including the lateral perforant pathway (LPP) and medial perforant pathway (MPP). The DG sends projections to the pyramidal cells in CA3 through mossy fibers. CA3 pyramidal neurons relay the information to CA1 pyramidal neurons through Schaffer collaterals. CA1 pyramidal neurons send back-projections into deep-layer neurons of the EC. CA3 also receives direct projections from EC layer II neurons through the PP. CA1 receives direct input from EC layer III neurons through the temporoammonic pathway (TA). The dentate granule cells also project to the mossy cells in the hilus and hilar INs, which send excitatory and inhibitory projections, respectively, back to the granule cells. Reproduced from Deng et al. (2010).

INs – are uniquely situated to control different aspects of pyramidal cell activity. Dendrite-targeting INs can directly gate dendritic integration of inputs and have been shown to directly modulate pyramidal cell burst spiking (Royer et al., 2012). Hippocampal-dendritic inhibition has also been implicated in efficient formation of contextual fear memories, work which I contributed to, but will not be discussing further (Lovett-Barron et al., 2014). Soma-targeting INs tightly control the output of hippocampal pyramidal cells, modulate theta-phase activity, and are robustly affected by behavioral state (Klausberger & Somogyi, 2008; Lovett-Barron et al., 2012; Klausberger et al., 2003). Interneuron-targeting INs generally express calretinin (CR) or vasointestinal peptide (VIP) and are located throughout the lamina of the HPC (Chamberland & Topolnik, 2012). Relatively less is known about their functional activity *in vivo*, but their connectivity provides a dysynaptic disinhibitory drive to hippocampal pyramidal cells. Local inhibition within the HPC is essential for the normal control of network activity and the disruption of hippocampal GABAergic INs has been linked to multiple psychological disorders (reviewed in Marín, 2012), including schizophrenia which I will discuss later (subsection 2.3.4).

### 1.2.2 Functional organization of the hippocampus

As described above (subsection 1.2.1), the HPC is fundamental to our understanding of how the brain processes spatial and episodic memory, but it also plays an important role in emotion and anxiety-related behaviors (Fanselow & Dong, 2010). The HPC is essential in modulating the hypothalamic-pituitary-adrenal axis, as HPC lesions disrupt the normal hormonal stress response (Jacobson & Sapolsky, 1991) and psychiatric disorders such as depression, posttraumatic stress disorder, and bipolar disorder, are associated with reduced HPC volume (Fanselow & Dong, 2010). These two cognitively distinct functions have been shown to segregate along the dorsal-ventral axis of the HPC: dorsal hippocampus (dHPC) is associated with spatial and episodic memory and ventral hippocampus (vHPC) with emotion, anxiety-related behaviors, social interaction, and fear (Moser & Moser, 1998; Fanselow & Dong, 2010; Strange et al., 2014). Supporting this dissociation, lesions of dHPC, but not vHPC, impair performance in a Morris water maze test of spatial memory (Moser et al., 1995) and taxi drivers recalling routes through a city show functional magnetic resonance imaging (fMRI) activation of posterior HPC, which corresponds to dHPC in rodents (Maguire et al., 1997). In contrast, lesions of vHPC in rodents reduced innate fear responses as

seen by increased time spent in the exposed arms of an elevated plus maze and affected the degree of social interaction (Fanselow & Dong, 2010; Strange et al., 2014). More recently, vHPC neurons have been shown to be active in social interaction experiments and reactivation of specific subsets showed memory retrieval and could be paired to an unconditioned stimulus (Okuyama et al., 2016).

In addition, the dorsal-ventral axis of the HPC also correlates with gradients of both afferent and efferent connections. Projections to the HPC-proper from the EC generally follow a mapping of the dorsal-ventral axis of the EC to the dorsal-ventral axis of the HPC (Strange et al., 2014). Additionally, the return projections from area CA1 back to the HPC follow the same mapping. This spatial-segregation of projections also applies to the upstream cortical projections to the EC which target specific dorsal-ventral locations such that brain regions more involved in spatial processing (such as the retrosplenial cortex) project to more dorsal EC and regions more associated with emotion (such as the infralimbic cortex) project to more ventral EC (Strange et al., 2014). Output projections from area CA1 follow a similar pattern. Dorsal HPC preferentially projects to regions involved in navigation, such as the retrosplinal and anterior cingulate cortices, while uniquely-vHPC projections target the olfactory bulb (which has been linked to depression), the amygdala, and the nucleus accumbens (Moser & Moser, 1998; Fanselow & Dong, 2010; Strange et al., 2014). The anatomical connectivity listed above are examples of differential connectivity and certainly not an exhaustive list, but they do highlight the underlying anatomy that gives rise to the episodic memory-emotion dichotomy within the HPC.

### 1.2.2.1 Pyramidal cell functional diversity

Beyond the overall organization along the dorsal-ventral axis of the HPC, principal cells in the HPC also vary in their genetic makeup, connectivity, and functional properties along the transverse (Igarashi et al., 2014) and radial (Slomianka et al., 2011) axes as well. In particular, the radial axis, which corresponds to neurodevelopmental age, can be divided into superficial and deep pyramidal cells with unique properties and connectivity (Angevine, 1965; Schlessinger et al., 1978; Deguchi et al., 2011). Deep pyramidal cells are generally larger, express *Vipr2* and *Sox5*, and they preferentially receive inputs from the septum and ventral striatum (Nielsen et al., 2010; Sørensen et al., 1993, 1995). Functionally, they show more burst firing, and generally contain more spatial information, which reflects as a higher fraction of place cells (Mizuseki et al., 2011). In contrast,

superficial pyramidal cells are smaller, and express *Calbindin-28k*, *Zbtb20*, and *Satb2* (Sloviter, 1989; Slomianka, 1992). As part of my extended projects, I worked with colleagues to further characterize *in vivo* functional properties and learning-related *in vivo* dynamics of pyramidal cells along the radial axis (section 6.3).

### 1.2.2.2 Hippocampal computations

Computational models of the HPC have long posited that the EC-DG-CA3 circuit was well positioned anatomically to perform pattern separator/completion computations (Marr, 1971; Treves & Rolls, 1994; Knierim & Neunuebel, 2016). The EC to DG connection is highly divergent, with 5 times as many DG granule cells as EC input cells (Amaral et al., 1990). In addition, DG granule cells are under heavy inhibitory control, as their very sparse activity has made them difficult to record from *in vivo* and their activity seems to readily remap to context manipulations (Neunuebel & Knierim, 2014; Leutgeb et al., 2007), perhaps the most direct measure of input decorrelation or PATTERN SEPARATION (Figure 1.4a). Hippocampal area CA3 in comparison is most notably characterized by its dense recurrent connections between pyramidal cells which inspired the proposal of CA3 as a Hebbian autoassociation network (Marr, 1971). Area CA3 receives excitatory inputs from both the strong ‘detonator’ synapses of DG granule cell Mossy fibers as well as perforant path inputs from the EC. These connections make the region much more excitable and are thought to support PATTERN COMPLETION (Figure 1.4b) by establishing attractor network dynamics that allows for the network to recall entire memories from partial cues (Treves & Rolls, 1992; Neunuebel & Knierim, 2014). Finally, the CA1 output node of the HPC has been suggested to play a role in novelty detection as a COMPARATOR (Vinogradova, 2001; Lisman & Otmakhova, 2001), as it has access to both the internal HPC processed information from CA3 Schaffer collaterals as well as direct temporoammonic path excitation from the EC (Figure 1.4c). While the role of area CA2 has been historically understudied, recent work has elucidated an important role for CA2 in social memory (Hitti & Siegelbaum, 2014), aggression (Wersinger et al., 2002), and time coding (Mankin et al., 2015).

In addition to specialized functions for hippocampal subfields, specific input streams to the HPC also serve distinct roles. In particular, the temporoammonic path inputs to CA1 include both medial entorhinal cortex (MEC) and lateral entorhinal cortex (LEC) projections which convey two

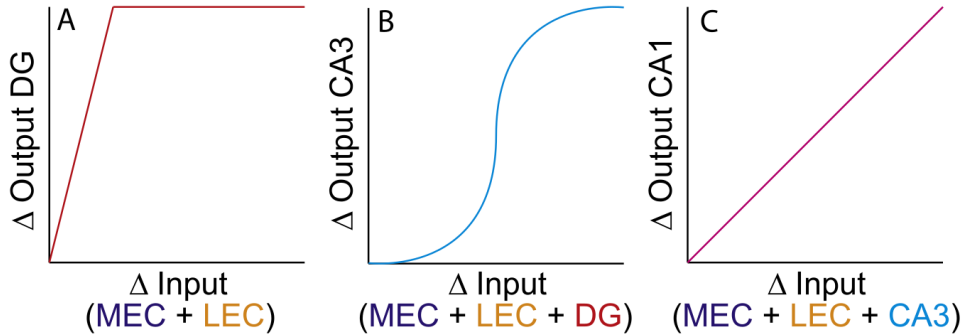


**Figure 1.4:** Hypothesized input-output curves for the DG, CA3, and CA1 regions of the hippocampus. The  $x$ -axis of each graph denotes the difference between the neural activity representations of two specific input patterns. The  $y$ -axis represents the difference between the corresponding output patterns. **A.** The DG is hypothesized to change its output patterns to a greater extent than the input patterns change (pattern separation). **B.** CA3 is hypothesized to show a sigmoidal relationship between  $\Delta\text{input}$  and  $\Delta\text{output}$ , performing pattern completion with small  $\Delta\text{input}$  and pattern separation with large  $\Delta\text{input}$ . **C.** CA1 is hypothesized to display a linear relationship between  $\Delta\text{input}$  and  $\Delta\text{output}$ . Reproduced from Knierim & Neunuebel (2016).

distinct streams of information. The MEC projection is the primary spatial input to CA1 and conveys the ‘where’ of an episodic memory. In contrast, LEC projections convey non-spatial, contextual and sensory information that contributes the ‘what’ components of episodic memory (Hargreaves et al., 2005; Dickerson & Eichenbaum, 2010; Eichenbaum et al., 2012). These two distinct input streams of spatial and non-spatial information also unequally project to CA1PC subpopulations (subsubsection 1.2.2.1), with MEC preferentially targeting proximal and deep CA1PCs, while LEC preferentially projects to distal and superficial CA1PCs (Masurkar et al., 2017). These inputs streams are not completely spatially separated, as within place cell populations differences in locations are encoded through global remapping and differences in context are encoded through rate remapping (see subsubsection 1.3.1.1; Leutgeb et al., 2005b). In agreement with this interpretation, the context-specific change in the active population of cells was impaired by lesions of LEC (Lu et al., 2013). Characterizing the *in vivo* activity of the inhibitory component of the LEC projection to CA1 was part of my work with collaborators that I will discuss briefly later (section 6.1).

### 1.2.3 Memory at the synapse

#### 1.2.3.1 Long-term potentiation

I have discussed the cognitive aspects of memory and the general brain regions involved, but what actually *is* memory? Mounting evidence points to specific changes at the synapses between cells and the molecular components that make this possible. The search for memory in the brain is in fact the search for HYSTERESIS, a dependence of the present activity of the brain on the past. The first physiological example of this phenomenon in the brain was described by Bliss & Lomo in 1973. In anesthetized rabbits they found that high-frequency stimulation of the perforant path inputs to the HPC resulted in the later enhancement of DG granule population activity (Bliss & Lomo, 1973). This long-term potentiation (LTP) effect has now been studied extensively, with much of the work being done at two model synapses: the sensory- to motor-neuron synapse governing the siphon-withdrawal reflex of *Aplysia californica* and synapses within the rodent HPC, primarily the Schaffer collateral synapse from CA3 to CA1 pyramidal cells (Kandel, 2001; Bailey et al., 2008). In both *Aplysia* and rodents, the molecular pathways giving rise to LTP have been well established. There are two primary stages of LTP: early, short-term LTP (E-LTP) which involves modification of pre-existing proteins at the synapse, and late, long-term LTP (L-LTP) which involves new protein synthesis and potentially the formation of new synapses (Frey et al., 1988; Bailey et al., 2008). These two distinct forms of LTP are reminiscent of short- and long-term memory, and have in fact been linked (Moser et al., 1998; Hernandez & Abel, 2008), mostly through the shared-dependence on NMDA-receptors.

#### 1.2.3.2 NMDA-receptor-dependent memory

Theoretical work had long posited that memory could be stored within neuronal networks by increasing the synaptic strengths between neurons that were active at the same time, effectively learning causal associations (Hebb, 1949; Marr, 1971). The NMDA-receptor (NMDAR)'s unique functional properties were recognized to make it well-suited as a coincidence detector. Most essentially, the NMDAR is blocked by magnesium in a voltage-dependent manner such that the block is released only when the postsynaptic neuron is depolarized, which when coupled with the NMDAR's slow activation and inactivation kinetics provides a time window for pre- and post-synaptic coinci-

dence detection (reviewed in Bliss & Collingridge, 1993). In addition, NMDARs have high calcium permeability, allowing for their opening to trigger the influx of calcium that initiates the molecular pathway leading to LTP (Bailey et al., 2008).

In the 1980's the study of acute hippocampal slices identified the NMDAR – an ionotropic glutamate receptor of which N-methyl-D-aspartate (NMDA) is a selective agonist – as being essential for the induction of LTP, but not for normal synaptic transmission (Collingridge et al., 1983). Around the same time, Richard Morris and colleagues were able to show that blocking NMDARs *in vivo* with an intraventricular infusion of the selective NMDAR antagonist R-2-amino-5-phosphonopentanoate (AP5) impaired mice on a spatial learning task (Morris et al., 1986). These two findings together laid the foundation for future work which points towards an essential role for NMDARs in learning and memory (Morris, 2013).

Cloning of the genes for the NMDAR subunits (Moriyoshi et al., 1991) allowed for their detailed characterization and eventual mouse lines with the genes manipulated. While knocking out *NR1* – the subunit necessary for forming a functional NMDAR – globally is lethal, mice were designed to selectively knockout *NR1* in specific hippocampal subregions – initially CA1 – using the *Cre/loxP* system which could be used to study the hippocampal-specific effect of NMDARs on memory (Tsien et al., 1996). Tsien et al. showed that CA1-specific knockout of NMDARs lead to impaired spatial memory in the hidden-platform water maze, but no impairment in the non-HPC-dependent landmark task (where the reward is marked by a large proximal cue). In addition, NMDARs have also been removed from the DG (McHugh et al., 2007) and CA3 (Nakazawa et al., 2002) where deficits were observed in pattern separation and pattern completion/associative recall, respectively, suggesting that these two functions do in fact reside in the DG/CA3 regions and they involve active synaptic plasticity. The selective removal of a single ion channel from individual subregions of the HPC strongly suggests an important role for hippocampal NMDARs and LTP, and thus synaptic plasticity, in spatial learning and memory (Tsien et al., 1996).

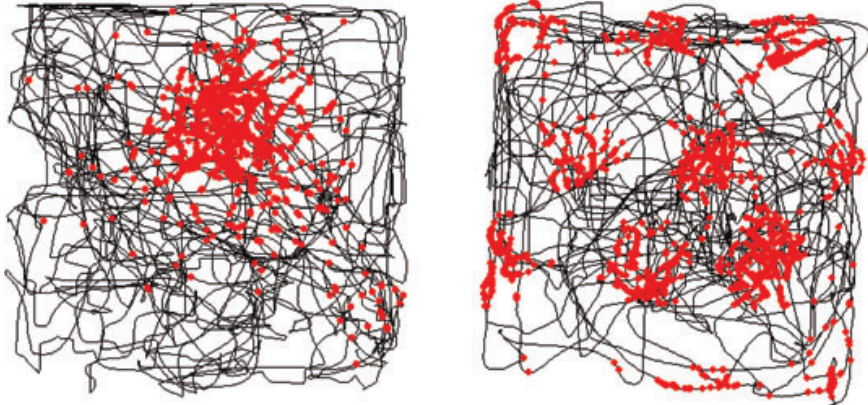


**Figure 1.5:** Place cell in the HPC (*left*) and grid cell in the MEC (*right*). Spike locations (*red*) are superimposed on the animal’s trajectory in the recording enclosure (*black*). Whereas most place cells have a single firing location, the firing fields of a grid cell form a periodic triangular matrix tiling the entire environment available to the animal. Reproduced from Moser et al. (2008).

## 1.3 Functional correlates of memory

### 1.3.1 Spatial maps

Perhaps the best-studied ‘engrams’ in the mammalian brain are hippocampal place cells. Throughout the HPC (DG, CA3, CA2, and CA1) there are principal cells that fire selectively at specific locations within an environment (PLACE CELLS). As an animal explores an environment these principal cells show sparse spatially-modulated changes in firing rates that are established rapidly and subsequently remain stable (O’Keefe & Dostrovsky, 1971; Thompson & Best, 1990; Frank et al., 2004). These place cells form an allocentric map of the environment, which is essential for normal episodic memory function (Smith & Mizumori, 2006; Nakazawa et al., 2004; Buzsáki & Moser, 2013). Our understanding of place cells is a uniquely well-characterized functional mapping of the real world multiple synapses from both sensory and motor cortices. In addition to place cells in the HPC, the MEC contains several categorized cell types involved in spatial navigation. These include GRID CELLS, which fire at regularly spaced intervals throughout an environment (Hafting et al., 2005; Moser et al., 2014), HEAD-DIRECTION CELLS (Taube, 2007), and BORDER or BOUNDARY-VECTOR CELLS, which fire at specific distances relative to the edges of an environment (Solstad et al., 2008). Together with place cells, these cells collectively form the cellular foundation for the mammalian navigation system.

### 1.3.1.1 Remapping

Place cells, like other forms of memory, are constantly trying to balance two competing constraints: on the one hand, their firing needs to be stable in order to be a helpful representation of the environment, but on the other hand, their firing needs to be plastic enough to constantly encode new environments, forget irrelevant information, and adapt to new features. Place cells changing their firing properties to incorporate new features of the world is known as REMAPPING (Muller & Kubie, 1987a; Leutgeb et al., 2005b; Colgin et al., 2008). A given place cell is defined by its spatial tuning – its place field – and its firing rate gain within the place field – the ratio of in vs. out of field firing. These seem to be independent factors, as either can remap separately. GLOBAL REMAPPING is the collective remapping of place field locations across a population of place cells. Alternatively, RATE REMAPPING is a change in place field gain, while place fields locations remain fixed.

Global remapping is generally triggered by discrete changes to environmental conditions (Leutgeb et al., 2004, 2005b), but can also be triggered by particularly salient events (Moita et al., 2004). The sudden and collective remapping of firing fields support the notion of place fields arising from discrete attractor states (Jeffery, 2011), though the discreteness of the transition seems to depend on the specifics of the environmental manipulations (Wills et al., 2005; Leutgeb et al., 2005a; Jezek et al., 2011). In contrast, rate remapping preserves firing fields (and grid cell firing), but the firing rate of place cells changes across the population. This separation of position and rate coding has lead to the hypothesis that they code for spatial and episodic memory, respectively (Leutgeb et al., 2005b). Indeed, while place field location is closely tied to grid cell activity in the MEC, rate remapping depends specifically on LEC inputs, which convey contextual information (Lu et al., 2013). It is possible to observe incomplete remapping, known as PARTIAL REMAPPING, though this generally refers to situations where subsets of cells respond to alternate competing spatial reference frames (Skaggs & McNaughton, 1998; Colgin et al., 2008).

### 1.3.1.2 Stability

The complete population remapping of global remapping and the ‘rate-only’ remapping of rate remapping do not tell a complete story of place fields firing dynamics. More generally, the STA-

BILITY of place cells populations varies with elapsed time and environment novelty, is affected by neuromodulation, and differs by hippocampal subfield. In area CA1, the place cell population changes over time, such that similarity of activity is greatest at short time scales and decays over time (Figure 1.6; Mankin et al., 2012). In contrast, place cell firing is more stable over time in CA3, providing a means to both stably represent a given environment and also distinguish different experience by recency. Place fields form rapidly (<10 min) and quickly stabilize (Frank et al., 2004) and can remain stable for months with the right conditions (Thompson & Best, 1990; Lever et al., 2002b; Ziv et al., 2013). This long-term stability of place fields is both NMDAR-dependent (McHugh et al., 1996; Kentros et al., 1998) and requires new protein synthesis (Agnihotri et al., 2004), in a similar manner as LTP (subsubsection 1.2.3.1) and other forms of declarative memory (Hernandez & Abel, 2008).

Several factors have additionally been shown to influence the stability of place cell tuning. Moita et al. trained mice in two chambers to establish separate place maps in both locations. After becoming familiar to both, rats underwent a contextual fear conditioning protocol in one of the chambers, which selectively induced remapping in that one chamber, while place cells in the control chamber remained stable (Moita et al., 2004). In addition, Kentros et al. showed that increasing spatial salience correlated with increased place field stability, and also showed that the stability could be modulated by systemic administration of dopamine D1/D5 receptor agonist/antagonists (Kentros et al., 2004), possibly through the dependence of CA1 LTP on D1/D5 receptor activity (Huang & Kandel, 1995). Place cell stability is a fundamental aspect of my main project (chapter 4), as I also looked at place field stability as it relates to context novelty and task demands. My main findings in wildtype mice agree with what was shown previously, but I also see disruptions in these normal stability mechanisms in *Df(16)A<sup>+</sup>/-* mice.

## 1.4 Summary

In summary, our memories are fundamental features of our identity. We now are beginning to understand not just the cellular and circuit substrates for memory, but also the conditions that effect their formation and stability. By expanding our knowledge of the basal brain state underlying memory, we can begin to understand not just the psychology of normal memory, but also how

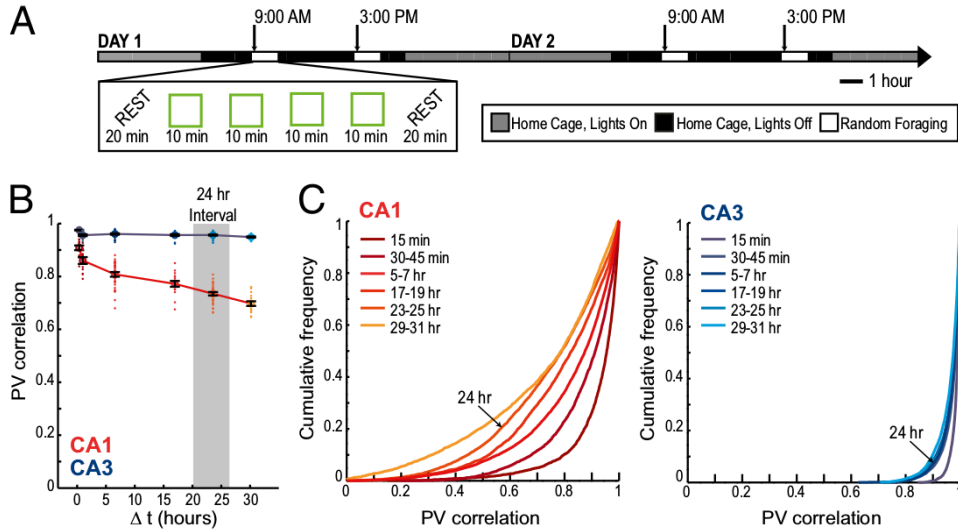


**Figure 1.6:** Place cell population stability over days differs by HPC subfield. When testing with a single enclosure shape, firing patterns of the CA3 network remained highly consistent for repetitions of the same environment over extended time intervals, whereas activity patterns in the CA1 network changed. **A.** An experimental design with a single enclosure shape. **B.** Population vector (PV) correlations between pairs of recordings are shown as dots. The black error bars report the mean  $\pm$  SEM for pair-wise comparisons at each time interval. Highly consistent firing patterns in the CA3 population were observed over time intervals of 30 minutes to 30 hours. In contrast, the CA1 network continued to show a pronounced monotonic decrease in firing similarity with time. **C.** Cumulative distribution functions for PV correlations between pairs of recordings at different time intervals. Reproduced from Mankin et al. (2012).

cellular and circuit failures give rise to memory impairments. In the next session I will discuss schizophrenia, and particularly how memory impairment is a core, debilitating symptom of the disease. By better understanding the precise way in which memory fails, we can hope to find ways to help strengthen these memories, while at the same time also learn more about what is essential for the normal functioning of the declarative memory system.

# Chapter 2

## Schizophrenia

### Overview

Schizophrenia is a chronic, debilitating disease affecting approximately 1% of the worldwide population (McGrath et al., 2008). In the United States, it is estimated that 20% of all schizophrenia patients are homeless and schizophrenia is associated with an approximately 20 year reduced life expectancy (Folsom et al., 2005; Tiihonen et al., 2009). A 2011 World Economic Forum report (Bloom et al., 2011) estimated that the global burden of mental illness – of which schizophrenia is a major contributor – would be more than 16 trillion US\$ over the next 20 years, or approximately 1-2% of the 2010 global GDP per year. Compared to all other non-communicable diseases, mental illness accounts for the most lost output, more than cardiovascular disease and cancer (Figure 2.1). The cost of schizophrenia in particular was estimated to be \$155 billion in the United States in 2013, 24% going to direct cost of treatment, and 75% coming from indirect costs including caregiving for patients and unemployment (Cloutier et al., 2016).

Schizophrenia is a syndrome defined by its symptoms, the most prominent of which is psychosis. Symptoms are generally classified into three main categories: positive, negative, and cognitive (Kay et al., 1987). Positive symptoms are behaviors not normally seen in healthy individuals and include hallucinations, delusions, suspiciousness, hostility, thought disorders, and movement disorders. Negative symptoms reflect missing or disrupted normal thought processes, including: blunted affect, social withdrawal, avolition, anhedonia, and difficulty in abstract thinking. Cognitive symptoms include attentional deficits, poor executive functioning, and both working and long-term

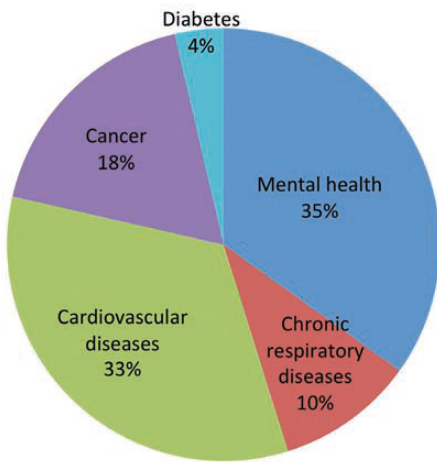


**Figure 2.1:** Breakdown of non-communicable disease cost by disease type. Reproduced from Bloom et al. (2011).

memory impairment, specifically in the domain of episodic semantic memory. While the positive symptoms, in particular hallucinations and delusions, might be the most prominent symptoms of schizophrenia, cognitive symptoms are present in up to 75% of schizophrenia patients and the severity of cognitive symptoms is strongly linked to functional outcomes (O'Carroll, 2000; Green, 1996; Keefe, 2007). This is particularly troubling since treatment options for the negative and cognitive symptoms of schizophrenia are extremely limited.

Since the underlying causes of schizophrenia are not known, treatment for patients with schizophrenia is limited to treating symptoms as they present. Treatment for schizophrenia patients primarily includes a combination of antipsychotic medication and psychosocial therapy. Patients' responses to antipsychotics varies widely, some experiencing complete remission of psychoses and others showing no alleviation of symptoms. Overall, following a first episode-psychosis, long-term antipsychotic treatment is effective in 30-40% of patients in preventing future psychoses (Boyer et al., 2007; Insel, 2010), leaving over half of all patients still experiencing psychotic episodes. More importantly, antipsychotic medication only aims to treat the positive symptoms of schizophrenia, such as hallucinations and delusions. There are limited treatment options for the debilitating cognitive deficits – including deficits in attention, executive function, and both working and episodic memory – which have proven to be the greatest barrier to rehabilitation (Lieberman et al., 2005; Harrison et al., 2001; O'Carroll, 2000; Hyman & Fenton, 2003).

Like most mental disorders, the underlying etiology of schizophrenia is most likely complex and heterogeneous, making the discovery of a single ‘monotherapy’ unlikely (Hyman & Fenton, 2003). For these reasons, there is growing appreciation that we need to better understand and treat sets of symptoms separately, particularly developing new drug interventions for the negative and cognitive symptoms of schizophrenia. Indeed, it seems likely that what today we call schizophrenia is in fact a collection of related disorders, some potentially common to other mental health diagnoses as well (Insel, 2010). This view of schizophrenia implies that by focusing on particular dysfunctions – such as episodic memory impairment – we can hope to find general therapeutic targets for diseases currently classified separately, and at the same time, by looking for convergence on to common endophenotypes we can identify treatment targets shared by patients with heterogeneous underlying etiology. Indeed, the core unit of computation for many of these cognitive functions seems likely to be ensembles of thousands of neurons working together as a NEURAL CIRCUIT. As we have learned more about the way neural circuits govern behavior in healthy individuals, the precise nature of cognitive deficits in patients, and the molecular changes that occur in schizophrenia, it is becoming clear the schizophrenia is at its core a neurodevelopmental dysfunction of neural circuits (Arguello & Gogos, 2012; Insel, 2010; Insel et al., 2010; Lewis & Levitt, 2002). Still, very little is known about the nature of neural circuit disruptions and how they lead to behavioral and cognitive dysfunction.

In the following sections I will expand upon some of the symptoms, brain abnormalities, and causative factors observed in schizophrenia patients, with a specific focus on aspects of the disease most relevant to my main research project (see chapter 4). I will discuss details of the memory deficits present in schizophrenia patients (section 2.1), with a particular focus on spatial and episodic memory impairments. I will present what we know about specific brain regions affected in schizophrenia patients, specifically focusing on the hippocampus (HPC) (section 2.2). Finally, I will lay out several proposed causes of schizophrenia including genetic risk factors, neurodevelopmental insults, alterations in neuromodulatory signaling, and disrupted glutamatergic and GABAergic machinery (section 2.3).

## 2.1 Memory deficits

Disruption in working and declarative memory are among the primary cognitive deficits observed in schizophrenia patients. The memory deficits present in schizophrenia are specific in that patients seem to have relatively spared implicit or procedural memory, while many patients present with striking deficits in declarative memory (see section 1.1), including both episodic memory – conscious recollection of events – and semantic memory – knowledge of people, place, objects, and facts (O’Carroll, 2000; Aleman et al., 1999; Gold et al., 2010). In addition to being specific, the observed memory deficits are also pervasive, in that they can not be accounted for by age, education, medication, or disease duration or severity (Ranganath et al., 2008) and are present in the majority of schizophrenia patients. As mentioned more generally about cognitive symptoms of schizophrenia, the severity of memory impairments in particular is one of the strongest predictors of longterm functional outcome among schizophrenia patients (Green, 1996), as failures in declarative memories provide the greatest barrier to steady employment.

The pattern of memory deficits observed in schizophrenia patients is consistent with disruptions in both the executive control and working memory functions associated with the prefrontal cortex (PFC) as well as with the longterm memory storage role of the HPC. Disorders that specifically arise from PFC lesions or dysfunction show a similar impairment in encoding and retrieval as seen in schizophrenia patients (Ranganath et al., 2008). Schizophrenia patients show specific impairment in working memory capacity and in the ability to work with memory held in working memory, both fundamental features of the PFC (Gold et al., 2010; Cannon et al., 2005). In addition, patients do not make use of the same semantic memory strategies as healthy individuals, though these impairments can at least in part be ameliorated by training or through restructuring of task stimuli – for example, blocked instead of unblocked word lists (Gold et al., 1992; Stone et al., 1998).

### 2.1.1 Spatial memory

As described in more detail above (see Spatial memory as episodic memory), memory for specific locations is one particular type of episodic memory that has provided tractable approaches for studying memory. While less recognized as a core symptom of schizophrenia, spatial memory deficits are well documented in schizophrenia patients (Boyer et al., 2007; Hanlon et al., 2006;

Wilkins et al., 2013; Weniger & Irle, 2008), but the underlying circuit level dysfunctions have rarely been investigated (Hayashi et al., 2015; Suh et al., 2013). A lack of general awareness of spatial memory deficits in schizophrenia patients is most likely attributable to the different approaches taken by clinical psychologists and basic research scientists. Deficits in verbal memory are among the most prominent cognitive deficits observed in schizophrenia patients (O'Carroll, 2000). The broad category of verbal memory reflects the nature of psychological tests used to assess memory deficits, they involve verbal discourse with the clinician. In practice verbal memory tests generally test either short-term working memory – with tests such as the Digit Span test which probes the number of items that one can remember and immediately recall – or longterm declarative memory. Longterm declarative memory tests includes remembering lists of potentially semantically grouped words or aspects of narrative stories. This longterm declarative memory component of verbal memory tests (referred to as SECONDARY VERBAL MEMORY) is particularly impaired in schizophrenia patients (Green, 1996).

In addition, the deficits observed in spatial memory seem to be specific to allocentric navigation, as compared to egocentric navigation. For example, a study by Wilkins et al. used a 4-on-8 virtual maze to distinguish between allocentric (referred to as ‘spatial’) and egocentric (‘response’) navigation strategies (Wilkins et al., 2013). The 4-on-8 virtual maze places participants in a virtual 8-arm radial maze with distal landmarks visible around the maze. In the first phase of the task 4 arms are blocked and the participants travel to the end of the 4 open arms to receive rewards. In the second phase all 8 arms are opened and the participants must learn to travel down the 4 newly-available arms to retrieve rewards. Finally, in the probe trials, all 8 arms are open, with rewards in the original 4 open arms, but now the walls of the arms are raised to occlude the distal landmarks. During these probe trials, participants who learned an egocentric strategy (e.g. visit the 1<sup>st</sup>, 3<sup>rd</sup>, 5<sup>th</sup>, & 6<sup>th</sup> arms clockwise around the maze) would still perform well, but those who learned an allocentric strategy (e.g. rewards are near the mountain, forest, lake, and sun) would perform poorly. The authors found that schizophrenia patients who used an allocentric navigation strategy performed significantly worse than healthy controls, but patients who used an egocentric navigation strategy performed similar to healthy individuals. This differential effect was also seen in learning to navigate a virtual park versus a virtual maze (Weniger & Irle, 2008) and in a virtual Morris water maze comparing hidden- and visible-platform trials (Hanlon et al., 2006). In agreement with the

well-characterized hippocampal deficits in schizophrenia patients (see subsection 2.2.1), allocentric navigation is primarily HPC-dependent (see subsection 1.1.1), while egocentric navigation relies on other brain regions unaffected by schizophrenia, principally the caudate nucleus (Hartley et al., 2003).

Spatial memory impairments in schizophrenia patients include not just deficits in allocentric spatial navigation, but in spatial working memory as well. For example, In a similar VR radial arm maze schizophrenia patients showed both working and reference memory impairments (Spieker et al., 2012). Piskulic et al. performed a meta-analysis of behavioral studies of schizophrenia patients and identified consistent spatial working memory deficits in schizophrenia patients (Piskulic et al., 2007). Additionally, HPC-PFC synchrony is disrupted in the *Df(16)A<sup>+-</sup>* mouse model of schizophrenia (see subsubsection 2.3.2.2) during a working memory task (Sigurdsson et al., 2010). Take together, this evidence points towards a clear fundamental disruption of spatial memory in schizophrenia patients.

## 2.2 Schizophrenia in the brain

Brain structural changes have been reliably identified in schizophrenia patients following a first episode of psychosis, and more recently, in high-risk individuals during the prodrome, prior to a clinical diagnosis. In particular, reductions in gray matter volume and a corresponding increase in lateral ventricle volume have been consistently demonstrated (Fusar-Poli et al., 2013; Shepherd et al., 2012). Tracking of clinically high-risk individuals has identified schizophrenia-related structural changes in the hippocampal formation, the cerebellum, the superior and medial temporal lobes, the insular cortex and the PFC (Cannon et al., 2015; Millan et al., 2016). Additionally, among the clinically high-risk population, continued progression towards schizophrenia can be predicted by monitoring gray-matter loss (Tognin et al., 2014), aiding in pre-symptomatic identification with the hope of early intervention treatments (see Schizophrenia as a neurodevelopmental disorder). While there are well-characterized deficits in schizophrenia patients in multiple other brain regions, including the PFC (Weinberger et al., 1986) and striatum (Simpson et al., 2010), my main research has been on hippocampal-dependent episodic memory impairment, so I will focus particularly on the HPC in the following sections.

### **2.2.1 The hippocampus in schizophrenia**

Of particular relevance to my primary thesis project, consistent behavioral, anatomical, and physiological studies of schizophrenia patients have all pointed towards the HPC as an integral region in disease pathology (Boyer et al., 2007; Bogerts et al., 1985; Jakob & Beckmann, 1986). Meta-analysis of quantitative functional magnetic resonance imaging (fMRI) studies found overall significant effect sizes of 0.37 and 0.39 for the left and right HPC respectively, corresponding to an approximately 4% reduction in bilateral hippocampal volume (Nelson et al., 1998). In addition, there was no effect of illness duration, which implies that either the HPC suddenly reduces in volume by 4% on the day of first-episode psychosis or the hippocampal volume reduction is already present prior to clinical disease onset, further supporting the neurodevelopmental etiology of schizophrenia (see subsection 2.3.2). The medial septum projections to the HPC are of particular interest, since the cholinergic projection has been linked to learning and memory (Parent & Baxter, 2004) and the GABAergic projection is known to target parvalbumin (PV)+ interneurons (INs) (Freund & Antal, 1988) which are altered in schizophrenia (see subsection 2.3.4). In addition, this projection has also been linked to aberrant behavior in an NMDA-receptor (NMDAR) antagonist model of schizophrenia (Ma et al., 2012). Despite these well-characterized features of hippocampal organization, it remains unknown how the function of these circuit motifs are altered in schizophrenia during hippocampal-dependent behaviors.

#### **2.2.1.1 Specific role of hippocampal area CA1**

There is growing evidence that hippocampal area CA1 is the first subregion affected in schizophrenia, and potentially the source of hippocampal deficits. Work by Schobel et al. used high-resolution (sub-millimeter pixel size) fMRI of baseline activity to compare schizophrenia patients to healthy controls. The authors particularly looked at regions previously associated with schizophrenia (the hippocampal formation, frontal cortex, basal ganglia, and amygdala) and found a preferential increase in cerebral blood volume (CBV) in schizophrenia patients in hippocampal area CA1 and orbitofrontal cortex, and a decrease in dorsolateral PFC (Schobel et al., 2009). In addition, the authors followed a prodromal population over two years and found that baseline CBV abnormalities specifically in hippocampal area CA1 predicted progression to psychosis. Finally, symptom

severity was also shown to correlate with CBV levels in area CA1. Follow-up work showed that hippocampal hypermetabolism spread from CA1 to other regions and prodromal CA1 hypermetabolism predicted post-psychosis hippocampal atrophy, and these effects are linked to deficient glutamate levels (see subsection 2.3.4; Schobel et al., 2013). Similarly, a recent study found that progressive hippocampal area CA1 volume loss correlated with disease progression and it spread from CA1 to other hippocampal subfields (Ho et al., 2017). In addition, the synaptic molecular machinery has been shown to be disrupted in area CA1 of schizophrenia patients, with a decrease in protein levels of PSD95, synaptophysin, and scaffolding proteins (Matosin et al., 2016). Finally, in my primary research project (chapter 4) I investigated the role of aberrant CA1 activity in spatial memory disruptions in a mouse model of schizophrenia, which further adds evidence for a central role of hippocampal area CA1 in schizophrenia.

### 2.3 Schizophrenia etiology

While the underlying cause of schizophrenia has remained elusive, and the search has been confounded by a high concordance with other psychiatric diseases (Kessler et al., 2005), collective evidence has pointed to several possible mechanistic pathways. Unlike Alzheimer’s disease or Parkinson’s disease where cell-death of specific cell types has been causally linked to disease progression, schizophrenia and many other psychiatric disorders exhibit no drastic cell loss or increased gliosis, and affected brain regions can span both cortical and subcortical regions, suggesting network or circuit dysfunctions (Uhlhaas & Singer, 2012; Lewis & Levitt, 2002). A clear genetic-risk component has been recognized for quite some time, which is perhaps most evident by an exponentially increasing risk for developing schizophrenia with relatedness to a schizophrenia patient (Rodriguez-Murillo et al., 2012). Additional risk factors are now becoming better understood as well, including shared family environment, male gender, advanced paternal age, perinatal events, and substance abuse (Lichtenstein et al., 2009).

In my primary research project (chapter 4) I studied a genetic mouse model of schizophrenia based on a human deletion in chromosome 22 that has been strongly associated with schizophrenia. In the following section I will generally discuss the genetic risk structure associated with schizophrenia, as well as some of the best-studied molecular hypotheses of schizophrenia etiology, particularly

the role of dopamine and excitation-inhibition imbalance.

### 2.3.1 Genetics

Current estimates suggest that schizophrenia is up to 80% heritable, arising from a large network of genetic abnormalities that predispose for schizophrenia (Ripke et al., 2011; Tandon et al., 2008), though most schizophrenia patients do not in fact have a family history of schizophrenia (Tandon et al., 2008; Rodriguez-Murillo et al., 2012). This suggests that either schizophrenia risk is conferred by many genes that individually have minimal effect, so go unnoticed unless combined with other risk factors (common disease, common allele, CDCA), or highly-penetrant individual mutations that are quickly selected against but arise *de novo* leading to schizophrenia (common disease-rare allele, CDRA). Current genetic research of schizophrenia focuses on three main approaches: genome-wide association (GWA) studies, identification of copy-number variants (CNVs), and full exome sequencing for individual mutations.

Linkage-based analysis has identified over 1000 proposed genes associated with schizophrenia, but many of these findings have failed to be replicated and their validity is questionable (<http://www.szgene.org>, Allen et al., 2008). Large scale GWA studies provide the ability to detect common genetic alleles which subtly contribute to schizophrenia predisposition (CDCA). A recent GWA study of 36,989 schizophrenia patients and 113,075 controls identified 108 genetic loci that reached genome-wide significance (Ripke et al., 2014). Of the 108 loci, 83 were novel regions not previously associated with schizophrenia, providing new potential therapeutic targets. Notable hits with previously recognized links to schizophrenia include: the D2 dopamine receptor (subsection 2.3.3), glutamatergic neurotransmission (subsection 2.3.4), and voltage-gated calcium channels.

CNVs have been shown to confer significant risk for schizophrenia and has highlighted the role of rare *de novo* mutations in schizophrenia (Rodriguez-Murillo et al., 2012). Advances in sequencing technologies now allows for the sequencing of large portions of the genome of schizophrenia patients, which has made possible the genome-wide unbiased search for CNVs in schizophrenia (Xu et al., 2011). A recent collaborative study of 21,094 schizophrenia patients and 20,227 controls identified significantly more CNVs present in the patient population (Marshall et al., 2016), a sign of generally more genetic mutations in schizophrenia patients and highlighting the link between schizophrenia and CNVs. This study specifically identified genes of synaptic function and mouse neuobehavioral

phenotypes as significantly affected and in particular identified 8 loci that reached genome wide significance, including the previously identified 22q11.2, which is the basis for the genetic model that I use in my experiments and I will discuss in detail below (subsubsection 2.3.2.1).

Sequencing the entire exomes of large populations of schizophrenia patients along with healthy controls provides the opportunity to identify rare, highly-penetrant, *de novo* mutations that drive schizophrenia susceptibility. One such study recently identified a loss-of-function mutation in *SETD1A* significantly associated with schizophrenia and present in 10 of the 4,264 genomes analyzed (Singh et al., 2016). *SETD1A* is among the 3% most constrained genes in the human genome, with no mutations found in any of the more than 9,000 matched controls, and only 2 in a separate 45,000 genome control analysis. *SETD1A* encodes an enzyme that catalyzes methylation in histone H3. Other genes in this family have also been associated with developmental disabilities and a separate GWA study analysis identified histone modification as one of the principal pathways affected in psychiatric disorders (O'Dushlaine et al., 2015).

#### **2.3.1.1 Gene pathway convergence**

The genetic architecture that predisposes for schizophrenia is undoubtedly complex. To go along with recent advances in sequencing technologies that has made it possible to identify mutations in individual genes throughout the genome as mentioned above, advances in bioinformatics and a growing genetic knowledge base have allowed us to better identify the biological pathways preferentially disrupted in schizophrenia. Mutations present in schizophrenia patients, but not the general population, cluster within several functional domains primarily focused on signaling networks controlling neurodevelopment and synaptic transmission, particularly neuregulin and glutamate pathways (Table 2.1; Walsh et al., 2008; Glessner et al., 2010). Additionally, a meta-analysis combining data from GWA, CNV, and single-nucleotide variation (SNV) studies identified gene networks related to axon guidance, neuronal cell mobility, synaptic function, and chromosomal remodeling (Figure 2.2; Gilman et al., 2012).

#### **2.3.2 Schizophrenia as a neurodevelopmental disorder**

Describing schizophrenia as a neurodevelopmental disorder primarily means that the pathology begins well before onset of symptoms, particularly while the brain is still developing. The typical

Pathway or process	P value
Signal transduction	0.012
Neuronal activities	0.049
Nitric oxide signaling	0.0002
Synaptic long-term potentiation	0.0005
Glutamate receptor signaling	0.003
ERK/MAPK signaling	0.004
Phosphatase and tensin homolog signaling	0.007
Neuregulin signaling	0.008
Insulin-like growth factor 1 signaling	0.008
Axonal guidance signaling	0.015
Synaptic long-term depression	0.017
G protein-coupled receptor signaling	0.034
Integrin signaling	0.036
Ephrin receptor signaling	0.042
Sonic hedgehog signaling	0.044

**Table 2.1:** Pathways and processes overrepresented by genes disrupted in schizophrenia cases. No pathways were overrepresented by genes disrupted in controls. Reproduced from Walsh et al. (2008).

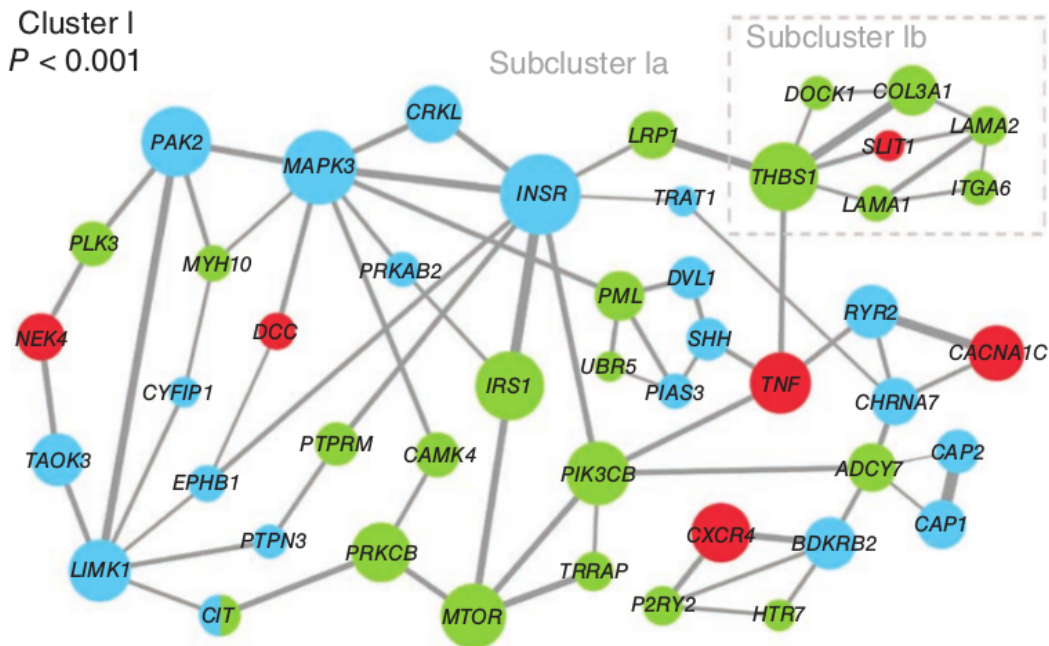


**Figure 2.2:** First cluster identified by the NETBAG+ approach. Cluster results from the combined set of schizophrenia-associated genetic variations: genes from *de novo* CNVs are in blue, genes from non-synonymous *de novo* SNVs are in light green and genes from GWA study-implicated regions in dark red. Edge widths are proportional to the strength of the likelihood score between the two genes, and node sizes are proportional to the gene's contribution to the overall cluster score. For simplicity, only the strongest two edges from each gene are shown. Cluster I was the best cluster from the combined set of all schizophrenia genetic variations ( $P<0.001$ ). Reproduced from Gilman et al. (2012).

age for a first psychotic episode is 18-25 years, though there is evidence for pre-diagnosis symptoms from birth cohort studies, including behavioral problems, general psychopathology, intellectual and language deficits, early motor delays, poor educational performance, and stunted physical growth (Welham et al., 2009). Additionally, prenatal (e.g. maternal malnutrition) and perinatal (e.g. infections) insults have shown modest links to schizophrenia (Lewis & Levitt, 2002). It's important to distinguish the long prodromal period of schizophrenia from more traditional neurodevelopmental disorders such as intellectual disability or autism. While schizophrenia disease progression may begin in early childhood, clear symptoms generally do not manifest until the second decade of life. This time course aligns with the refinement of excitatory and inhibitory synapses associated with adolescence, so it may be that early-in-life genetic and environmental factors aren't exposed until a critical period later in life (Figure 2.3; Insel, 2010).

### **2.3.2.1 22q11.2 deletion syndrome**

Perhaps the best-established and well-studied CNV linked to schizophrenia is a deletion present in human chromosome 22 (22q11.2; Karayiorgou et al., 1995; Chow et al., 2006; Karayiorgou et al., 2010). Individuals with 22q11.2 deletion syndrome (22q11.2DS) exhibit a spectrum of cognitive deficits as children, and  $\approx 30\%$  of them develop schizophrenia in adolescence or early adulthood, accounting for up to 2% of all schizophrenia cases (Stark et al., 2008). Several variants of the deletion have been identified, but the critical region seems to cover 1.5 megabases including approximately 35 known genes (Figure 2.4). Children with 22q11.2DS have clear cognitive impairments, reflected in a low full scale IQ, general language delays, and impairments in nonverbal, spatiotemporal and numerical tasks, in addition to general deficits in attention and working memory (Karayiorgou et al., 2010). By early adulthood, around one third of 22q11.2DS patient are diagnosed with schizophrenia, making 22q11.2DS one of the highest known risk factors for developing schizophrenia, possibly only behind having closely related family members with schizophrenia (Murphy et al., 1999). Importantly, while 22q11.2DS is additionally associated with other psychiatric disorders through adolescence, by adulthood strict diagnoses are fairly specific for schizophrenia and those who are diagnosed with schizophrenia are generally indistinguishable from schizophrenia patients without the 22q11.2 deletion (Karayiorgou et al., 2010).

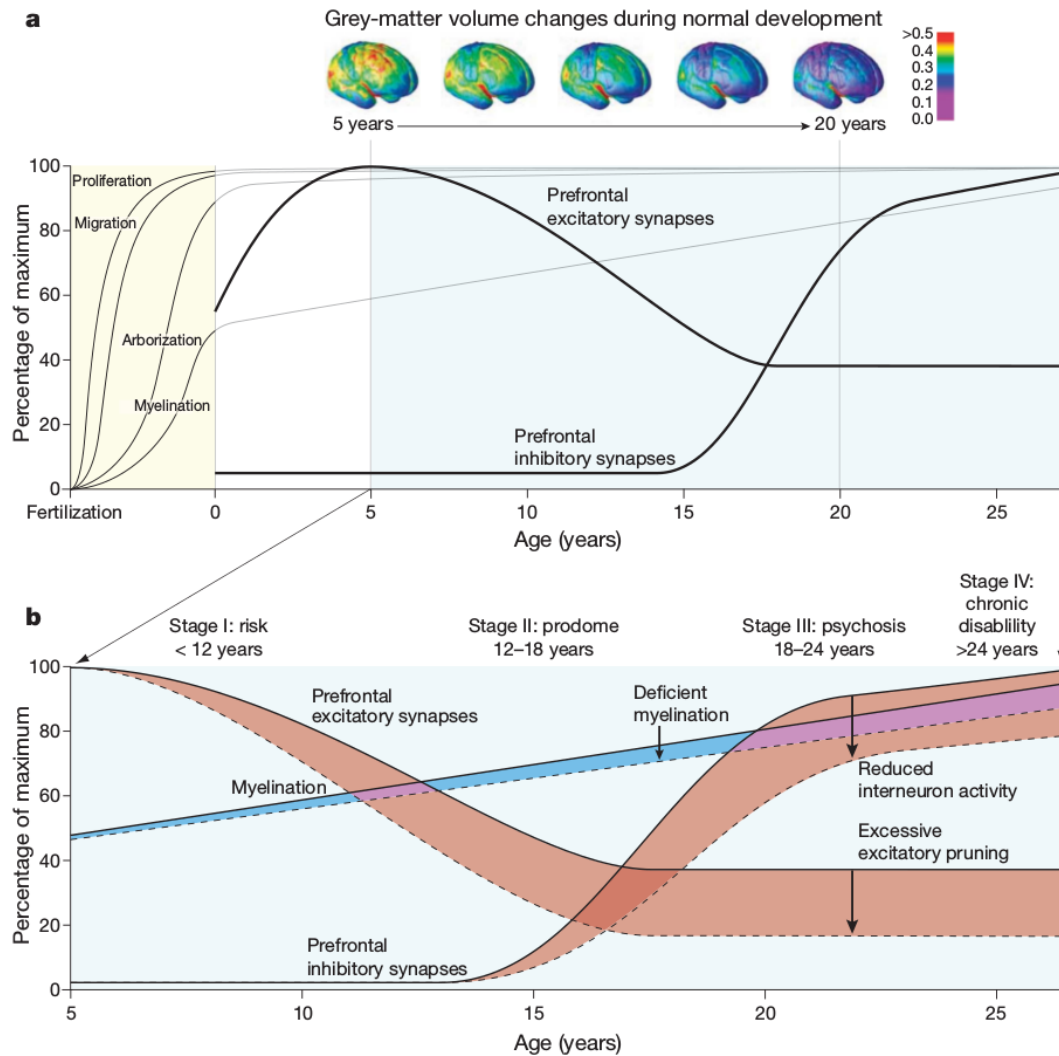


**Figure 2.3:** Neurodevelopmental model of schizophrenia. **a.** Normal cortical development involves proliferation, migration, arborization (circuit formation) and myelination, with the first two processes occurring mostly during prenatal life and the latter two continuing through the first two post-natal decades. The combined effects of pruning of the neuronal arbor and myelin deposition are thought to account for the progressive reduction of grey-matter volume observed with longitudinal neuroimaging. Beneath this observed overall reduction, local changes are far more complex. Data from human and non-human primate brain indicate increases in inhibitory and decreases in excitatory synaptic strength occurring in prefrontal cortex throughout adolescence and early adulthood, during the period of prodrome and emergence of psychosis. **b.** The trajectory in children developing schizophrenia could include reduced elaboration of inhibitory pathways and excessive pruning of excitatory pathways leading to altered excitatory-inhibitory balance in the prefrontal cortex. Reduced myelination would alter connectivity. Although some data support each of these possible neurodevelopmental mechanisms for schizophrenia, none has been proven to cause the syndrome. Detection of prodromal neurodevelopmental changes could permit early intervention with potential prevention or preemption of psychosis. Reproduced from Insel (2010).

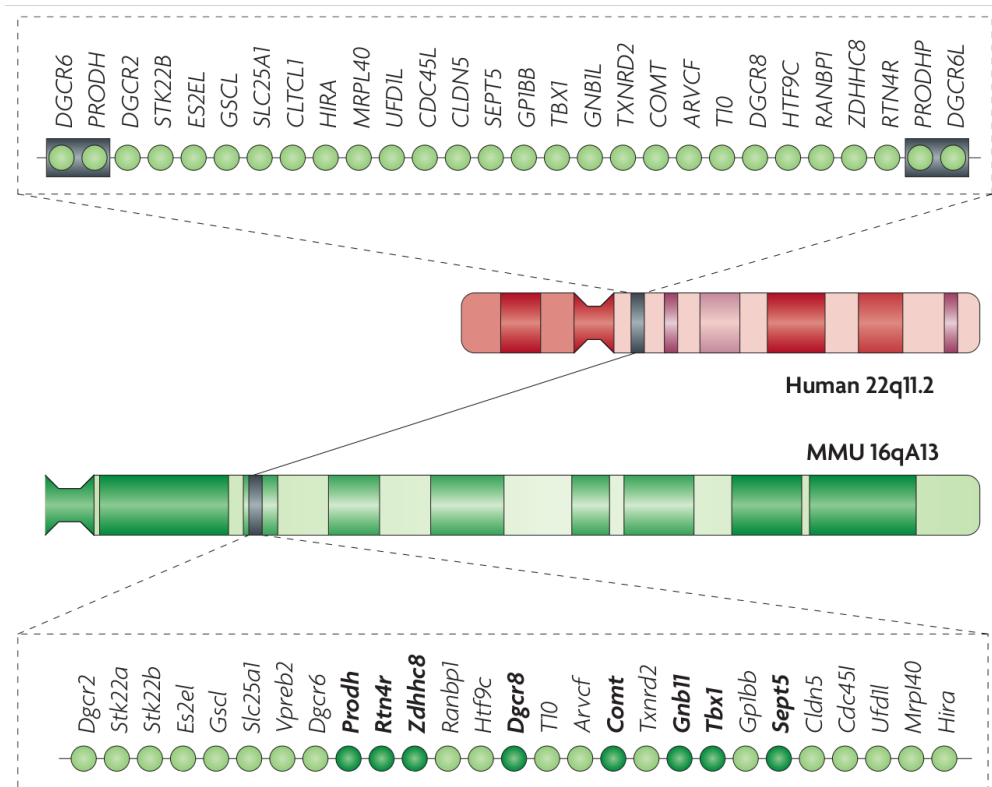


**Figure 2.4:** Genes involved in the human 22q11.2 deletion and syntenic region in the mouse genome deleted in the *Df(16)A<sup>+/−</sup>* mouse model. Modified from Karayiorgou et al. (2010)

### **2.3.2.2 *Df(16)A<sup>+-</sup>* mouse model of 22q11.2DS**

Advances in understanding the genetic component of schizophrenia predisposition have led to the development of etiologically-validated mouse models of schizophrenia which will allow for the direct analysis of *in vivo* neuronal network activity and identification of circuit dysfunctions present in the disease. The homologous region to human 22q11.2 in the mouse chromosome (16qA13) is highly conserved (Figure 2.4), with only one gene not present in the mouse (clathrin, heavy polypeptide-like 1, CLTCL1) and one gene that is duplicated in the human region is only present as a single copy in the mouse (DiGeorge syndrome critical region 6, DGCR6p; Karayiorgou et al., 2010). Several mouse models have been designed which delete various size regions from 16qA13, but I will focus on the particular model that I used in my experiments (*Df(16)A<sup>+-</sup>*) which deletes the largest region, encompassing all of the syntenic region (Stark et al., 2008).

Behavioral tests on the *Df(16)A<sup>+-</sup>* mouse model have shown increased non-specific anxiety in open field and light-dark transition tasks, impaired sensorimotor gating by measuring startle response during prepulse inhibition (PPI), impaired spatial working memory in a delayed non-matching to place T-maze task, impaired working memory, and decreased freezing in a contextual fear conditioning paradigm, which could reflect either impaired contextual memory or the inability to associate the unconditioned stimuli with the context in which it was presented (Drew et al., 2011; Stark et al., 2008; Sigurdsson et al., 2010). Additionally, a study of immediate early gene expression using c-Fos staining following exposure to a novel environment found significantly fewer CA3 pyramidal cells active and a trend in the same direction for CA1 pyramidal cells (CA1PCs) as well, which is suggestive of deficits in contextual-episodic memory, though in a direct test of spatial memory in a Morris water maze, no deficit was found (Drew et al., 2011). Finally, recent work in the *Df(16)A<sup>+-</sup>* mouse has identified a hippocampal area CA2-specific reduction in PV+ INs, a corresponding decrease in inhibitory activity onto CA2 pyramidal cells, and a deficit in CA2-dependent social memory (Piskorowski et al., 2016).

*In vivo* neurophysiology experiments have additionally identified several deficits in this mouse model. Experiments in hippocampal slices from *Df(16)A<sup>+-</sup>* mice revealed decreased inhibition of CA1PCs and induction protocol-specific deficits in Schaffer collateral long-term potentiation (LTP) (Drew et al., 2011). In a paper by Sigurdsson et al., the authors found that synchrony between

the HPC and PFC was disrupted in the *Df(16)A<sup>+/−</sup>* mouse model during a working memory task that generally relies on increased synchrony between those two brain regions and in which the *Df(16)A<sup>+/−</sup>* mice showed a learning deficit (Sigurdsson et al., 2010). In addition, they found that baseline synchrony predicted later task performance, suggesting a basal disruption in functional connectivity. More recently, Hamm et al. recorded neuronal activity in primary visual cortex of *Df(16)A<sup>+/−</sup>* mice and found several indications for altered local coordination and synchrony among the neuronal population, leading to the hypothesis that disrupted local attractors lead to aberrant activity in schizophrenia (Hamm et al., 2017).

Taken together, the *Df(16)A<sup>+/−</sup>* mouse model of the human schizophrenia-linked 22q11.2 deletion syndrome effectively recapitulates cognitive deficits seen in schizophrenia patients, including increased anxiety, impaired executive control, and deficits in spatial and episodic memory. Modeling these cognitive deficits in a mouse model allows us to directly investigate underlying cellular and circuit dysfunctions. I will discuss this topic in detail in chapter 4, where I describe experiments studying spatial-reward memory in this etiologically-validated mouse model in order to dissect altered hippocampal circuitry in schizophrenia. I will discuss the specifics later, but I found similar behavioral deficits as Drew et al.; normal baseline spatial-reward memory and deficits when faced with contextual changes, but also a robust spatial memory impairment in a task-dependent manner.

### 2.3.2.3 Individual genes within the 22q11.2 locus

The individual genes within the 22q11.2 locus have been characterized to varying degrees. Mouse models of DiGeorge critical region 8 (*Dgcr8*) haploinsufficiency – a micro RNA (miRNA) processing gene affected by 22q11.2 deletion – show similar working memory deficits as the *Df(16)A<sup>+/−</sup>* mouse model of the entire 22q11.2 deletion (Stark et al., 2008). In addition, these mice have modest alterations in PFC neuronal morphology and increased short-term synaptic depression in mPFC layer 5 (Fenelon et al., 2011). Suppression of a miRNA gene within the 22q11.2 locus (*miR-185*) has been shown to recapitulate some of the findings in the *Df(16)A<sup>+/−</sup>* mouse, including simpler dendritic morphology and decreased spine density (Xu et al., 2013). Additionally several interventions have been successful in reversing some of these miRNA-related abnormalities, providing potential therapies and highlighting the advantage of targeting specific molecular pathways disrupted in disease. Repression of the downstream target of *miR-185* (*Mirta22*) in *Df(16)A<sup>+/−</sup>* primary cultures reverses

the structural abnormalities (Xu et al., 2013) and an activator of DGCR8 (Cobalt(III) protoporphyrin IX) can help compensate for reduced expression levels and restore *miR-185* levels in mice (Barr et al., 2015). In addition, recent work currently in press, has introduced a loss-of-function mutation in *Mirta22* to the *Df(16)A<sup>+/−</sup>* mouse, rescuing behavioral deficits (Diamantopoulou et al., in press). Collectively these mutations implicate miRNA processing in schizophrenia disease risk and provide potential targets for therapeutic intervention.

ZDHHC8 is a palmitoyltransferase within the 22q11.2 locus that specifically targets proteins involved in axonal growth and branching. Reintroducing ZDHHC8 in primary *Df(16)A<sup>+/−</sup>* cultures rescues impairments in dendritic growth and synapse number, and ZDHHC8 deficiency has been shown to specifically disrupt protein localization to the axonal tip as well as disrupt AKT/GSK3 $\beta$  signaling (Mukai et al., 2008, 2015).

Finally, as mentioned below (subsection 2.3.3), dopamine misregulation seems to be a core feature of schizophrenia. Two genes are present in the 22q11.2 locus related to dopamine synthesis and processing: *Comt* and indirectly *Prodh*. COMT has been shown to modulate dopamine clearance in the PFC, as extracellular dopamine clearance was 2 times slower in *Comt* knockout mice (Käenmäki et al., 2010). PRODH is an enzyme that metabolizes L-proline which can modulate glutamatergic and GABAergic transmission, and has been independently linked to schizophrenia (Liu et al., 2002; Crabtree et al., 2016). *Prodh*-deficient mice are hypersensitive to psychosis-inducing, dopamine-increasing amphetamine, and this is exaggerated by inhibition of COMT (Paterlini et al., 2005). Thus, the deletion of both of these genes in 22q11.2DS provides two ‘hits’ which may cooperatively increase the risk of dopamine-dysfunction and schizophrenia.

### 2.3.3 Dopamine

The earliest mechanistic hypotheses for the disease progression of schizophrenia involves disruption in normal dopamine signaling (Matthysse, 1973). This hypothesis revolves around the positive symptoms of schizophrenia, specifically the hallucinations and delusions which can be both induced and prevented through modification of dopamine levels in the brain. In particular, compounds that generally increase the level of dopamine (e.g. amphetamine, LSD) lead to hallucinations similar to those experienced by schizophrenia patients (Angrist, 1994; Lieberman et al., 1987). Conversely, for over 60 years the primary treatment for schizophrenia has been antipsychotic medications (Delay

et al., 1952), which were first shown to increase the metabolism of dopamine (Carlsson & Lindqvist, 1963) and are now known to function primarily as D2 dopamine receptor antagonists (Kapur & Mamo, 2003). The general effectiveness of classical antipsychotics (e.g. haloperidol) and the newer atypical antipsychotics (e.g. clozapine) in treating the positive symptoms of schizophrenia suggested a central role for dopamine in the more general neuropathophysiology of schizophrenia, but this insight has failed to expand beyond the direct treatment of psychotic episodes. Indeed, while D2 dopamine receptor antagonists work well for many patients in managing psychotic episodes, these treatments have done very little in improving functional outcomes, as the more debilitating negative and cognitive symptoms remain untreated (Insel, 2010).

The role of dopamine in schizophrenia is now realized to be more nuanced than a simple consequence of a brain-wide hyperdopaminergic state. While D2 dopamine receptor antagonist antipsychotic treatments do help manage psychotic episodes in many schizophrenia patients, in some these treatments show no effect. Additionally, post-mortem measurements of dopamine levels in schizophrenia patients, as well as *in vivo* measurements of dopamine activity, have not been entirely consistent across studies, and more importantly, across patients (Davis et al., 1991). This inconsistency is most likely reflective of variability in underlying disease etiology, and points to a lack of a singular disease pathology, instead suggesting a collection of underlying brain dysfunctions that funnel towards shared pathways and a commonly identified set of expressed symptoms.

#### **2.3.3.1 Dopamine in the striatum**

One brain region in particular, the striatum, has been identified as a potential target for altered dopamine signaling. Using radiolabeled L-dopa, presynaptic dopamine levels have been consistently shown to be elevated in the striatum of schizophrenia patients (reviewed in Howes et al., 2007). At the same time, also in the striatum, D2/3 dopamine receptors (the primary receptor subtypes in this brain region) are modestly (10-20%) elevated, independent of treatment with antipsychotic drugs (reviewed in Howes & Kapur, 2009). Studies have also found evidence for increased dopamine uptake in the striatum, and post-mortem studies have found elevated dopamine and dopamine metabolite levels in the striatum (Simpson et al., 2010). In addition, post-mortem studies have reported increased levels of striatal dopamine D2 receptors in un-medicated human patients compared to unaffected controls, suggesting a possible source of dopamine mis-regulation (Cross et al.,

1981).

In order to study this potential schizophrenia pathway, Kellendonk et al. characterized a striatal dopamine hyper-activity mouse model that over-expresses the dopamine D2 receptor (D2R-OE) specifically in the striatum (Kellendonk et al., 2006). They showed that increased D2 dopamine receptor activity in the striatum leads to deficits in PFC-dependent working-memory tasks and an increased dopamine-induced excitability in PFC cells. The mesolimbic pathway is a potential mechanism of action, where striatal medium spiny neurons (MSNs) have altered excitability due to over-expression of D2 dopamine receptors which then project to the ventral tegmental area (VTA) dopaminergic neurons, which in turn project to the PFC, which feeds back on to striatal MSNs. Recent work has shown that both the tonic and burst firing rates of VTA neurons are altered in the D2R-OE mouse model, though neurons in the substantia nigra are unaffected, despite both being dopaminergic centers that receive strong projections from the striatum (Krabbe et al., 2015).

#### 2.3.4 Excitation and inhibition

It has additionally been proposed that an imbalance in the levels of excitatory and inhibitory activity during development underlies schizophrenia (Insel, 2010; Coyle, 2006; Yizhar et al., 2011). Similar to how the effectiveness of D2 dopamine-receptor targeting antipsychotics gave rise to the ‘dopamine hypothesis’ of schizophrenia, one of the main pieces of evidence in support of a ‘glutamate hypothesis’ of schizophrenia etiology is the effect of NMDAR modulators in schizophrenia patients. NMDAR antagonists, such as phencyclidine and ketamine, induce psychoses in healthy subjects reminiscent of hallucinations observed in schizophrenia patients (Javitt, 1991; Krystal et al., 1994) and have also been shown to cause similar spatial memory deficits as in schizophrenia patients along with corresponding aberrant activity in the HPC (Morgan et al., 2014). Schizophrenia patients are also particularly sensitive to the effect of these drugs, as they worsen psychotic events. In addition, NMDAR antagonists induce schizophrenia-like symptoms in mice (Inta et al., 2010). Finally, despite poor blood-brain barrier penetrance, NMDAR agonists significantly improve negative symptoms in schizophrenia patients. Specifically, drugs targeting the NMDAR glycine binding site show potential to alleviate symptoms (Tsai et al., 1998; Coyle, 2012).

Postmortem analysis has found mixed, and generally not robust, changes in NMDAR levels in schizophrenia patients relative to healthy controls, but increased levels of NMDAR antagonists does

seem to be consistent. In particular, reduced glutamate and reduced catabolism of an endogenous NMDAR antagonist (N-acetylaspartylglutamate) was found selectively in the HPC and PFC (Tsai, 1995). Also, postmortem studies have found decreased levels of pre-synaptic GABAergic machinery, including GAT, GAD67, and PV, in both the PFC and HPC (Coyle, 2006; Zhang & Reynolds, 2002; Konradi et al., 2011). In particular, schizophrenia patient have shown decreased levels of PV leading to hypofunction of PV+ INs in the PFC as well as decreased numbers of PV+ INs in the HPC (Zhang & Reynolds, 2002; Lewis et al., 2005), especially in area CA2 (Knable et al., 2004). Recent work from Piskorowski et al. has shown that reduction in PV+ INs in area CA2 of the *Df(16)A<sup>+-</sup>* mouse has profound effects on pyramidal cell excitability and disrupts CA2-dependent social memory (Piskorowski et al., 2016). In agreement with the well-established memory deficits present in schizophrenia patients (see section 2.1), PV+ INs are also especially important for normal memory processing (Korotkova et al., 2010; Murray et al., 2011; Donato et al., 2013). One possible link between these excitatory and inhibitory pathways was identified by Grunze et al., who showed that GABAergic INs in hippocampal area CA1 are 10 times more sensitive to NMDAR-antagonist than pyramidal cells, and thus elevated NMDAR-antagonists levels would have a disynaptic disinhibitory effect on pyramidal cells leading to disrupted pattern recognition (Grunze et al., 1996). Despite this significant histological evidence, there is currently limited data available on how the *in vivo* activity of hippocampal GABAergic INs is altered in schizophrenia.

## 2.4 Summary

Schizophrenia is a devastating disorder of psychoses and cognitive deficits. Hallucinations and psychoses are treatable to varying degrees of success, leaving the cognitive deficits as the least treatable and largest barrier to functional recovery. Episodic memory impairment is a core component of the cognitive deficits in schizophrenia. The hippocampus is necessary for normal episodic memory in healthy individuals and is consistently identified as being altered in schizophrenia patients. By making use of a genetic mouse model of schizophrenia (*Df(16)A<sup>+-</sup>*) made possible by the growing understanding of the network of genetic mutations predisposing for schizophrenia, I will show specific functional correlates of impaired hippocampal activity during an episodic memory task that I identified in my primary thesis project (chapter 4).

# Chapter 3

## Techniques

### 3.1 *In vivo* two-photon Ca<sup>2+</sup> imaging

All of my experiments revolved around two-photon (Denk et al., 1990) Ca<sup>2+</sup> imaging in hippocampal area CA1 of awake head-fixed mice (Dombeck et al., 2007) using genetically-encoded calcium indicators (GECIs, Knöpfel, 2012), in particular GCaMP6f (Chen et al., 2013). These methods are based in general on the advances of Dombeck et al. who established the first awake *in vivo* two-photon recordings in mice and later imaged hippocampal place cells (Dombeck et al., 2010). *In vivo* Ca<sup>2+</sup> imaging provides several essential advantages over *in vivo* electrophysiological approaches which I made use of in my thesis work. First, a typical field of view will contain 500-1000 pyramidal cells, allowing me to rapidly collect data from a large number of cells. This large population sampling was a fundamental part of all of my experiments, but most critical in quantifying the nature of reward enrichment in my goal-oriented learning (GOL) task (subsection 4.2.10) and our work on characterizing the activity of the very low-firing rate dentate gyrus (DG) granule cells (section 6.2). Second, actually seeing the cells that I was recording from allowed me to register fields of view from day-to-day and reliably track the same cells for up to 2 weeks. The main experimental task that I used (subsection 3.2.2) was a 9-day protocol and tracking the same cells across those 9 days was essential. A similar protocol was also used in our work characterizing diversity in pyramidal cells along the radial axis of CA1 (section 6.3) and this project also critically took advantage of the imaging method by visually identifying superficial and deep CA1 pyramidal cell imaging planes. Finally, Ca<sup>2+</sup> imaging allows for recording activity from cellular compartments

other than the soma – such as dendrites, axons, and even synaptic boutons. These same recordings are technically very difficult with electrophysiological approaches, and most likely impossible to do over long timescales. I took advantage of this ability in imaging axons and boutons of long-range inhibitory projections (LRIPs) from lateral entorhinal cortex (LEC) to *stratum locunosum-moleculare* in CA1 (see section 6.1) as our lab has also done in the past (Kaifosh et al., 2013; Lovett-Barron et al., 2014).

During my thesis work, the most significant upgrade to our imaging capabilities was the addition of resonant scanning capabilities, which allowed for an up to 10-fold increase in both temporal and spatial resolution, thus greatly improving the quality of our imaging data. The upgrade also required a corresponding upgrade to our analysis pipeline and server design to handle the significantly increased quantity of data acquired.

## 3.2 Head-fixed behavior

In order to allow for two-photon  $\text{Ca}^{2+}$  imaging in awake mice, I needed to design all behavioral tasks to work while mice are head-fixed under a two-photon microscope (Figure 3.1). Our primary imaging apparatus most directly combines the work of Dombeck et al. and Royer et al.. Dombeck et al. performed the first two-photon  $\text{Ca}^{2+}$  imaging experiments of hippocampal area CA1 place fields and their work provided the basis for our viral GECI strategy and surgery procedure (Dombeck et al., 2010). Royer et al. designed a feature-rich head-fixed treadmill for the study of place cells, which was the basis of our original treadmill design (Royer et al., 2012). While the core apparatus was in place when I began experiments, extensive upgrades were necessary to optimally run my head-fixed learning tasks. I, along with colleagues in the lab, redesigned the wheels, axles, and platform to minimize friction and facilitate running while head-fixed. We designed a RFID-tag and quadrature encoding-based system to accurately track position over many laps to within <0.5 cm. We designed new treadmill belts that consist of multiple fabrics sewed together with various cues scattered throughout, which together convey all the spatial information used by mice to anchor place cell maps. I added features to our in-house behavioral control software to allow for reward schedules that depend on the spatial location of the mouse on the treadmill. These improvements allowed for the design of new head-fixed behaviors, described below.

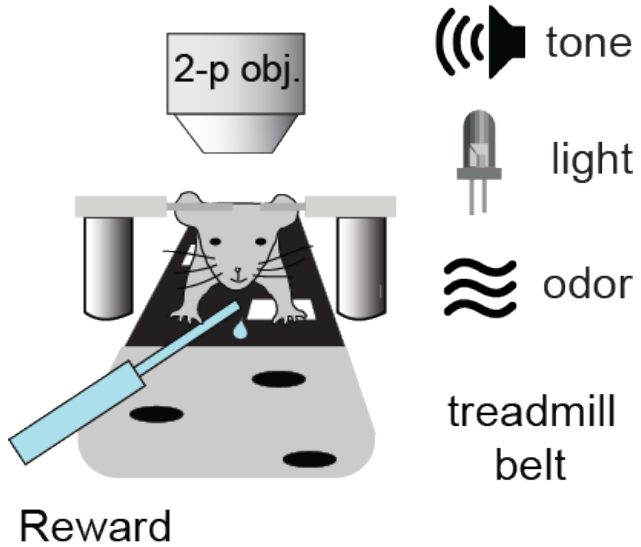


**Figure 3.1:** Schematic of treadmill design for head-fixed awake two-photon  $\text{Ca}^{2+}$  imaging. Mice are head-fixed underneath the objective a two-photon microscope (2-P OBJ.) while they run on a fabric belt consisting of multiple materials with local cues dispersed throughout (TREADMILL BELT). Water-deprived mice learn to run for water rewards delivered through a lick port placed in front of them (REWARD), which also includes a capacitance sensor to record the timing of each lick (not shown). Throughout the task, mice can experience different contextual modes as changes are made to the background, non-spatially-modulated pure tones (TONE), blinking colored LED (LIGHT), and odors (ODOR).

### 3.2.1 Random foraging

The first task we designed was a simple random foraging task where mice run to get water, but don't need to learn about any particular location on the belt in order to get water rewards. All head-fixed paradigms begin with 1-2 weeks of training where mice learn to lick for water from a lick port while needing to run progressively farther each session in order to receive another reward (see subsection 4.4.3). Mice were either operantly rewarded (they must lick to receive water) at random intervals along the belt or non-operantly at a fixed location. This allowed me to look at baseline stability of spatial maps with two-photon  $\text{Ca}^{2+}$  imaging over days or weeks (see subsection 4.2.9 & subsection 7.2.7).

### 3.2.2 Goal-oriented learning

In order to study spatial learning and memory while simultaneously imaging functional activity of hippocampal area CA1 place cells, we developed a head-fixed goal-oriented learning task. The task has been used by me to study spatial memory in a mouse model of schizophrenia (subsubsection 7.2.7).

section 4.4.3.2), by Nathan Danielson to study functional diversity within CA1 pyramidal cells (section 6.3), and is now being used by many other people in Attila’s lab. Freely-moving assays of spatial memory in rodents traditionally include the Morris water maze, Barnes maze, or cheese board maze (see subsection 1.1.2). While head-fixed under a two-photon microscope, mice are constrained to run in effectively a one-dimensional environment (similar to freely moving linear track paradigms) and there are limited options to experimentally assay choices made by the mice. They key features that we were trying to design in the task were:

1. Mice are able to learn a specific rewarded location on the treadmill that is otherwise un-cued.
2. Mice learn the task over several trials to allow for determining a ‘learning curve’.
3. A behavioral readout that is sensitive to subtle variations in ability to learn.
4. Be able to flexibly manipulate the reward and environment parameters to probe mice’ ability to learn the task.

Our GOL task requires mice to run laps along our multi-fabric, feature-rich circular treadmill belt (for task schematic, see Figure 4.1). The mice are water-restricted, so we use water delivered through a lick port as a reward. Each lap there is one spatial region (REWARD ZONE, usually a 20-cm window) on the belt where the mice can operantly receive water rewards: if they lick they get water, if they do not lick, they don’t. The reward will ‘dry up’ after after a fixed amount of time has passed since the mouse entered the reward zone that lap (usually 3 seconds). Not all mice will run for water rewards at all, and not all mice will perform this task, but many are able to (1). We generally give the mice 9 sessions to learn the reward location. Some mice will find the reward immediately, but even those that do, they continue to improve and stabilize their performance over the 9 sessions (2). By measuring the capacitance of the lick port, we can detect changes when the mouse licks, providing us an accurate measure of the time (and the mouse’s location on the belt) when each lick occurs. The operant nature of the reward schedule requires the mice to lick everywhere along the belt to sample each location and find the correct position that will be rewarded. As the mice learn the reward zone, they suppress licking away from the reward and will then only lick at the reward zone. We have used multiple measures to quantify this behavior, but generally look at the fraction of licks in the reward zone as a measure of learning (3). This particular

measure can be misleading if the mice lick everywhere along the belt, but then lick robustly once they receive the first drop of water, but in practice we do not see this behavior. In addition we often look at measures such as ANTICIPATORY LICKING, which quantify the fraction of licks directly preceding the reward, but crucially exclude licks in response to water delivery, though this measure has proven to be less-sensitive to learning. Finally, the setup allows the experimenter to move the reward to any arbitrary location along the belt, swap out belts to modify the environment, and manipulate non-spatial odor/tone/light cues to change the surrounding context (4).

### 3.3 Data analysis pipeline

A typical 10 minute imaging session generates a  $\approx$ 15 GB raw movie that needs to be processed down to a single spatial tuning vector for each of approximately 500 cell somas in the field of view. Processing each movie requires identifying regions of interest (ROIs), extracting fluorescent signals from each ROI, cleaning up each trace by calculating changes in fluorescence, identifying significant  $\text{Ca}^{2+}$  events, aligning  $\text{Ca}^{2+}$  event times to the mouses' position in the behavioral environment, and finally calculating place fields for each cell. Place fields from a single session can tell us how the mice represent the environment in a given session, but to address some of the more interesting questions I wanted to ask how these representations changed over time. For this, I needed to register ROIs from day-to-day and compare the tuning of the population as a whole over time, but also track changes in the tuning of individual pyramidal cells from session-to-session. All of these steps need to be performed fast, reliably, and as automatically as possible. Over the course of my PhD thesis work, I, along with other members of Attila's Lab (especially Patrick Kaifosh and Nathan Danielson), developed a set of programs and tools to complete all of these steps mentioned above. I will focus here on the pieces that I personally originated or was the primary contributor to, but Attila's lab is collaborative by design and all the code we use is shared, so multiple people have contributed to most aspects of the analysis pipeline.

#### 3.3.1 Initial processing

Imaging data acquired through our microscope software (PraireView) is stored as an individual TIFF image file for every frame of every plane and channel. This can lead to over 30,000 files

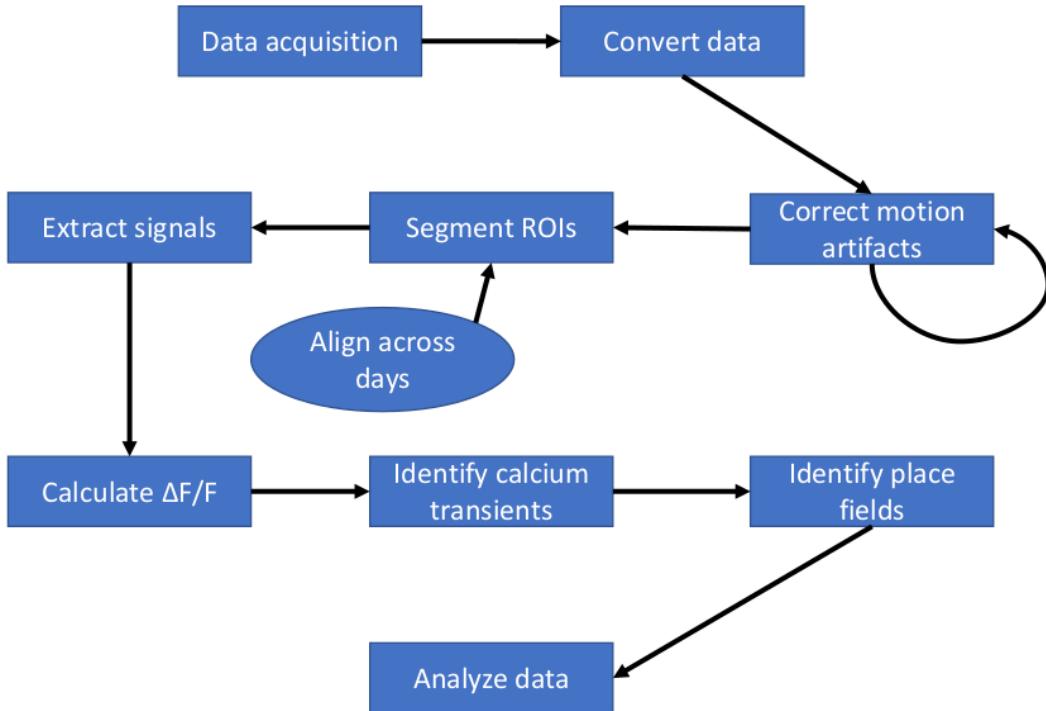


**Figure 3.2:** Data analysis pipeline. Schematic represents the various steps of processing performed on all data.

per 10 minute recording session, which very quickly becomes difficult to manage. So, the first step after running an experiment is to move all the data to a special SCRATCH folder on our lab server, where I have a script constantly running to convert all of the data into one large HDF5 file (<https://www.hdfgroup.org/HDF5/>). This format allows us to store all of the data in a 5-dimensional (Time × Plane × Row × Column × Channel) indexable structure for easy iteration and viewing of the data. The script checks every individual TIFF file, writes it to the HDF5 file, verifies the integrity of the new HDF5 file, and then moves the new file to a permanent place on the server while deleting the original TIFF files.

At this point the data is now properly formatted for estimation and correction of motion-induced imaging artifacts using our SIMA software package (chapter 5).

### 3.3.2 Signal processing

After signals are extracted for each ROI the next step is to quantify the change in fluorescence over time, as absolute fluorescent values are not interpretable in isolation. Calculating the change in

fluorescent over time is simple in theory:

$$\Delta F/F(t) = \frac{F(t) - F_\circ}{F_\circ},$$

though in practice there are many complications that any algorithm needs to be robust to. The primary concern is a non-stationary baseline fluorescence, as drift in the baseline intensity can be mistaken for physiological activity, when in fact it is usually due to an experimental artifact. The most common problem is for the baseline to decay over the course of long recordings, caused by water evaporation/leaking from under the objective, bleaching of the  $\text{Ca}^{2+}$  indicator, movement of the tissue out of focus, or some combination of these factors. While not particularly common, these things do occur and thus need to be accounted for.

Our particular baseline calculation method is based off of Jia et al. (2011). In brief, we first smooth the signal with a boxcar smoothing window of width  $\tau_1$  and then for every time-point choose the baseline to be the minimum value of this smoothed signal within a  $\tau_2$  window. This effectively implies that there should be a  $\tau_1$  size window every  $\tau_2$  seconds that is absent of any  $\text{Ca}^{2+}$  transients or other large fluctuations. For hippocampal area CA1 pyramidal cells imaged with GCaMP6f in a well-trained mouse running on a 2-meter long treadmill, we found that  $\tau_1 = 3$  seconds and  $\tau_2 = 60$  seconds worked well. As an additional step to aid the robustness of the precise window sizes, we also implemented an iterative procedure where after calculating  $\Delta F/F$  we identified significant  $\text{Ca}^{2+}$  events (see subsubsection 4.4.10.1) and then re-calculated the  $\Delta F/F$  while removing the identified  $\text{Ca}^{2+}$  transients from the baseline. This prevents errors in the baseline calculation for any cells that do not have a 3 second period of quiescence every minute, and was generally repeated 3 times to ensure an accurate baseline calculation.

### 3.3.3 Place cell identification

Pyramidal cells in the mammalian hippocampus fire at specific locations within an environment. We developed an algorithm to reliably identify cells that had a significantly higher mutual information between the mouse's position and the  $\text{Ca}^{2+}$  activity of the cell than expected by chance. The overall goal of our analytical approach is to identify as un-biased a population of spatially-tuned cells as possible. In particular, we aim to avoid biases in place field width, number of place fields per cell,

location of place fields on the belt, or overall cell activity/firing rate level. In addition, unlike with electrophysiological data,  $\text{Ca}^{2+}$  events have a finite duration that we needed to account for on a per-cell basis.

In brief, we calculate the occupancy normalized transient rate histogram for each cell with bin sizes ranging from 2 cm to 100 cm. In addition, for each bin size we also rotate the binning through all the possible shifts, such that, for example, if a cell fired transients over any continuous 20 cm segment of the belt, there would be a 20 cm bin that contained all of the transients.

We then calculate the spatial information for each of these bin sizes and bin shifts and take the maximum value as the true spatial information of that cell. We then shuffle all of the transients within each cell, re-calculate the occupancy normalized transient rate histogram for each bin size and shift as described above, again take the maximum spatial information for this particular shuffle, and then create a distribution of spatial information values across shuffles. This distribution empirically defines our spatial information confidence threshold for the particular pattern of transient durations and timings for the particular cell.

Additional details of this method can be found in subsubsection 4.4.11.1.

### 3.3.4 Lab Analysis Bundle (LAB)

Over the years, as the lab and our code base grew, the collection of scripts, classes, and functions used for our analysis became hard to mention and difficult for new members to learn. In order to stabilize the code for future members, I spearheaded an effort to clean-up, refactor, and document all of the code we used in the lab. This became the Lab Analysis Bundle (LAB), which is a complete Python package hosted privately on GitLab (<https://gitlab.com>). The package is easily installable using standard Python packaging tools, with well-defined dependencies. As part of refactoring the code, I added automatic documentation to the core functions and standardized the API. The lab code repository is now in a much more manageable structure that has successfully been passed on to future lab members.

The LAB contains all of the tools needed to analyze behavior and imaging data acquired in Attila’s lab. The core components are:

- Standardized representation of all experimental **metadata**, including mouse information,

experiment start time, and exact behavioral parameters.

- Scripts for **processing** of imaging data from raw movies to extracted traces for each ROI.
- Access to all of the **behavioral data** acquired during the experiment, such as licking and position information.
- Object-oriented **structure** to work with collections of mice and experiments.
- **Analysis methods** to calculate behavioral (e.g. fraction of licks near rewards) and functional (e.g. place field correlation) metrics.
- Generalized **plotting** functions that work the output of any analysis function.
- **Automatic analysis scripts** to quickly perform standard analyses as soon as imaging data is processed.

Below is an example analysis that will plot a histogram of place field widths for all recorded sessions from one mouse.

```
1 import matplotlib.pyplot as plt
2 import lab
3
4 # Parse experiments metadata
5 expts = lab.ExperimentSet('behavior_jeff.xml')
6 # Pull out one particular mouse
7 mouse = expts.grabMouse('jz119')
8 # Find all sessions that were imaged
9 expt_grp = lab.classes.pcExperimentGroup(mouse.imagingExperiments())
10
11 # Calculate the width of all place fields
12 pf_width = lab.analysis.place_cell_analysis.place_field_width(expt_grp)
13
14 # Plot a histogram of all the place field widths
15 ax = plt.axes()
16 lab.plotting.plot_dataframe(
17     ax, [pf_width], plot_method='hist', labels=['jz119'],
18     activity_label='Place field width (cm)')
```

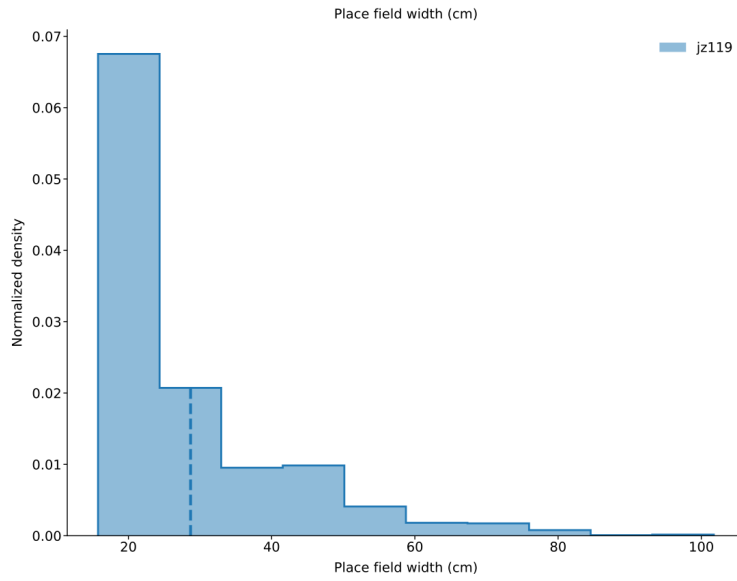


**Figure 3.3:** Example of using LAB to collect experiments, calculate a place cell metric, and plot the data.

### 3.3.5 Place cell stability

Quantifying the stability of spatial maps is fundamental to most of my thesis work. There are five commonly used methods for quantifying similarity that I implemented in our analysis package that I will touch on briefly:

- place cell recurrence
- place field correlation
- population vector correlation
- centroid shift
- firing rate overlap

Place cell **RECURRANCE PROBABILITY** is defined between a pair of sessions as the fraction of place cell for the first session that are still identified as place cells in the second session. The null hypothesis that the place cell populations are independent both days would suggest a recurrence probability equal to the fraction of place cells in the second session. This measure captures the stability of the spatially-active population from session-to-session.

PLACE FIELD (PF) CORRELATION is the correlation between the tuning curve of a cell at two different time points. I subdivided the treadmill belt into 100 evenly-sized bins (each  $\approx$ 2 cm), so every place cell is defined by a 100-element vector of occupancy-normalized  $\text{Ca}^{2+}$  transient rates (see Place cell identification). The correlation between these vectors gives the place field correlation for that pair of sessions, and these values can be averaged across cells to give a measure of the population stability. While this is perhaps the most commonly used metric of place cell stability, it is not our preferred measure for quantifying stability of  $\text{Ca}^{2+}$  transient-defined place cells. For  $\text{Ca}^{2+}$  data, a perfect place cell will fire a single large transient in the same spatial bin every lap. This can lead to very spatially-sparse rate maps, as compared to spike-based activity. Consequently, if the firing location shifts very minimally the preferred firing spatial bins may no longer overlap at all, leading to a correlation close to 0, when in fact, the firing has not changed very much.

POPULATION VECTOR (PV) CORRELATION is similar to PF correlation but measures the correlation across cells at each spatial bin, instead of the correlation across spatial bins for each cell. This metric is calculated by ‘stacking’ place field tuning curves for each cell, and then calculating the correlation between the activity of all the cells at the *same location* from two different sessions. For my experiments I always binned the data into 100 evenly spaced bins, so for every pair of session I calculate the correlation between 100 population vectors corresponding to each of the 100 spatial bins. This metric can be used in two separate ways. First, by averaging across spatial bins we can determine the mean stability of *positions* instead of *cells*, a subtle, but sometimes meaningful distinction. Also, if we do not average across positions, we can use this measure to look for positions that are specifically more/less stable, such as around the reward location.

CENTROID SHIFT is defined per cell as the distance between the center of its place field in two sessions. We use two separate measures to identify the centroid of a place field. The first is the more traditional measure, which is the center of mass of transients along the belt. We define the centroid of each place field separately, so we only use transients that occurred within the place fields when calculating the centroid, and then take the centroid of the place field that had the peak transient rate. In general, I calculated the centroid shift as the absolute value of the distance between the centroids as a fraction of belt, so all values are on [0, 0.5]. An alternative version of the centroid shift ignores place fields and instead represents every transient on the unit circle such that the angle

is the position on the circular treadmill and the length is inversely related to the occupancy of that position. By taking the vector sum of these transient vectors, we can calculate a SPATIAL TUNING VECTOR, for each cell for each session (for more details see, subsubsection 4.4.11.2). Finally, the centroid shift is then defined by the minimum angle between two spatial tuning vectors. This implementation does not care about place fields, so it is defined for every cell that fires at least 1 transient, which is how I looked at stability of the entire pyramidal cell population. The main caveat with this measure is that multi-peaked place fields will not be handled correctly, as for example, a place cell with two peaks will have a spatial tuning vector that falls between them.

FIRING RATE OVERLAP is the similarity of firing rate for a cell between two session. It is simply defined as:

$$\frac{\min r_1, r_2}{\max r_1, r_2},$$

where  $r_1$  and  $r_2$  are the firing rates on the first and second session respectively. This definition means that overlap is defined on  $[0, 1]$ , with a value of 1 corresponds to the cell having the same firing rate on both sessions, and a value of 0 corresponds to a cell that was silent one of the two sessions. This measure is not defined if the cell was silent both sessions, so those cells were excluded from all analysis. I generally used transient frequency as a proxy for firing rate, but measures such as the mean of the  $\text{Ca}^{2+}$  trace or the area under the  $\text{Ca}^{2+}$  trace during transients worked as well.

## Part II

# Projects

## Chapter 4

# Impaired hippocampal place cell dynamics in a mouse model of the 22q11.2 deletion<sup>1</sup>

Hippocampal place cells represent the cellular substrate of episodic memory. While place cell ensemble activity reorganizes to support learning, place cells must also maintain stable representations to facilitate memory recall. Despite extensive research, the learning-related role of place cell dynamics in health and disease remains elusive. We employed chronic two-photon Ca<sup>2+</sup> imaging in hippocampal area CA1 of wild-type and *Df(16)A<sup>+/−</sup>* mice, an animal model of 22q11.2 deletion syndrome, one of the most common genetic risk factors for cognitive dysfunction and schizophrenia. We found that goal-oriented learning in wild-type mice was supported by stable spatial maps and the robust remapping of place fields toward the goal location. *Df(16)A<sup>+/−</sup>* mice showed a significant learning deficit, and this finding was accompanied by both a reduction of spatial map stability and the absence of goal-directed place cell reorganization. These results expand on our understanding of hippocampal ensemble dynamics supporting cognitive flexibility during learning and provide the first direct demonstration of their disruption in a model of 22q11.2-associated cognitive dysfunction.

---

<sup>1</sup>This work has been previously published (Zaremba et al., 2017b,a) and is joint work with the coauthors.

## 4.1 Introduction

Episodic memory, the encoding of personal experience organized in space and time, represents a fundamental aspect of cognition, crucial for learning about the world and normal functioning in everyday life. Episodic memory dysfunction, stemming from the inability to learn and recall contextual, spatial, and temporal details of specific events (Dickerson & Eichenbaum, 2010; Eichenbaum, 2000), is a highly debilitating symptom of various neurological, cognitive and psychiatric disorders, including schizophrenia (SCZ) (Dere et al., 2010; Leavitt & Goldberg, 2009). In the case of SCZ, episodic memory impairments are consistently reported (Aleman et al., 1999; Schaefer et al., 2013) and largely untreatable (Green, 1996; Ibrahim & Tamminga, 2011; Keefe, 2007). More generally, cognitive deficits in SCZ appear to be the strongest predictor of patients' functional outcomes irrespective of the underlying disease etiology (Green, 1996; Ranganath et al., 2008). Understanding the neural circuit dynamics that supports episodic memory and the manner in which it fails will provide vital clues to the understanding and treatment of cognitive deficits in psychiatric disorders.

To this end, we studied a well characterized animal model of cognitive dysfunction and SCZ, the *Df(16)A<sup>+-</sup>* mouse model of the 22q11.2 deletion syndrome (22q11.2DS). 22q11.2 deletions are responsible for variable childhood cognitive deficits and behavioral phenotypes as well as adult psychiatric illness, most notably SCZ (Biswas & Furniss, 2016; Schneider et al., 2014). Deletion carriers have a 30-fold increased risk to develop SCZ, accounting for 1-2% of cases of sporadic forms of the disease (Karayiorgou et al., 2010; Xu et al., 2008) and there are no major clinical differences in the core SCZ phenotype between individuals with SCZ who are 22q11.2 deletion carriers and those who are not (Bassett et al., 2003, 1998). Importantly, *Df(16)A<sup>+-</sup>* mice, recapitulate many cognitive and behavioral deficits seen in 22q11.2 deletion carriers and SCZ patients in general, as well as disease-related anatomical and functional alterations in the hippocampus and frontal cortex (Glausier & Lewis, 2013; Scariati et al., 2016; Schmitt et al., 2015, 2016; Spencer et al., 2004; Uhlhaas & Singer, 2010; Weinberger et al., 2016). These alterations include deficits in synapse formation, plasticity, and long-range functional connectivity (Drew et al., 2011; Mukai et al., 2008; Stark et al., 2008; Fenelon et al., 2013; Mukai et al., 2015; Sigurdsson et al., 2010; Tamura et al., 2016), pointing to the conservation of disease pathways across species and enabling the formulation of specific hypotheses for underlying psychopathology.

Cognitive dysfunction in SCZ patients manifests as deficits associated with several spatial memory domains, such as deficits in spatial navigation reference memory, spatial working memory, and episodic memory (Hanlon et al., 2006; Piskulic et al., 2007; Ranganath et al., 2008; Schaefer et al., 2013; Wilkins et al., 2013). Furthermore, SCZ is linked to impaired performance in basic spatial tasks, such as the mental rotations of letters and objects (de Vignemont et al., 2006) and also to more complex tasks (Landgraf et al., 2011; Weniger & Irle, 2008), such as visuo-spatial working memory (see review Piskulic et al., 2007). In particular, patients with SCZ have an impaired ability to process contextual information (Barch et al., 2003; Cohen et al., 1999; Maren et al., 2013), frequently exhibit perseverative behaviors in tasks requiring cognitive flexibility (Crider, 1997; Leeson et al., 2009; Morice, 1990), and a failure to switch between cognitive strategies in spatial, relational and associative memory tasks (Armstrong et al., 2012; Hanlon et al., 2006; Sheffield et al., 2012; Wilkins et al., 2013).

The well documented role of the hippocampus in spatial and episodic memory (Burgess et al., 2002; Buzsáki & Moser, 2013; Dickerson & Eichenbaum, 2010; Eichenbaum, 2000; Eichenbaum & Cohen, 2014), combined with morphological and functional alterations of the hippocampus in SCZ patients (Narr et al., 2004; Vita et al., 2006; Witthaus et al., 2010; Zhou et al., 2008; Heckers & Konradi, 2010; Meyer-Lindenberg et al., 2005; Tamminga et al., 2010; Collin et al., 2011; Debbané et al., 2006; Flahault et al., 2012) and disruptions in functional connectivity (Harrison et al., 2001; Hutcheson et al., 2015), collectively point to a central role for the hippocampus in the pathophysiology of cognitive memory deficits in SCZ (Achim & Lepage, 2005; Bast, 2011). In particular, physiological and morphological alterations are reported specifically in hippocampal CA1 output node in SCZ patients (Narr et al., 2004; Zierhut et al., 2013), suggesting a potentially primary role for area CA1 in hippocampal pathophysiology in SCZ. Nevertheless, learning-related neural population dynamics under pathological conditions remain largely unexplored.

Neural circuits in the mammalian hippocampus support episodic memory by providing cognitive representations of spatial and contextual aspects of an experience (Burgess et al., 2002; Buzsáki & Moser, 2013; Eichenbaum, 2000; O'Keefe & Dostrovsky, 1971). At the neuronal level, principal cells in the hippocampus are selectively active in specific locations within an environment (place cells: O'Keefe & Dostrovsky, 1971), forming the cellular basis of the fast high-capacity declarative memory system (Buzsáki & Moser, 2013). At the ensemble level, place cells collectively form cognitive

maps of space (Hartley et al., 2014; Leutgeb et al., 2005c; O’Keefe & Dostrovsky, 1971; O’Keefe & Nadel, 1978; Moser et al., 2015), which are proposed to be expressions of individual memories (Moser et al., 2015; Buzsáki & Moser, 2013), and the long-term stability of hippocampal spatial representation is a widely posited prerequisite for reliable spatial learning (Kentros et al., 2004; Lever et al., 2002a; Mankin et al., 2012; Thompson & Best, 1990; Ziv et al., 2013). Consistent with this view, place cells modify their preferred firing fields to incorporate both contextual (Colgin et al., 2008; Karlsson & Frank, 2008; Leutgeb et al., 2005b, 2004; Muller & Kubie, 1987b; Wilson & McNaughton, 1994) and non-spatial information, including salient sensory information, as well as internal state of the animal (Frank et al., 2000; Kobayashi et al., 1997; Moita et al., 2004; Pastalkova et al., 2008; Wood et al., 1999), while at the same time, place maps are also modulated by proximal cues in an environment, which can serve as local landmarks to support allocentric navigation (Deshmukh & Knierim, 2013; Knierim & Hamilton, 2011; Knierim & Rao, 2003). Importantly, it has been repeatedly demonstrated that place maps incorporate goal-related information during learning (Breese et al., 1989; Fyhn et al., 2002; Dupret et al., 2010a; Gothard et al., 1996; Hok et al., 2007; Hollup et al., 2001a; Kobayashi et al., 1997), and that place coding is altered during behaviors requiring increased attention (Kentros et al., 2004; Markus et al., 1995; Muzzio et al., 2009). In particular, goal-directed reorganization of place cells was found to predict memory performance (Dupret et al., 2010a). Therefore, monitoring hippocampal ensemble dynamics provides a tractable entry point for understanding – at the cellular and neural population levels – how genetic mutations associated with cognitive dysfunction and psychiatric disorder lead to circuit abnormalities and the emergence of learning deficits. While studies have examined the role of place cells in supporting spatial and episodic memory, the roles of spatial map stability and plastic reorganization of place cell populations during learning remain poorly understood, especially as they relate to disease-associated cognitive dysfunction.

Two-photon  $\text{Ca}^{2+}$  imaging during head-fixed behaviors (Danielson et al., 2016b; Dombeck et al., 2010) allows for the chronic recording of physiological activity from individual CA1 place cells, as well as their ensemble activity as a whole. Chronic imaging provides a unique opportunity to follow changes in individual place cells over days and understand how a SCZ-related mutation affects local activity in the final output node ream of the hippocampus. In light of the well documented deficits in memory functions and cognitive flexibility in SCZ, we aimed to develop a spatially-guided reward

learning task for head-fixed mice, during which task demands could be readily switched from initial reward learning in a novel context, to maintenance of a reward location memory following context manipulation, and finally to learning a new reward location in a now familiar context. By tracking the activity of hippocampal area CA1 place cell populations with chronic two-photon Ca<sup>2+</sup> imaging in *Df(16)A<sup>+/−</sup>* mice and wild-type (WT) littermates through each phase of this learning task, we identified specific aspects of place cell map stability that evolved with learning, as well as alterations in the stability and plasticity of these cognitive maps in the mutant mice. In addition, we analyzed place cell maps during random foraging in a task-free context and found that the spatial map stability differences were specific to the more cognitively challenging learning conditions. Our findings highlight the reduced stability and impaired goal-directed reorganization of hippocampal place cells as fundamental components of 22q11.2 deletion-linked cognitive dysfunction.

## 4.2 Results

### 4.2.1 Head-fixed goal-oriented learning paradigm

We injected mice with AAV1/2(*Synapsin-GCaMP6f*) in dorsal hippocampal area CA1 to express the genetically-encoded Ca<sup>2+</sup> indicator GCaMP6f (Chen et al., 2013) in neurons located in the CA1 pyramidal layer (see Mice and viruses). Mice were implanted with a head-post and imaging window to provide long-term optical access to the CA1 pyramidal layer (Danielson et al., 2016b; Kaifosh et al., 2013; Lovett-Barron et al., 2014). In order to facilitate chronic two-photon functional imaging from hippocampal CA1 place cells (Danielson et al., 2016b; Dombeck et al., 2010) during learning of a spatial navigation task, we used a head-fixed variation of goal-oriented learning (Danielson et al., 2016b) (GOL, Figure 4.1) tasks that have been previously used in freely-moving rodents (Dupret et al., 2010a) (see Comparison of GOL task to freely-moving goal-directed learning task in Dupret et al.). For this, we first trained water-deprived mice to run on a linear treadmill (Danielson et al., 2016a,b; Royer et al., 2012) and then on the first day of the experiment introduced the mice to a novel environmental context, consisting of a feature-rich fabric belt and specific background non-spatial odor, tones, and blinking light patterns (Figure 4.2). Operant water rewards were available at a single unmarked location on the belt; if the mouse licked in the correct location they received a water reward, but no water was administered if they did not lick in the reward

## Goal-Oriented Learning

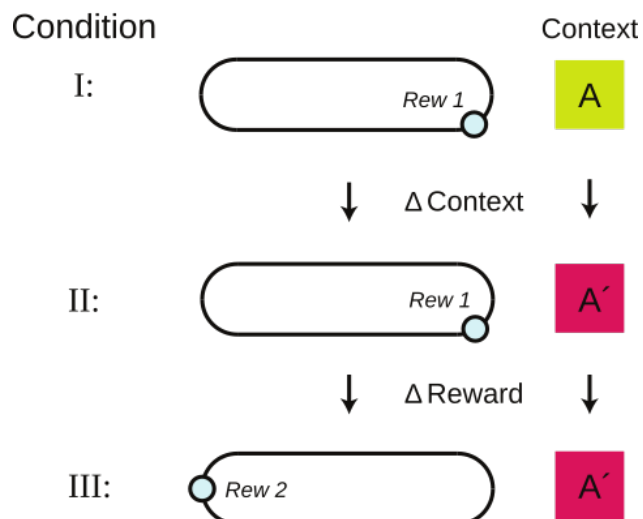


**Figure 4.1:** Mice spend 3 days in each condition. Context A and Context A' are composed of different auditory, visual, olfactory, and tactile cues (see Contexts), varied between Condition I and Condition II. The hidden reward location (blue circles, Rew 1 and Rew 2) is switched between Condition II and Condition III.

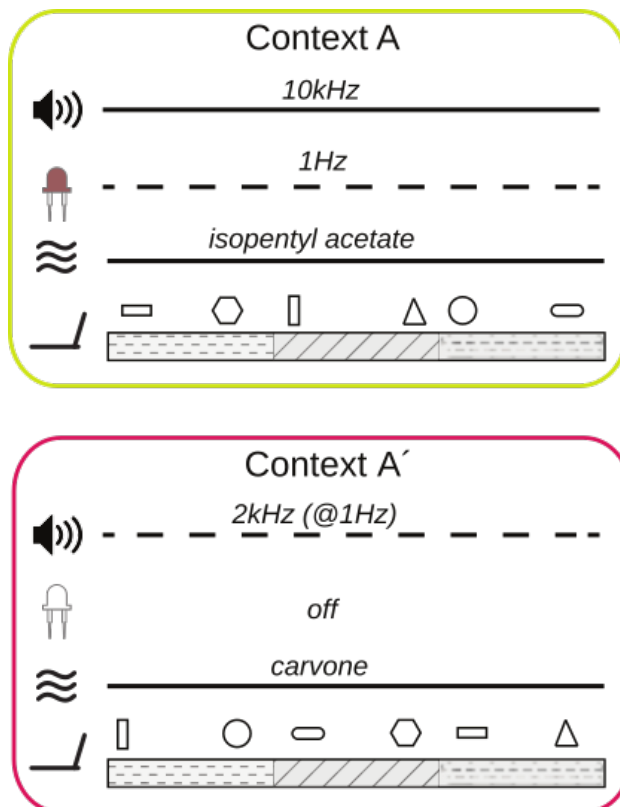


**Figure 4.2:** Context A and Context A' are composed of different auditory, visual, olfactory, and tactile cues (see Methods)

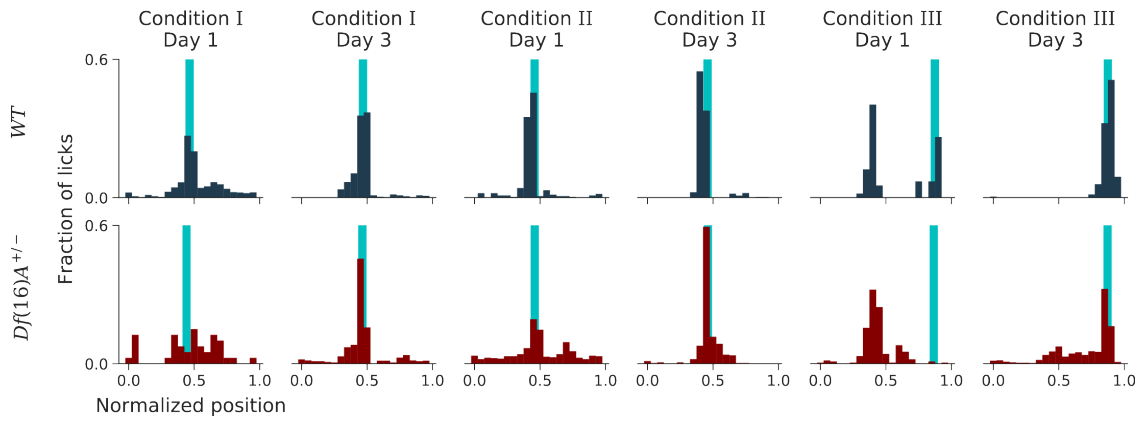


**Figure 4.3:** Example histograms of lick counts by position for a WT (blue) and a *Df(16)A<sup>+-</sup>* (red) mouse on the first and last day of each Condition. Cyan bars depict reward locations. As learning progresses, licking becomes increasingly specific for the reward location.

location or if they licked outside the reward location (Condition I, 3 days, 3 sessions per day). We recorded the time of each lick as well as the position of the mouse on the treadmill in order to both determine when to deliver water rewards and to provide a readout of learning. As the mice learned the reward location they switched from exploratory licking along the entire belt, to focused licking only at the reward location, suppressing licking at other locations (Figure 4.3). In order to test the ability of mice to adjust to changes in the task conditions, we challenged mice by exposing them to an altered context (same sequence of belt materials, shuffled local cues, different non-spatial odor, tone, and light, see Contexts), while maintaining the same reward location relative to the belt fabric sequence (Condition II, 3 days, 3 sessions per day). During the last part of the task, we changed the location of the hidden reward while maintaining the familiar context from Condition II (Condition III, 3 days, 3 sessions per day). As a point of clarity, we use the term ‘context’ to refer to the entire environment and set of features present during the experiment, including the fabric belts, local cues, non-spatial odor, tone, and light, the head-fix apparatus and the microscope itself, but importantly not the un-cued reward location. Also, ‘position’ is always in reference to the sequence of three distinct belt fabrics, which were always in the same order throughout all Conditions of the experiment.

#### **4.2.2 *Df(16)A<sup>+/−</sup>* mice are impaired in GOL task following changes in both context and reward location**

Our overall behavioral analysis on the GOL task revealed general differences among genotypes (Two-way RM ANOVA all days and Conditions, main effect of Genotype:  $p=0.004$ ; main effect of Condition: n.s.), which developed in a condition dependent manner (Two-way RM ANOVA, Condition  $\times$  Genotype interaction:  $p=0.036$ ). In more detail, we found that both *Df(16)A<sup>+/−</sup>* mice and wild-type (WT) littermates had a similar ability to learn the initial location of the hidden reward, as assessed by the suppression of un-rewarded licks outside of the reward zone and an increase in the fraction of licks within the reward zone (Condition I, two-way RM ANOVA, main effect of Day:  $p<0.0001$ ; Genotype  $\times$  Day interaction and main effect of Genotype: n.s.; Figures 4.3, 4.4). During this initial learning period, both WT and *Df(16)A<sup>+/−</sup>* mice explored the task at similar levels (velocity, lap rate, lick rate, Figure 4.5). A change in the environmental context (Condition II) had no detectable effect on WT animals, as their learning of the reward location in the new context continued to improve until their performance plateaued. However, this contextual manipulation impacted learning in the *Df(16)A<sup>+/−</sup>* mice, as their task performance dropped on the first day and was overall worse than WT mice during Condition II (Condition II, two-way RM ANOVA, main effect of Genotype:  $p=0.031$ ; main effect of Day:  $p=0.033$ ; Genotype  $\times$  Day interaction: n.s.; Figures 4.3, 4.4). Moreover, changing the reward location while maintaining a familiar context (Condition III) challenged *Df(16)A<sup>+/−</sup>* mice to a greater degree than WT animals, as they were significantly impaired in acquiring the new reward location (Condition III, two-way RM ANOVA, main effect of Day:  $p<0.0001$ ; main effect of Genotype:  $p=0.019$ ; Genotype  $\times$  Day interaction: n.s.; Figures 4.3, 4.4). Overall locomotor and licking performance was not different between the two groups (laps per session:  $p=0.770$ ; lick rate:  $p=0.686$ ; Figure 4.6e,f). Thus, although *Df(16)A<sup>+/−</sup>* mice are initially able to perform a spatially-guided reward task, learning deficits are revealed by manipulation of task parameters, specifically the environmental context or the reward location.

We noticed during the task that *Df(16)A<sup>+/−</sup>* mice appeared to be relatively more impaired at the start of each day, so to identify genotypic differences in the consolidation of the task memory overnight, we compared the task performance at the beginning and the end of the day during

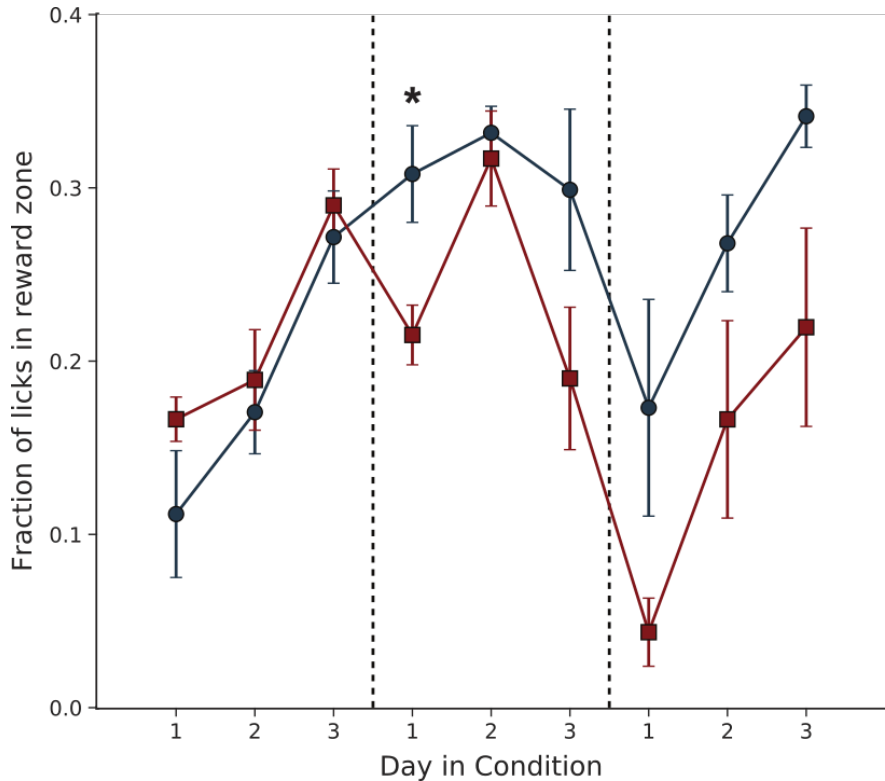


**Figure 4.4:** Learning performance of WT and *Df(16)A<sup>+/−</sup>* mice based on fraction of licks in the reward zone (Two-way RM ANOVA, all days and Conditions, n=6 mice per genotype, main effect of Genotype:  $F(1,10)=13.634$ ,  $p=0.004$ ; Genotype  $\times$  Condition interaction:  $F(2,40)=3.946$ ,  $p=0.036$ ; main effect of Condition: n.s.) for each day and Condition (Condition I, two-way RM ANOVA, main effect of Day:  $F(2,20)=28.235$ ,  $p<0.0001$ ; Condition II, two-way RM ANOVA, main effect of Genotype:  $F(1,10)=6.297$ ,  $p=0.031$ ; main effect of Day:  $F(2,20)=4.076$ ,  $p=0.033$ ; Condition II post-hoc for individual days with Bonferroni correction, day 1:  $p=0.015$ ; Condition III, two-way RM ANOVA, main effects of Day:  $F(2,20)=15.762$ ,  $p<0.0001$ ; main effect of Genotype:  $F(1,10)=7.768$ ,  $p=0.019$ ; effects not listed: n.s.). \* $p<0.05$ .

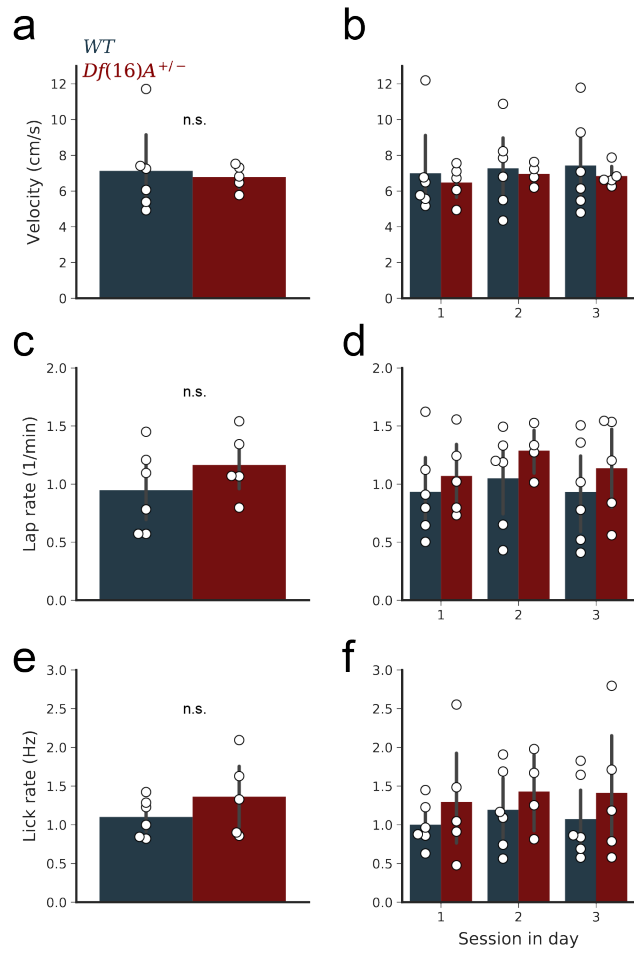


**Figure 4.5:** a. Mean velocity (excluding stationary time) during Condition I for WT and *Df(16)A<sup>+/−</sup>* mice. (WT:  $7.123 \pm 1.002$ , n=6 mice; *Df(16)A<sup>+/−</sup>*:  $6.778 \pm 0.312$ , n=5 mice; independent samples T-test, t=0.302, p=0.769). b. Velocity during Condition I separated by session within each day (two-way ANOVA for session and genotype, all n.s.). c,d. Lap rate (as in a,b) (WT:  $0.947 \pm 0.147$ , n=6 mice; *Df(16)A<sup>+/−</sup>*:  $1.164 \pm 0.128$ , n=5 mice; independent samples T-test, t=-1.087, p=0.305; two-way ANOVA for session and genotype, all n.s.). e,f. Lick rate (as in a,b) (WT:  $1.100 \pm 0.101$ , n=6 mice; *Df(16)A<sup>+/−</sup>*:  $1.362 \pm 0.312$ , n=5 mice; independent samples T-test, t=-1.102, p=0.299; two-way ANOVA for session and genotype, all n.s.). Both WT and *Df(16)A<sup>+/−</sup>* mice show similar levels of activity during the initial learning period, as well as across sessions within each day.

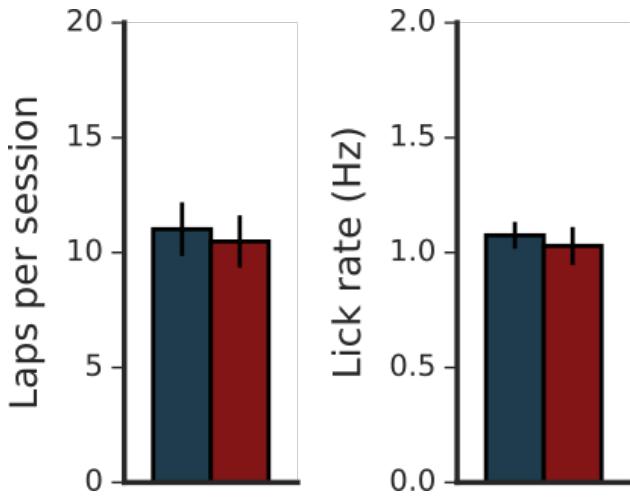


**Figure 4.6:** Left, Mean number of laps per session aggregated by mouse (WT:  $11.018 \pm 1.279$ , n=6 mice,  $Df(16)A^{+/‐}$ :  $10.482 \pm 1.246$ , n=6 mice, independent samples T-test:  $t=0.300$ ,  $p=0.770$ ). Right, Mean lick rate per mouse (WT:  $1.075 \pm 0.064$ , n=6 mice,  $Df(16)A^{+/‐}$ :  $1.029 \pm 0.090$ , n=6 mice, independent samples T-test:  $t=0.416$ ,  $p=0.686$ ).

each condition (Figure 4.7). During Condition I – in which we observed no learning deficit in the  $Df(16)A^{+/‐}$  mice – both WT and  $Df(16)A^{+/‐}$  mice performed at comparable levels throughout the day, and both performed better at the end of the day than at the beginning (Condition I, two-way RM ANOVA, main effect of Session:  $p=0.025$ ; main effect of Genotype and Genotype  $\times$  Session interaction: n.s.). During Condition II – in which we observed an overall decrease in task performance in the  $Df(16)A^{+/‐}$  mice – we found that the  $Df(16)A^{+/‐}$  animals performed poorly on the first session of each day, before reaching WT performance levels by the end of the day (Condition II, two-way RM ANOVA, main effect of Session:  $p<0.0001$ ; Genotype  $\times$  Session interaction:  $p=0.030$ ; main effect of Genotype: n.s.). Finally, during Condition III – in which we observed the most robust learning deficit in the  $Df(16)A^{+/‐}$  mice – we found that  $Df(16)A^{+/‐}$  mice performed significantly worse throughout the entire day (Condition III, two-way RM ANOVA, main effect of Genotype:  $p=0.030$ ; main effect of Session:  $p<0.0001$ , Genotype  $\times$  Session interaction: n.s.). Collectively, these results indicate that deficits in overnight consolidation likely contributed to the differences we observed between genotypes.

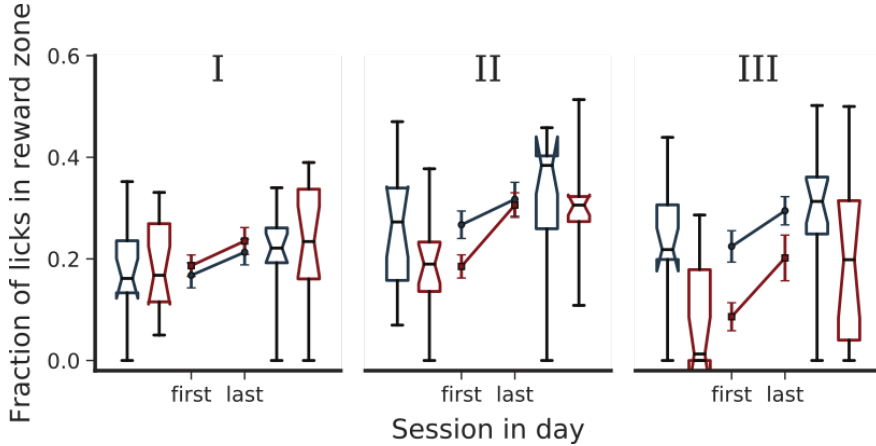


**Figure 4.7:** Learning performance for WT and *Df(16)A<sup>+/−</sup>* mice on the first and last session of each day by Condition. Across all conditions, both genotypes perform better at the end of the day. During Condition I, WT and *Df(16)A<sup>+/−</sup>* mice performs similarly throughout the day (two-way RM ANOVA, main effect of Session:  $F(1,10)=6.901$ ,  $p=0.025$ ; main effect of Genotype and Genotype  $\times$  Session interaction: n.s.), while in Condition II *Df(16)A<sup>+/−</sup>* mice were more impaired at the start of the day (two-way RM ANOVA, main effect of Session:  $F(1,10)=40.506$ ,  $p<0.0001$ ; Genotype  $\times$  Session interaction:  $F(1,10)=6.404$ ,  $p=0.030$ ; main effect of Genotype: n.s.), and in Condition III they additionally never reached WT levels (two-way RM ANOVA, main effect of Genotype:  $F(1,10)=6.433$ ,  $p=0.030$ ; main effect of Session:  $F(1,10)=53.237$ ,  $p<0.0001$ ; Genotype  $\times$  Session interaction: n.s.).

#### 4.2.3 Smaller, less diffuse place cell population in *Df(16)A<sup>+/−</sup>* compared to WT mice

We used two-photon  $\text{Ca}^{2+}$  imaging of large neuronal populations in the CA1 pyramidal layer during the GOL task to assess basic coding properties of place cells (Figure 4.8). Spatially-tuned  $\text{Ca}^{2+}$  transients (Dombeck et al., 2007) (Figure 4.9) were detected in both WT and *Df(16)A<sup>+/−</sup>*, mice however we found that the fraction of identified neurons that exhibited place cell place cell properties was about 25% less in *Df(16)A<sup>+/−</sup>* mice compared to WT mice across all sessions (place cell fraction: WT:  $0.2553 \pm 0.0109$ ; *Df(16)A<sup>+/−</sup>*:  $0.1924 \pm 0.0079$ ;  $p<0.0001$ ; Figure 4.10a). This effect is not driven by a silent fraction of cells in the *Df(16)A<sup>+/−</sup>* mice or differences in our sampling of the pyramidal cells between the genotypes, as cumulatively over all imaging sessions the available place cell population was similar (lifetime place coding:  $p=0.244$ ; Figure 4.11a). Instead, we see that individual cells were identified as place cells in fewer sessions (fraction of sessions a place cell:  $p<0.0001$ ; Figure 4.11b). Furthermore, the spatial tuning of individual place cells in *Df(16)A<sup>+/−</sup>* mice was less diffuse, as indicated by differences in the number of place fields per place cell (place

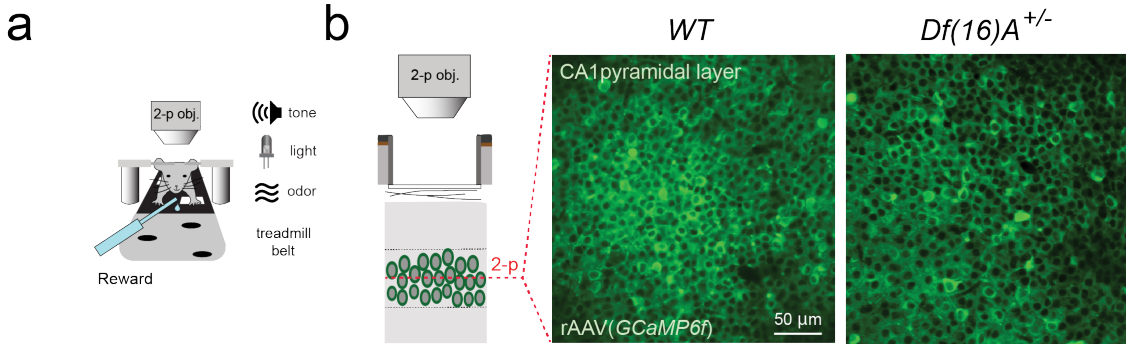


**Figure 4.8:** a. Schematic of head-fixed behavioral setup. b. Left: schematic of two-photon  $\text{Ca}^{2+}$  imaging in the CA1 pyramidal layer. Representative two-photon fields of view across the pyramidal layer showing cross-sections of GCaMP6f-expressing cell bodies from a WT (middle) and  $Df(16)A^{+/-}$  (right) mouse. 179–621 regions of interest (ROIs, see subsection 4.4.2) corresponding to cell bodies were imaged chronically in each field of view.

fields per place cell:  $p < 0.0001$ ; Figure 4.10b), slightly narrower place fields (place field width:  $p < 0.0001$ ; Figures 4.10c, Figure 4.11e), less variability in  $\text{Ca}^{2+}$  transient firing location (circular variance;  $p < 0.0001$ ; inset averaged by mouse,  $p = 0.0491$ ; Figure 4.10d), and less out-of-field firing (transient specificity:  $p < 0.0001$ ; Figure 4.11d). Overall, the significant decrease in the fraction of spatially-tuned cells and altered firing field properties suggests a disruption in the processing of spatial information in the pathological hippocampal network of  $Df(16)A^{+/-}$  mice.

#### 4.2.4 Spatial map is less stable in $Df(16)A^{+/-}$ compared to WT mice

To examine the evolution of spatial maps throughout the GOL task we repeatedly imaged the same populations of individually-identified neurons throughout the 27 sessions across 9 days during the GOL task (cells per mouse, mean  $\pm$  s.d.; WT:  $463 \pm 37$ ,  $n=6$  mice;  $Df(16)A^{+/-}$ :  $479 \pm 84$ ,  $n=5$  mice), and looked at two aspects of stability: place cell population stability (recurrence probability: probability of a cell being identified as a place cell in paired sessions) and individual pyramidal cell firing stability (centroid shift: distance between centroid of firing in paired sessions). Combining all conditions and sessions, we found that individual place cells recurred (Ziv et al., 2013) from day-to-day significantly above chance levels in WT and  $Df(16)A^{+/-}$  mice (recurrence probability: WT vs. shuffle:  $p = <0.0001$ ;  $Df(16)A^{+/-}$  vs. shuffle:  $p < 0.0001$ ; Figure 4.12a), but a significantly smaller fraction of place cells re-occurred from day-to-day in  $Df(16)A^{+/-}$  than WT mice (WT vs.  $Df(16)A^{+/-}$ :  $p < 0.0001$ ; inset by mouse,  $p = 0.028$ ; Figure 4.12a). This decreased overlap in place

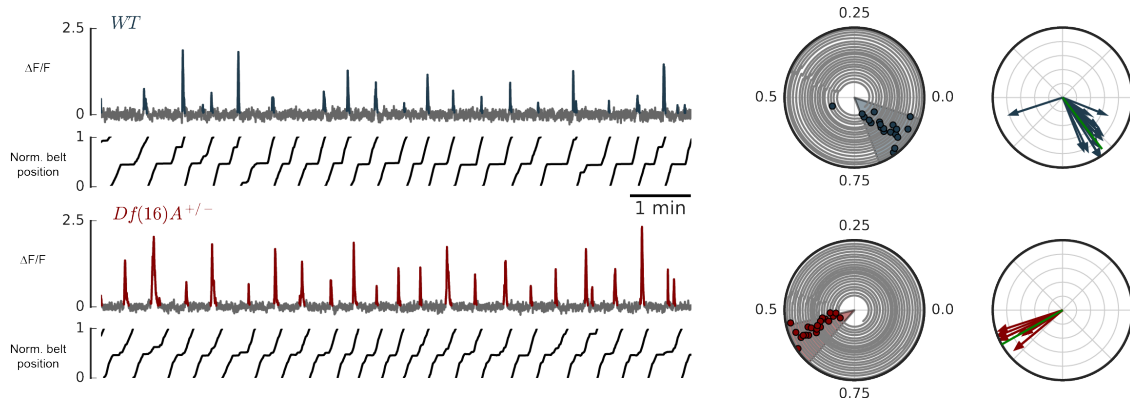


**Figure 4.9:** Example  $\text{Ca}^{2+}$  traces and spatial tuning. Left, GCaMP6f  $\text{Ca}^{2+}$  fluorescence ( $\Delta F/F$ ) traces from two example spatially-tuned CA1 place cells in WT and  $Df(16)A^{+/-}$  mice during 10 minute sessions. Significant  $\text{Ca}^{2+}$  transients are highlighted in blue/red, and treadmill position is shown below the traces. Middle, polar trajectory plots showing significant running-related transients for the same example cells. The animals' position (angle) over time (radius) is gray, the onset times of significant running-related calcium transients are shown as colored circles. Shaded areas denote place fields. Right, transient vector plots showing the position (angle) and occupancy-normalized weight of each running-related transient (radius), as used to calculate occupancy-normalized transient rate histograms and transient circular variance. Green lines indicate transient resultant vector (the magnitude is  $1 - \text{circular variance}$ ).

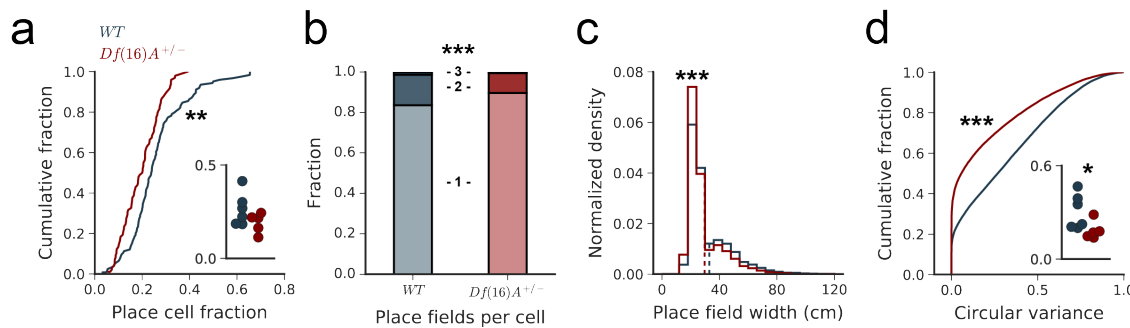


**Figure 4.10:** Compared to WT,  $Df(16)A^{+/-}$  mice had a decreased fraction of cells per experiment with significant spatial information (place cell fraction: WT:  $0.2553 \pm 0.0109$ , n=124 sessions;  $Df(16)A^{+/-}$ :  $0.1924 \pm 0.0079$ , n=98 sessions; Mann-Whitney U, U=4214.5,  $p < 0.0001$ ; inset averaged by mouse, independent samples T-test,  $t = 1.620$ ,  $p = 0.140$ ; a), fewer multi-peaked place cells (place fields per place cell; WT:  $1.180 \pm 0.004$ , n=12571 PC\*sessions;  $Df(16)A^{+/-}$ :  $1.110 \pm 0.004$ , n=7683 PC\*sessions; Pearson chi-square test:  $\chi^2 = 228.650$ ,  $p < 0.0001$ ; Mann-Whitney U, U= $4.53 \times 10^7$ ,  $p < 0.0001$ ; e), narrower place fields (place field width; WT:  $32.531 \pm 0.135$ , n=12571 PC\*sessions;  $Df(16)A^{+/-}$ :  $29.532 \pm 0.144$ , n=7683 PC\*sessions; Mann-Whitney U, U= $4.123 \times 10^7$ ,  $p < 0.0001$ ; f), and lower circular variance (WT:  $0.310 \pm 0.0013$ , n=43068 cell\*sessions;  $Df(16)A^{+/-}$ :  $0.189 \pm 0.0014$ , n=27397 cell\*sessions, Mann-Whitney U, U= $4.21 \times 10^8$ ,  $p < 0.0001$ ; inset averaged by mouse, Welch's T-test,  $t = 2.327$ ,  $p = 0.0491$ , g). \* $p < 0.05$ , \*\* $p < 0.01$ , \*\*\* $p < 0.001$ .

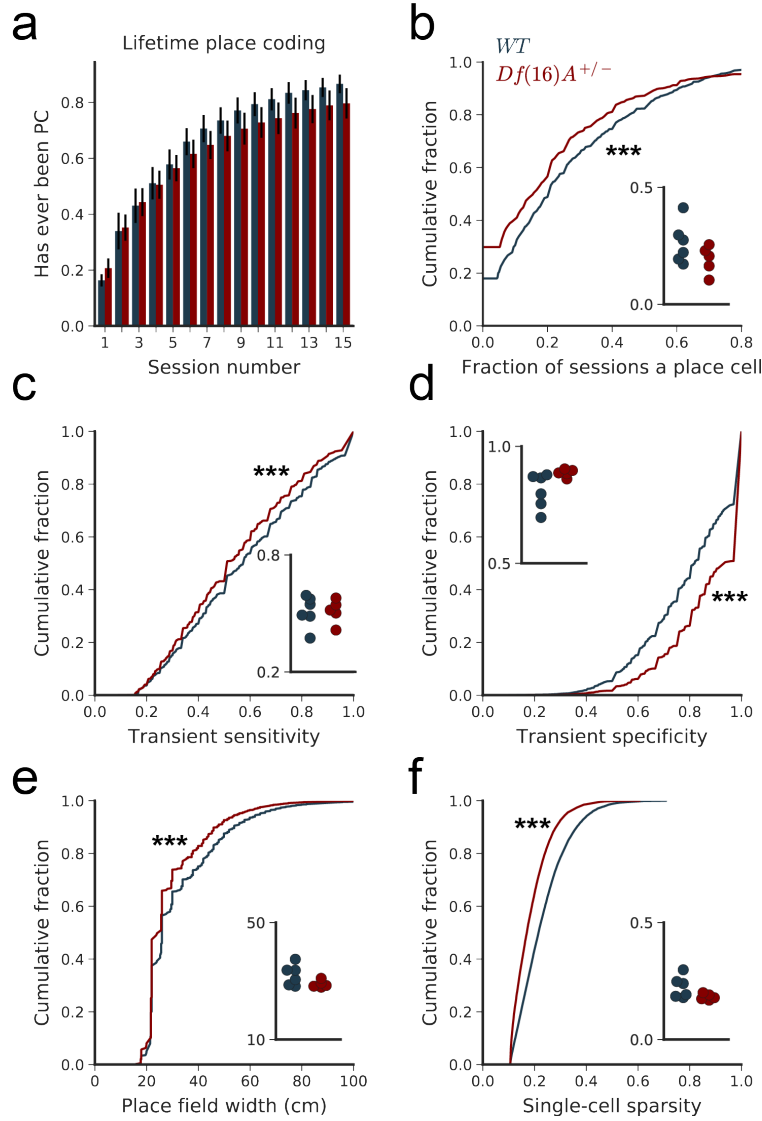


**Figure 4.11:** a. Lifetime place coding percentage, the fraction of ROIs that were ever identified as a place cell by the nth session imaged (lifetime place coding, Cox Regression,  $B=0.222$ ,  $p=0.244$ ). b. Fraction of all sessions imaged that an ROI was identified as a place cell (fraction of sessions a place cell; WT:  $0.254 \pm 0.004$ ,  $n=3162$  cells; *Df(16)A<sup>+/−</sup>*:  $0.214 \pm 0.004$ ,  $n=3322$  cells; Mann-Whitney U,  $U=4.55 \times 10^6$ ,  $p<0.0001$ ), averaged within mice (inset; independent sample T-test,  $t=1.517$ ,  $p=0.164$ ). c. Transient sensitivity, defined as the fraction of laps in which a transient occurred in the place field (WT:  $0.5786 \pm 0.00218$ ,  $n=12524$  place cell\*sessions; *Df(16)A<sup>+/−</sup>*:  $0.5445 \pm 0.0027$ ,  $n=7664$  place cell\*sessions; Mann-Whitney U,  $U=4.4 \times 10^7$ ,  $p<0.0001$ ), averaged within mice (inset, independent samples T-test,  $t=0.0142$ ,  $p=0.989$ ). d. Transient specificity, defined as the fraction of transients that occurred in the place field (WT:  $0.795 \pm 0.0161$ ,  $n=12571$  place cell\*sessions; *Df(16)A<sup>+/−</sup>*:  $0.872 \pm 0.0018$ ,  $n=7683$  place cell\*sessions; Mann-Whitney U,  $U=3.59 \times 10^7$ ,  $p<0.0001$ ), averaged within mice (inset; Welch's T-test,  $t=2.427$ ,  $p=0.0544$ ). e. Place field width (WT:  $32.09 \pm 0.125$ ,  $n=14833$  place fields; *Df(16)A<sup>+/−</sup>*:  $29.25 \pm 0.136$ ,  $n=8529$  place fields; Mann-Whitney U,  $U=5.5 \times 10^7$   $p<0.0001$ ), averaged within mice (inset, Welch's T-test,  $t=1.990$ ,  $p=0.0911$ ). f. Single-cell sparsity (WT:  $0.2325 \pm 0.001$ ,  $n=12571$  ROI\*sessions; *Df(16)A<sup>+/−</sup>*:  $0.186 \pm 0.001$ ,  $n=8683$  ROI\*sessions; Mann-Whitney U,  $U=3.35 \times 10^7$ ,  $p<0.0001$ ), averaged within mice (inset, Welch's T-test,  $t=2.064$ ,  $p=0.0852$ ). \*\*\* $p<0.001$

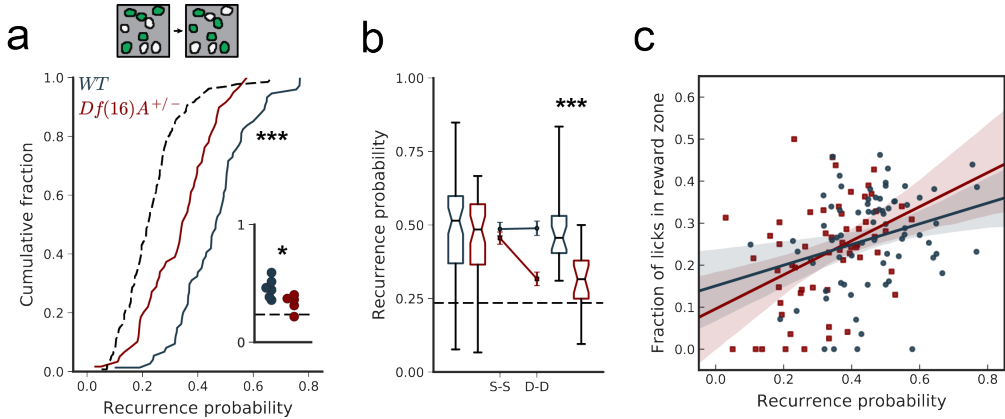


**Figure 4.12:** a. (top) Example of place cell recurrence. In a given field of view, a subset of all cells has significant spatial tuning each day (place cells, green). The overlap in this population is the recurrence probability (40% in this example). (bottom) Distribution of recurrence fractions from day-to-day for WT and *Df(16)A<sup>+/−</sup>* mice for all sessions (dotted line is cell-identity shuffle distribution: WT:  $0.456 \pm 0.015$ , n=74 sessions, *Df(16)A<sup>+/−</sup>*:  $0.327 \pm 0.017$ , n=59 sessions, shuffle:  $0.229 \pm 0.009$ , n=133 sessions; WT vs. shuffle: Welch's T-test,  $t=12.64$ ,  $p=<0.0001$ ; *Df(16)A<sup>+/−</sup>* vs. shuffle: Welch's T-test,  $t=5.124$ ,  $p<0.0001$ ; WT vs. *Df(16)A<sup>+/−</sup>*: independent samples T-test,  $t=5.72$ ,  $p<0.0001$ ) and aggregated by mouse (inset, gray bar is cell-identity shuffle: WT vs. *Df(16)A<sup>+/−</sup>*: independent samples T-test,  $t=2.611$ ,  $p=0.028$ ). b. Mean fraction of cells that reoccur as place cells from session-to-session (S-S) or day-to-day (D-D) for WT and *Df(16)A<sup>+/−</sup>* mice (dotted line is mean place cell fraction; two-way ANOVA for elapsed time and genotype; main effect of Genotype:  $F(1,152)=8.199$ ,  $p=0.0048$ ; main effect of Time:  $F(1,152)=4.434$ ,  $p=0.0369$ ; Time  $\times$  Genotype interaction:  $F(1,152)=6.493$ ,  $p=0.0118$ ; post-hoc analysis, WT vs. *Df(16)A<sup>+/−</sup>*, S-S:  $t=0.988$ ,  $p=0.325$ ; D-D:  $t=5.012$ ,  $p<0.0001$ ). c. Correlation of place cell recurrence with performance throughout the task. Solid line is linear regression fit, shaded regions are 95% confidence intervals calculated from bootstrap resampling (Pearson's correlation coefficient, WT:  $0.288$ ,  $p=0.013$ ; *Df(16)A<sup>+/−</sup>*:  $0.416$ ,  $p=0.001$ ; WT correlation vs. *Df(16)A<sup>+/−</sup>* correlation, Fisher Z transformation of correlations, GLM model, Univariate Analysis of Variance: Genotype  $\times$  Recurrence interaction:  $F(1,132)=0.599$ ,  $p=0.440$ ). \* $p<0.05$ , \*\*\* $p<0.001$

cell population in the *Df(16)A<sup>+/−</sup>* mice primarily driven by decreased stability overnight, as this difference was not observed within day from session-to-session (two-way ANOVA; Genotype  $\times$  Elapsed Time interaction:  $p=0.0118$ ; post-hoc analysis, WT vs. *Df(16)A<sup>+/−</sup>*, S-S:  $p=0.325$ ; D-D,  $p<0.0001$ ; Figure 4.12b), again suggesting a disruption in overnight consolidation, as seen with the *Df(16)A<sup>+/−</sup>* behavioral performance (see Figure 4.7).

We next looked at the shift in firing locations in both WT and *Df(16)A<sup>+/−</sup>* mice to assess the similarity of spatial tuning from day-to-day. We found that while preferred firing locations of all cells were more stable than chance in both genotypes (centroid shift: WT vs. shuffle:  $p<0.0001$ ; *Df(16)A<sup>+/−</sup>* vs. shuffle:  $p<0.0001$ ; Figure 4.13a; place field correlation: WT vs. shuffle:  $p<0.0001$ ; *Df(16)A<sup>+/−</sup>* vs. shuffle:  $p<0.0001$ ; Figure 4.14a), the spatial tuning in *Df(16)A<sup>+/−</sup>* mice was signifi-

cantly less stable day-to-day compared to WT mice (centroid shift: WT vs.  $Df(16)A^{+/-}$ :  $p<0.0001$ ; inset by mouse:  $p=0.030$ ; Figure 4.13a; place field correlation: WT vs.  $Df(16)A^{+/-}$ :  $p<0.0001$ ; Figure 4.14a). Also, just as the active place cell population overlap was similar within day between WT and  $Df(16)A^{+/-}$  mice, spatial tuning was also not different between WT and  $Df(16)A^{+/-}$  mice from session-to-session within the same day (centroid shift: two-way ANOVA, Genotype  $\times$  Elapsed Time interaction:  $p=0.0696$ ; post-hoc analysis, WT vs.  $Df(16)A^{+/-}$ , S-S:  $p=0.694$ ; D-D,  $p=0.0047$ ; Figure 4.13b; place field correlation: Genotype  $\times$  Elapsed Time interaction:  $p=0.0051$ ; post-hoc analysis, WT vs.  $Df(16)A^{+/-}$ , S-S:  $p=0.613$ ; D-D,  $p<0.0001$ ; Figure 4.14b). Taken together, spatial maps are less stable in  $Df(16)A^{+/-}$  than WT mice from day-to-day (but not from session-to-session), as seen by lower recurrence of place cells and a larger shift in spatial tuning centroids, reflecting severely disrupted spatial maps in the  $Df(16)A^{+/-}$  mutant mice.

#### 4.2.5 Task performance correlates with spatial map stability

Stability of place fields over time is thought to provide basis for spatial and episodic learning (Kentros et al., 2004; Mankin et al., 2012; Thompson & Best, 1990; Ziv et al., 2013). If so, we expect that the relative stability of these maps would reflect the ability of mice to perform in our GOL task. Indeed, on a per-session basis the overlap in the identity of place cells from day-to-day correlated with learning performance across all conditions of the GOL task for both groups (recurrence probability vs. fraction of licks in reward zone: Pearson's correlation coefficient, WT: 0.288,  $p=0.013$ ;  $Df(16)A^{+/-}$ : 0.416,  $p=0.001$ ; Figure 4.12c), suggesting that this coding strategy is implemented by both WT and  $Df(16)A^{+/-}$  mice, though the overall decreased population stability in the  $Df(16)A^{+/-}$  mice contributes to the impaired task performance – the  $Df(16)A^{+/-}$  mice are shifted lower on the recurrence-performance curve. In a similar manner to recurrence probability, place cell firing location stability also correlated with task performance for the WT mice and trended similarly in the  $Df(16)A^{+/-}$  mice (centroid shift vs. fraction of licks in reward zone: Pearson's correlation coefficient, WT: -0.306,  $p=0.008$ ;  $Df(16)A^{+/-}$ : -0.218,  $p=0.097$ ; Figure 4.13c; place field correlation; Spearman's correlation coefficient, WT: 0.335,  $p=0.004$ ; Pearson's correlation coefficient,  $Df(16)A^{+/-}$ : 0.224,  $p=0.088$ ; Figure 4.14c). In addition, as is suggested by the overall correlation of task performance with stability, the trajectory of these metrics by Condition mirrors the trajectory of the behavioral deficit in the task. Namely, just as we did not see a difference in

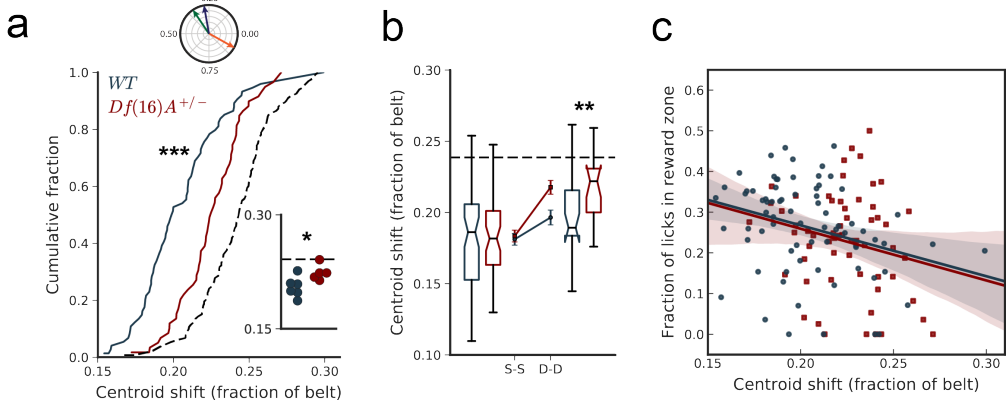


**Figure 4.13:** d. (top) Preferred spatial tuning is represented as a vector where the angle is the position on the treadmill of maximal activity. Across three sessions (green, blue, orange lines) spatial preference is generally stable (green to blue sessions), though salient events or changes to the environment can induce remapping (blue to orange session). The centroid shift is the angle between these vectors, represented as the fraction of the belt. (bottom) Distribution of mean centroid shift from day-to-day per session (dotted line is cell-identity shuffled distribution: WT:  $0.204 \pm 0.003$ , n=74 sessions, *Df(16)A<sup>+/−</sup>*:  $0.224 \pm 0.003$ , n=59 sessions, shuffle:  $0.242 \pm 0.002$ , n=133; WT vs. shuffle: independent sample T-test,  $t=-9.42$ ,  $p<0.0001$ ; *Df(16)A<sup>+/−</sup>* vs. shuffle: independent samples T-test,  $t=-4.25$ ,  $p<0.0001$ ; WT vs. *Df(16)A<sup>+/−</sup>*: independent samples T-test,  $t=-4.71$ ,  $p<0.0001$ ), and aggregated by mouse (inset, gray bar is cell-identity shuffle; independent samples T-test,  $t=2.58$ ,  $p=0.0295$ ). e. Mean centroid shift from session-to-session (S-S) or day-to-day (D-D) for WT and *Df(16)A<sup>+/−</sup>* mice (dotted line is mean centroid shift, two-way ANOVA for elapsed time and genotype; main effect of Genotype:  $F(1,152)=2.693$ ,  $p=0.103$ ; main effect of Time:  $F(1,152)=20.378$ ,  $p<0.0001$ ; Time × Genotype interaction:  $F(1,152)=3.340$ ,  $p=0.0696$ ; post-hoc analysis, WT vs. *Df(16)A<sup>+/−</sup>*, S-S:  $t=0.394$ ,  $p=0.694$ ; D-D:  $t=2.985$ ,  $p=0.0047$ ). f. Correlation of mean day-to-day stability with performance throughout the task. Solid line and shaded regions as in d (Pearson's correlation coefficient, WT:  $-0.306$ ,  $p=0.008$ ; *Df(16)A<sup>+/−</sup>*:  $-0.218$ ,  $p=0.097$ ; WT correlation vs. *Df(16)A<sup>+/−</sup>* correlation, Fisher Z transformation of correlations, GLM model, Univariate Analysis of Variance: Genotype × Stability interaction:  $F(1,132)=0.268$ ,  $p=0.605$ ). \* $p<0.05$ , \*\* $p<0.01$

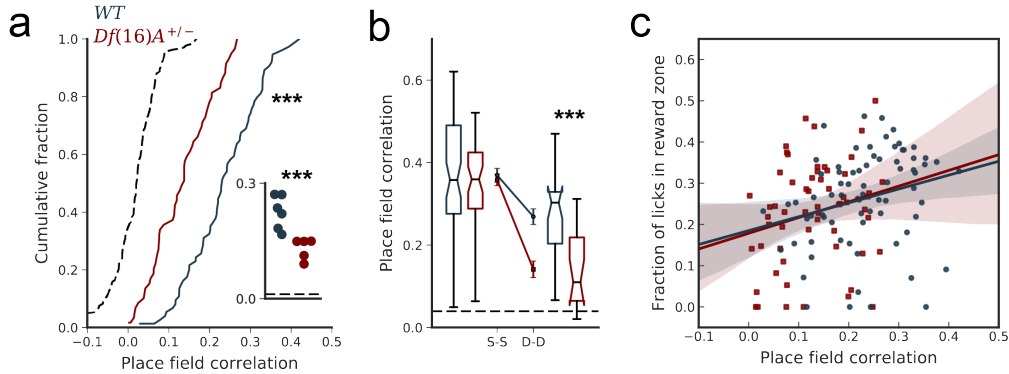


**Figure 4.14:** Place field correlation showed an overall similar effect as centroid shift (see Figure 4.13). a. Compared to WT mice, *Df(16)A<sup>+/−</sup>* mice show a significant overall decrease in place field correlation (WT:  $0.232 \pm 0.010$ , n=74 sessions; *Df(16)A<sup>+/−</sup>*:  $0.130 \pm 0.010$ , n=59 sessions; shuffle:  $0.0238 \pm 0.005$ , n=133; WT vs. shuffle: Welch's T-test;  $t=18.87$ ;  $p<0.0001$ ; *Df(16)A<sup>+/−</sup>* vs. shuffle: Welch's T-test,  $t=9.89$ ,  $p<0.0001$ ; WT vs. *Df(16)A<sup>+/−</sup>*, independent samples T-test,  $t=7.143$ ,  $p<0.0001$ ; inset aggregated by mouse: WT vs. *Df(16)A<sup>+/−</sup>*: independent samples T-test,  $t=2.584$ ,  $p=0.0295$ ). b. Place fields were more stable from session-to-session than day-to-day and the *Df(16)A<sup>+/−</sup>* mice were less stable across elapsed time (two-way ANOVA for time elapsed and genotype, main effect of Genotype:  $F(1,152)=5.710$ ,  $p=0.0181$ ; main effect of Time:  $F(1,152)=55.329$ ,  $p<0.0001$ ; Time  $\times$  Genotype interaction:  $F(1,152)=8.074$ ,  $p=0.00511$ ; S-S, WT vs. *Df(16)A<sup>+/−</sup>*:  $t=0.507$ ,  $p=0.613$ ; D-D, WT vs. *Df(16)A<sup>+/−</sup>*:  $t=4.455$ ;  $p<0.0001$ ). c. Task performance correlates with the session-mean place field correlation for WT mice (Spearman's correlation coefficient= $0.335$ ,  $p=0.004$ ) and trends similarly for *Df(16)A<sup>+/−</sup>* mice (Pearson's correlation coefficient= $0.224$ ,  $p=0.088$ ).

behavior during Condition I (Figure 4.15a, see Figure 4.4), stability is also similar between WT and *Df(16)A<sup>+/−</sup>* mice during Condition I, but while the WT place cell population continues to stabilize in Condition II and III, the *Df(16)A<sup>+/−</sup>* population stability drops off as the task demands change (Figure 4.15b: two-way ANOVA, main effect of Genotype,  $p=0.048$ ; Genotype  $\times$  Condition interaction,  $p=0.083$ ; post-hoc analysis comparing genotype, Condition I and II, n.s., Condition III,  $p=0.016$ ). Thus, the learning strategy employed by both genotypes does involve the formation and maintenance of stable hippocampal spatial maps, but the stability of these maps is impaired in *Df(16)A<sup>+/−</sup>* mice – particularly from day-to-day and when the task demands change – as reflected in their decreased performance on the GOL task.

#### 4.2.6 Goal-oriented learning requires dorsal hippocampal area CA1 and relies on allocentric navigational strategies

To confirm the necessity of the hippocampus to our GOL task, we pharmacologically silenced bilateral dorsal hippocampus area CA1 using the GABA<sub>A</sub>-receptor agonist muscimol during initial

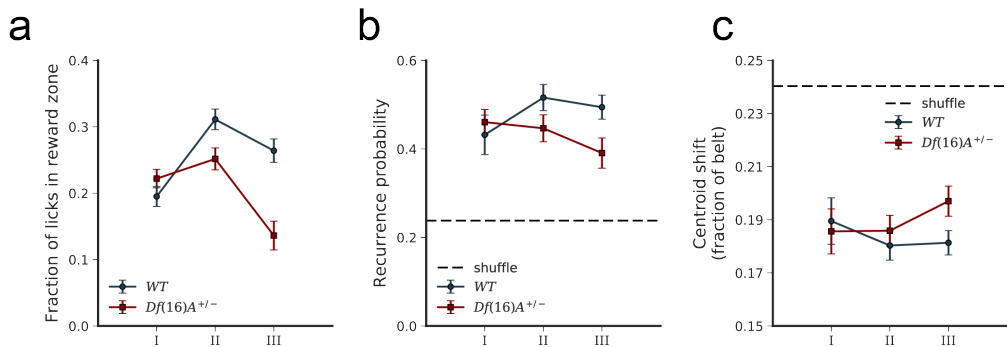


**Figure 4.15:** Task performance and population stability by genotype follows similar trajectories across Conditions; that is to say, performance and stability are similar in Condition I, slightly impaired in the *Df(16)A<sup>+/-</sup>* mice during Condition II and most different during Condition III (three-way ANOVA, Genotype  $\times$  Metric  $\times$  Condition interaction:  $F(4,549)=0.484$ ,  $p=0.747$ ; Condition  $\times$  Genotype interaction:  $F(2,549)=11.982$ ,  $p=<0.0001$ ; Metric *times* Genotype interaction:  $F(2,549)=0.771$ ,  $p=0.463$ ; Metric  $\times$  Condition interaction:  $F(4,549)=1.503$ ,  $p=0.200$ ; Condition I, all metrics, WT vs. *Df(16)A<sup>+/-</sup>*: independent samples T-test:  $t=-1.194$ ,  $p=0.234$ ; Condition II, all metrics, WT vs. *Df(16)A<sup>+/-</sup>*: independent samples T-test:  $t=2.67$ ,  $p=0.0081$ ; Condition III, all metrics, WT vs. *Df(16)A<sup>+/-</sup>*: Welch's T-test:  $t=5.586$ ,  $p<0.0001$ ).  
a. Fraction of licks in the reward zone by condition (two-way ANOVA, main effect of Genotype  $p<0.0001$ , main effect of Condition  $p<0.0001$ , Genotype  $\times$  Condition interaction  $p<0.0001$ ). b. Recurrence probability by condition (two-way ANOVA, main effect of Genotype  $p=0.048$ , main effect of Condition  $p=0.505$ , Genotype  $\times$  Condition interaction  $p=0.083$ ). c. Mean centroid shift by condition (two-way ANOVA, main effect of Genotype  $p=0.284$ , main effect of Condition  $p=0.620$ , Genotype  $\times$  Condition interaction  $p=0.347$ ).

learning of a fixed reward location. Mice ran in a single Condition (same reward location, belt, local cues, and non-spatial cues, identical to the initial learning conditions of Condition I) for 4 days (3 sessions per day) with the first group of mice receiving a bilateral local infusion of muscimol to dorsal hippocampus 30 minutes before the start of the first trial for the first 3 days and then saline on the fourth day. The second group of mice was infused with saline for the first 3 days and then muscimol on the fourth day. Mice in which their dorsal hippocampus was silenced during initial learning of the reward location performed significantly worse than mice with an active hippocampus (Days 1-3, muscimol to saline vs. saline to muscimol:  $p<0.0001$ ; Figure 4.16), indicating that silencing dorsal hippocampus activity results in decreased ability to learn a hidden reward zone. On the fourth day, the mice that had received muscimol infusions now received saline infusions and these mice still perform poorly on the task, showing that the silencing of the hippocampus was not merely suppressing the expression of goal oriented learning, but that instead they are just beginning to learn the reward location. In further support of the hippocampal-dependence of this task, mice that successfully learned the task with an active hippocampus over the first three days had their dorsal hippocampus silenced during the fourth day and showed a significant decrease in goal oriented behavior (saline to muscimol, Days 1-3 vs. Day 4:  $p=0.0235$ ), and now performed similar to the initially silenced training group (Day 4, saline to muscimol vs. muscimol to saline:  $p=0.535$ ).

Allocentric and path integration navigational strategies are thought to be two complementary attributes of the hippocampal-entorhinal navigational-memory circuitry (Buzsáki & Moser, 2013; Etienne & Jeffery, 2004; Gothard et al., 1996; Moser et al., 2015). While in our head-fixed GOL task, local cues and fabric segments of the treadmill belt are aimed to primarily provide an allocentric reference frame for spatial map during learning, mice can in principle also use egocentric, path integration strategies to find the reward location. In order to elucidate the relative contribution of allocentric navigation and path integration in the learning task, we carried out experiments in which we imaged WT mice in the absence of local cues on the treadmill belt, where we find that place cells were practically absent (place cell fraction, cue-rich vs. cue-free:  $p=0.004$ ; Figure 4.17a,b) and the tuning of all cells was significantly more diffuse (circular variance, cue-rich vs. cue-free:  $p<0.0001$ ; Figure 4.17c). Furthermore, in the case of path integration, we would expect that during transition between Condition I and II, when fabric transitions are the only features remaining constant, place cells near the fabric transitions would be more stable than place cells farther from the fabric

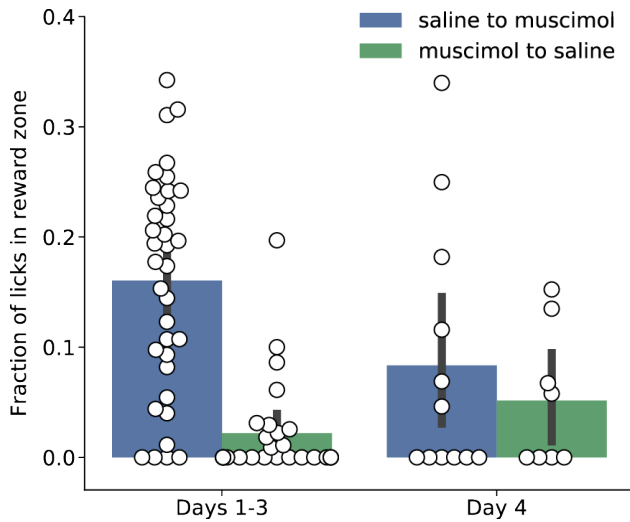


**Figure 4.16:** During initial learning of a reward location, local inactivation of CA1 lead to significantly reduced task performance (Days 1-3, muscimol to saline vs. saline to muscimol: Mann-Whitney U,  $U=126.5$ ,  $p<0.0001$ ). In addition, mice which received saline infusion during the first three initial learning days performed significantly worse on the fourth day when they were infused with muscimol (saline to muscimol, Days 1-3:  $0.221 \pm 0.053$ ,  $n=36$  sessions; Day 4:  $0.084 \pm 0.034$ ,  $n=12$  sessions; Mann-Whitney U,  $U=111$ ,  $p=0.0235$ ) and now performed at a similar level to mice which were initially infused with muscimol (Day 4, saline to muscimol vs. muscimol to saline: independent samples T-test,  $t=0.633$ ,  $p=0.535$ ).

transitions, as errors in path integration would accumulate with distance (Etienne & Jeffery, 2004; Gothard et al., 1996). We carried out analyses in which we compared the stability of spatial tuning from the last day of Condition I to the first session of Condition II by dividing cells into three groups based on which third of the treadmill belt they were active in at the end of Condition I – before the fabric transitions, after the fabric transitions, and in the middle of the fabric segments. We found no difference in stability contributable to the distance of the initial preferred tuning to the nearest fabric transition (two-way ANOVA, main effect of Binned Distance:  $p=0.977$ ; Figure 4.17d). These results together suggest that egocentric navigational strategies would be insufficient to maintain place cell firing, and thus mice indeed primarily employ allocentric navigational strategies for learning in the head-fixed GOL task.

#### 4.2.7 Disrupted sharp wave-ripple activity in *Df(16)A<sup>+/−</sup>* mice

Decreased task performance following long-delays (overnight period) coupled with the decreased recurrence and similarity of neuronal ensemble activity from day-to-day suggests a consolidation deficit in the *Df(16)A<sup>+/−</sup>* mice. Reactivation and consolidation of memories of previous experi-

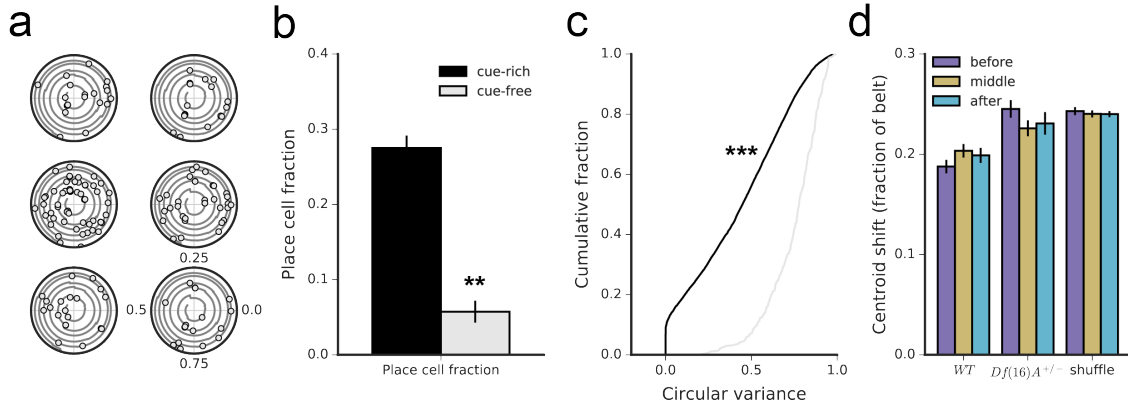


**Figure 4.17:** a. The 6 most spatially tuned cells (lowest circular variance) on a burlap belt, plotted as in Figure 4.9. b. Place cell fraction on a ‘cue-rich’ and ‘cue-free’ belt during RF (cue-rich:  $0.275 \pm 0.017$ , n=56 sessions; cue-free:  $0.057 \pm 0.018$ , n=3 sessions; independent samples T-test,  $t=3.006$ ,  $p=0.004$ ). c. Transient circular variance on a ‘cue-rich’ and ‘cue-free’ belt during RF (cue-rich:  $0.427 \pm 0.003$ , n=7828 cell\*sessions; cue-free:  $0.746 \pm 0.008$ , n=375 cell\*sessions; Mann-Whitney U,  $U=4.99 \times 10^5$ ,  $p<0.0001$ ). d. Centroid shift of cells from the last day of Condition I to the first session of Condition II separated by tuning preference relative to fabric transitions – the only features that remain constant between the two contexts. WT tuning is generally more stable (WT vs. *Df(16)A<sup>+/</sup>*, independent samples T-test:  $t=-4.96$ ,  $p<0.0001$ ; see Figure 4.21), but neither genotype shows increased stability near the fabric transitions (two-way ANOVA, main effect of binned Distance:  $F(2,24)=0.024$ ,  $p=0.977$ ). \* $p<0.05$ , \*\*\* $p<0.001$

ences are thought to occur during sharp wave-ripples (SWRs) – large-amplitude, short-duration, high-frequency events detected in the local field potential (Buzsaki, 2015; Diba & Buzsaki, 2007; Dupret et al., 2010a; Foster & Wilson, 2006; Jadhav et al., 2012; Kudrimoti et al., 1999; Wilson & McNaughton, 1994) during quiet wakefulness and sleep. To assess SWR activity in WT and *Df(16)A<sup>+/</sup>* mice, in a separate cohort of mice we implanted electrodes in hippocampal area CA1 to record the local field potential and detect SWRs (Figure 4.18a,b, see subsubsection 4.4.11.6) during a head-fixed random foraging task on a featureless burlap belt. During periods of immobility, we found that *Df(16)A<sup>+/</sup>* mice had significantly more SWRs ( $p<0.001$ ; Figure 4.19a), though the SWRs were irregular, as reflected by a higher mean ripple band-power ( $p<0.001$ ; Figure 4.19b) and a higher peak frequency in the ripple-band ( $p<0.001$ ; Figure 4.19c). To ensure the robustness of the result, we varied the SWR detection threshold and found that these effects held across SWR event detection thresholds (significance as noted in figure; Figure 4.20). Dysregulation of hippocampal excitability during periods of rest in *Df(16)A<sup>+/</sup>* mice, as manifest by increased SWR frequency and power, provides a possible mechanism behind the failure to efficiently retain a memory of the reward location by the *Df(16)A<sup>+/</sup>* mice.

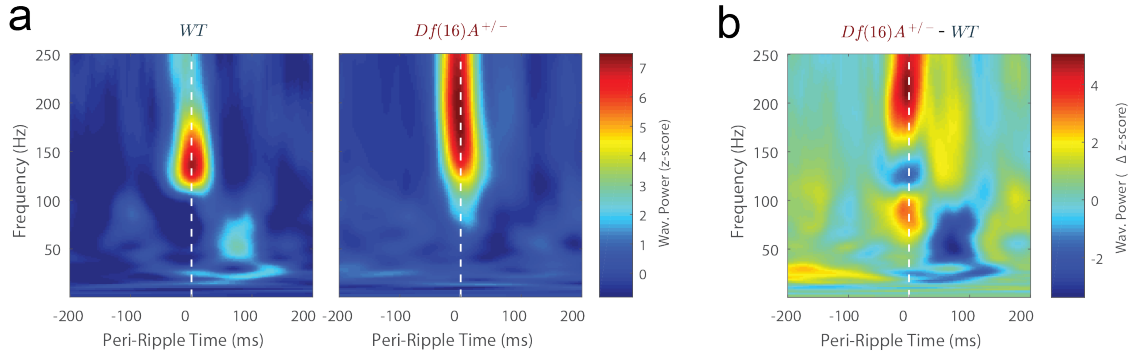


**Figure 4.18:** a. Mean SWR wavelet power for WT (left) and *Df(16)A<sup>+/−</sup>* (right) mice. b. Difference (*Df(16)A<sup>+/−</sup>* - WT) of mean SWR wavelet power in a.

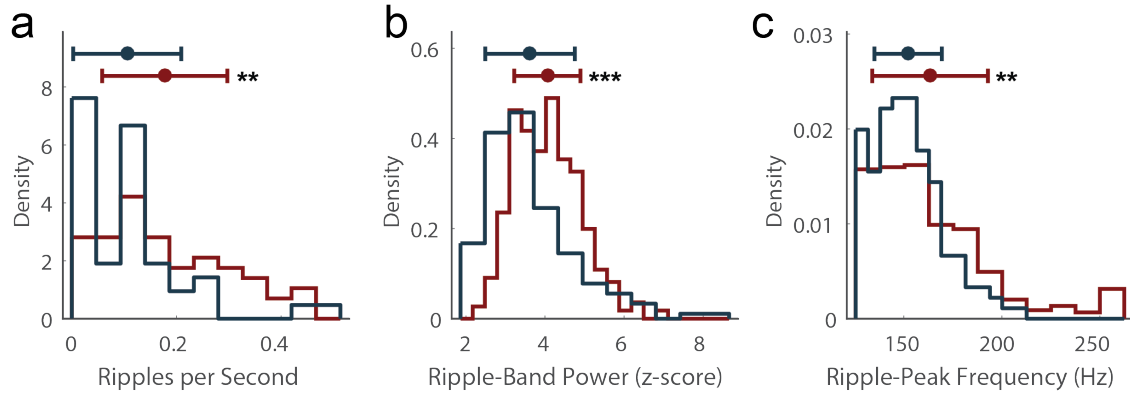


**Figure 4.19:** a. Rate of SWRs during stationary bouts (mean  $\pm$  SD; WT:  $0.106 \pm 0.103$ , n=45 stationary intervals; *Df(16)A<sup>+/−</sup>*:  $0.178 \pm 0.120$ , n=61 stationary intervals; Wilcoxon rank-sum test, h=3777.5, p=0.00096). b. Mean wavelet power (mean  $\pm$  SD; WT:  $3.622 \pm 1.133$ , n=145 sharp-wave ripples; *Df(16)A<sup>+/−</sup>*:  $4.060 \pm 0.838$ , n=357 sharp wave-ripples; Wilcoxon rank-sum test, h=98423, p<0.0001). c. Frequency with maximum power (mean  $\pm$  SD; WT:  $152.190 \pm 17.174$ , n=145 sharp wave-ripples; *Df(16)A<sup>+/−</sup>*:  $163.391 \pm 29.485$ , n=357 sharp wave-ripples; Wilcoxon rank-sum test, h=94798, p=0.00066).

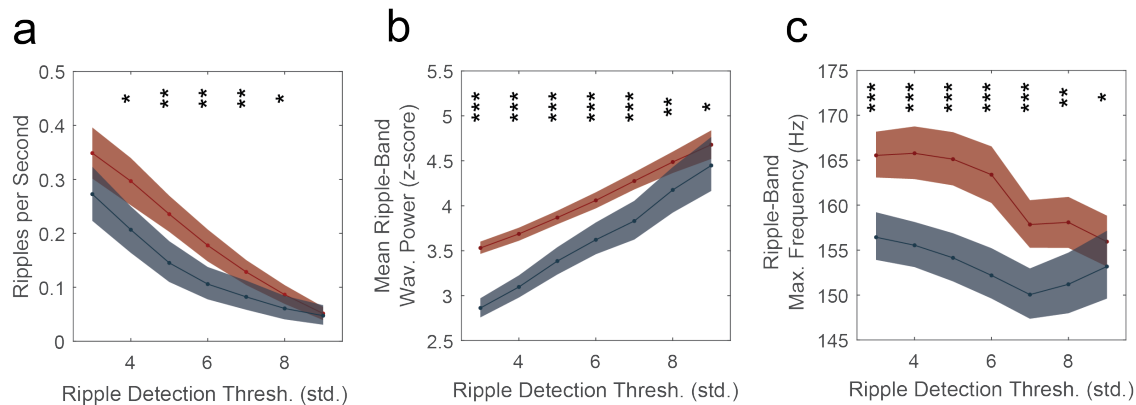


**Figure 4.20:** Same as Figure 4.19 for several SWR detection thresholds (significance by Wilcoxon rank-sum test as marked). \*p<0.05, \*\*p<0.001, \*\*\*p<0.0001

#### **4.2.8 Change in context induces disrupted place cell stability in *Df(16)A<sup>+/−</sup>* mice**

In addition to deficits following the overnight period, *Df(16)A<sup>+/−</sup>* mice showed significantly impaired performance after a change in context during Condition II in the GOL task (Condition II, Day 1; see Figures 4.3 & 4.4) – a change in both the non-spatial (tone, light, and odor) and proximal spatial cues (shuffled local cues on belt, constant fabric sequence). When we compared the day-to-day stability of place fields in WT and *Df(16)A<sup>+/−</sup>* mice across this transition (Condition I-Day 3 to Condition II-Day 1) we found that place fields in WT mice were significantly more stable than in *Df(16)A<sup>+/−</sup>* mice ( $p=0.0055$ ; Figure 4.21a). Since this change of local cues from Condition I to Condition II dissociates ‘position’ relative to the sequence of fabrics and ‘position’ relative to the cues, we looked at coding of space relative to these two distinct reference frames in the WT and *Df(16)A<sup>+/−</sup>* mice. First, we looked at all the place cells that were active near a cue on the last day of Condition I and asked if on the first day in Condition II it fired closer to that same cue (‘cue-preferring’) or the position relative to the fabric sequence where the cue was previously (‘position-preferring’, see Methods). We found a significantly different distribution of cue-preferring and position-referring cells between WT and *Df(16)A<sup>+/−</sup>* mice ( $p<0.0001$ ; Figure 4.21b), with notably fewer position-preferring cells in the *Df(16)A<sup>+/−</sup>* mice and a significantly lower ratio of cue- to position-preferring cells ( $p=0.0131$ ; Figure 4.21c). Again, importantly, in Condition II the location of the hidden reward does not change relative to the fabric sequence, so the lack of cells that track ‘position’ in the *Df(16)A<sup>+/−</sup>* mice is consistent with the increased disruption in task performance and the decreased stability of the population relative to the fabric sequence in the *Df(16)A<sup>+/−</sup>* mice. Thus, we see that changes to the non-spatial context and the shuffling of local cues induced remapping and disrupted the stability of spatial maps in *Df(16)A<sup>+/−</sup>* mice significantly more than in WT mice, and in particular, fewer cells remained anchored to the belt reference space.

#### **4.2.9 Task-dependent stabilization of place cells is impaired in *Df(16)A<sup>+/−</sup>* mice**

To better understand the conditions in which place cell stability is affected in the *Df(16)A<sup>+/−</sup>* mice, we next aimed to separate baseline place cell stability from the demands of a spatial learning task. In a separate random foraging (RF) paradigm, where there is no learning of a particular reward po-

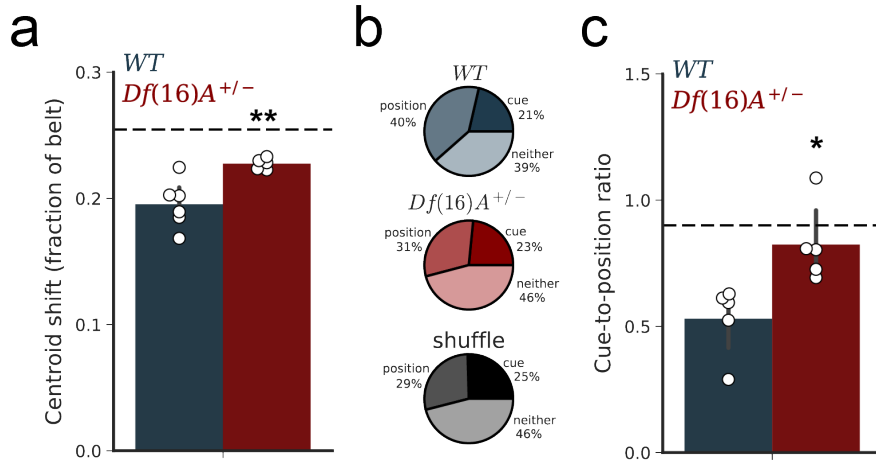


**Figure 4.21:** a. Mean centroid shift from the last day of Condition I to the first day of Condition II (WT:  $0.195 \pm 0.008$ , n=6;  $Df(16)A^{+/-}$ :  $0.227 \pm 0.002$ , n=5; independent samples T-test:  $t=-3.626$ ,  $p=0.0055$ ). b. Fraction of all cells classified as place-preferring, cue-preferring, or neither (pooled across mice) for WT,  $Df(16)A^{+/-}$  and shuffled data (Pearson chi-square test:  $\chi^2=85.7776$ ,  $p<0.0001$ ). c. Ratio of the number of cue-preferring to place-preferring cells per mouse for WT and  $Df(16)A^{+/-}$  mice (independent samples T-test:  $t=-3.172$ ,  $p=0.0131$ ). \* $p<0.05$ , \*\* $p<0.01$

sition involved, we trained water-deprived mice to run head-fixed on a similar cue-rich belt. In this task the reward schedule was changed such that water was presented to the mice probabilistically as they ran, independent of both position on the belt and whether or not they lick (Figure 4.22a). From day-to-day, preferred firing locations were more stable than expected by chance in both WT and  $Df(16)A^{+/-}$  mice (WT:  $0.222 \pm 0.004$ , n=30 session pairs;  $Df(16)A^{+/-}$ :  $0.220 \pm 0.004$ , n=42 session pairs; shuffle:  $0.244 \pm 0.002$ , n=72; WT vs. shuffle:  $p<0.0001$ ;  $Df(16)A^{+/-}$  vs. shuffle:  $p<0.0001$ ), but in contrast to during the GOL task, they were not significantly different from each other (WT vs  $Df(16)A^{+/-}$ :  $p=0.653$ ; Figure 4.22b). More specifically, the WT spatial tuning is significantly stabilized in the GOL task while the  $Df(16)A^{+/-}$  spatial tuning is not (two-way ANOVA, Genotype  $\times$  Task interaction,  $p=0.0322$ , main effects, n.s.; WT, GOL vs. RF:  $p=0.022$ ;  $Df(16)A^{+/-}$ , GOL vs. RF:  $p=0.579$ ; Figure 4.22c). This suggests that the presence of a spatially-salient reward location selectively stabilizes hippocampal spatial masks in WT mice, a phenomenon absent from  $Df(16)A^{+/-}$  mice.

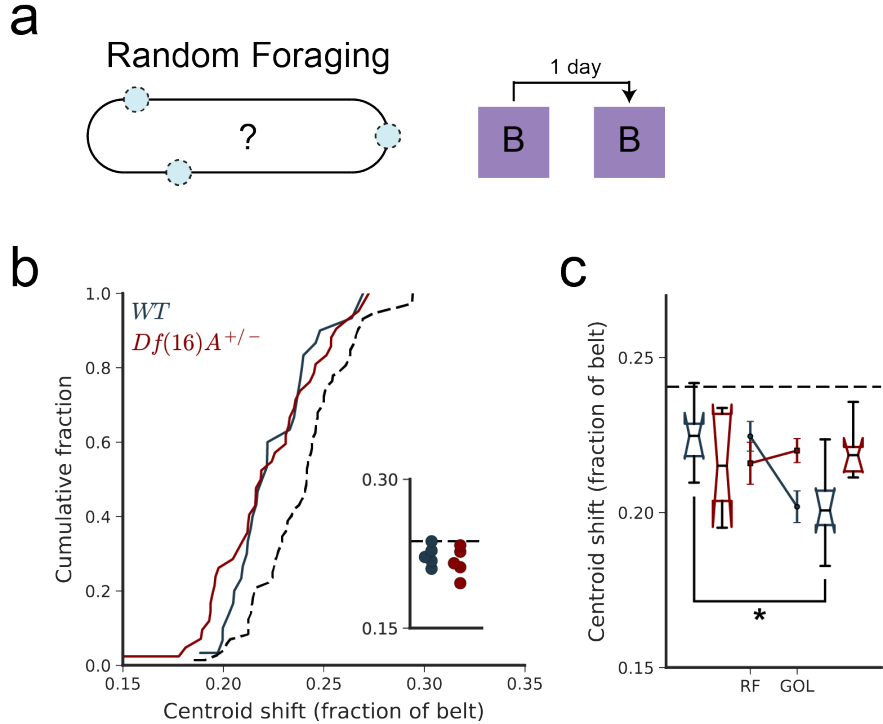


**Figure 4.22:** a. Schematic of Random Foraging (RF) task. Rewards are presented randomly throughout the belt in the same context: same belt fabric sequence, different auditory, visual, olfactory, and tactile cues. b. Distribution of mean centroid shift per session from day-to-day during Random Foraging task (dotted line is cell-identity shuffled distribution; WT:  $0.222 \pm 0.004$ , n=30 session pairs; *Df(16)A<sup>+/−</sup>*:  $0.220 \pm 0.004$ , n=42 session pairs; shuffle:  $0.244 \pm 0.002$ , n=72; WT vs. shuffle: independent sample T-test:  $t=-5.05$ ,  $p<0.0001$ ; *Df(16)A<sup>+/−</sup>* vs. shuffle: Welch's T-test,  $t=-5.12$ ,  $p<0.0001$ ; WT vs *Df(16)A<sup>+/−</sup>*: independent samples T-test:  $t=0.451$ ,  $p=0.653$ ) and aggregated by mouse (inset, gray bar is cell-identity shuffle; WT vs. *Df(16)A<sup>+/−</sup>*: independent samples T-test:  $t=0.799$ ,  $p=0.448$ ). c. Comparison of mean centroid shift per mouse in the RF and GOL tasks (GOL data replotted from Figure 4.13b; two-way ANOVA, Genotype  $\times$  Task interaction,  $p=0.0322$ , main effects, n.s.; WT, GOL vs. RF:  $p=0.022$ ; *Df(16)A<sup>+/−</sup>*, GOL vs. RF:  $p=0.579$ ). \* $p<0.05$ .

#### **4.2.10 Enrichment of goal location by place cells in WT, but not *Df(16)A<sup>+/−</sup>* mice**

Place maps incorporate goal-related information during learning (Breese et al., 1989; Dupret et al., 2010b; Fyhn et al., 2002; Gothard et al., 1996; Hok et al., 2007; Hollup et al., 2001a; Kobayashi et al., 1997), and over-representation of goal locations by place cells has been shown to correlate with learning performance during goal-directed spatial learning tasks (Dupret et al., 2010a; Hollup et al., 2001a). While we did not observe place cell enrichment during initial goal learning in a novel context (Condition I) or the subsequent change of context (Condition II), upon learning of the new reward location in an already familiar context (Condition III), we found robust organized remapping of place cells towards the new reward location in WT mice, though this goal-directed reorganization was strikingly absent in *Df(16)A<sup>+/−</sup>* mice (two-way RM ANOVA: Genotype × Condition × Day interaction:  $p<0.0001$ ; Conditions I & II: no significant effect of Genotype:  $p=0.749$  and  $p=0.065$ , respectively; Condition III, Genotype × Day interaction:  $p<0.0001$ ; main effect of Genotype:  $p=0.002$ ; post-hoc analysis with Bonferroni correction for multiple comparisons, Day 3:  $p<0.0001$ ; Figures 4.23 & 4.24). Additionally, we found that the magnitude of place cell enrichment at the goal location correlated with learning performance in WT mice (Pearson Correlation,  $Z=0.362$ ,  $p=0.023$ ; Figure 4.25) but not in *Df(16)A<sup>+/−</sup>* mice (Pearson Correlation,  $Z=-0.068$ ,  $p=0.791$ ; Figure 4.25). The lack of enrichment during certain phases of our GOL task – Conditions I and II for WT mice and all Conditions for *Df(16)A<sup>+/−</sup>* mice – suggests that the learning performance is primarily determined by the initial formation and maintenance of stable spatial maps during these Conditions (see Figures 4.12, 4.13, & 4.14), though an alternative, improved, goal-enrichment strategy is available to WT mice. Thus, place cell enrichment supports learning of new reward locations in a familiar context in WT animals, while in *Df(16)A<sup>+/−</sup>* mice enrichment does not influence task performance, which may account for their significantly worse performance during this phase of the GOL task.

#### **4.2.11 WT place fields shift towards the new reward location**

Several aspects of place cell population dynamics may explain the enrichment of firing fields at the goal location in the familiar context, for example: place cells within the reward zone may be more likely to recur as place cells with stable place fields; existing place fields may shift towards

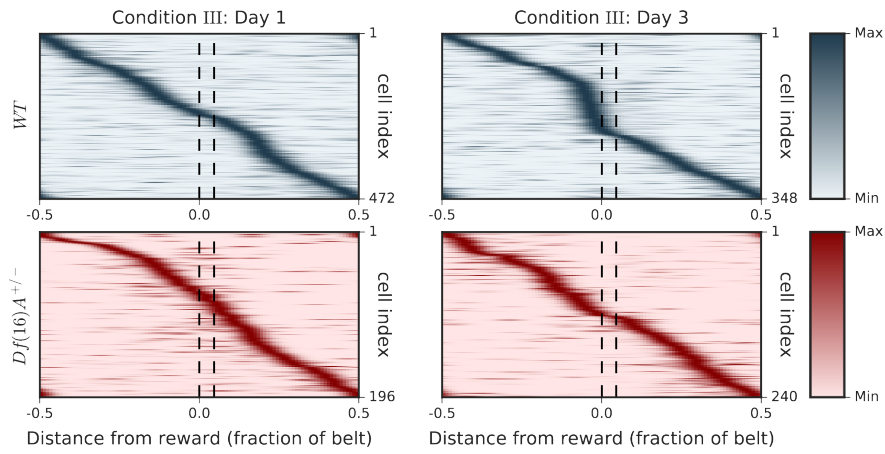


**Figure 4.23:** Tuning profiles for all place cells in both WT and  $Df(16)A^{+/-}$  mice on the first and last day of Condition III. Each row is an individual place cell. The intensity corresponds to the normalized transient rate in each spatial bin along the  $x$ -axis. Goal location is between dotted lines. WT mice show more place cells near the reward by day 3, an enrichment lacking in  $Df(16)A^{+/-}$  mice.

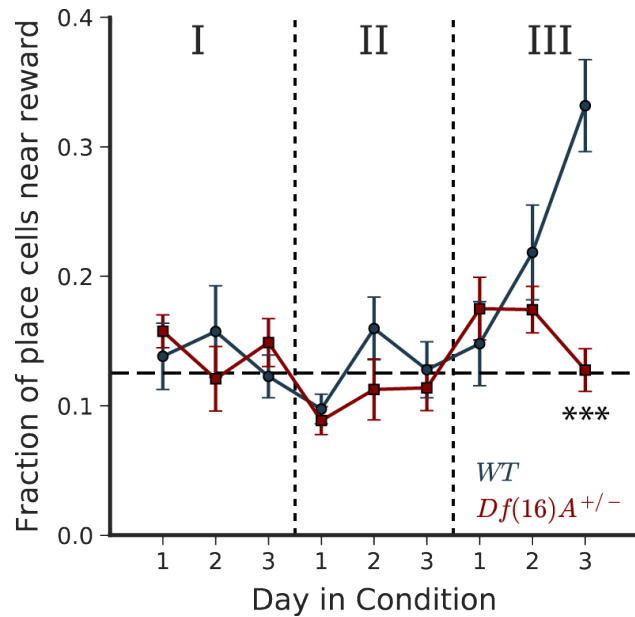


**Figure 4.24:** Fraction of place cells near the goal location (within  $\frac{1}{16}$  of the belt length) across all days of the experiment. Dotted line is uniformly distributed fraction (two-way RM ANOVA: Genotype  $\times$  Condition  $\times$  Day interaction:  $F(4,124)=10.684$ ,  $p<0.0001$ ; Condition I & II: no significant effect of Genotype:  $F(1,31)=0.104$ ,  $p=0.749$  and  $F(1,31)=3.668$ ,  $p=0.065$ ; Condition III: Genotype  $\times$  Day interaction:  $F(2,62)=18.149$ ,  $p<0.0001$ ; main effect of Genotype:  $F(1,31)=12.051$ ,  $p=0.002$ ; post-hoc analysis with Bonferroni correction for multiple comparisons, Day 3:  $t=4.669$ ,  $p=0.00017$ ). \*\*\* $p<0.001$

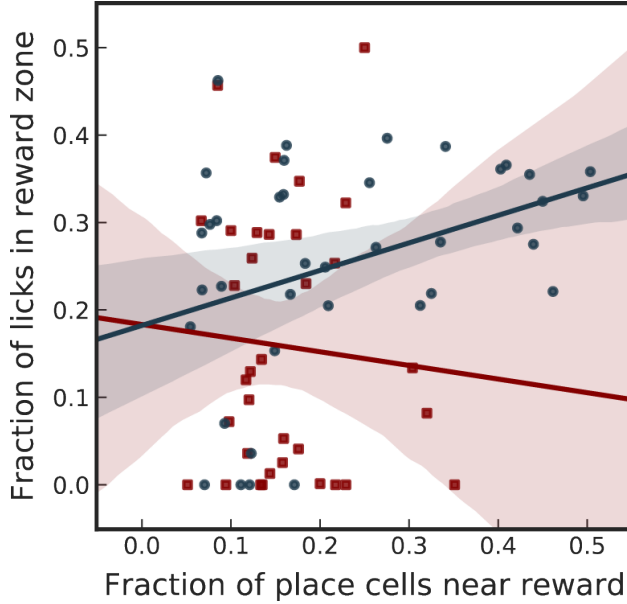


**Figure 4.25:** Place cell goal-zone enrichment correlation with task performance during Condition III in WT, but not *Df(16)A<sup>+/−</sup>*, mice (WT: Pearson Correlation: 0.362, p=0.023; *Df(16)A<sup>+/−</sup>*: Pearson Correlation: -0.068, p=0.791). Linear regression and confidence intervals as in Figure 4.12c.

the reward (Lee et al., 2006b); or place fields at the reward location may be selectively stabilized compared to place fields farther away (Figures 4.26 & 4.27). In order to distinguish between these possibilities, we used WT mouse data from sessions during Condition III to calculate the session-to-session place cell recurrence probability as well as the mean and variance of the place field centroid shift, as a function of the original place field's distance from the reward location (see subsubsection 4.4.11.5). We found a slight increase in recurrence probability of place cells that were active immediately preceding the reward (Figure 4.28), though this effect is not strong enough to lead to reward location enrichment (see below). Interestingly, place fields drifted towards a location on the belt just after the reward zone, such that fields preceding it tended to shift forwards and fields following it tended to shift backwards (Figure 4.29a,b). In addition, place fields just after the reward location shifted more consistently, as evidenced by a relatively lower place field shift variance (Figure 4.29a,c).

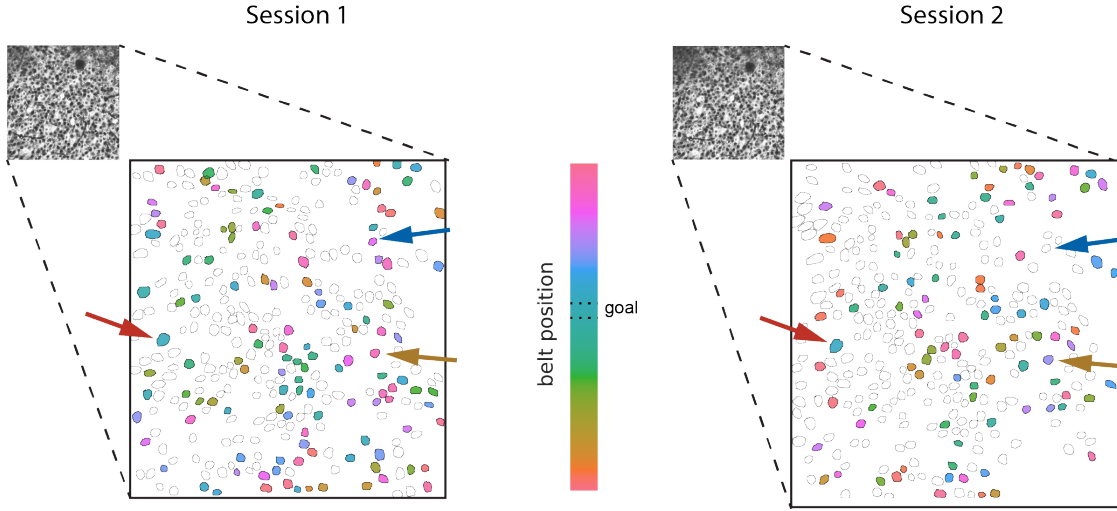


**Figure 4.26:** Example fields of view from two consecutive sessions. Background is time-averaged GCaMP6f movie. Place cells are colored corresponding to their spatial tuning within each session. The color bar shows the mapping of place field location on the belt. The reward zone for these sessions was between the dotted lines. Place fields are generally stable (red arrow), but some shift their place field (yellow arrow), while others stop being spatially active (blue arrow).

#### 4.2.12 Modeling of place cell dynamics suggests that place fields shift is the primary factor leading to reward enrichment

To determine the effect of these place fields stability properties on population-level spatial coding we next built a simple model of place cell stability and goal-oriented remapping. Our model assumes that every cell has a preferred spatial tuning each day, which is either latent (non-place cell) or expressed as significant spatial activity (place cell). This assumption is supported by the observation that even when a cell is not identified as a place cell, it retains a ‘memory’ of the last time it was spatially active; firing closer to the old place field than expected by chance. Specifically, for all place cells from pairs of experiments separated by one session, the mean place field centroid shift variance between those two sessions was independent of the spatial information in the middle session (Figure 4.30).

At each iteration (similar to 1 elapsed session) of the model (Figure 4.31) non-place cells transition to place cells with a fixed probability calculated from the data ( $P_{on}$ ) and place cells recur as place cells with the position-dependent recurrence probability calculated above ( $P_{recur}(x_i)$ , see Figure 4.28). Additionally, all cells shift their preferred spatial tuning direction and the new firing position is randomly drawn from a von Mises distribution with position-dependent offset ( $\mu(x_i)$ ,

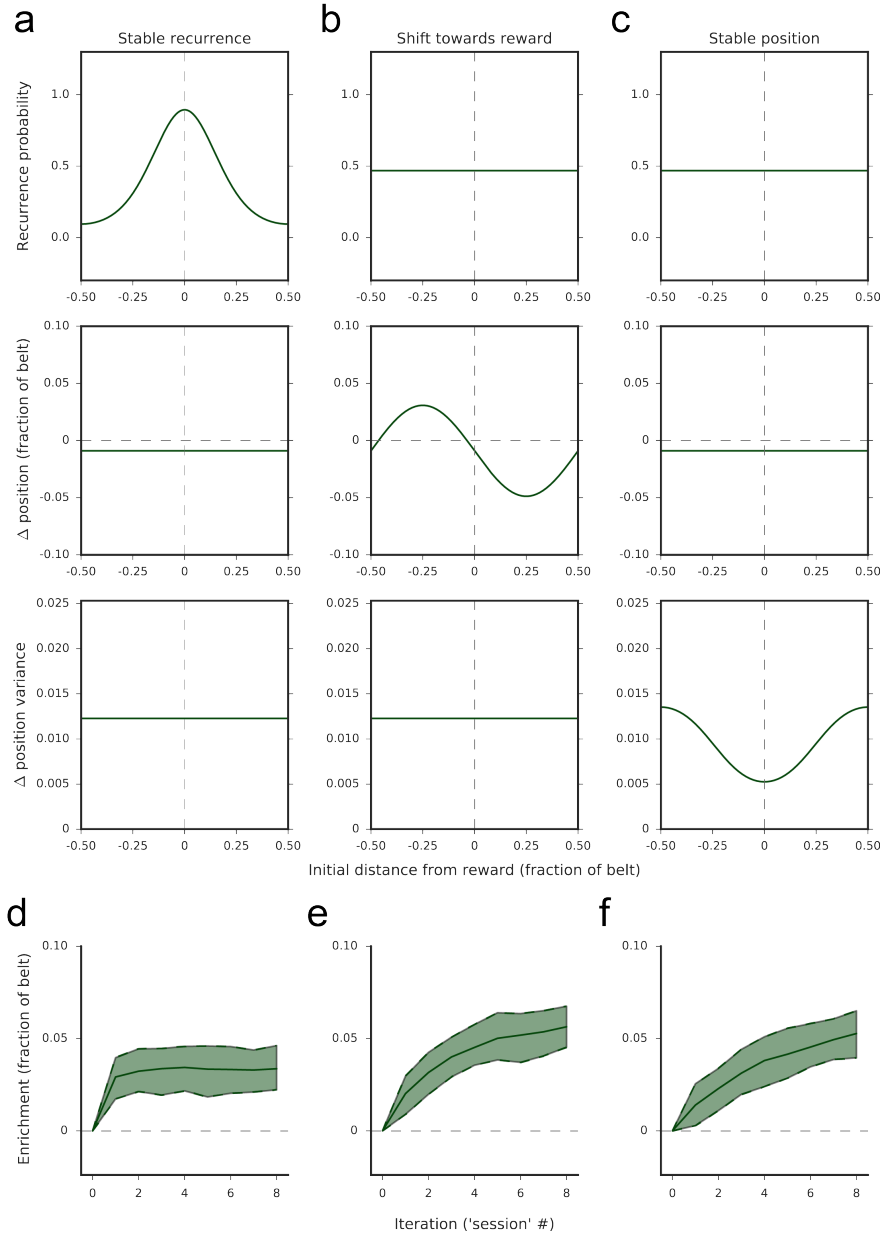


**Figure 4.27:** Comparison of three theoretical methods by which place cells could enrich a goal location. a. Place fields could be generally stable, but place cells near the reward are more likely to reoccur as place cells from session-to-session. (top) Recurrence probability as a function of distance from reward. (middle) Mean place field centroid shift as a function of distance from reward. (bottom) Mean place field shift variance as a function of distance from reward. b. Place cells could reoccur at equal probability along the belt, but place fields shift towards the reward location such that fields before the reward shift forward and fields after the reward shift backwards. Plots as in a. Place fields shifting towards the reward also leads to enrichment in our model. c. Place fields might not shift uniformly towards the reward, but if fields are generally stable, the ones near the reward could shift less than ones farther away. Plots as in a. d-f. Using the parameters from a-c, our enrichment model suggests all three hypothetical models could lead to enrichments: (d) increased place cell recurrence at reward position, (e) place fields shifting towards the reward location, or (f) place fields near the reward shifting less than ones away from the reward.

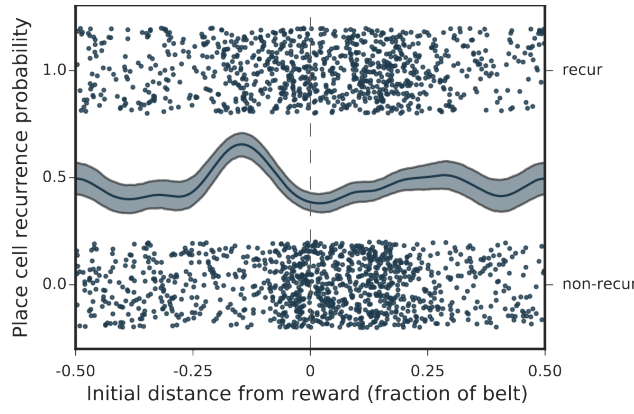


**Figure 4.28:** Recurrence probability as a function of original distance from the reward. For all pairs of consecutive sessions during Condition III, each place cell during the first session is plotted with the centroid of its place field along the  $x$ -axis and whether or not it was also a place cell in the second session on the  $y$ -axis (top cluster is place cell in second session, bottom cluster is not a place cell, random  $y$ -axis jitter within each cluster for visualization). Cyclic logistic regression fit with 95% confidence interval from cross-validation plotted on left axis.

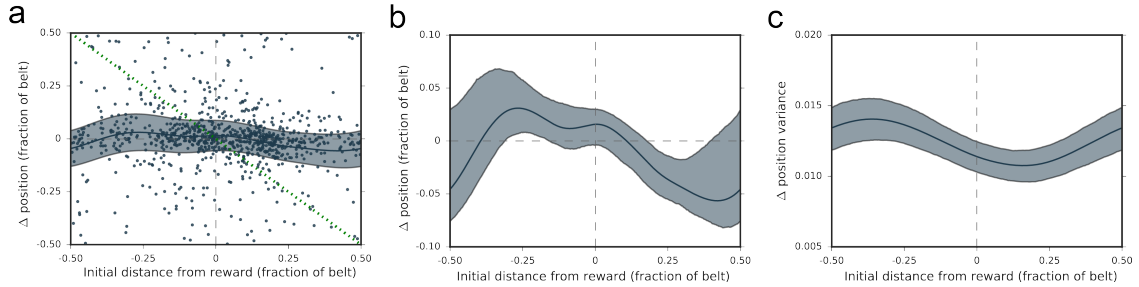


**Figure 4.29:** a. Session-to-session place field shift as a function of original distance from the reward. For all pairs of consecutive sessions during Condition III, each place cell during the first session is plotted with the centroid of its place field along the  $x$ -axis and the change in centroid position in the second session along the  $y$ -axis. Data is fit as a continuous series of von Mises distributions for each position, with the offset (solid line) and variance ( $\frac{1}{\kappa}$ , where  $\kappa$  is the concentration parameter) shown. Green dotted line denotes cells that move directly to the reward position in the second session. b. Same offset curve (solid line, shaded region is 90% confidence interval calculated from refitting bootstrap resampled data) as in a. Positive values to the left of the zero-crossing and negative values to the right correspond to drift towards the reward position. c. Same variance fit as in a. (shaded region represents 90% confidence interval calculated from refitting bootstrap resampled data) plotted independently. Place field shift is most consistent (minimum variance) at a position that corresponds to the most stable place field location from b, just after the goal location.

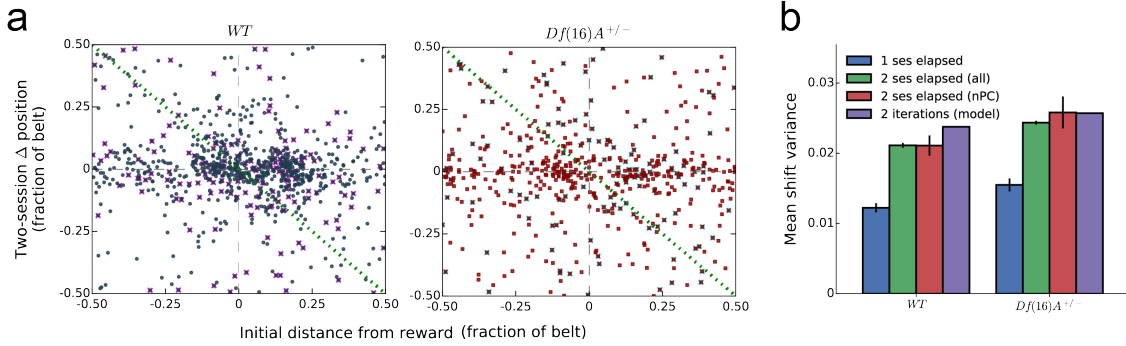


**Figure 4.30:** a. Scatter plots of original position versus position shift after 2 elapsed sessions for WT and  $Df(16)A^{+/-}$  mice. Cells that were not a place cell in the middle session are marked in magenta and cyan for WT and  $Df(16)A^{+/-}$  data, respectively. Even cells that were not a place cell in the intervening session still cluster around 0, suggesting that they retain some latent place preference that is either not expressed or not detectable. Vertical dashed line denotes reward location. Horizontal dashed line marks fields that do not shift at all. Green diagonal dashed line marks fields that remap directly to the reward location. b. Mean place field shift variance across all positions for cells paired by 1 session elapsed, 2 sessions elapsed, 2 sessions elapsed for cells that were not a place cell in the intervening session, and 2 iterations of the model. Two-session elapsed place cells are equally stable whether or not the cell was a place cell in the middle session, which is also the same as two iterations of the model.

see Figure 4.29b) and concentration ( $\kappa(x_i)$ , see Figure 4.29c).

By simulating the same number of session transitions as in our experimental paradigm we see the gradual enrichment of the goal location similar to the observed enrichment that we saw in the WT mice during Condition III (Figure 4.32). In contrast, when we fit the model from data taken from Condition I or II, we do not see enrichment of the reward location, in agreement with the experimental data (Figure 4.33). To assess which particular factor is driving goal enrichment, we created a *flat* model for comparison by setting each of the position-dependent model parameters equal to the mean across all positions, effectively removing the dependence on the distance to reward by flattening out the fits, and as expected, with these parameters we do not see any enrichment (Figure 4.32). We next swapped parameters one-by-one between our WT model and *flat* model and re-ran the simulation, so as to see the effect of each parameter on the final goal enrichment. Flattening out either the recurrence probability or the place field shift variance resulted in very little change to the final level of place field enrichment with otherwise WT parameters. In contrast, by flattening out the place field shift, the population enrichment of the reward location completely disappeared (Figures 4.34 & 4.35). In addition, if we take the *flat* model and only replace the place field shift with the WT fit, we now see place field enrichment of the goal location (Figure 4.34a).

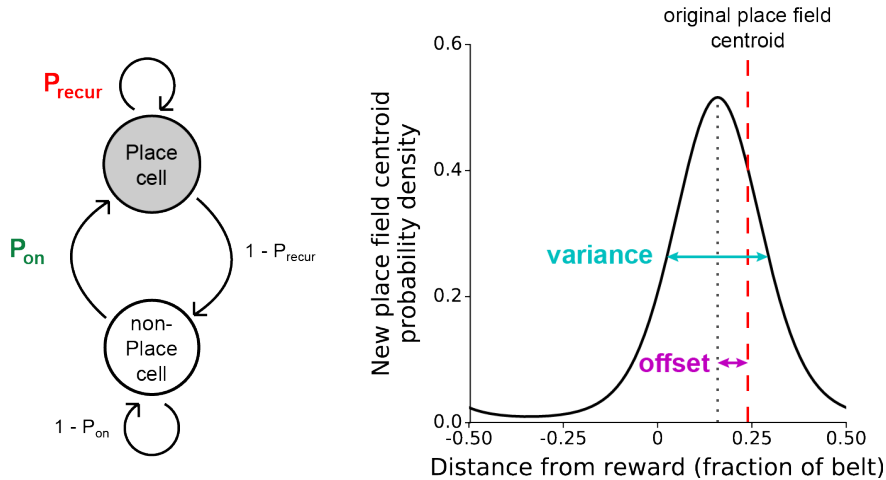


**Figure 4.31:** Schematic of place cell recurrence (left) and stability (right) model including the four parameters that were fit from our data: non-place cell-to-place cell transition probability ( $P_{on}$ ), place cell recurrence probability by position ( $P_{recur}$ ), session-to-session place field shift variance, and session-to-session place field shift offset.

We conclude that place field enrichment of goal locations is driven by an active recruitment of place fields shifting coherently towards the reward location.

#### 4.2.13 Modeling of place cell dynamics corroborates the absence of enrichment in the $Df(16)A^{+/-}$ mice through lack of place field shift towards reward

While we saw robust place field enrichment of the reward location in WT mice following a change in the reward location, population enrichment was completely absent in  $Df(16)A^{+/-}$  mice. In order to gain insight into the lack of enrichment, we calculated the recurrence probability, place field shift, and place field shift variance as a function of distance from reward during Condition III with the  $Df(16)A^{+/-}$  data, as we did with the WT data. All three parameters show no dependence on position for the recurrence probability, place field shift, or the place field shift variance (Figure 4.36a-d). Consistent with previous studies (Mehta et al., 1997) across the entire belt on average place fields shifted slightly backwards (Figure 4.36c) and when we simulated session-to-session place field shifts with our model we do not see any enrichment of the goal location (Figure 4.36e,f). We conclude that while WT place fields shift toward the reward location, leading to an over-representation of this location, this effect is disrupted in  $Df(16)A^{+/-}$  mice.

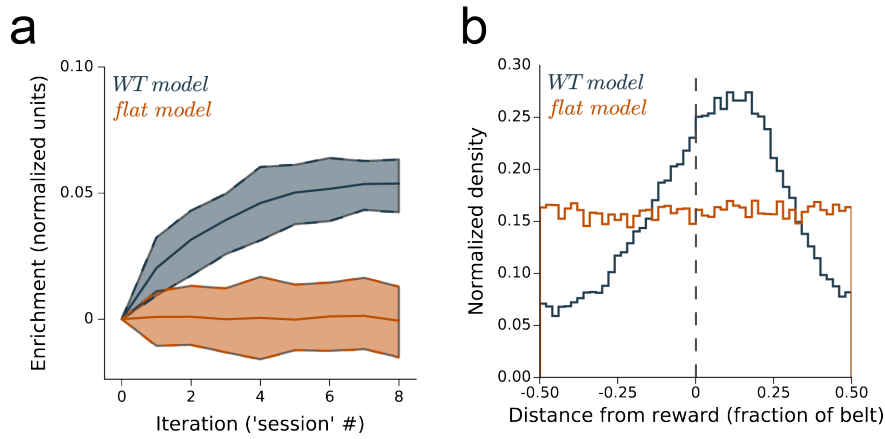


**Figure 4.32:** a. Mean population enrichment by simulated iteration for WT and *flat* parameter sets ( $\pm 90\%$  confidence intervals from 100 simulations). WT parameters reproduce the enrichment observed during Condition III. b. Final distribution of place fields after 8 iterations for WT and *flat* parameters. Vertical dashed line denotes reward location.

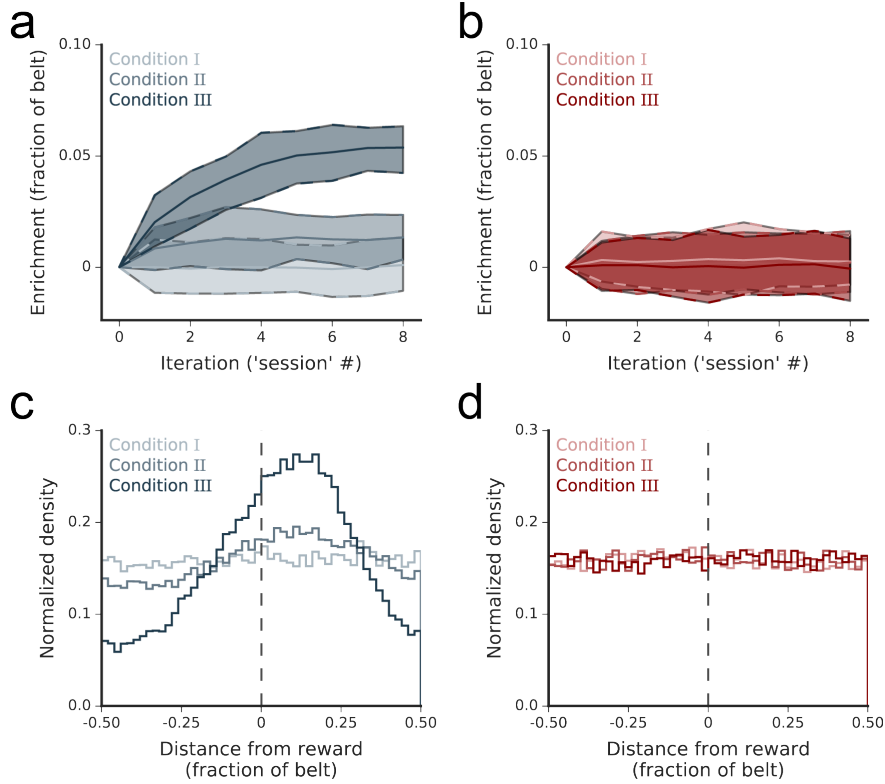


**Figure 4.33:** Our model of place cell enrichment only produces goal location enrichment with parameters fit from WT mice during Condition III. a,b. Enrichment by iteration with parameters fit from each of the three Conditions of the task for (a) WT and (b) *Df(16)A<sup>+-</sup>* mice (as in Figures 4.32a & 4.36e). c,d. Final distribution of place fields after 8 iterations for each set of parameters fit from (c) WT and (d) *Df(16)A<sup>+-</sup>* mice (as in Figures 4.32b & 4.36f).

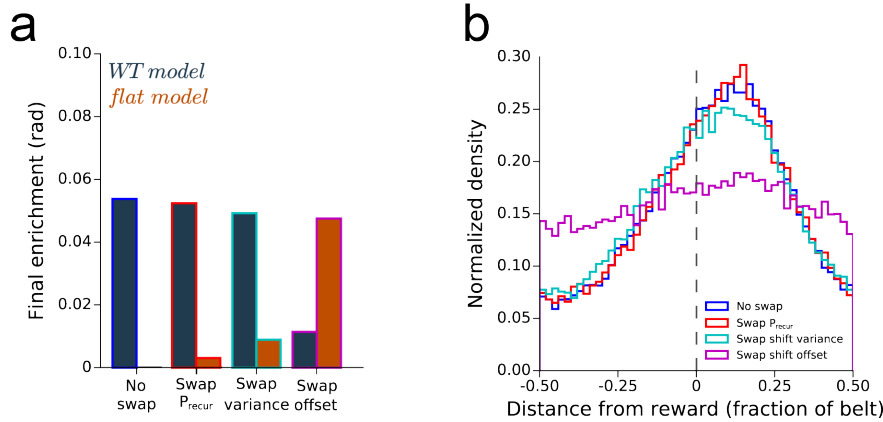


**Figure 4.34:** a. Mean population enrichment after 8 iterations with true fit parameters and then swapping each set of position-dependent parameters individually between WT and *flat*: recurrence probability ( $P_{recur}$ ), place field shift variance, and place field shift offset. b. Final WT place field distributions after 8 iterations with the same parameter swaps as in a. Mean place field shift (offset) toward the reward is revealed as the main factor underlying enrichment in GOL.

### 4.3 Discussion

Our study provides the first comparative characterization of learning-related neural population dynamics in the hippocampus with chronic cellular-resolution functional imaging in wild-type and mutant mice carrying a SCZ-predisposing genetic lesion. We found that mice carrying the 22q11.2 deletion, one of the strongest genetic risk factors for cognitive dysfunction and SCZ, exhibit compromised stability and plasticity of hippocampal place cell maps during spatially guided reward learning. Broadly interpreted, our results provide further insight into the normal roles of neuronal ensemble stability and plastic reorganization under specific learning conditions. Further, we show that genetic mutations predisposing to neuropsychiatric and cognitive disorders can lead to learning deficits through disruptions in these fundamental features of hippocampal population dynamics.

#### 4.3.1 Hippocampal place cell dynamics depend on both the task and the specific task parameters in goal-directed learning

Long-term stability of hippocampal spatial representation is a widely posited prerequisite for reliable spatial learning (Kentros et al., 2004; Lever et al., 2002a; Mankin et al., 2012; Thompson & Best, 1990; Ziv et al., 2013). By tracking hippocampal place cell dynamics over different phases of a multiday learning task, our study extends previous findings by showing a positive correlation

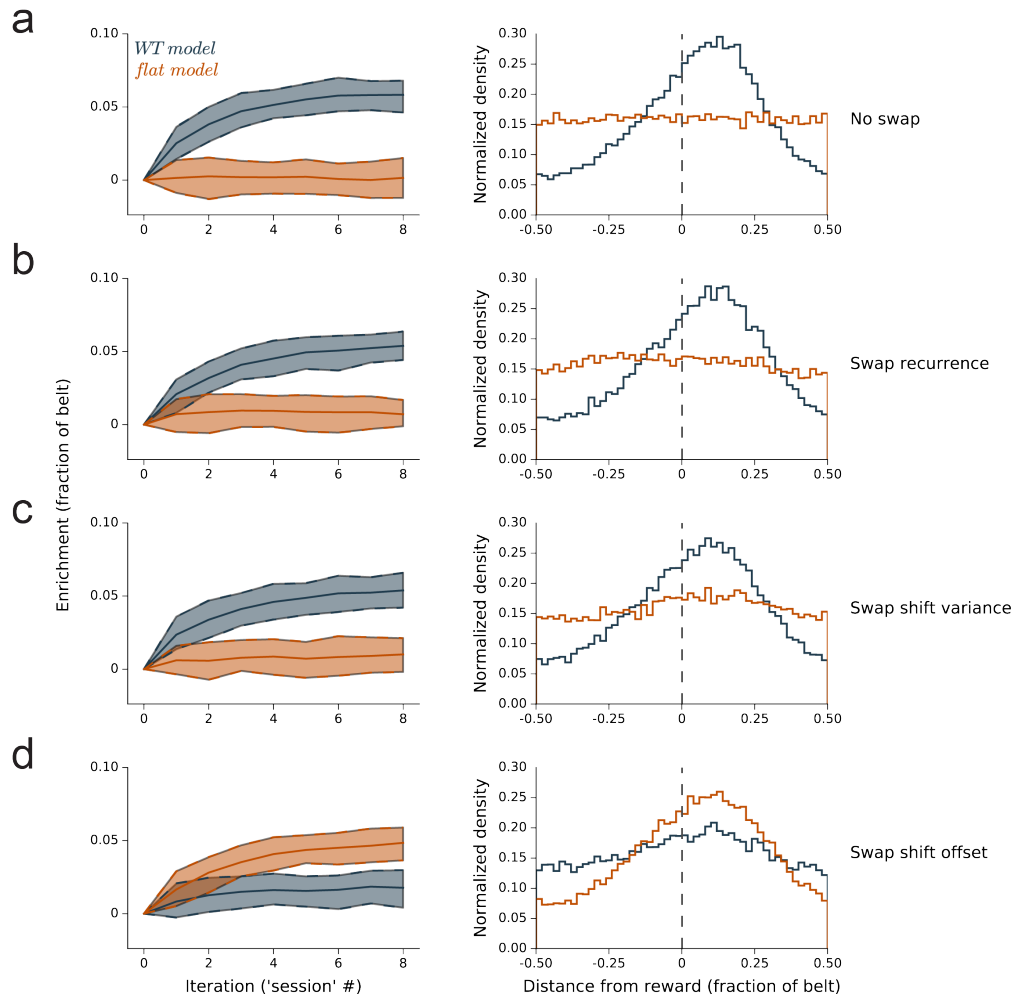


**Figure 4.35:** Mean enrichment by iteration (left, 90% confidence interval shading determined from 100 simulations) and histogram of distributions of place fields after the final iteration (right, data pooled across all simulations, vertical dashed line denotes reward location) for each parameter individually swapped between WT and *flat* models. a. No swap. b. Swap place cell recurrence probability ( $P_{recur}$ ). c. Swap session-to-session place field shift variance. d. Swap session-to-session place field shift offset. Swapping shift offset has the largest effect, as the *flat* model with only the WT shift offset parameters leads to enrichment, while the WT model with the *flat* shift offset parameters does not.

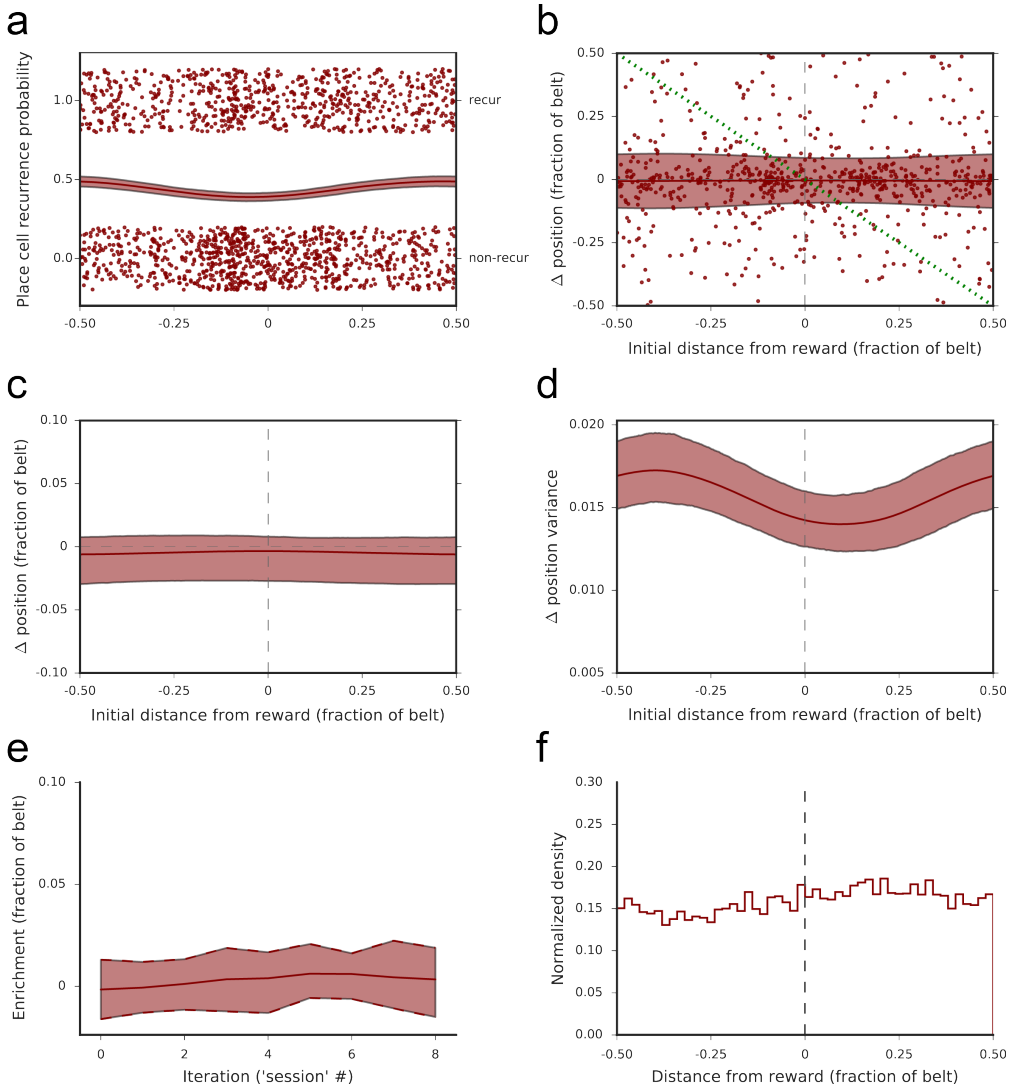


**Figure 4.36:** a. Place cell recurrence by distance from reward as in Figure 4.28. b. Session-to-session place field shift as a function of original distance from the reward as in Figure 4.29a. c,d. Place field shift and variance fits from b as in Figure 4.29b,c (shaded region is 90% confidence interval calculated from refitting bootstrap resampled data). e. Unlike WT model, enrichment model with  $Df(16)A^{+/-}$  parameters shows no enrichment (see Figure 4.32a). f. Final distribution of place fields after 8 iterations for  $Df(16)A^{+/-}$  parameters.

between place cell map stability and learning performance in both WT and *Df(16)A<sup>+/−</sup>* mice (see Figures 4.12c, 4.13c, & 4.14c). Indeed, task performance and spatial map stability for each genotype followed a similar trajectory as task demands changed; more specifically, task performance and stability were most similar during Condition I, *Df(16)A<sup>+/−</sup>* mice were slightly impaired in Condition II, and the largest difference was observed in Condition III (see Figure 4.15). These findings strongly suggest that the neural coding strategy employed during all phases of a spatial reward learning task relies on the formation and maintenance of stable hippocampal representations, both in terms of place cell identity and place field location. Our results also show task-dependent stabilization of spatial maps in WT mice, as WT place fields were significantly more stable in the GOL task than during random foraging, an effect possibly mediated by the attentional demands of GOL (Kentros et al., 2004; Kobayashi et al., 1997; Markus et al., 1995; Monaco et al., 2014). In contrast, place field stability between GOL and RF tasks was indistinguishable in *Df(16)A<sup>+/−</sup>* mice, indicative of a failure to conditionally stabilize spatial maps instrumental in finding rewarded locations (see Figure 4.22c). However, *Df(16)A<sup>+/−</sup>* mice were comparable to WT littermates in their ability to initially learn a reward location, as well as in baseline place cell stability, which suggests that the *Df(16)A<sup>+/−</sup>* learning deficit was related to the stabilization and rearrangement of spatial maps in response to changing task demands (Condition I, see Figures 4.3, 4.4, & 4.15).

Our results also suggest that the memory deficit throughout the GOL task may result from impaired consolidation processes. *Df(16)A<sup>+/−</sup>* mice were capable of solving this task, but they were significantly impaired at the beginning of each day (Figure 4.7) and spatial maps are significantly less stable overnight, compared to the WT mice (Figures 4.12b, 4.13b, & 4.14b). In that respect, the altered SWR activity we observe in the *Df(16)A<sup>+/−</sup>* mice may underlie the decreased stability of spatial maps. SWRs are thought to support reactivation and consolidation of memories of previous experiences and planned future experiences (Buzsaki, 2015; Diba & Buzsaki, 2007; Foster & Wilson, 2006; Jadhav et al., 2012; Kudrimoti et al., 1999), and the strength of SWR-related reactivation has been shown to correlate with subsequent memory expression (Dupret et al., 2010a). Although we did not directly assess place cell reactivation, the increased rate of SWRs we observe in the *Df(16)A<sup>+/−</sup>* mice could reflect either a failure to selectively reactivate task-related representations, or a compensatory mechanism, as aberrant SWRs are not efficiently consolidating task memories. Relatedly, abnormalities in hippocampal place cell dynamics found in *Df(16)A<sup>+/−</sup>* mice

may reflect the inefficient replay of place cell firing patterns during rest or sleep, a phenomenon causally linked to spatial memory consolidation (de Lavilleon et al., 2015). The increased rate of SWRs in *Df(16)A<sup>+/−</sup>* mice is similar to the effect seen in calcineurin knockout mice and in mice expressing dominant negative DISC1, both of which have behavioral phenotypes reminiscent of SCZ (Altimus et al., 2015; Suh et al., 2013), indicating that these alterations are common features across genetically distinct mouse models of SCZ.

Our results also indicate that distinct hippocampal coding strategies may be employed under varying task demands. Learning of a reward location in novel environments was primarily supported by the stability of spatial maps, while learning of a change in reward location in an otherwise familiar environment was additionally dependent on the plasticity of these maps, as place cells shift toward the new reward location in WT mice (Figure 4.34). Here it is important to consider that prior studies of goal-directed spatial learning were mostly performed in familiar environments (Breese et al., 1989; Dupret et al., 2010a; Fyhn et al., 2002; Hok et al., 2007; Hollup et al., 2001a; Kobayashi et al., 1997), in which animals were habituated to the experimental settings prior to testing. Our results here are in line with previous observations showing that prominent changes in place cell firing in response to goal or reward occur when the pattern of the reinforcement was changed in the same environment (Breese et al., 1989; Fyhn et al., 2002; Kobayashi et al., 1997; Markus et al., 1995), and in particular, following translocation of a reward location (Breese et al., 1989; Kobayashi et al., 1997). Of particular note is the work by Hollup et al., where place field enrichment was found during the probe trial in an annular water maze task, and the study by Dupret et al., in which goal-enrichment was tested following several trials in the same maze. As learning demands change across conditions in our task – from learning in a novel context (Condition I); maintaining the reward memory after contextual manipulation (Condition II); and learning a new reward location in a familiar context (Condition III) – the neural correlates of learning are also expected to change. Previous literature has also demonstrated that place fields undergo experience-dependent stabilization over multiple days during the transition from a novel to familiar context (Cacucci et al., 2007; Frank et al., 2004; Hill, 1978; Karlsson & Frank, 2008; Leutgeb et al., 2004; Wilson & McNaughton, 1993). Therefore, one potential explanation for the lack of reward-related enrichment during Conditions I and II is that goal-directed place cell dynamics are obscured by conflicting demands related to the formation of a stable contextual

representations. Additional changes within a stabilized, or well encoded, context, such as the incorporation of reward-related information, could occur through goal-directed reorganization of place fields, resulting in overrepresentation of place fields near the reward in WT mice (see Figures 4.24 & 4.33). This interpretation is consistent with previous studies demonstrating the effect of environmental novelty on experience-dependent shifts and directionality of CA1 place fields (Mehta et al., 1997; Navratilova et al., 2012; Roth et al., 2012; Lee & Knierim, 2007), and more broadly, with the proposed role of CA1 in novelty detection (Duncan et al., 2012; Karlsson & Frank, 2008; Larkin et al., 2014; Nitz & McNaughton, 2004; Vinogradova, 2001; Lever et al., 2002b).

We find that wild-type place fields before the reward tended to shift forward, while place fields after the reward shifted backwards during learning of a new reward location in a familiar environment (Figure 4.29a,b). This finding is consistent with prior observation of gradual shift of spatial correlates of neuronal firing toward goal location (Lee et al., 2006a). This slight bias (maximal mean shift of  $\approx 5\%$  of the belt length) was sufficient to produce robust goal zone enrichment (2.5 times more place cells near the reward position than expected by chance, Figure 4.24), which was also captured in our model of place cell dynamics (Figures 4.32 & 4.34). The lack of enrichment in novel contexts and in the *Df(16)A<sup>+/−</sup>* mice in general (Figures 4.24 & 4.33) suggests that conflicting demands of forming stable context representations could interfere with goal-directed place cell dynamics. While it is also possible that a subset of the goal-enriching cells are reward cells that directly follow the reward, the larger effect is the gradual drift of the entire place cell population towards the reward, not the active recruitment of reward cells directly remapping to the reward location (lack of cells clustered around green dotted line, Figure 4.29a). While the higher overall stability and the increased reward-directed remapping in WT mice might seem paradoxical, we actually observed an organized restructuring of firing patterns in WT animals, and the magnitude of these shifts were still less than the disorganized firing pattern changes we observed in *Df(16)A<sup>+/−</sup>* mice.

In contrast to their WT littermates, *Df(16)A<sup>+/−</sup>* mice failed to ever employ this goal location enrichment coding strategy and are significantly delayed in learning the new reward location. The fact that the *Df(16)A<sup>+/−</sup>* mice were still able to improve their behavioral performance despite their lack of goal-related remapping implies that *Df(16)A<sup>+/−</sup>* mice rely on other alternative, albeit less efficient, strategies to find the reward location. Although we find that self-motion generated

information in the absence of external cues is not sufficient for the maintenance of stable firing fields in our task, local cues and fabric segments of the belt which primarily provide a reference frame for allocentric navigation could, in principle, also serve as anchors to reduce error accumulation in path integration (Etienne & Jeffery, 2004; Gothard et al., 1996). *Df(16)A<sup>+/−</sup>* mice did not track position as accurately as WT mice when local cues are shuffled (Condition II, Day 1; see Figures 4.24 & 4.21a) indicating that *Df(16)A<sup>+/−</sup>* mice overly rely on local cues (but not the fabric segments, see Figure 4.17d) and potentially egocentric navigational strategies. While we did not attempt to disentangle the relative contribution of the complementary allocentric and egocentric spatial navigation strategies in our head-fixed task, this interpretation is broadly consistent with the impaired allocentric and intact egocentric memory found in patients with SCZ (Agarwal et al., 2015; Weniger & Irle, 2008). Nonetheless, this topic deserves further exploration.

#### 4.3.2 Potential mechanisms underlying impaired place cell dynamics and learning deficits in *Df(16)A<sup>+/−</sup>* mice

While the precise mechanisms underlying disrupted spatial map stability and plastic reorganization in the *Df(16)A<sup>+/−</sup>* mice remains to be determined, they could result from deficits in local circuit dynamics or in long-range communication, both of which would presumably be attributable to the deficiency of one or more genes in the 22q11.2 locus. The former may be due to local excitatory/inhibitory imbalance, altered synaptic plasticity and NMDA-receptor function, which are known to affect place field stability and spatial learning (Kentros et al., 2004; McHugh et al., 1996; Tsien et al., 1996) and may be related to previously reported anatomical and functional alterations in both pyramidal cells and interneurons in the CA1 subfield of *Df(16)A<sup>+/−</sup>* mice (Drew et al., 2011; Mukai et al., 2008) and in SCZ in general (Coyle, 2012; Crabtree & Gogos, 2014). Such alterations would result in destabilization of synapses and dendritic spines (Fenelon et al., 2013; Mukai et al., 2015), disrupting local assemblies formation in learning (Holtmaat & Caroni, 2016). In addition, long-range communication deficits might involve deviant neuromodulation, as there is a well-characterized dopamine deficit in SCZ patients (Howes & Kapur, 2009) that could underlie aberrant neuromodulatory reward signal.

The observed decrease in the fraction of spatially-tuned cells and altered firing field properties at the neuronal population level, although only partially corroborated in the level of mouse population,

could partially be an additional contributor to the disruption in the processing of spatial information in the pathological hippocampal network of *Df(16)A<sup>+/−</sup>* mice. Nevertheless, the potential relevance of unimodal and narrower place fields we tend to observe in the *Df(16)A<sup>+/−</sup>* mice to the accuracy and capacity of population coding may depend on task demands. Indeed, multiple studies have reported that in larger environments, more neurons are recruited to be place cells, many cells have multiple fields, and place fields are wider compared to small spaces (Fenton et al., 2008; Park et al., 2011; Kjelstrup et al., 2008; Rich et al., 2014). Analogously, in our study, unimodal and narrower place fields may be sufficient to provide an accurate or even improved spatial coding by combining the independent location estimates from individual cells under basal conditions in the *Df(16)A<sup>+/−</sup>* mice. In contrast, during modification of task contingencies, place cells with multiple fields and high rate of spatial information may increasingly contribute to population coding in WT, but not in the *Df(16)A<sup>+/−</sup>* mice. Lastly, larger place fields have been linked to improved memory in Hussaini et al. (2011) where forebrain-specific deletion of HCN1 leads to larger and more stable place fields in the CA1 and enhanced spatial memory, indicating that narrower place fields are not always beneficial for spatial memory. Thus, overall, the decrease in the fraction of spatially-tuned cells and altered firing field properties at the neuronal population level, although only partially corroborated in the level of mouse population, despite not being the primary underlying mechanism of altered place cells population dynamics, could contribute to the disruption in the processing of spatial information in the pathological hippocampal network of *Df(16)A<sup>+/−</sup>* mice.

Affected brain regions in SCZ patients in general, and 22q11.2DS patients and the *Df(16)A<sup>+/−</sup>* mouse model specifically, are not limited to the hippocampus. While in our study we focused on the hippocampal area CA1, altered long-range communication of the hippocampus with other cortical areas is likely to be relevant for the interpretation of learning deficits and the altered place cell dynamics we observed at this main output node of the hippocampus in the *Df(16)A<sup>+/−</sup>* mice. In this respect, it is important to note that these learning deficits were revealed by manipulation of the environmental context and the reward location, conditions requiring cognitive flexibility. A deficit in memory recall, which emerges upon introduction of contextual changes, seems to interfere with the learned information in a genotype specific manner. Sustained stability in WT mice is paired with learning efficiency, while in *Df(16)A<sup>+/−</sup>* mice a decline in performance is associated with decreased stability of spatial maps. In *Df(16)A<sup>+/−</sup>* mice, the decreased fraction of

cells tracking the place reference frame following a shuffling of the local cues during the GOL task (Figure 4.21b,c) suggests a misattribution of salience to irrelevant cues, inducing global remapping in the mutant mice. These behavioral and neuronal abnormalities collectively point to impaired interactions between the prefrontal cortex (PFC) and hippocampus, a feature of both SCZ patients and animal models of SCZ (Sigurdsson & Duvarci, 2015; Mukai et al., 2015; Sigurdsson et al., 2010; Tamura et al., 2016). Bidirectional interactions between the hippocampus and the PFC play a critical role in normal memory processing (Eichenbaum, 2017; Navawongse & Eichenbaum, 2013; Place et al., 2016; Preston & Eichenbaum, 2013; Simons & Spiers, 2003; Miller & Cohen, 2001), as they support cognitive and behavioral flexibility, switching between learned perceptual sets, reversal learning, and rule-guided switching between strategies (Ragozzino et al., 1999b,a; Birrell & Brown, 2000; Mala et al., 2015; Floresco et al., 2008; Rich & Shapiro, 2007). Deficits resulting from impaired cognitive and strategic control of the PFC over hippocampal memory processes are therefore expected to be most apparent under conditions of memory distraction or interference. In this framework, impaired learning performance and reduced place map stability during a context switch may reflect the impaired ability of the mutant mice to ignore the irrelevant dimensions of the context in order to retrieve and maintain the appropriate hippocampal memory of the reward location. Analogously, the prominent learning deficit and lack of goal-directed remapping during the change in reward location may reflect the failure of mutant mice to suppress inappropriate reactivation of the now un-rewarded location and the altered SWR activity in the *Df(16)A<sup>+/</sup>* mice may reflect impaired functional synchronization between the hippocampus and the PFC during memory processing (Jadhav et al., 2016; Jones & Wilson, 2005; Peyrache et al., 2011; Siapas et al., 2005; Sigurdsson et al., 2010; Wierzynski et al., 2009). Together, our findings resemble both the rigid, perseverative behaviors that characterize patients with SCZ (Crider, 1997; Leeson et al., 2009; Morice, 1990), as well as the failure to switch between cognitive strategies seen in spatial, relational and associative inference memory tasks in patients with schizophrenia and psychotic disorders (Armstrong et al., 2012; Colgin et al., 2008; Hanlon et al., 2006; Sheffield et al., 2012; Wilkins et al., 2013).

### **4.3.3 Relevance of *Df(16)A<sup>+/-</sup>* mouse model of 22q11.2 deletion syndrome for cognitive deficits in SCZ**

Our findings indicate that impaired stability and the inability of hippocampal place fields to re-organize in response to salient information together represent important neuronal correlates of cognitive and behavioral inflexibility in *Df(16)A<sup>+/−</sup>* mice. Given that the memory deficit revealed by the GOL task is reminiscent of episodic memory deficits and learning impairments in 22q11.2 deletion carriers (McCabe et al., 2011) seen in spatial learning (Hanlon et al., 2006; Wilkins et al., 2013) and reversal tasks (Debbané et al., 2008; Leeson et al., 2009), we propose that the impaired hippocampal ensemble dynamics is a central component of cognitive memory dysfunctions emerging from the 22q11.2DS. Further, our findings may generalize to SCZ cases arising from other genetic causes (Rodriguez-Murillo et al., 2012), as the 22q11.2DS is a bona fide SCZ predisposition locus (Marshall et al., 2016), and there is a large body of data suggesting that there are no major clinical differences in the core SCZ phenotype between individuals with SCZ who are 22q11.2 deletion carriers and those who are not (Bassett et al., 2003, 1998). In a manner indistinguishable between SCZ patients with and without the 22q11.2 deletion, cognitive dysfunction is a key manifestation of SCZ that often precedes psychotic symptoms (Larson et al., 2010; Reichenberg, 2010; Seidman et al., 2010), is highly correlated with functional outcome (Green et al., 2004; Kahn & Keefe, 2013; Rosenheck et al., 2006), and is a robust indicator of the risk of developing a psychotic illness (Butcher et al., 2012; Goldenberg et al., 2012; Schneider et al., 2014; Vorstman et al., 2015). Therefore, this convergence suggests that investigations of 22q11.2DS as a genetic model for elucidating neurobiological mechanisms underlying the development of cognitive dysfunction is likely to have wide implications and could lead to novel treatments aimed at counteracting the effects of diverse disease mutations under the assumption that the diversity of dysfunction that occurs at the molecular, cellular and synaptic levels could be functionally convergent at the level of altered neuronal ensembles (Crabtree & Gogos, 2014; Lisman, 2012; Mukai et al., 2015).

Together, this study expands our understanding of the neuronal dynamics underlying goal-oriented learning under normal conditions, and it associates the disruption of these dynamics with learning deficits observed in a genetic model of SCZ. Our findings suggest that the impaired capacity of hippocampal place cells populations to maintain stable representations while still allowing for

plastic reorganization during learning may be fundamental components of the pathophysiology of cognitive memory deficits in SCZ. Our study provides important new insights into the pattern of neuronal ensemble malfunction in cognitive and psychiatric disorders as well as a foundation for dissecting the molecular and cellular mechanisms underlying this malfunction that may ultimately enable the successful development of long needed treatments for improving cognitive deficits in neuropsychiatric disorders.

## 4.4 Methods

All experiments were conducted in accordance with the US National Institutes of Health guidelines and with the approval of the Columbia University Institutional Animal Care and Use Committee.

### 4.4.1 Mice and viruses

For all experiments we used adult (8-12 weeks) male and female *Df(16)A<sup>+-</sup>* and wild-type (WT) littermates that have been backcrossed into C57BL/6J background for over ten generations. Hemizygous *Df(16)A<sup>+-</sup>* mice carry a 1.3-Mb deficiency on chromosome 16 syntenic to the human 22q11.2 region encompassing 27 genes from the *Dgcr2* gene to the *Hira* gene (Mukai et al., 2008; Stark et al., 2008). Mice were housed in the Columbia University vivarium (1-5 mice per cage) and were maintained on a 12-h light/dark cycle. Experiments were performed during the second half of the light portion of the cycle. GCaMP6f expression in neurons located in the hippocampal CA1 pyramidal layer was induced with a recombinant adeno-associated virus (rAAV) expressing GCaMP6f under a Synapsin promoter [rAAV1/2(Synapsin-GCaMP6f)]. Viral delivery to dorsal CA1 was performed by stereotactically injecting 50 nL (10-nL pulses) of rAAV at three dorsoventral locations using a Nanoject syringe (-2.3 mm AP, -1.5 mm ML, -0.9, -1.05, and -1.2 mm DV relative to Bregma). Optimal levels of viral expression of GCaMP6f occur 3-4 weeks post-injection. A subset of *Df(16)A<sup>+-</sup>* mice were crosses with mice expressing Cre-recombinase under interneuron promoters (*Som*, *Pvalb*, *VIP*) (Lovett-Barron et al., 2014) to identify interneurons located in the CA1 pyramidal layer in order to exclude them from further analysis. However, none of these crosses completely label the interneuron population in the pyramidal layer (data not shown), therefore putative interneurons were identified and excluded from image analysis based on morphological

criteria (see section 4.4.10). In total, 6 WT mice (5 males and 1 female) and 6 *Df(16)A<sup>+/−</sup>* mice (4 males and 2 females) were used for behavioral analysis. One of the male *Df(16)A<sup>+/−</sup>* mice was excluded from the imaging analysis due to poor quality of the imaging window. Experimenters were blind to mouse genotype throughout the experiment and initial data pre-processing steps.

#### **4.4.2 Imaging window implant**

Mice were surgically implanted with an imaging window over the left dorsal hippocampus along with a steel headpost for head-fixation during the experiments. Imaging cannulas were constructed by adhering (Norland optical adhesive) a 3-mm glass coverslip (64-0720, Warner) to a cylindrical steel cannula (3.0 mm diameter, 1.5 mm height). The surgical protocol was performed as described previously (Kaifosh et al., 2013; Lovett-Barron et al., 2014; Danielson et al., 2016b). Analgesia was continued for three days post-operatively.

#### **4.4.3 Behavioral training**

##### **4.4.3.1 Run training**

After recovery from surgery, but before the beginning of the behavioral experiments, mice were water deprived (>85% pre-deprivation weight) and habituated to handling and to the experimental setup including imaging equipment (shutter sounds, laser, objective). Next, water-deprived mice were head-fixed and trained to operantly lick to receive water rewards (water delivered in response to tongue contact with a capacitive sensor) at random hidden locations while running on a single-fabric, cue-free treadmill for 10 days (15-min trial/day). Mice initially received 40 randomly placed rewards per lap, and the reward frequency was decreased until the mice ran reliably for 3 randomly placed rewards per lap at a rate of at least one lap per minute. Upon entering the reward zone, a drop of water is delivered in response to every other lick from the mouse. Water delivery stops either when the mouse travels 10 cm past the beginning of the reward zone or 3 seconds has elapsed. Randomization of reward zones during training encouraged mice to continuously run and lick simultaneously.

#### **4.4.3.2 Goal-oriented learning**

The reward location was fixed to a 20-cm reward zone within the  $\approx$ 2 meter long treadmill belt (180-200 cm) during context presentation as described below (Contexts). Under this set up, each mouse was trained to learn the initial reward position for  $3 \times 10 separated by  $\approx$ 1 hour for 3 consecutive days (days 1-3, Context A, Condition I, 9 sessions total). We then changed the treadmill belt and non-spatial context and mice were given  $3 \times 10 for 3 consecutive days (days 4-6, Context A', Condition II) under this changed context. During Condition III of the experiment, the reward zone was moved to a new location, while the other features of the belt and context were kept the same as in Condition II. Mice were given  $3 \times 10 for 3 consecutive days in order to learn the new reward position (days 7-9, Context A', Condition III).$$$

#### **4.4.3.3 Random foraging**

Water deprived mice were trained to run for water rewards that were randomly administered non-operantly throughout the belt. When the experiment started, mice received on average 3 water rewards per lap, but their position from lap-to-lap remained random. Mice ran two sessions per day, either in the same context or in paired contexts as described below (Contexts).

#### **4.4.4 Behavioral readout**

We used the location and quantity of licks in order to measure performance on the goal-directed task. As a measure of learning, we computed the fraction of licks in the goal window, where the goal window is spatio-temporally defined as the time when the animal is eligible for rewards (within both the 20-cm spatial zone and the 3-second temporal window).

#### **4.4.5 Comparison of GOL task to freely-moving goal-directed learning task in Dupret et al.**

The GOL task used in this study was motivated by the cheeseboard maze task used by Dupret and colleagues (Dupret et al., 2010a). The hidden reward cheeseboard maze used in Dupret et al. requires rats to learn the location of hidden food rewards over successive trials. In their primary task these locations were un-cued and following learning rats would travel directly to each baited

location to retrieve the food reward. In order to facilitate chronic two-photon functional imaging from hippocampal CA1 place cells throughout learning, we designed this head-fixed paradigm for mice on a linear treadmill instead of a freely-moving maze. Our head-fixed goal-oriented learning task requires mice to learn the unmarked ('hidden') location (single location instead of three in Dupret et al.) of water rewards (instead of food) over successive laps (instead of discrete trials). Mice search for these rewards by sampling the lick port, which only dispenses water in the correct location, while traversing a circular treadmill. In Dupret et al. rats moved around the cheeseboard maze and sampled each well to find the baited reward locations. Both tasks use measures of behavioral efficiency to determine the degree of learning; in Dupret et al. the authors looked at the length of the path taken by the mice to collect all of the rewards, and in our task we are in effect looking for the suppression of wasted/unrewarded licks. In essence, both of these tasks require animals to remember a location in space where a reward had previously been received and effectively return to that reward location to receive another reward. Both of these tasks depend on normal activity in hippocampal area CA1 to complete this task (Figure 4.16).

#### 4.4.6 Stimulus presentation

Visual, auditory, and olfactory stimuli were presented and all behavior signals digitized as described previously (Danielson et al., 2016b; Kaifosh et al., 2013; Lovett-Barron et al., 2014). In order to track the linear position of the treadmill, we established three registration anchors at known positions along the belts and interpolated between them using a quadrature encoded movement signal tied to the rotation of the treadmill wheels. Registration anchors were marked by radio-frequency identification (RFID) buttons (16 mm, 125 kHz, SparkFun Electronics) at evenly spaced positions along the belt, and were detected when they passed over a fixed RFID reader (ID-12LA, SparkFun). The rotational quadrature signal was produced by marking treadmill wheels with offset tick marks, and this signal was encoded by a pair of photodiodes (SEN-0024, SparkFun) aligned to the wheels (<0.5 cm resolution).

#### 4.4.7 Contexts

Distinct multisensory contexts were created by using the system described in our previous work (Lovett-Barron et al., 2014). This included presentation of a constant odor (carvone or isopentyl

acetate), blinking red LED (100 ms duration at 1 Hz or off), and a pure tone (10 kHz) or continuous beeps (2 kHz, 100 ms duration at 1 Hz). All spatial information was presented to the mice via the treadmill belts. The 2 meter long imaging belts used in these experiments were constructed by stitching together 3 fabrics and then adhering six local tactile cues. Paired contexts (Context A and Context A') consisted of 2 belts with an identical sequence of 3 fabrics and the same local cues, but the order of the cues was randomized between the two belts. Preservation of the fabric order allowed for comparison of spatial representations between contexts. In addition, each belt was paired with a unique multisensory context, such that when a mouse experiences Context A' after Context A, the belt will be the same fabric sequences as in Context A, but a new local cue order, and there will be a change in the background odor, light, and tone. The composition of the first context (A) was randomized between mice.

#### 4.4.8 Hippocampal inactivation

To selectively silence dorsal hippocampus during the GOL task, we infused the GABA-agonist muscimol (Sigma) through chronically implanted cannulae. Guide cannulae (24-gauge stainless steel) were implanted in wildtype C57BL/6J mice bilaterally over dorsal area CA1 (anteroposterior, -1.7 mm; mediolateral,  $\pm$ 1.5 mm; dorsoventral, -1.0 mm) and plugged with dummy cannulae (31-gauge stainless steel wire) matching the inner dimension of the guide cannula. The injection cannulae (31-gauge stainless steel) extended 0.5 mm past the end of the guide cannulae, targeting CA1. Surgical procedures were similar to those for imaging window implantation except that a modified headpost was used to accommodate the bilateral guide cannulae. Following implantation, mice were given 3 days to recover before head-fixation habituation, followed by 2 weeks of GOL task training (see Behavioral training).

To test for effects of dorsal hippocampus silencing on GOL, we used a modified GOL task paradigm that consisted of a single condition (all days same belt, context, and reward location). On the first day, mice were randomly divided into two groups (saline n=4, and muscimol n=3). The saline group was infused with 0.9% saline (0.15  $\mu$ L at 0.25  $\mu$ L/min) for the first 3 days (3 sessions per day, 30 minutes between sessions) and then switched to muscimol (0.15  $\mu$ L of 1  $\mu$ g/ $\mu$ L at 0.25  $\mu$ L/min) on the fourth day as a reversal trial. The muscimol group received the opposite drug schedule; muscimol on the first three days and saline on the fourth. To allow for drug

diffusion, Injection cannulae were left in place for two minutes following infusion. Mice were briefly head-restrained on a separate training treadmill during drug infusion. Infusions were performed sequentially (one hemisphere at a time) with a 5- $\mu$ L Hamilton Syringe and micro-infusion pump (World Precision Instruments). Following infusions, the dummy cannulae were replaced and mice returned to the homecage for 30 minutes before behavior training/testing.

#### 4.4.9 *In vivo* 2-photon imaging

All imaging was conducted using a two-photon 8kHz resonant scanner (Bruker). We acquired 300  $\mu$ m  $\times$  300  $\mu$ m images (512 $\times$ 512 pixels) at 7-30 Hz using a 920-nm laser (50-100 mW, Coherent) through the approximate midline of the CA1 pyramidal cell body layer. In order to align the CA1 pyramidal layer with the horizontal 2-photon imaging plane, we adjusted the angle of the mouse's head using two goniometers ( $\pm 10^\circ$  range, Edmund Optics). All images were acquired with a Nikon 40 $\times$  NIR water-immersion objective (0.8 NA, 3.5 mm WD) in distilled water. Green (GCaMP6f) fluorescence was detected with a GaAsP PMT (Hamamatsu Model 7422P-40). A custom dual stage preamp was used for optimal signal amplification prior to digitization (Bruker).

#### 4.4.10 Data processing for Ca<sup>2+</sup> imaging

All imaging data were analyzed using the SIMA software package written in Python <https://github.com/losonczylab/sima> (Kaifosh et al., 2014). Motion artifact correction was achieved by implementing a plane-wise version of the 2D Hidden Markov Model (Dombeck et al., 2010; Kaifosh et al., 2013, 2014). Segmentation was performed on each field-of-view (FOV) by manually drawing polygons around GCaMP6f labeled somata for the first imaged session of each FOV. Polygons were drawn along the inner edge of the cytosolic border to minimize neuropil contamination. Putative interneurons in the pyramidal layers, predominantly GABAergic basket cells (Bezaire & Soltesz, 2013; Freund & Buzsáki, 1996; Klausberger & Somogyi, 2008); were identified and excluded from further analysis based on their multipolar morphologically larger soma diameter compared to CA1 pyramidal cells (Ambros-Ingerson & Holmes, 2005; Gulyas et al., 1999; Papp et al., 2013) and higher baseline and nuclear fluorescence, consistent with their higher baseline tonic firing rate *in vivo* (Klausberger et al., 2003; Klausberger & Somogyi, 2008; Lapray et al., 2012; Varga et al., 2012). Regions of interest were imported in to the SIMA project's ROI Buddy graphical user interface

(Kaifosh et al., 2014), and were transformed to the other imaging sessions of the same FOV using a piecewise-affine transformation. The tool also allowed for registration of the regions of interest (ROIs) across experiments, allowing us to track identified cells across imaging sessions. GCaMP6f fluorescence time-series were extracted from the ROIs using SIMA as previously described (Kaifosh et al., 2014). We computed the relative fluorescence changes ( $\Delta F/F$ ) as previously described (Jia et al., 2011), with uniform smoothing window  $\tau_1 = 3$  seconds and baseline size  $\tau_2 = 60$  seconds.

#### 4.4.10.1 Identification of calcium transients

To identify significant calcium events, we modified a method first implemented in Dombeck et al. 2007, and has since been used both by our lab (Danielson et al., 2016a,b; Lovett-Barron et al., 2014) and others (Dombeck et al., 2010; Rajasethupathy et al., 2015). The general idea is that for a  $\Delta F/F$  calcium trace, positive and negative deflections from 0 should occur with equal probability for any noise associated with the photon counting or image acquisition and also for un-correctable motion along the dorsal-ventral axis (z-axis) of the mouse. This assumption allows us to empirically calculate the false positive rate for each putative event, and thus identify a duration and amplitude threshold above which an event has a fixed (5%) maximum false-positive rate; the level at which there are 20 times more positive events than negative events. To implement this approach, we identify putative events by finding consecutive imaging frames that start 2 standard deviations above or below the mean, ends when the signal falls back down to 0.5 standard deviations above/below the mean, and lasts for at least 250 ms. These events are classified by their duration and amplitude (in units of standard deviations,  $\sigma$ ), binned into 0.5  $\sigma$  amplitude and 250 ms duration bins. For each bin we calculate the associated false positive rate as the ratio of negative to positive events. Significant calcium transients are thus defined at the positive events from amplitude-duration bins with a false-positive rate less than or equal to 5%.

#### 4.4.11 Data analysis

##### 4.4.11.1 Selection of spatially-tuned cells

When evaluating the spatial tuning of pyramidal cells, we restricted our analysis to running-related epochs, defined as consecutive frames of forward locomotion (an imaging frame in which at least

one forward pair of beam breaks occurred) at least 1 second in duration and with a minimum peak speed of 5 cm/sec. Consecutive epochs separated by < 0.5 seconds were merged. Running-related transients were defined as those that were initiated during a running-related epoch.

In order to identify cells with significant spatial tuning, we calculated the spatial information relative to an empirically calculated shuffle distribution. For each cell we first computed the spatial information content (Skaggs et al., 1993) as

$$I_N = \sum_{i=1}^N \lambda_i \ln \frac{\lambda_i}{\lambda} p_i$$

where  $\lambda_i$  and  $p_i$  are the transient rate and fraction of time spent in the  $i^{th}$  bin,  $\lambda$  is the overall firing rate, and  $N$  is the number of bins. We computed  $I_N$  for multiple values of  $N = \{2, 4, 5, 10, 20, 25, 50, 100\}$ . We then created 1000 random reassessments of the transient onset times within the running-related epochs and re-computed the values of  $I_N^s$ , where  $s$  is the index of the shuffle. To roughly correct for biases in the calculation of mutual information, we then subtracted the mean of this null distribution from all estimates to obtain values

$$\hat{I}_N = I_N - \frac{1}{1000} \sum_{s=1}^{1000} I_N^s.$$

Finally, we computed a single estimate of the information content for the true transient onset times,

$$\hat{I} = \max_N \hat{I}_N,$$

and for the shuffles,

$$\hat{I}_s = \max_N \hat{I}_N^s.$$

The spatial tuning p-value was taken as the fraction of values of  $s$  for which  $\hat{I}$  exceeded  $\hat{I}_s$ . Cells falling in the top 5% of their respective shuffle distributions were classified as place cells on the basis of their spatial information content.

For all cells, rate maps were formed by dividing the number of transients initiated in each spatial bin by the occupancy of that bin. We calculated rate maps with 100 position bins and smoothed with a Gaussian kernel ( $\sigma = 3$  bins). In order to define place fields for cells that were identified

as containing significant spatial information, we fit each local maximum in the rate map with a Gaussian, merged overlapping putative-fields, and then discarded any with an area less than 50% of the largest.

#### 4.4.11.2 Place cell properties

For each cell, we calculated a spatial tuning vector

$$\sum_j \frac{e^{i\theta_j}}{o(\theta_j)},$$

where  $\theta_j$  is the position of the mouse at the onset time of the  $j^{th}$  running transient, and  $o(\theta_j)$  is the fraction of running frames acquired at position  $\theta_j$ . The circular variance is defined as 1 minus the magnitude of this mean resultant vector (smaller values convey sharper tuning specificity). Transient sensitivity is defined for a place cell as the fraction of laps in which a significant  $\text{Ca}^{2+}$  transient occurred in a place field. Transient specificity is defined as the fraction of significant  $\text{Ca}^{2+}$  transients that occurred within a place field. Single-cell sparsity is defined as in Ahmed & Mehta 2009:

$$s = \frac{\left(\frac{1}{n} \sum_i r_i\right)^2}{\frac{1}{n} \sum_i (r_i^2)},$$

where  $r_i$  is the transient rate in in spatial bin  $i$  out of  $n$  total bins. Lifetime place coding is the fraction of all cells that were ever previously identified as a place cell by the  $n^{th}$  session they were imaged.

#### 4.4.11.3 Remapping analysis

Recurrence probability was defined for a given pair of experiments as the fraction of place cells in the first experiment that were also identified as a place cell in the second experiment. The centroid shift for each cell was defined as the distance between the spatial tuning vectors calculated for a pair of experiments. As noted above (see Goal-oriented learning) the actual treadmill belts used for the experiments ranged from 180 to 200 cm, so we normalized the values to the length of the belt to directly compare centroid shift values. These values range on the interval  $[-0.5, 0.5]$  and the units have been labeled ‘fraction of belt’. For Figures 4.13, 4.21, & 4.22, we plot the absolute value

of this shift. A cell was required to have fired at least 1 transient in both experiments for inclusion. In our analysis of cell firing location following the shifting of local cues, we define a ‘cueness’ metric for all cells that fired within  $\pm 5\%$  (belt units) of the cue before cue shift, as:

$$c = \frac{d_p}{d_p + d_c},$$

where  $d_p$  is the distance from the activity centroid after cue shift to the position on the fabric sequence where the preferred cue was before the cue shift, so  $d_p = 0$  means that cell maintained it’s firing at the location where the cue had been. We defined  $d_c$  similarly as the distance from activity centroid after cue shift to the new position of the cue after the cue shift, so  $d_c = 0$  means that cell’s activity followed the movement of the cue exactly (and a value of 0.5 means it is now at the opposite side of the belt). So, the cueness metric,  $c$ , has a value of 1 for a cell that followed the cue and a value of 0 for a cell that stayed at the original cue position. All cells with a cueness value  $>0.67$  were classified as ‘cue-preferring’ and all cells with a value  $<0.33$  were classified as ‘place-peferring’. Cueness shuffle distributions were calculated by randomizing the cell identity before and after the cue shift. The fraction of place fields near the reward was defined as the fraction of place cells with a spatial tuning vector within of a belt length of the reward zone.

#### 4.4.11.4 Shuffle distributions

For recurrence probability shuffle distributions, we selected every pair of experiments and we calculated the fraction of place cells in the first experiment that were still place cells in the second experiment (recurrence probability) as well as the fraction of all cells in the second experiment that were identified as place cells (recurrence probability chance level). We pooled this chance level calculation across all pairs of experiments in both genotypes to create the shuffle CDF and inset bar. Centroid shift and place/cue-preferring shuffle distributions were calculated by randomly choosing 10,000 pairs of activity centroids (taken from correctly paired experiments, but ignoring cell identity) and calculating the difference in centroid position or the distance to the cue/position.

#### 4.4.11.5 Recurrence and stability by position

Recurrence and stability as a function of position were calculated from all data during Condition III – the only condition during which we detected remapping towards the reward location. For every session, we first identified the significantly spatially-tuned cells, and then for these place cells we calculated the activity centroid position relative to the reward location (positions after the reward are positive, before the reward are negative). In order to get a continuous estimate of recurrence as a function of position, we used nonparametric logistic regression to fit a cyclic cubic spline to whether a place cell recurred (1) or not (0) for all place cell pairs of sessions. Over-fitting was controlled for by leave-one-out cross-validation, which determined an appropriate smoothness penalty on the spline. Confidence intervals were calculated by generating 1000 new datasets of the same size as the original by resampling with replacement. Splines were fit to each new dataset, and the confidence interval was defined as the 5th and 95th percentile of the fit values (Wang & Wahba, 1995; Hastie et al., 2009).

Session-to-session place field shift by position was modeled as a continuous series of von Mises distributions, defined as:

$$VMS = f(x|\mu, \kappa) = \frac{e^{\kappa \cos x - \mu}}{2\pi I_0(\kappa)},$$

where  $x$  is the distance from the reward,  $I_0$  is the modified Bessel function of order 0,  $\mu$  is the offset (mean of the distribution), and  $\kappa$  is the concentration ( $\frac{1}{\kappa}$  is analogous to variance). Both the offset and concentration parameters are assumed to change smoothly across the belt. We first fit the mean shift (offset) of place fields as a function of their initial position as a cyclic cubic spline, minimizing mean squared error between the predicted and actual second session shift. Using this fit as the offset for the von Mises distributions, we fit the concentration factor again as a cyclic cubic spline, minimizing the negative log-likelihood of the actual data. Similar to above, over-fitting was controlled by leave-one-out cross-validation to determine the penalty on the second derivative of the splines. Confidence intervals were calculated by resampling the original dataset as described above.

#### 4.4.11.6 LFP acquisition and sharp wave-ripple analysis

Wide-band signals were acquired at 25 kHz using a digital acquisition system (Intan Technologies, Los Angeles) from 2 WT and 2 *Df(16)A<sup>+/−</sup>* mice. For each mouse, LFP signals from a 4-channel silicon probe (NeuroNexus, Ann Arbor) centered around the *stratum pyramidale* layer of CA1 were recorded for 20 minutes while the mouse was head-fixed on a cue-free treadmill belt, with randomly distributed water rewards. LFP signals were subsequently derived by band-pass filtering wide-band signals between 0.1 and 625 Hz, and down-sampling to 1250 Hz. For each animal, a ‘pyramidal layer’ recording site was chosen based on the amplitude of LFP ripple-events, and its location dorsal to the sites showing prominent negative sharp-waves which are visible in the *stratum radiatum*. LFP signals originating in the pyramidal layer during epochs that did not show evidence of muscle-related electrical artifacts and in which the animal was immobile (velocity < 3 cm/s) were included in the analysis. Gabor wavelet spectrograms were computed between 1 and 250 Hz - power within each frequency band was subsequently z-scored within each session. In order to detect SWR events, the pyramidal layer LFP’s were band-pass filtered at the ripple-band frequency (125 to 250 Hz), rectified, smoothed with a 25-ms STD Gaussian kernel, and z-scored. For the main analysis, ripples were detected as ‘trigger’ peaks at least 6 standard deviations above the mean, with the Ripple ‘edges’ set at 2 standard deviations above the mean. The ‘trigger’ thresholds were also varied between 2 and 9 standard deviations above the mean. Across all conditions, candidate ripple events occurring within 30 ms of each other were concatenated, and only ripples lasting at least 30 ms were included. Ripple incidence rates were calculated by binning immobility epochs into non-overlapping 30 second bins and calculating the ripple incidence within these bins.

#### 4.4.11.7 Modeling goal-directed remapping

All parameters in our model of session-to-session recurrence and remapping were fit from our WT and *Df(16)A<sup>+/−</sup>* place cell data separately for each Condition. For the *flat* model, recurrence, shift offset, and shift variance were all set to the mean across all positions from the WT fits. Our model assumes that every cell has a preferred spatial tuning each day, and a subset of cells express this spatial preference each session (place cells). At each iteration of the model a fixed fraction of non-place cells become spatially-active:  $P_{on}$  (WT: 24.83%; *Df(16)A<sup>+/−</sup>*: 20.58%). Place cells

remain spatially-active as place cells with a position-dependent recurrence probability:  $P_{recur}(x_i)$ . Finally, all cells shift their place field location, with the new position being drawn from a von Mises distribution with position-dependent offset and concentration as described previously:

$$P(x_{i+1}|x_i) = VMS(x_i + \mu(x_i), \kappa(x_i)).$$

For all simulations, we ran 8 iterations, similar to the 8 transitions between the 9 sessions within each Condition of our experiment. We calculated the mean enrichment as the mean absolute centroid distance to the reward across all place cells minus the expected mean distance from the reward (0.25). For all model simulations, initial spatial tuning and place cell identity were chosen pseudo-randomly; initial place cell identities and masks were randomized until the mean distance to the reward was <0.00001, but then held constant across 100 simulations of 8 iterations. For enrichment by iteration curves (Figures 4.32a, 4.36e, 4.33a,b, & 4.35) the mean and 90% confidence intervals are calculated from the 100 simulations. Final distribution histograms (Figures 4.32b, 4.34b, 4.36f, 4.33c,d, & 4.35) are aggregated across all simulations. In order to compare the influence of each set of parameters to the final enrichment, we re-ran the simulation with each of the parameters swapped between WT and *flat* fits (Figures 4.34 & 4.35). For example, the WT enrichment for ‘swap  $P_{recur}$ ’ is the simulation run with all WT-fit parameters, except with  $P_{recur}$  being the same for all positions and equal to the mean.

#### 4.4.11.8 Statistics

Behavioral results were analyzed with Repeated Measures two-way ANOVA. All data was tested for equal variance (Levene’s test) and for normal distribution (Kolmogorov-Smirnov normality test). Means were compared by two-sample unpaired t-tests, unless the variances were significantly different or the data was not normally distributed, in which case. the Welch’s t-test or Mann-Whitney U test was used respectively. Wilcoxon rank sum test was used for comparing genotypes in SWR data. Chi-square test, cox regression, or two-ANOVA were used for all other individual parameter comparisons. Post hoc pairwise analysis was performed with Bonferroni corrections for multiple comparisons. Linear regression analysis with Pearson’s correlation coefficient was calculated for correlations of behavioral performance with place cell stability and enrichment (Figures 4.12c, 4.13c,

& 4.14c). Comparisons of significant correlations between groups were performed with GLM after Z-score transformation with Z-transformed variable in *x*-axis as a covariate. Cox regression was used to compare lifetime place coding between genotypes (Figure 4.11a). Unless otherwise noted, values are plotted as mean  $\pm$  standard error of the mean.

## Chapter 5

# SIMA: Python software for analysis of dynamic fluorescence imaging data<sup>1</sup>

When we began this project, *in vivo* Ca<sup>2+</sup> was a relatively new technique in neuroscience, and more relevantly, there were no publicly available tools to aid in the processing and analysis of the large amounts of data generated by these experiments. To help fill this void and progress our own research, we developed a collection of Python tools to help with the analysis steps common to all Ca<sup>2+</sup> experiments, namely: motion correction, ROI segmentation, registering ROIs across sessions, and signal extraction. We released all of the code for both the SIMA package and the ROI Buddy GUI under a free license, and continue to maintain the collaborative project on GitHub: <https://github.com/losonczylab/>. We designed SIMA with the goal for it to work with many different data formats, be easily extensible with new features, and be as simple to work with as possible.

In the sections below I will go through the main features and overview from our paper (Kaifosh et al., 2014), with slightly more emphasis on the areas I personally contributed to the most: ROI registration and signal extraction. Extensive documentation for the SIMA package and ROI Buddy GUI is available at <http://www.losonczylab.org/sima/>. Software and source code can be downloaded from the Python Package Index: <https://pypi.python.org/pypi/sima>. The source code repository is maintained on GitHub: <https://github.com/losonczylab/sima>.

---

<sup>1</sup>This work has been previously published (Kaifosh et al., 2014) and is joint work with the coauthors. The open source SIMA project is the joint work of many contributors.

## 5.1 Abstract

Fluorescence imaging is a powerful method for monitoring dynamic signals in the nervous system. However, analysis of dynamic fluorescence imaging data remains burdensome, in part due to the shortage of available software tools. To address this need, we have developed SIMA, an open source Python package that facilitates common analysis tasks related to fluorescence imaging. Functionality of this package includes correction of motion artifacts occurring during *in vivo* imaging with laser-scanning microscopy, segmentation of imaged fields into regions of interest (ROIs), and extraction of signals from the segmented ROIs. We have also developed a graphical user interface (GUI) for manual editing of the automatically segmented ROIs and automated registration of ROIs across multiple imaging datasets. This software has been designed with flexibility in mind to allow for future extension with different analysis methods and potential integration with other packages. Software, documentation, and source code for the SIMA package and ROI Buddy GUI are freely available at <http://www.losonczylab.org/sima/>.

## 5.2 Introduction

Two-photon fluorescence imaging of neuronal populations has proven to be a powerful method for studying dynamic signals in neural circuits. For example, imaging of genetically-encoded fluorescent  $\text{Ca}^{2+}$  indicators (Looger & Griesbeck, 2012) has been widely applied to simultaneously monitor the activity in large populations of spatially, morphologically, or genetically identified neurons. These methods can be implemented *in vivo* in awake rodents (Dombeck et al., 2007; Komiyama et al., 2010; Lovett-Barron et al., 2014), providing the potential to study the molecular, anatomical, and functional properties of neurons responsible for behavior (Kerr & Denk, 2008; O'Connor et al., 2010). Relative to the electrophysiological approaches traditionally used to study neuronal activity *in vivo*, two-photon imaging provides the advantages of recording activity in entire local populations without spike-sorting ambiguities or bias towards highly active neurons, imaging activity in subcellular compartments such as axons or dendrites, and tracking the same neurons across experiments spanning multiple days. Additionally, fluorescence imaging can be used to measure other signals, such as membrane potentials and neurotransmitter release (Looger & Griesbeck, 2012).

To facilitate the analysis of data from dynamic fluorescence imaging experiments, we have

developed two software tools: the Sequential IMaging Analysis (SIMA) Python package, and the ROI Buddy graphical user interface (GUI). The SIMA package can be used for motion correction, automated segmentation, and signal extraction from fluorescence imaging datasets. The ROI Buddy GUI allows for editing and annotating ROIs within a given imaging session, as well as registering ROIs across imaging sessions acquired at different times. The output data resulting from analysis with SIMA can either be directly analyzed using the NumPy/SciPy tools for scientific computing (Oliphant, 2007; Jones et al., 2001), or can be exported to common formats allowing for subsequent analysis with other software. The SIMA package and ROI Buddy GUI can be run on Linux, Windows, and MacOS operating systems, have been made freely available under an open source license, and require only other freely available open source software.

I provide here a brief overview of the SIMA package and ROI Buddy GUI. Section 5.3 explains the capabilities of these software tools and how they can be used. Section 5.4 explains details of the algorithms that have been implemented to provide this functionality.

### 5.3 Functionality

The SIMA package and ROI Buddy GUI provide a variety of functionality outlined in Figure 5.1. To give an overview of this functionality, we provide sample code for typical use in the case in which the raw imaging data is contained in two NumPy arrays named `channel_A` and `channel_B`, (other possibilities for input data formats are discussed in subsection 5.3.1), and in which the output data is to be stored in the location `/save/path.sima`. Throughout our code examples, we assume that the SIMA package has been imported with the `import sima` Python command.

With just a few lines of code, the user can correct motion artifacts in the data, and then segment the resulting `ImagingDataset` object to identify ROIs:

```
dataset = sima.motion.hmm([[channel_A, channel_B]], '/save/path.sima')  
dataset.segment()
```

If the data lack motion artifacts (e.g. fluorescence imaging in *ex vivo* brain slices), the motion correction step can be replaced with direct initialization of an `ImagingDataset` object. The full set of commands in this case is as follows:

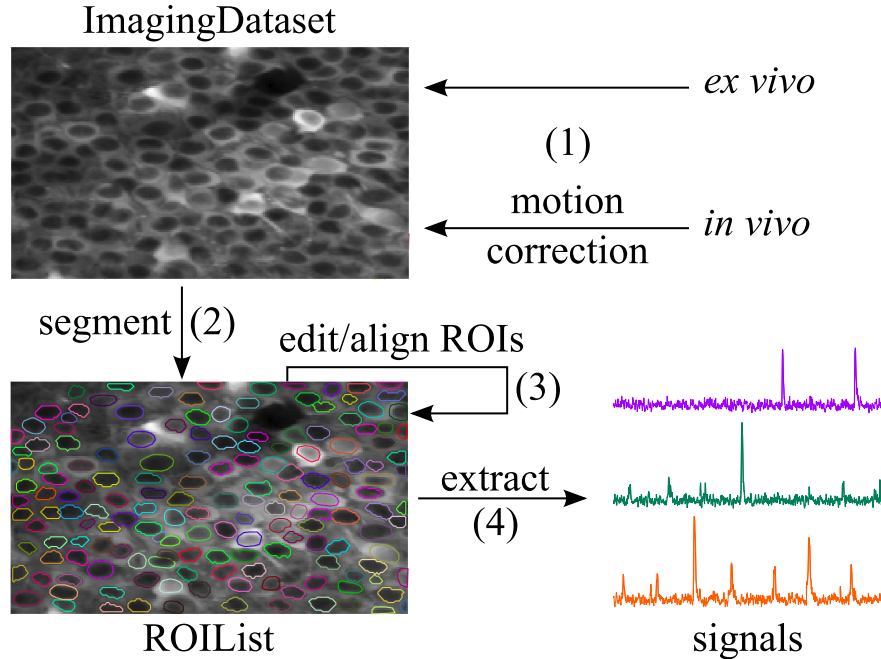


**Figure 5.1:** Workflow supported by SIMA. (1) An **ImagingDataset** object is first created either directly from the raw data or from the output of the motion correction algorithm. (2) ROIs are generated by automatic segmentation. (3) The ROI Buddy GUI can be used to edit the automatically generated ROIs and to automatically register ROIs across multiple datasets. (4) Dynamic fluorescence signals are extracted from the imaging data and ROIs.

```
dataset = sima.ImagingDataset([[channel_A, channel_B]], '/save/path.sima')
dataset.segment()
```

In either case, the result of these commands is an **ImagingDataset** object containing the raw or motion-corrected imaging data and the automatically generated ROIs. This object is permanently stored in the location `/save/path.sima` so that it can be reloaded at a later time.

Following automated segmentation, the generated ROIs can be manually edited with the ROI Buddy graphical user interface (GUI). This GUI can be used to delete erroneous ROIs, add missing ROIs, merge ROIs that have been incorrectly split, and adjust the shapes and positions of existing ROIs. The ROI Buddy GUI can also be used to register ROIs across multiple datasets acquired at different times, allowing for assessment of long-term changes in neural activity.

Once the ROIs have been edited and registered, the **ImagingDataset** object can be loaded in Python again, and then dynamic fluorescence signals can be extracted from the ROIs as follows:

```
dataset = sima.ImagingDataset.load('/save/path.sima')
```

```
dataset.extract()
```

The extracted signals are permanently saved with the `ImagingDataset` object and can be accessed at any time with the command `dataset.signals()`. For further analysis with external software, the signals can be exported using the command `dataset.export_signals('/export/path.csv')`.

The remainder of this section contains more detailed discussion of each of the stages of this workflow. This discussion complements the API documentation that is available online at the project's website: <http://www.losonczylab.org/sima>.

### 5.3.1 Object classes and input formats

The SIMA package follows an object-oriented design. The central object class around which the package is structured is the `ImagingDataset`. Objects of this class can be created either by direct initialization or as the output of the motion correction function call. Direct initialization of an `ImagingDataset` object requires two mandatory arguments: (1) the raw imaging data formatted according to the requirements discussed below, and (2) the path where the `ImagingDataset` object is to be saved. Names for the channels may be specified as an optional argument. Once created, `ImagingDataset` objects are automatically saved to the designated location and can be loaded at a later time with a call to the `ImagingDataset.load` method.

A single `ImagingDataset` object can contain imaging data from multiple simultaneously recorded optical channels, as well as from multiple *cycles* (i.e. continuous imaging epochs/trials) acquired at the same imaging location during the same imaging session. To allow for this flexibility, the raw imaging data used to initialize the `ImagingDataset` object must be packaged into a list of lists, whose first index runs over the cycles and whose second index runs over the channels. For example, if the raw data is stored in an object called `data`, then the element `data[i][j]` corresponds to the `j`th channel of the `i`th cycle.

The formating requirements for each such element of the aforementioned list of lists are designed to allow for flexible use of SIMA with a variety of data formats. The sole requirement is that each element be specified as a Python iterable object satisfying the following properties: (1) the iterable may not be its own iterator, i.e. it should be able to spawn multiple iterators that can be iterated over independently; (2) each iterator spawned from the iterable must yield image frames in the

form of two-dimensional NumPy arrays; and (3) the iterable must survive Python’s pickling and unpickling methods for saving and loading objects.

A simple example of an object that satisfies these requirements is a three-dimensional NumPy array, with the first index corresponding to the frame, the second to the row, and the third to the column. Therefore, data in any format can be analyzed with SIMA following conversion to a NumPy array. We also implemented the `sima.iterables.MultiPageTIFF` object class for creating SIMA-compatible iterables from multi-page TIFF files, and the `sima.iterables.HDF5` object class for creating iterables from HDF5 files. For example, a two-channel dataset can be initialized from TIFF files as follows:

```
iterables = [[sima.iterables.MultiPageTIFF('channel1.tif'),
              sima.iterables.MultiPageTIFF('channel2.tif')]]

dataset = sima.ImagingDataset(iterables, '/save/path.sima',
                               channel_names=['GCaMP', 'tdTomato'])
```

Compared to converting data from TIFF or HDF5 files to NumPy arrays, use of these custom iterables is advantageous because there is no need to duplicate the data for separate storage in a second format. Furthermore, less data need be held in memory at any one time because the `MultiPageTIFF` or `HDF5` iterables allow for imaging data to be loaded one frame at a time on an as-needed basis.

Importantly, the SIMA package has been designed to allow for flexible extension with additional custom iterable classes analogous to the `MultiPageTIFF` class. Such extensions can be developed to allow SIMA to use data from any required input format. Therefore, users wishing to use SIMA with other data formats have two options: (1) to convert the data to a format already supported such as a TIFF stack or NumPy array, or (2) to extend SIMA by creating a new iterable type to support the desired data format.

### 5.3.2 Motion correction

During *in vivo* laser-scanning microscopy, the animal’s movements cause time-dependent displacements of the imaged brain region relative to the microscope and thus introduce substantial artifacts into the imaging data. These artifacts are especially problematic when attempting to extract

transient fluorescence signals from very small structures, such as dendritic branches and synaptic boutons (e.g. Kaifosh et al., 2013). Since individual pixels are acquired at different times during laser scanning microscopy, motion artifacts can occur within a single frame and cannot be corrected by simple frame alignment methods. To allow for correction of these within-frame motion artifacts, the SIMA package includes line-by-line motion correction software (Figure 5.2) that we developed (Kaifosh et al., 2013) by extending upon the hidden Markov model (HMM) approach used previously (Dombeck et al., 2007).

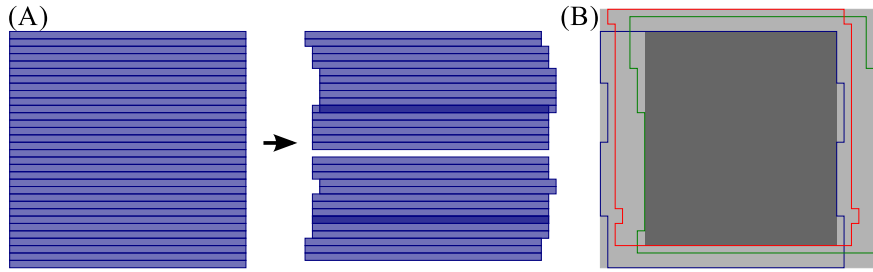


**Figure 5.2:** Line-by-line correction of within-frame motion artifacts. **(A)** Schematic diagram showing a single imaging frame before (left) and after (right) line-by-line motion correction. A separate displacement is calculated for each sequentially acquired line from the laser scanning process. As a result, some pixel locations may be accounted for multiple times (darker blue), while others may not be imaged in a given frame (white gap). **(B)** Overlay of different regions imaged by different frames due to motion. The light gray region indicates the maximum frame-size that can be selected for the motion correction output, such that all pixels locations that were ever imaged are within the frame. The dark gray region indicates the default and minimum frame-size that can be selected for the motion correction output, such that all pixels within the frame are within the field of view at all times.

A call to the hidden Markov model motion correction function `sima.motion.hmm` returns a motion-corrected `ImagingDataset` object. This function takes the same arguments used to directly initialize an `ImagingDataset` object, as well as additional arguments for specifying parameters for the motion correction procedure. One optional argument allows for specification of the number of states retained at each step of the Viterbi algorithm. Retaining a larger number of states may in some cases result in more accurate displacement estimates, though at the expense of longer runtimes. The maximum allowable displacement in the horizontal and vertical directions can also be specified. Use of this restriction can improve the quality of the estimated displacements by ruling out unreasonably large estimates. Optionally, a subset of the channels can be selected for use in estimating the displacements, which will then be used to correct artifacts in all channels. This option is useful in cases where there is a sparse or highly dynamic channel with signals of interest,

and an additional static channel providing a stable reference for motion correction.

Once the motion artifacts are corrected, the frames of the resulting `ImagingDataset` show static imaged structures, but a field of view that moves from frame to frame (Figure 5.2B). Typically, a frame size larger than that of the original images is required to display the full spatial extent that was imaged during the session. Relatedly, the area imaged during all frames is smaller than that of the original images. To determine the spatial extent of the corrected image series that will be retained for further analysis, the `hmm` function takes an additional optional argument, the `trim_criterion`, which specifies the fraction of frames for which a location must be within the field of view in order to be retained for further analysis. By default, the edges of the corrected images are conservatively trimmed to retain only the rectangular region that remains within the field of view during all imaging frames.

### 5.3.3 Segmentation and ROIs

The SIMA package allows for automated segmentation of the field of view with a call to the `ImagingDataset.segment` method. The `segment` method takes arguments that allow for specification of the approach to be used and an optional label for the resulting set of ROIs, which are saved with the `ImagingDataset`. Arguments specific to the particular method can also be passed into this method call. The SIMA package currently contains two implemented segmentation methods, '`normcut`' and '`ca1pc`', both of which are based on the normalized cuts approach (Shi & Malik, 2000).

A call to the `segment` method returns an `ROIList` object, which contains the segmented ROI objects. As well, ROI objects can be initialized independently in one of four ways: (1) with a mask, typically a NumPy array, indicating the weight of each pixel (see subsection 5.4.2), (2) with a list of polygons, each consisting of a list of vertices, (3) using ROI Buddy (see subsection 5.3.4), or (4) by importing a set of ROIs created in ImageJ (Schneider et al., 2012). Masks can either be binary, to select a subset of pixels, or real-valued, as in the case of weights resulting from principal or independent component analysis. Polygons are treated equivalently to binary masks. ROIs typically consist of a single polygon, however multiple polygons are useful for marking structures that leave and re-enter the imaging plane.

Additionally ROI objects have the following optional attributes: `id`, `label`, and `tags`. The

`label` attribute is a descriptor for the `ROI` used for referencing the region within one imaging session. The `id` of an `ROI` object is an identifier used to track the region over multiple imaging sessions, such that two `ROI` objects from different experiments that have the same `id` are understood to correspond to the same neuron/dendrite/bouton. The `id` values are automatically set during `ROI` registration with the `ROI` Buddy GUI. The `tags` attribute is a set of strings associated with the `ROI`, used for sorting or marking the `ROIs` based on morphological, genetic, or other criteria. These `tags` can also be modified from within the `ROI` Buddy GUI or during analysis of fluorescence signals to aid in the selection and sorting of `ROIs` during subsequent analysis.

#### 5.3.4 Manual ROI Editing

The `ROI` Buddy GUI can be used to view and edit the automated segmentation results or to manually draw new `ROIs`. When the user loads an `ImagingDataset` object, the time-averaged images are displayed as a static background on which `ROI` objects are displayed. The underlying static image can be toggled between each of the imaged channels, and optionally a contrast-enhanced “processed” image can be displayed. Each `ROI` object, consisting of one or more polygons, is displayed with a unique color over this background. If multiple `ROIList` objects are associated with an `ImagingDataset` (automatically generated and manually edited sets, for example), the active set is selectable via a drop-down menu. The user can also toggle between simultaneously loaded `ImagingDataset` objects, which is useful for rapidly switching between multiple imaging sessions of the same field of view in order to verify the `ROIs` during editing.

Once the `ImagingDataset` and `ROI` objects are loaded in the GUI, the user can edit, delete, and add new `ROIs` as polygons while in the GUI’s “Edit” mode. All `ROIs` are directly editable, allowing for the user to adjust individual vertices or translate the entire `ROI`. In addition, separate polygons can be merged either into a single multiple-polygon `ROI` or, if the polygons are overlapping, into a single polygon `ROI`. The interface also allows the user to directly set the `label` and `tags` properties of each `ROI` described in subsection 5.3.3.

#### 5.3.5 ROI Registration

To track the same structures over multiple imaging sessions of the same field of view (Figure 5.3), the `ROI` Buddy GUI also supports the registration of `ROIs` from different `ImagingDataset` objects.

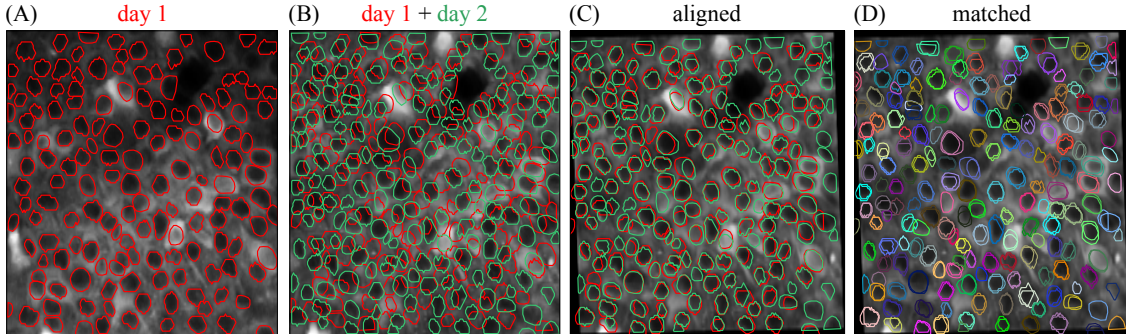


**Figure 5.3:** Registration of ROIs across imaging sessions acquired on two different days. (A) ROIs (red) and time-averaged image for the first imaging session. (B) ROIs (green) and time-averaged image for the second imaging session, with ROIs for the first imaging session (red) shown for comparison. (C) Same as (B) but with an affine transformation applied to align the time-averaged image and ROIs from day 2 to those of day 1. (D) Same as (C) but with the ROIs colored by their automatically determined shared identities across both imaging sessions.

In the GUI’s “Align” mode, affine transformations are estimated to align the time-averaged images of the currently active `ImagingDataset` with each of the other loaded sets. These transformations are then applied to the respective `ROI` objects to transform them all into the space of the active `ImagingDataset` (Figure 5.3C). This allows ROIs to be imported from one set on to the active `ImagingDataset` or for all of the ROIs to be viewed simultaneously over the time-averaged image of a single `ImagingDataset`. The ROIs are then automatically identified across imaging datasets based on their degree of overlap following transformation. The `id` attributes of co-registered `ROI` objects are set to be equal, thus allowing for tracking of the same regions over multiple imaging sessions.

When displayed in the GUI, co-registered `ROI` objects are colored identically for easy visual inspection of the registration results (Figure 5.3D). Groups of co-registered ROIs can be manually modified by removing and adding `ROI` objects to correct any errors in the automated registration. The `tags` can also be propagated across co-registered ROIs from different `ImagingDataset` objects.

### 5.3.6 Signal extraction

Signal extraction is accomplished by the `ImagingDataset.extract` method. This `extract` method can take several optional arguments. The `ROIList` to be used can be specified in cases where there are multiple `ROIList` objects (e.g. one that has an automatically generated and another that has been manually edited) associated with the `ImagingDataset`. If multiple optical channels are

present, the channel to be used for extraction can be specified. If the ROIs are either polygons or a binary masks, the `extract` method can optionally exclude pixels that overlap between ROIs in order to reduce artifactual correlations between adjacent ROIs.

The output of the `extract` method is a Python dictionary, which is also automatically saved as part of the `ImagingDataset` object. This dictionary contains (1) the raw extracted signals, (2) a time-averaged image of the extracted channel, (3) a list of the overlapping pixels, (4) a record of which `ROIList` and channel were used for extraction, and (5) a timestamp. Additionally, a verification image is saved as a PDF file showing the extracted ROIs and overlapping pixels overlaid on the time-averaged image. Once the signals are extracted, they can be accessed at any time with a call to the `ImagingDataset.signals` method.

### 5.3.7 Exporting data

The SIMA package is intended to provide support for early stages of data analysis, such that subsequent analysis of the extracted signals can be performed with separate software. In cases where all analysis is performed using Python, no exporting is necessary, since the SIMA objects can be used in conjunction with other Python code. In other cases, data from SIMA objects can be easily exported into standard formats, including TIFF images and CSV text files.

Such exporting of data can be performed at various stages of data processing with the SIMA package. For example, those wishing to use SIMA solely for motion correction can export the motion-corrected time series with a call to the `ImagingDataset.export_frames` method. This method takes as its argument the filenames with which the exported data will be saved, formatted as a list of lists of strings organized similarly to the input data (see subsection 5.3.1). Additional optional arguments can be used to specify the output file format, whether to scale the intensity values to the full range allowed by the output file format, and whether to fill in unobserved rows (Figure 5.2A) of motion corrected images with values from adjacent frames. Time-averaged images can similarly be exported with the `ImagingDataset.export_averages` method.

If SIMA is also used for signal extraction, then the extracted signals can be exported to a CSV file with the `ImagingDataset.export_signals` method. The resulting CSV file contains the `id`, `label`, and `tags` for each ROI, and the extracted signal from each ROI at each frame time.

## 5.4 Software details

### 5.4.1 ROI Registration

To estimate affine transformations between pairs of time-averaged images, we used the function `getAffineTransform` from OpenCV. Once ROIs are transformed into the same reference space, the ROI Buddy GUI can automatically estimate the degree of similarity between each pair of ROIs from different `ImagingDataset` objects by calculating the Jaccard index, defined as the area of the intersection divided by the area of the union. ROIs are then clustered with the unweighted pair group method with arithmetic mean (UPGMA) hierarchical clustering algorithm (Sokal & Michener, 1958), with distances between ROIs given by the reciprocal of the Jaccard index for that pair. ROI pairs from the same `ImagingDataset` are assigned infinite distance to prevent co-clustering of ROIs from the same imaging session. The termination criterion for clustering is set such that pairs of ROIs in a cluster have a minimum Jaccard index of 0.25. The objects of each cluster are then assigned a common `id` attribute, allowing for identification of the same region over multiple imaging sessions.

### 5.4.2 Signal extraction

In discussing the extraction procedures, we use the notation  $w_{ip}$  to denote the weighting of the  $p$ th pixel by the  $i$ th ROI. For polygon or binary mask ROIs, created with SIMA’s automated segmentation or the ROI Buddy GUI, or imported from ImageJ,  $w_{ip}$  is defined as  $\frac{1}{N_i}$  for pixels  $p$  within the ROI and 0 elsewhere, where  $N_i$  is the number of pixels in the  $i$ th ROI.

The simplest case for extraction occurs when the same pixel locations are imaged in every frame. In this case, we calculate the signal by a simple weighting of the normalized fluorescence intensities from each pixel. Specifically, the signal of the  $i$ th ROI at time  $t$  is calculated as

$$s_{it} = \sum_p w_{ip} \cdot \frac{f_{pt}}{f_p}, \quad (5.1)$$

with  $f_{pt}$  denoting the intensity of the  $p$ th pixel in the frame at time  $t$ , and  $f_p$  denoting the average intensity across all frames at pixel location  $p$ .

When extracting signals following correction of within-frame motion artifacts, the situation is

complicated by the fact that not all pixel locations are observed in each frame. To derive a method for extracting these signals, we first note that the simple extraction method (Equation 5.1) reduces to the least-squares error estimate for a simple linear model in which the pixel intensities are related to the underlying ROI signals as follows:

$$\frac{f_{pt} - f_p}{f_p} = \sum_i a_{pi}(s_{it} - s_i^*),$$

with the coefficients  $a_{pi}$  defined as the entries of the pseudoinverse of the matrix with entries given by the weights  $w_{ip}$ , and with  $s_i^*$  set as  $\sum_p w_{ip}$ . Given this model, when a subset  $P_t$  of the pixels are imaged in the frame taken at time  $t$ , the least squares estimate of the signal is given by

$$s_{it} = \sum_p w_{ipt} \cdot \frac{f_{pt} - f_p}{f_p} + \sum_p w_{ip}.$$

Here, the time-dependent coefficients  $w_{ipt}$  are defined as the entries of the pseudo-inverse of the matrix with entries  $a_{pi}$  for all pixels  $p$  in  $P_t$ .

A few special cases are worth mentioning. For non-overlapping ROIs, this formula reduces to

$$s_{it} = \frac{\sum_p w_{ip}^2}{\sum_{p \in P_t} w_{ip}^2} \cdot \sum_{p \in P_t} w_{ip} \frac{f_{pt} - f_p}{f_p} + \sum_p w_{ip}.$$

In cases of binary mask or polygon ROIs, the above formula simplifies to

$$s_{it} = \frac{1}{N_{it}} \cdot \sum_{p \in P_{it}} \frac{f_{pt}}{f_p},$$

where  $P_{it}$  is the set of pixels in the  $i$ th ROI that were imaged at time  $t$ , and  $N_{it}$  the number of pixels in this set. In cases in which no pixels of a given ROI are imaged in a given frame, a not-a-number (`numpy.NaN`) value is recorded in place of that ROI's signal at that time.

# Chapter 6

## Additional Projects

### 6.1 Gating of hippocampal activity, plasticity, and memory by entorhinal cortex long-range inhibition<sup>1</sup>

The cortico-hippocampal circuit is critical for storage of associational memories. Most studies have focused on the role in memory storage of the excitatory projections from entorhinal cortex to hippocampus. However, entorhinal cortex also sends inhibitory projections, whose role in memory storage and cortico-hippocampal activity remains largely unexplored. We found that these long-range inhibitory projections enhance the specificity of contextual and object memory encoding. At the circuit level, these g-aminobutyric acid (GABA)-releasing projections target hippocampal inhibitory neurons and thus act as a disinhibitory gate that transiently promotes the excitation of hippocampal CA1 pyramidal neurons by suppressing feedforward inhibition. This enhances the ability of CA1 pyramidal neurons to fire synaptically evoked dendritic spikes and to generate a temporally precise form of heterosynaptic plasticity. Long-range inhibition from entorhinal cortex may thus increase the precision of hippocampal-based long-term memory associations by assessing the salience of mnemonic information to the immediate sensory input.

(Basu et al. 2016)

This project was primarily the work of Jayeeta Basu, who performed the slice physiological

---

<sup>1</sup>This work has been previously published (Basu et al., 2016) and is joint work with the coauthors.

recordings, though I performed and analyzed all *in vivo* imaging experiments. Dr. Basu characterized a long-range inhibitory projection (LRIP) from lateral entorhinal cortex (LEC) to the *stratum lacunosum moleculare* of hippocampal area CA1, which gated a specific form of input timing-dependent plasticity between CA3 Schaffer collaterals and CA1 pyramidal cells. In addition, Dr. Basu showed that interrupting this projection *in vivo* affected both context and object recognition memory. As further evidence for the *in vivo* role of these LRIPs from LEC to CA1, I imaged these fibers in CA1 while mice were running and exposed to various sensory stimuli.

We found that LEC inhibitory axons in CA1 showed robust responses to aversive (air puff), appetitive (water), and contextual (tone and light) stimuli. (Figure 6.1). In addition, these responses were coherent across buttons on a single axons and individual boutons responded to more than 2 stimuli at a higher rate than chance, together suggesting that there is a subpopulation of LEC inhibitory projecting cells which preferentially encode contexts as a whole (Figure 6.2).

## 6.2 Distinct contribution of adult-born hippocampal granule cells to context encoding<sup>2</sup>

Adult-born granule cells (abGCs) have been implicated in cognition and mood; however, it remains unknown how these cells behave *in vivo*. Here, we have used two-photon calcium imaging to monitor the activity of young abGCs in awake behaving mice. We find that young adult-born neurons fire at a higher rate *in vivo* but paradoxically exhibit less spatial tuning than their mature counterparts. When presented with different contexts, mature granule cells underwent robust remapping of their spatial representations, and the few spatially tuned adult-born cells remapped to a similar degree. We next used optogenetic silencing to confirm the direct involvement of abGCs in context encoding and discrimination, consistent with their proposed role in pattern separation. These results provide the first *in vivo* characterization of abGCs and reveal their participation in the encoding of novel information. (Danielson et al. 2016a)

While this project is the primary work of the first author, the behavioral apparatus, experi-

---

<sup>2</sup>This work has been previously published (Danielson et al., 2016a) and is joint work with the coauthors.

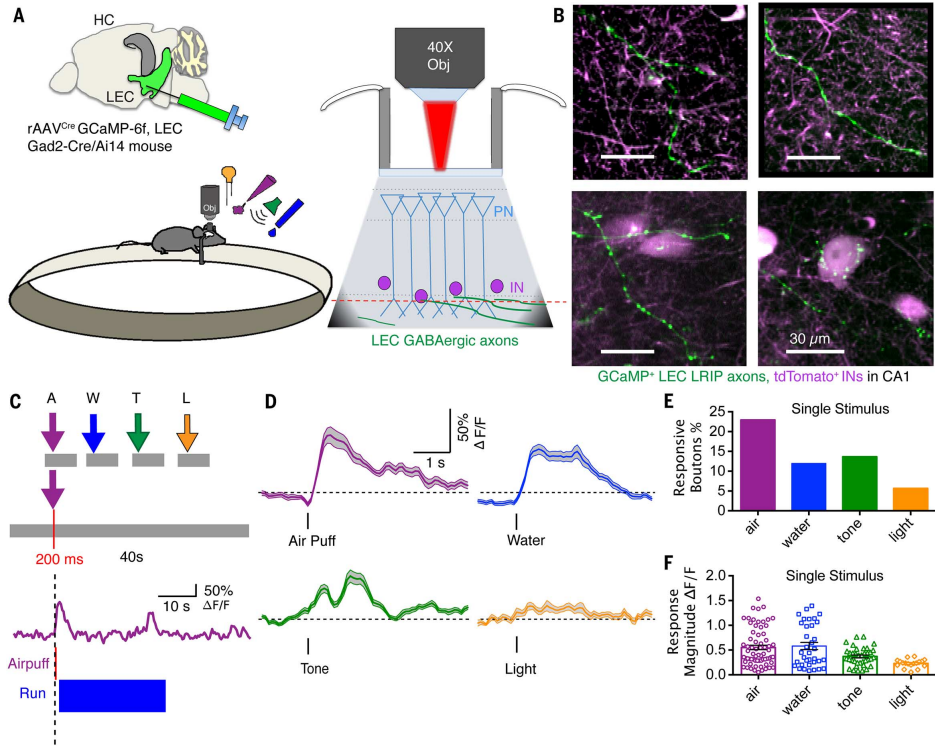


**Figure 6.1:** Functional imaging of sensory coding in LEC LRIPs present in SLM of CA1. **A)** Diagram of in vivo imaging experiment. GCaMP6f was expressed in dorsal LEC, by injecting Cre-dependent rAAV in *Gad2-Cre/Ai 14* mice that also expressed tdTomato in all GABAergic neurons. A 40× water immersion objective was used for two-photon imaging through a cranial window over CA1 in head-fixed awake mice during multimodal sensory and behavioral stimuli presentation. **(B)** Four examples of time-averaged images of GCaMP6f fluorescence in LEC LRIP axons in SLM (green) with tdTomato labeling CA1 interneurons (magenta). **(C)** Experimental design of single-stimulus protocol. Imaging was performed in blocks of four trials, each 40 seconds in duration. After a  $10 \pm 3$  s baseline, one of four types of stimuli – aversive air puff (A), water drop (W), tone (T), or light (L) – was presented in random order for 200 ms, except the water drop was limited to 50 ms to prevent satiation. Each block was repeated to obtain at least five trials per stimulus. The animal’s behavioral response (running and licking) was monitored.  $\Delta F/F$  traces showing increased  $\text{Ca}^{2+}$  signal in a single bouton on an LRIP axon in response to air puff. **(D)** Mean ( $\pm$  SEM)  $\Delta F/F$   $\text{Ca}^{2+}$  signal (PSTH) from responsive ROIs to indicated stimuli. **(E)** Percentage of responsive boutons to the stimuli (air = 22.92%, water = 11.96%, tone = 13.64%, and light = 5.65%). **(F)** Scatter and mean ( $\pm$  SEM) plots of  $\Delta F/F$  signals from individual responsive boutons (air =  $0.55 \pm 0.05$ , n = 68; water =  $0.58 \pm 0.07$ , n = 35; tone =  $0.37 \pm 0.03$ , n = 37; light =  $0.23 \pm 0.02$ , n = 18).

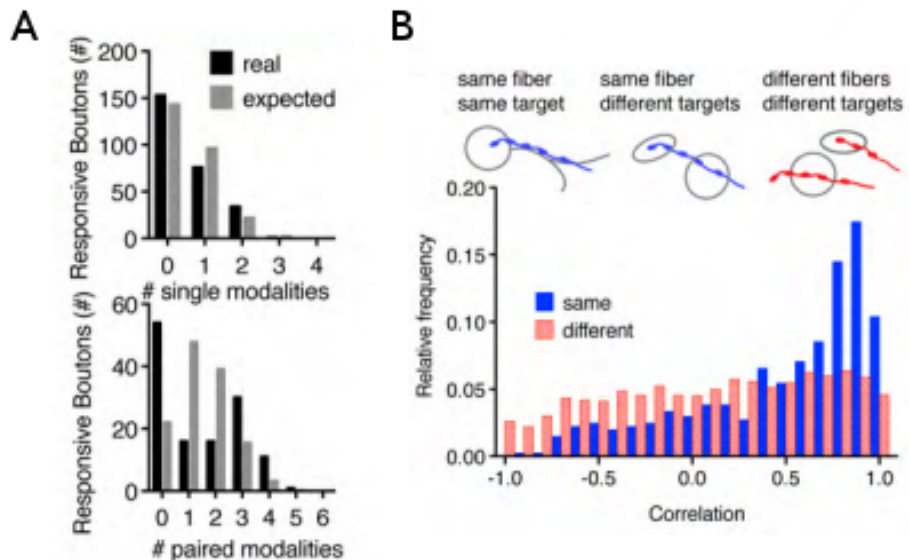


**Figure 6.2:** Responsive properties of LRIP boutons. (A) Histogram bar plots of the number of responsive boutons (*y*-axis) as a function of the number of stimulus modalities (*x*-axis) to which a given bouton responds, either with a single sensory stimulus (above) or two stimuli presented simultaneously (below). The experimental data is plotted in black while the distribution expected if the stimuli and bouton responses were independent is in gray. For single stimulus presentations, very few boutons respond to more than one type of stimulus, following the predictions for independent responses ( $P = 0.01659$ ). In contrast, paired stimuli evoke  $\text{Ca}^{2+}$  responses in a greater than expected number of boutons ( $P < 0.03$ ), perhaps the influence of a single overlapping stimulus in paired modalities (e.g. bouton responding to airpuff alone would likely respond to all three pairings with air; A+T, A+L, A+W). (B) Relative frequency distribution of bouton-bouton  $\text{Ca}^{2+}$  response correlation coefficients for all identifiable bouton pairs originating from the same axon segment (solid blue,  $r = 0.488 \pm 0.017$ ,  $n = 808$ ) versus boutons from different axons (cross-hatched red,  $r = 0.115 \pm 0.009$ ,  $n = 3992$ ;  $P < 0.0001$ , Mann-Whitney U test). Response similarity was determined by calculating the z-scored response magnitude for each stimulus for each bouton and then comparing the responses of pairs of boutons by calculating the correlation between their responses across all stimuli.

mental paradigms, and analysis tools were all developed jointly. In particular, this manuscript was Attila Losonczy’s lab’s first publication of head-fixed two-photon calcium imaging of place cells in mice, so relied upon co-developed upgrades to the behavioral apparatus (section 3.2), the imaging processing pipeline (section 3.3), and analysis of place cell data (subsection 3.3.3 & subsection 3.3.5).

### 6.3 Sublayer-specific coding dynamics during spatial navigation and learning in hippocampal area CA1<sup>3</sup>

The mammalian hippocampus is critical for spatial information processing and episodic memory. Its primary output cells, CA1 pyramidal cells (CA1 PCs), vary in genetics, morphology, connectivity, and electrophysiological properties. It is therefore possible that distinct CA1 PC subpopulations encode different features of the environment and differentially contribute to learning. To test this hypothesis, we optically monitored activity in deep and superficial CA1 PCs segregated along the radial axis of the mouse hippocampus and assessed the relationship between sublayer dynamics and learning. Superficial placemaps were more stable than deep during headfixed exploration. Deep maps, however, were preferentially stabilized during goal-oriented learning, and representation of the reward zone by deep cells predicted task performance. These findings demonstrate that superficial CA1 PCs provide a more stable map of an environment, while their counterparts in the deep sublayer provide a more flexible representation that is shaped by learning about salient features in the environment.

(Danielson et al. 2016b)

This project was the primary work of the first author, Nathan Danielson, but again a lot of the experimental designs, tools, and procedures were developed collaboratively: goal-oriented learning (GOL) task (subsection 3.2.2, Figure 6.4), place cell stability metrics (subsection 3.3.5, Figure 6.5), and reward enrichment analysis (Figure 6.6).

These results showed that superficial and deep pyramidal cells could store separable spatial maps: stable maps of space and context-dependent conjunctive representations, respectively. The

---

<sup>3</sup>This work has been previously published (Danielson et al., 2016b) and is joint work with the coauthors.

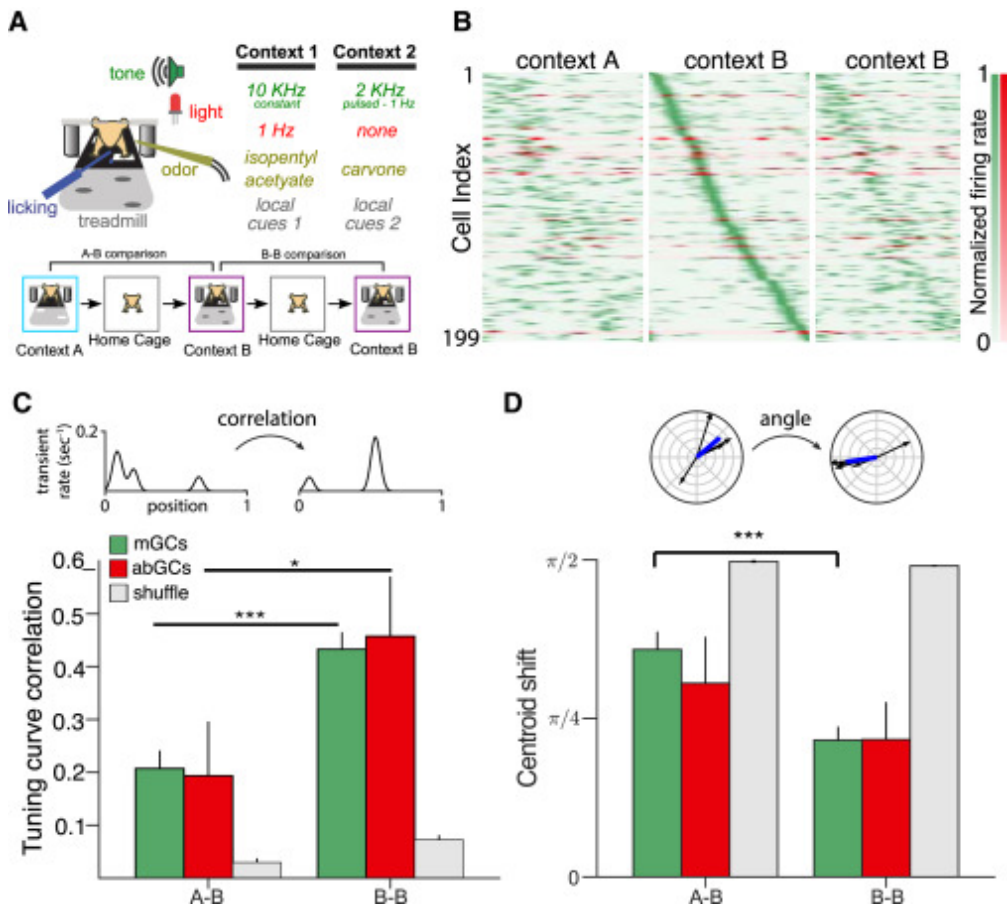


**Figure 6.3:** Contextual coding by adult-born and mature granule cells. (A) Experimental schematic. Mice ran for three 12-min sessions in contexts A, B, and B (1 hr between runs). A and B refer to either context 1 or 2 (chosen randomly for each experiment). (B) Remapping of spatial rate maps across sequential context exposures. Smoothed calcium transient rates, normalized to peak for each cell, are plotted as a function of position during three contextual exposures (A, B, B). Cells (mGCs, green; abGCs, red) are ordered according to the position of peak activity during the first exposure to context B. Data is shown for GCs with sufficient tuning specificity and activity ( $p < 0.1$ , at least four transients) in at least one experiment. (C and D) Context specificity of spatial representations. Tuning curve correlations of 1D rate maps (C) and centroid shifts (angle between tuning directions) (D) between sequential exposures to different (A-B) or the same (B-B) contexts for all cells shown in (B) (A-B: n = 180 mGCs, 14 abGCs; B-B: n = 174 mGCs, 9 abGCs). The rate map correlations of both populations were more similar in the B-B condition than in A-B (Mann-Whitney U, mGCs:  $U(150) = 5,291$ ,  $p < 0.001$ ; abGCs:  $U(18) = 23.0$ ,  $p < 0.05$ ). In mGCs the tuning shift was larger in the A-B condition than in B-B, although this did not reach significance in abGCs (mGCs:  $U(150) = 5,714$ ,  $p < 0.001$ ; abGCs:  $U(18) = 40.0$ ,  $p = 0.34$ ). In both conditions, the similarity of spatial representations exceeded chance levels as estimated by shuffling cell identity (gray). Error bars are mean  $\pm$  SEM.

developmental origin of the superficial-deep distinction (subsubsection 1.2.2.1) makes these results especially interesting in light of the neurodevelopmental etiology of schizophrenia and my results. Spatial maps in the *Df(16)A<sup>+/</sup>* mice were much less stable which could reflect superficial-CA1-specific wiring deficits.

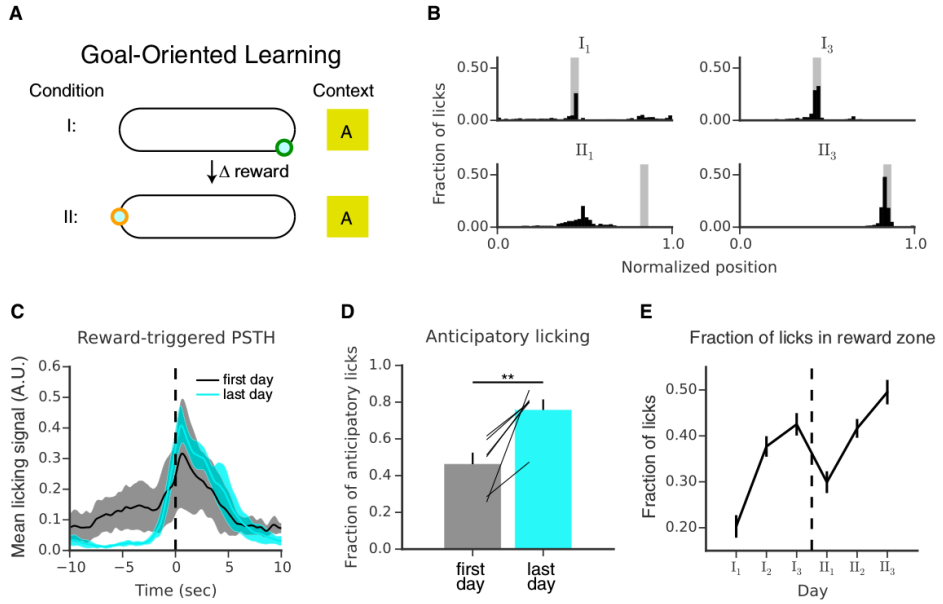


**Figure 6.4:** GOL task for head-fixed imaging. (A) Schematic of the goal-oriented learning (GOL) task. Mice ( $n = 6$ ) searched for an unmarked reward zone, and water rewards were administered only when the mice licked within the fixed 10-cm goal. At the end of condition I, the reward was moved to a new location of the belt, and the experiment was repeated (condition II). The same context (A) was maintained throughout. (B) Representative licking data from four individual experiments from one mouse performing the task. The fraction of total licks is plotted as a function of position on the belt (50 bins, 4 cm per bin). The reward zone is shaded gray. On the first day of the experiment, the mouse licked diffusely throughout the belt as it searched for the hidden reward zone. By the last day of condition I, the mouse licked selectively at the reward location. After the reward was moved, the mouse continued to lick at the original reward location. It eventually reverted to an exploratory licking state, and by the end of condition II the mouse selectively licked at the new reward location. (C) Peri-stimulus time histogram (PSTH) of licking rate triggered on reward zone entry for the first (black) and last (cyan) days of each condition. PSTHs were calculated for each mouse and smoothed with a 1-s Hamming filter. Shaded regions indicate mean  $\pm$  SD across mice. Licking was initially diffuse. By the last day, licking outside the reward zone was largely suppressed and rose sharply prior to reward zone entry, reflecting the expectation of reward. The effect was highly consistent across mice. (D) Anticipatory licking (fraction of non-reward zone licks in the 10 cm preceding the reward) increased significantly by the end of learning ( $n = 6$  mice,  $p < 0.01$ , paired t-test). Error bars indicate mean  $\pm$  SEM across mice. (E) The fraction of licks occurring within the reward zone aggregated by recording session and plotted by day (mean  $\pm$  SEM across mice). Over time, licking became more selective for the reward zone.

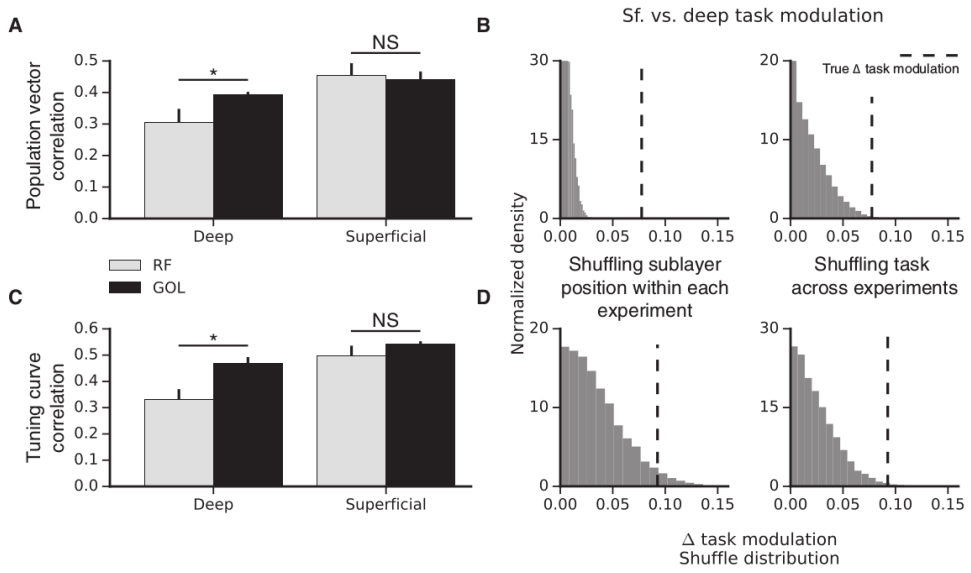


**Figure 6.5:** Sublayer-specific modulation of activity by the GOL task. (A) Stability in the B-B condition of RF compared to session-to-session stability in GOL (similar elapsed time of 90 min.). Deep, but not superficial, CA1 PCs showed a significant increase in PV correlation in the GOL task as compared to RF ( $n = 7$  RF mice, 6 GOL mice; deep,  $p < 0.05$ ; superficial,  $p = 0.36$ ; Mann-Whitney U test). Error bars indicate mean  $\pm$  SEM across animals. (B) The magnitude of the task modulation was compared across sublayers by performing two shuffling procedures: randomizing cell identity and randomizing task identity. Both comparisons suggested the magnitude of task modulation was greater for deep than for superficial cells ( $p < 0.001$ ,  $p < 0.01$ ). (C) The same analysis was performed with tuning curve correlation. Deep, but not superficial, CA1 PCs showed a significant increase in tuning curve correlation in the GOL task as compared to RF ( $n = 7$  RF mice, 6 GOL mice; deep,  $p < 0.05$ ; superficial,  $p = 0.11$ ; Mann-Whitney U test). Error bars indicate mean  $\pm$  SEM across animals. (D) Both shuffles showed the magnitude of the task modulation was greater for deep than superficial ( $p < 0.01$ ,  $p < 0.01$ ).

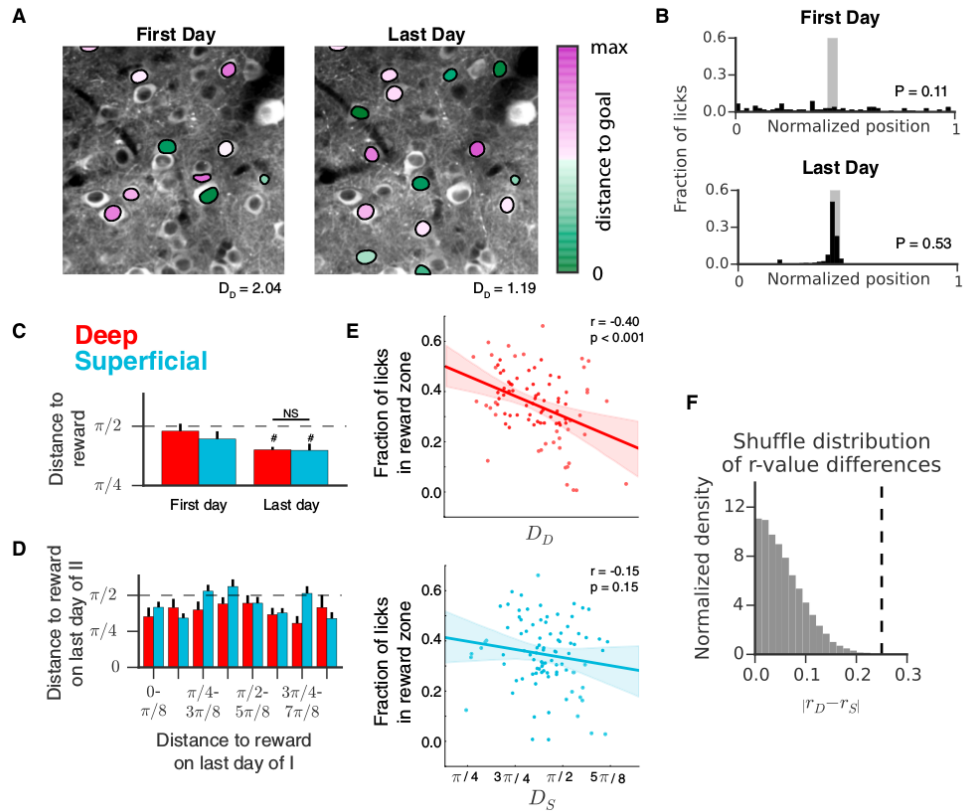


**Figure 6.6:** Reward zone representation versus performance on the GOL task. (A) Time-averaged images of the deep sublayer from two different recording sessions are shown in grayscale. Identified place cells from each session are overlaid and colored according to the distance of their centroid to the reward (green, near; purple, away). The mean distance to the reward zone is indicated (radians). (B) As in Figure 6.4B, licking distributions from the two experiments corresponding to (A). (C) Mean distance of each place cell centroid to the reward on first and last days of the experiment. On the last day, the mean distance to reward was significantly different from the chance level of  $\pi/2$  for both sublayers (dashed line;  $n = 6$  mice; one sample t-test; deep,  $p < 0.001$ ; superficial,  $p < 0.05$ ), but was not significantly different between sublayers ( $n = 6$  mice,  $p = 0.95$ , paired t-test). Error bars indicate mean  $\pm$  SEM across animals. (D) We did not detect a relationship between distance to reward at the end of condition II with distance at the end of I, sublayer, or with the interaction (type II ANOVA,  $n = 172$  deep, 336 superficial place cells,  $F(\text{distance end of I}) = 0.10$ ,  $p(\text{distance end of I}) = 0.76$ ;  $F(\text{layer}) = 0.54$ ,  $p(\text{layer}) = 0.46$ ;  $F(\text{interaction}) = 0.11$ ,  $p = 0.74$ ). The dashed line represents the mean distance expected in the case of a uniform place field distribution, and error bars indicate mean  $\pm$  SEM across cells. (E) Fraction of licks in reward zone (P) plotted against  $D_D$  (top) and  $D_S$  (bottom). Individual points represent single recording sessions. The dashed line indicates the linear fit with the 95% confidence interval shaded. We observed a significant relationship between  $D_D$  and P ( $n = 91$  sessions,  $r = 0.40$ ,  $p < 0.001$ , Pearson's R), but not between  $D_S$  and P ( $n = 91$  sessions,  $r = 0.15$ ,  $p = 0.15$ , Pearson's R). (F) In order to directly compare the sublayers' relationships to performance on the GOL task, we compared the magnitude of the difference in correlation coefficients (0.25, dashed line) relative to a null distribution. The true difference (dashed line) fell outside the shuffle distribution ( $p < 0.001$ ).

## **Part III**

# **Conclusions**

# Chapter 7

## Conclusions

### 7.1 Summary

In the preceding chapters I have laid out an understanding of memory in general, but also more specifically spatial-episodic memory, the structure in the brain that supports it (the hippocampus) and place cells as the functional units of these memories (chapter 1). I have explained the symptoms that define schizophrenia, particularly the cognitive deficits which are most relevant for functional recovery, yet least treatable, and identified some of the underlying genetic risk factors and proximate causes (chapter 2). I described the techniques that I employed in my experiments as well as the tools I developed to run the experiments and analyze the data (chapter 3). I next presented my primary thesis work; the characterization of hippocampal area CA1 pyramidal cell functional alterations during spatial learning in the *Df(16)A<sup>+/−</sup>* mouse model of schizophrenia (chapter 4). In addition, in collaboration with graduate student colleagues, I developed a Python package for the initial processing of Ca<sup>2+</sup> imaging data that we have released to the broader neuroscience community (chapter 5). Supplementing my primary project, I also helped characterize the *in vivo* functional properties of long-range inhibitory projections from lateral entorhinal cortex to CA1, adult-born neurons among the dentate gyrus granule cell population, and developmentally separable sub-populations of pyramidal cells within area CA1 (chapter 6).

### 7.1.1 What we learned about memory

By performing some of the first functional, awake, *in vivo* imaging experiments in the hippocampus (HPC), I characterized the *in vivo* activity of novel circuit elements and identified neural correlates of learning. In particular, I have shown that:

- The stability of place cell populations – both in the identity and tuning of those cells – correlates with learning of a spatial reward task.
- The memory encoding strategy employed by the HPC varies depending on the specifics of the task demands.
- Place cell enrichment of the reward location can support learning of spatial rewards and this enrichment arises from the coherent shift of place fields towards the reward location.
- Place cells retain latent tuning information even during sessions when they are not active, providing further evidence for separate codes for spatial and episodic memory (Leutgeb et al., 2005b).
- Long-range inhibitory projections from the lateral entorhinal cortex (LEC) convey salient, contextual information to the HPC, providing a disinhibitory gating mechanism to refine hippocampal contextual representations.
- Adult-born granule cells have higher firing rates and are less spatially-tuned than mature granule cells, supporting their role in context discrimination and pattern separation.
- Superficial and deep CA1 pyramidal cells independently modulate their activity during learning, providing distinct substrates for stable and dynamic representations of space.

Depending on the specific task demands, the HPC can support learning and memory either by providing stable spatial representations for other brain regions – such as the prefrontal cortex – or by dynamically reconfiguring to explicitly internally represent the salient features of the environment. The finding that stable maps always correlated with learning, but place cell reward enrichment only did sometimes, implies that a stable spatial map coexists with a salience-weighted map. Superficial and deep pyramidal cells may provide the distinct cellular substrates to support these two maps

simultaneously. The salience instructive signal could come from direct neuromodulatory inputs to the HPC or from contextual LEC inputs, such as the long-range inhibitory projection (LRIP) – and possibly the two in combination.

It's worth noting that while my main work primarily looked to understand aberrant hippocampal activity in the *Df(16)A<sup>+/</sup>* mouse during spatial-reward learning task, my data also is interesting from the reverse perspective of understanding normal hippocampal function during a spatial-reward learning task. We have shown that the *Df(16)A<sup>+/</sup>* mouse is a model of impaired global remapping (context stability) and goal-related remapping (enrichment), two fairly complicated properties of neuronal circuits that would otherwise be very difficult, if not impossible, to manipulate. From this perspective, my data provides evidence that inducing global remapping or preventing reward-zone place cell enrichment impairs spatial-reward memory.

### 7.1.2 What we learned about schizophrenia

Functional imaging in an etiologically-validated mouse model of schizophrenia provided insights into the hippocampal circuit disruptions that underlie hippocampal-dependent behavior. In particular, by imaging CA1 pyramidal cell activity throughout a goal-oriented learning (GOL) task, I've shown that:

- *Df(16)A<sup>+/</sup>* mice can perform spatial navigation tasks, just less efficiently, which is similar to what has been observed in schizophrenia patients.
- *Df(16)A<sup>+/</sup>* mice are specifically impaired as task demands increase.
- Spatial maps are less stable, both in cell identity and spatial tuning, in the *Df(16)A<sup>+/</sup>* mice, providing a plausible functional explanation for impaired hippocampal-dependent behaviors.
- Minor changes to context resulted in global remapping only in *Df(16)A<sup>+/</sup>* mice, lending support to the idea of schizophrenia as a disorder of aberrant salience.
- The specific cognitive strategy of place cell enrichment of salient features (goal zones) is inaccessible to the *Df(16)A<sup>+/</sup>* mice, forcing them to rely on less-efficient alternate strategies.
- *Df(16)A<sup>+/</sup>* spatial maps do not show any evidence of shifting towards the reward, which was implicated in my remapping model to be driving reward enrichment.

Stable place cell maps, in and of themselves, do not provide information about where to find salient features, such as rewards. Despite this, stable maps do help spatial reward learning in both wildtype and *Df(16)A<sup>+/−</sup>* mice, which suggests that downstream regions make use of this information – potentially regions which have also been implicated in schizophrenia pathology, such as the basal ganglia and prefrontal cortex. The HPC is clearly not the only brain region affected by schizophrenia, but it is a key component of the cognitive systems disrupted in schizophrenia, including declarative memory, which has been my focus.

In general, I've shown disruptions in neuronal ensemble activity in a genetic model of schizophrenia that directly relate to behavioral deficits. These behaviors are similar to symptoms observed in schizophrenia patients and the functional deficits I identified were in the evolutionarily-conserved hippocampal circuit, so they may translate to human patients as well.

## 7.2 Future directions

### 7.2.1 Context generalization

My GOL task tested two fundamentally different aspects of spatial memory: (1) how do spatial maps change in response to small changes to the environment (Condition I & II)? and (2) how do spatial maps support the encoding of salient reward locations (Condition II & III)? I found an interesting differential effect between WT and *Df(16)A<sup>+/−</sup>* mice in both of these tasks, so it would be interesting to explore each of these in more detail. In particular, my context remapping results suggests that the *Df(16)A<sup>+/−</sup>* mice mis-attend to stimuli that the wildtype mice ignore, which manifests as an over-separation of similar contexts as seen by impaired task performance and also the global remapping of spatial maps between the two similar contexts. This could be looked at in more detail by systematically modifying the two contexts to have varying degrees of symmetry and look at similarity of spatial maps between the two contexts while performing a context discrimination task.

The EC-DG-CA3 circuit has been implicated in ‘pattern separation’ and ‘pattern completion’ as a means for distinguishing similar contexts and generalizing to slightly different contexts (see subsubsection 1.2.2.2). My work on adult-born granule cells (abGCs) highlighted their role in context discrimination (section 6.2) and there is also evidence that adult neurogenesis may be altered

in schizophrenia (reviewed in, Toro & Deakin, 2007), which is perhaps not surprising given the developmental origin of schizophrenia (subsection 2.3.2). Recording from abGCs in the *Df(16)A<sup>+/</sup>* mouse model may provide insight into possible disruptions of adult neurogenesis in schizophrenia.

Alternatively, non-spatial, contextual information arrives to the HPC through a distinct circuit pathway which includes a LRIP from the LEC (see subsubsection 1.2.2.2). I performed the first awake, *in vivo* functional imaging recordings of this projection which confirmed that they carry information about salient features of the environment (see section 6.1 & Basu et al. (2016)). This projection may be driving the observation of aberrant salience in the *Df(16)A<sup>+/</sup>* mice, and potentially more generally in schizophrenia patients.

### 7.2.2 Hippocampal GABAergic interneurons

Hippocampal GABAergic interneurons (INs) provide robust control of the local hippocampal circuit (subsubsection 1.2.1.2). Disruptions in both excitatory synaptic machinery and interneuron networks have been implicated as a possible root cause of schizophrenia progression, though beyond gross neuroanatomical differences, the specific functional disruptions in GABAergic INs in schizophrenia are not well understood (see subsection 2.3.4). Goal-oriented learning-related reorganization of hippocampal CA1 interneuron activity has been recently demonstrated (Dupret et al., 2013), suggesting that CA1 GABAergic interneuron activity is closely tied to learning-related remapping of place cell ensembles, but the role of genetically-identified HPC GABAergic inhibitory circuits during normal and diseased learning and memory has not been characterized. In particular, the paper by Dupret et al. shows that interneuron activity evolves with pyramidal cell activity as learning progresses and place cells enrich the reward location. It is tempting to infer that interneuron activity is shaping pyramidal cell activity profiles, as it is possible that local INs could provide the needed signal to shift place cell firing towards the reward location. By recording the activity of dendrite-, soma-, and interneuron-targeting INs during the GOL task I can look for altered activity during Condition III, when the *Df(16)A<sup>+/</sup>* mice failed to show any reward enrichment, and also performed poorly on the task. I acquired preliminary data from each of these subclasses of INs and while I do not yet have conclusive results, initial analysis showed interesting differences in running modulation of VIP+ interneuron-targeting INs. This suggests that there may be deficits in the precise timing of the release of inhibition to allow for learning during spatial navigation.

### 7.2.3 Functional dissection of population dynamics with *in vivo* imaging during alternate hippocampus-dependent behaviors in the *Df(16)A<sup>+-</sup>* mouse

Goal-oriented learning, as a test of spatial-episodic memory, was the first behavior – beyond simple random-foraging tasks – that we attempted to train the head-fixed *Df(16)A<sup>+-</sup>* mice to perform. It would also be very interesting to analyze behaviors related to other cognitive domains with well-known deficits in the *Df(16)A<sup>+-</sup>* mice. The *Df(16)A<sup>+-</sup>* mice have a well-established deficit in contextual fear conditioning (CFC, Stark et al., 2008) – they freeze less than wildtype mice – and we have already adapted CFC for head-fixed imaging (hfCFC, Lovett-Barron et al., 2014). Our hfCFC paradigm uses an air-puff to the snout, instead of a foot shock, as the unconditioned stimulus (US) and lick suppression, instead of freezing, as the conditioned response (CR), so we would need to confirm that the *Df(16)A<sup>+-</sup>* still showed a behavioral deficit with this potentially milder US. Based on work by Moita et al. (Moita et al., 2004), I would expect to see place cell remapping selectively induced in the wildtype mice in the conditioned context, but not in the *Df(16)A<sup>+-</sup>* mice. In addition, we have shown that SST+ interneurons in CA1 effectively filter out the CS from the representation of the conditioned context (Lovett-Barron et al., 2014), so disrupted interneuron activity in the *Df(16)A<sup>+-</sup>* mice could lead to contamination of the conditioned context representation in the HPC by the US, leading to the observed deficit in freezing. This would also be generally consistent with my finding that the *Df(16)A<sup>+-</sup>* mice are differentially affected by small changes to the contextual environment (subsection 4.2.8) and the schizophrenia conceptual framework that suggests that mis-attribution of salience may be the fundamental underlying dysfunction (Kapur, 2003; van Os & Kapur, 2009).

Another interesting behavior for future study is prepulse inhibition (PPI), where the magnitude of the acoustic startle response to a loud noise is markedly reduced by preceding the tone with a milder stimulus. The *Df(16)A<sup>+-</sup>* mouse shows decreased PPI, and this behavior involves the septo-hippocampal cholinergic projection in particular (Koch, 1996; Swerdlow et al., 2001). This task should be fairly straightforward to establish as a head-fixed paradigm. As place cells and running activity would not necessarily be relevant for this task, I could instead use an immobilization chamber in place of the treadmill that I used throughout my previous experiment. Mice quickly adapt to this form of restraint and other members of our lab regular make use of this technique.

The aversive stimulus could be either an air-puff as we've used in the past, or a mild shock delivered through the immobilization chamber. By imaging the cholinergic septo-hippocampal projections in HPC area CA1 we could determine if they are altered in the *Df(16)A<sup>+/−</sup>* mouse model, and if so, we could potentially attempt to correct the aberrant activity using optogenetics or pharmacogenetics approaches.

#### 7.2.4 Sharp wave-ripples in *Df(16)A<sup>+/−</sup>* during goal-oriented learning

We looked at baseline sharp wave-ripples (SWRs) in WT and *Df(16)A<sup>+/−</sup>* mice and found aberrant activity characterized by increased high-frequency power and an increased number of SWR events (subsection 4.2.7). This is a very interesting initial finding that could be a fundamental aspect of memory deficits in this mouse. SWRs are fundamental to the consolidation and recall of episodic memories (reviewed in, Buzsaki, 2015). They have specifically been shown to increase in frequency following rewarded trials in a spatial memory task (Singer & Frank, 2009). In the work by Dupret et al. which is conceptually similar to my GOL task (see subsection 4.4.5), the authors found that the fraction of cells that participated in SWRs during the task (the more cells ‘remembering’) and the similarity of place maps reactivated after the task during SWRs with the place maps near the reward locations during the task (the better they ‘remembered’ the reward) correlated with task performance. By recording SWR activity during and immediately after our GOL task we could look for disruptions in SWRs directly related to task performance. Based on our initial findings and the above mentioned work, I would hypothesize to see aberrant SWR activity specifically after the task, during the time most critical for consolidation to long-term memory. This could explain why we see learning similar to WT mice in the *Df(16)A<sup>+/−</sup>* mice during the day, but a large deficit following the overnight period (Figure 4.7).

#### 7.2.5 Reward cells

In spatial reward learning tasks, there is evidence of REWARD CELLS among the place cell population that follow the reward location as it moves (Hok et al., 2007). It has been suggested that their firing can predict reward memory recall – their activity directly precedes the onset of reward licking. I actively searched through my data for evidence of reward cells and was not able to find any. This cell population would be interesting to study in general, as the formation and stability of this cell

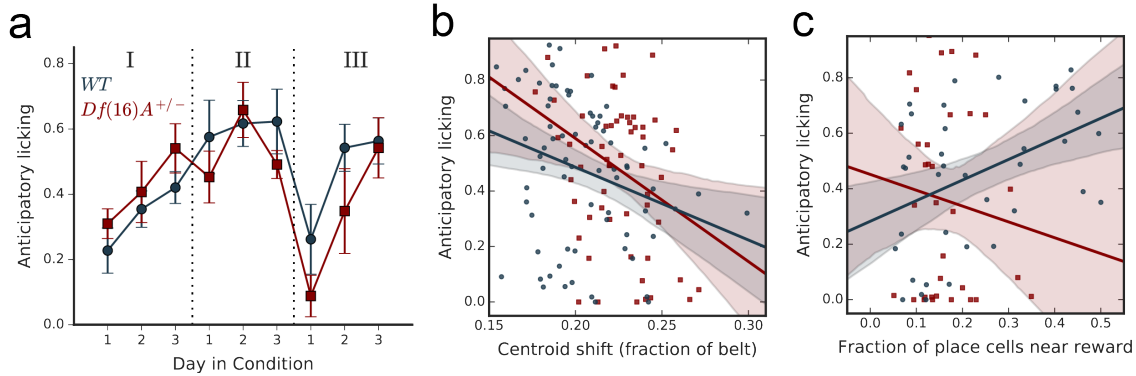


**Figure 7.1:** Mice anticipate the reward location and the anticipation is predicted by stable spatial maps. a. Task performance across all conditions of the task (two-way RM ANOVA, Genotype  $\times$  Condition interaction,  $p=0.060$ ). b. Task performance and centroid shift correlation (centroid shift vs. fraction of licks in reward zone, Pearson's correlation coefficient, WT: -0.282,  $p=0.015$ ;  $Df(16)A^{+-}$ : -0.343,  $p=0.008$ ). c. Task performance and goal zone place cell enrichment during Condition III (fraction of place cells near reward vs. fraction of licks in reward zone, Pearson's correlation coefficient, WT: 0.418,  $p=0.008$ ;  $Df(16)A^{+-}$ : -0.119,  $p=0.503$ ).

population over time has not been thoroughly investigated and they could have large implications for spatial reward learning. Also, in the  $Df(16)A^{+-}$  mice, their absence might also be reflective of their impaired task performance. To facilitate finding these cells, it would be helpful to modify the GOL task to include more than two reward locations. Instead of changing the context and then the reward, I could instead change the reward twice. This would help to identify cells that actually represented all three reward locations at the end of each Condition.

### 7.2.6 Further exploring place field shift modeling result

How do place cells throughout the environment coherently shift their firing fields towards the reward location (Figures 4.29 & 4.34)? The underlying mechanism driving this coherent shift remains unknown. Our result shows a symmetric shift towards the reward location, so some signal – which could be local to CA1 or from another brain region – needs to anticipate the reward position in order to shape the firing of place fields that precede the reward. We do see anticipatory licking leading up to the reward location that predicts tasks performance (Figure 7.1), so this information is clearly represented somewhere. Three possibilities that I would like to further investigate are that enrichment originates in the entorhinal cortex and is inherited by CA1, that neuromodulatory signals shape the tuning curves, or the local inhibitory circuit shifts firing fields towards the reward.

Hippocampal area CA1 receives a direct project from the entorhinal cortex via the temporoammonic pathway, which could shape their activity in a task- and learning-dependent manner. Grid cells in the medial entorhinal cortex are thought to contribute to a cognitive map of space by providing a metric framework for direction and distance (Hafting et al., 2005; Jeffery, 2015) and these cells directly project to hippocampal area CA1 (Zhang et al., 2013), though the nature of their influence on CA1 place cell activity is currently debated (Wills et al., 2010; Langston et al., 2010; Koenig et al., 2011; Brandon et al., 2011). Recent studies (Krupic et al., 2015; Stensola et al., 2015) have found evidence for warping of grid spacing to salient anchors points (walls), so it is tempting to speculate about a similar warp of grid cell spacing by the learned reward position. While we did not record from area CA3 cells in the current study, previous studies (Dupret et al., 2010a) have shown similar goal-directed remapping in CA1, but no remapping in CA3, leading to the possibility that area CA1 place cell activity is driven by stable CA3 representations and updated with environmental sensory input (border cells) and self-motion cues (grid cells) from the entorhinal cortex (Bush et al., 2014). Particularly, an increasing gradient of grid spacing centered about the reward would provide the perception of slower movement, thus delaying the firing of cells tuned to distance from boundaries and shifting all place cells towards the reward. The nature of border cells in a one-dimensional head-fixed environment is not entirely obvious, though there are salient belt fabric transitions that could similarly anchor a cognitive reference frame. This interpretation predicts that after reward learning, a given grid module will have an increased scale, with spacing maximal farthest away from the reward (largest shift) and smallest near the reward (smallest shift). Also, under conditions of grid cell map warping, we would expect a correlation between the local density of grid fields and the density of place cells. By recording either grid cells directly from the medial entorhinal cortex or grid cell axons that project to CA1, we could directly test these predictions.

Alternatively, CA1 could itself be the source of enrichment. The shift in firing field that we observed shows a symmetric ‘pull’ of fields towards the reward. This suggests a synaptic gain function that peaks at the reward and falls off symmetrically in both directions. Neurochemical gradients along the belt could modulate the synaptic plasticity window in this space-dependent manner. Alternatively, GABAergic control of pyramidal cell firing could also instill this learning rule on the pyramidal cell population. Both neuromodulation in general and hippocampal GABAergic interneuron activity in particular have been implicated in schizophrenia disease progression, which

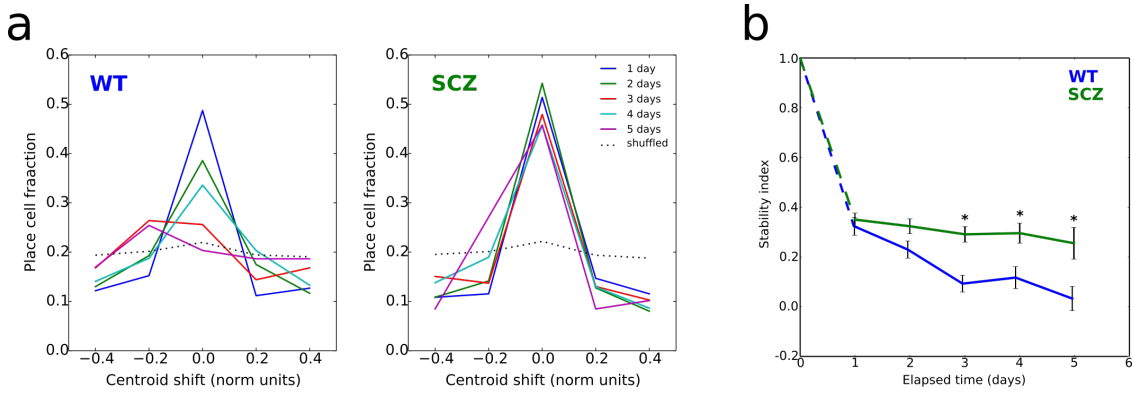


**Figure 7.2:**  $Df(16)A^{+/-}$  place fields are hyper-rigid over the course of a week. a. Histograms of centroid shift over a varying number of elapsed days for wildtype (left) and  $Df(16)A^{+/-}$  (right) mice. The sharp peak at zero shows that cells are generally stable day-to-day, but while the stability of the wildtype mice falls off (the curve flattens) over the course of 5 days, the  $Df(16)A^{+/-}$  place fields stay hyper-stable. b. Place cell recurrence probability as a function of elapsed time. Similar to centroid shift, the place cell population also is hyper-stable in the  $Df(16)A^{+/-}$  mice.

could explain the lack of enrichment in  $Df(16)A^{+/-}$  mice.

### 7.2.7 Long term stability in place cell population

One of my first experiments with the  $Df(16)A^{+/-}$  mouse was to look at the long-term stability of CA1 spatial maps in a similar manner as Ziv et al. (Ziv et al., 2013). Mice were trained to run head-fixed on our same cue-rich multi-fabric belts as I used in the GOL task, but only for 1 session each day and the water reward was presented non-operantly once per lap at the same location every day. I recorded CA1 pyramidal cell activity for at least 6 days without changing any aspects of the task. By looking at the stability between spatial maps at progressively longer elapsed intervals I found that while the wildtype stability decreased from 1 day elapsed to 5 days elapsed, the  $Df(16)A^{+/-}$  spatial maps were surprisingly rigid for the entire 6 days (Figure 7.2).

Ziv et al. actually found the wildtype mice to be more stable than what I observed, but I think this can be contributed to differences in task protocol. In their task, mice were running in an already familiar environment, so the stability observed was reflective of an already stabilized spatial map. In contrast, in our task the belt that conveys all of the spatial information was novel on day 1, therefore we observed the normal stabilization that occurs over the first few days of exposure to a novel environment. This interpretation suggests that the  $Df(16)A^{+/-}$  mice immediately stabilize their spatial maps so that they don't allow for the normal stabilization process to occur.

This data needs further follow-up to completely interpret the results. There was really no spatial learning in this version of the task. Mice received water as long as they continued to run, it was delivered automatically every lap, and they didn't need to remember where that location was. The first experiment I would run would be to change the reward schedule to require learning and memory. Instead of a non-operant reward every lap, I would make it similar to the GOL task; one rewarded zone where the water is only delivered if the mice actually lick there. In this case I would expect to see several factors alternatively driving stability or rigidity. First, wildtype mice showed a task-dependent stabilization from day-to-day, so we might see this effect over longer timescales as well. Second, in Condition III of my GOL task I observed place cell enrichment of the reward location in the wildtype mice, which could manifest as transient instability as cells remap to the reward, but then increased stability as they stabilize. Finally, I observed neither of those effects in *Df(16)A<sup>+/</sup>* mice, so I don't necessarily expect this change to affect the stability of the *Df(16)A<sup>+/</sup>* place fields.

In addition, to see if the decreased stability in the wildtype mice relative to Ziv et al. is truly due to environment novelty, we could either over-train the mice on the same belt on which we will eventually record place cell activity, or extend the protocol to 10 or more days so that we can alternatively discard the first few days and look at long-term stability relative to day 3 or 4. I would expect to see increased stability in the wildtype mice, back to the level observed initially in the *Df(16)A<sup>+/</sup>* mice. Assuming that both of these proposed manipulations increase stability in the wildtype mice, but don't affect the already increased *Df(16)A<sup>+/</sup>* stability, this would confirm an aberrantly fast place map rigidity in novel environments, and would suggest deficient novelty signaling in the *Df(16)A<sup>+/</sup>* mice, which may be linked to aberrant neuromodulatory signaling of novelty or generally with the proposed role of CA1 in novelty detection (Li et al., 2003; Barry et al., 2012; Larkin et al., 2014; Nitz & McNaughton, 2004).

### 7.2.8 Neuromodulators in the hippocampus of *Df(16)A<sup>+/</sup>* mice

Both principal neurons and local GABAergic interneurons are targeted by afferents from neuromodulatory nuclei, including cholinergic and GABAergic projections from the medial septum (MS) (Klausberger & Somogyi, 2008), serotonergic and glutamatergic projections from the raphe nuclei (Varga et al., 2009), dopaminergic projections from the ventral tegmental area (VTA) (Gasbarri

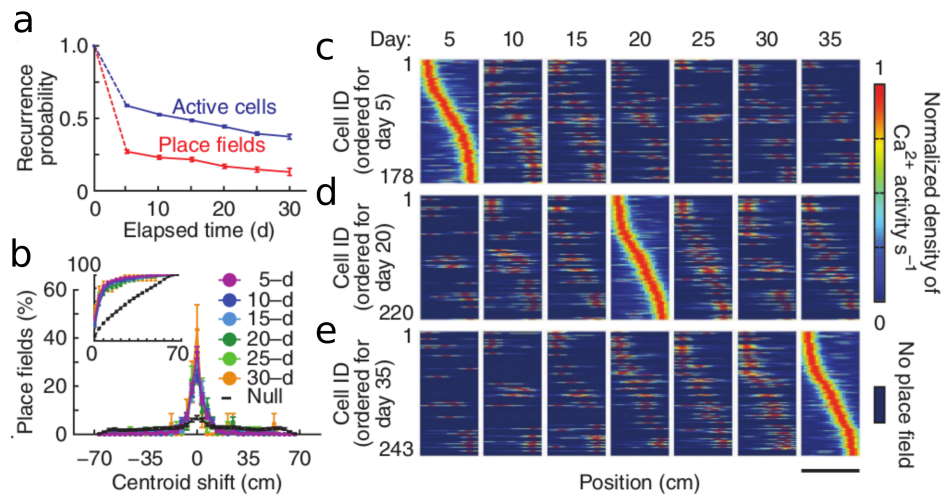


**Figure 7.3:** Place fields are spatially invariant and temporally stochastic while preserving a stable representation at the ensemble level. (a) If a cell had  $\text{Ca}^{2+}$  activity in one session, the odds (blue data) that it also did in a subsequent session declined with time. If a cell had a statistically significant place field in one session, the odds (red data) that it had a place field in a subsequent session also declined with time. Mean  $\pm$  s.e.m. (b) Distributions of centroid shifts (colored by days between sessions, mean  $\pm$  s.e.m.) were indistinguishable (Kolmogorov-Smirnov test,  $P \geq 0.17$ ), sharply peaked at zero and highly distinct from the null hypothesis that place fields would randomly relocate ( $P = 4 \times 10^{-67}$ , Kolmogorov-Smirnov test). Inset, cumulative histograms of shift magnitudes; 74-83% were  $\leq 7$  cm. Median shift (3.5 cm) was much less than the median place field width (24 cm). (c-e) Place-field maps for cells found on multiple days, ordered by place fields' centroid positions on day 5 (c), day 20 (d) or day 35 (e). Data pooled across four mice. Reproduced from Ziv et al. (2013).

et al., 1997) and noradrenergic projections from the locus coeruleus (Foote et al., 1983). The functional consequences of these projections is not completely understood, but place cell stability can be affected by salience, novelty, and attention, which has been shown to act through neuromodulatory inputs, including dopamine and acetylcholine. Of these neuromodulatory projections, the dopaminergic-VTA and cholinergic-MS projections are of particular interest, since there is already extensive literature relating dopamine to schizophrenia (Davis et al., 1991) and the cholinergic projection is involved in normal hippocampal learning and memory (Parent & Baxter, 2004). Despite these well-characterized features of hippocampal neuromodulation, it remains unknown how the function of these circuits are altered in schizophrenia during hippocampal-dependent behaviors.

To search for aberrant salience/novelty/attention signaling in the *Df(16)A<sup>+/−</sup>* mice I could directly image the activity of the dopaminergic and cholinergic axons projecting from the ventral tegmental area and medial septum, respectively, to area CA1 of the HPC. Dopamine is proposed to signal salience or reward (Berridge & Robinson, 1998), so based on my findings of mis-attention to minor changes in the environment (subsection 4.2.8) and generally impaired reward learning in the *Df(16)A<sup>+/−</sup>* mice (subsection 4.2.2), I suspect that I will see an overactive VTA dopamine projection, which might manifest as an indiscriminate increased activity rate, disruptions in the more precise timing of firing around the reward, and/or altered trajectory of activity across days during learning as compared to wildtype mice. Dopamine is also involved in the long-term stability of place cells (subsubsection 1.3.1.2), so aberrant dopamine activity may also explain the impaired stability of *Df(16)A<sup>+/−</sup>* spatial maps (subsection 4.2.4). In addition, the septal-cholinergic projection has been specifically implicated in novelty detection (Jeewajee et al., 2008; Barry et al., 2012), and the *Df(16)A<sup>+/−</sup>* mice appear to have a familiarity-specific deficit in our GOL task (subsection 4.2.10), so I suggest that we might see abnormal septal-cholinergic activity in the *Df(16)A<sup>+/−</sup>* mice.

# Bibliography

- Achim, A. M. & Lepage, M. (2005). Episodic memory-related activation in schizophrenia: meta-analysis. *Br J Psychiatry*, 187, 500–509.
- Agarwal, S. M., Danivas, V., Amaresha, A. C., Shivakumar, V., Kalmady, S. V., Bose, A., Narayanaswamy, J. C., & Venkatasubramanian, G. (2015). Cognitive mapping deficits in schizophrenia: Evidence from clinical correlates of visuospatial transformations. *Psychiatry Res*, 228, 304–311.
- Agnihotri, N. T., Hawkins, R. D., Kandel, E. R., & Kentros, C. (2004). The long-term stability of new hippocampal place fields requires new protein synthesis. *Proceedings of the National Academy of Sciences of the United States of America*, 101, 3656–61.
- Ahmed, O. J. & Mehta, M. R. (2009). The hippocampal rate code: anatomy, physiology and theory. *Trends in neurosciences*, 32, 329–38.
- Aleman, A., Hijman, R., de Haan, E. H., & Kahn, R. S. (1999). Memory impairment in schizophrenia: a meta-analysis. *The American journal of psychiatry*, 156, 1358–66.
- Allen, N. C., Bagade, S., McQueen, M. B., Ioannidis, J. P. A., Kavvoura, F. K., Khouri, M. J., Tanzi, R. E., & Bertram, L. (2008). Systematic meta-analyses and field synopsis of genetic association studies in schizophrenia: the SzGene database. *Nature Genetics*, 40, 827–834.
- Altimus, C., Harrold, J., Jaaro-Peled, H., Sawa, A., & Foster, D. J. (2015). Disordered ripples are a common feature of genetically distinct mouse models relevant to schizophrenia. *Mol Neuropsychiatry*, 1, 52–59.
- Amaral, D. G., Ishizuka, N., & Claiborne, B. (1990). Neurons, numbers and the hippocampal network. In *Understanding the Brain Through the Hippocampus: The Hippocampal Region as a Model for Studying Brain Structure and Function*, J. Storm-Mathisen, J. Zimmer, & O. P. Ottersen, eds. pp. 1–11.
- Ambros-Ingerson, J. & Holmes, W. R. (2005). Analysis and comparison of morphological reconstructions of hippocampal field CA1 pyramidal cells. *Hippocampus*, 15, 302–315.
- Angevine, J. B. (1965). Time of neuron origin in the hippocampal region. An autoradiographic study in the mouse. *Experimental neurology*. Supplement, pp. Suppl 2:1–70.
- Angrist, B. M. (1994). Amphetamine psychosis: clinical variations of the syndrome. In *Amphetamine and Its Analogs*, A. K. Cho & D. S. Segal, eds. (Academic Press), pp. 387–414.
- Arguello, P. A. & Gogos, J. a. (2012). Genetic and cognitive windows into circuit mechanisms of psychiatric disease. *Trends in Neurosciences*, 35, 3–13.

- Armstrong, K., Kose, S., Williams, L., Woolard, A., & Heckers, S. (2012). Impaired associative inference in patients with schizophrenia. *Schizophr Bull*, 38, 622–629.
- Aronov, D. & Tank, D. W. (2014). Engagement of Neural Circuits Underlying 2D Spatial Navigation in a Rodent Virtual Reality System. *Neuron*, 84, 442–456.
- Astur, R. S., Ortiz, M. L., & Sutherland, R. J. (1998). A characterization of performance by men and women in a virtual Morris water task:. *Behavioural Brain Research*, 93, 185–190.
- Bailey, C., Barco, A., Hawkins, R., & Kandel, E. (2008). Molecular studies of learning and memory in Aplysia and the hippocampus: A comparative analysis of implicit and explicit memory storage. In *Learning and memory: A Comprehensive Reference*, Volume 4. pp. 11–29.
- Barch, D. M., Carter, C. S., MacDonald 3rd, A. W., Braver, T. S., & Cohen, J. D. (2003). Context-processing deficits in schizophrenia: diagnostic specificity, 4-week course, and relationships to clinical symptoms. *J Abnorm Psychol*, 112, 132–143.
- Barnes, C. A. (1979). Memory deficits associated with senescence: a neurophysiological and behavioral study in the rat. *Journal of comparative and physiological psychology*, 93, 74–104.
- Barr, I., Weitz, S. H., Atkin, T., Hsu, P., Karayiorgou, M., Gogos, J. A., Weiss, S., & Guo, F. (2015). Cobalt(III) Protoporphyrin Activates the DGCR8 Protein and Can Compensate microRNA Processing Deficiency. *Chemistry and Biology*, 22, 793–802.
- Barry, C., Heys, J. G., & Hasselmo, M. E. (2012). Possible role of acetylcholine in regulating spatial novelty effects on theta rhythm and grid cells. *Frontiers in neural circuits*, 6, 5.
- Bassett, A. S., Chow, E. W., AbdelMalik, P., Gheorghiu, M., Husted, J., & Weksberg, R. (2003). The Schizophrenia Phenotype in 22q11 Deletion Syndrome. *American Journal of Psychiatry*, 160, 1580–1586.
- Bassett, A. S., Hodgkinson, K., Chow, E. W., Correia, S., Scutt, L. E., & Weksberg, R. (1998). 22q11 deletion syndrome in adults with schizophrenia. *Am J Med Genet*, 81, 328–337.
- Bast, T. (2011). The hippocampal learning-behavior translation and the functional significance of hippocampal dysfunction in schizophrenia. *Curr Opin Neurobiol*, 21, 492–501.
- Basu, J., Zaremba, J. D., Cheung, S. K., Hitti, F. L., Zemelman, B. V., Losonczy, A., & Siegelbaum, S. A. (2016). Gating of hippocampal activity, plasticity, and memory by entorhinal cortex long-range inhibition. *Science*, 351, aaa5694–aaa5694.
- Berridge, K. C. & Robinson, T. E. (1998). What is the role of dopamine in reward: Hedonic impact, reward learning, or incentive salience? *Brain Research Reviews*, 28, 309–369.
- Bezaire, M. J. & Soltesz, I. (2013). Quantitative assessment of CA1 local circuits: knowledge base for interneuron-pyramidal cell connectivity. *Hippocampus*, 23, 751–785.
- Birrell, J. M. & Brown, V. J. (2000). Medial frontal cortex mediates perceptual attentional set shifting in the rat. *J Neurosci*, 20, 4320–4324.
- Biswas, A. B. & Furniss, F. (2016). Cognitive phenotype and psychiatric disorder in 22q11.2 deletion syndrome: A review. *Res Dev Disabil*, 53-54, 242–257.

- Bliss, T. V. & Collingridge, G. L. (1993). A synaptic model of memory: long-term potentiation in the hippocampus. *Nature*, 361, 31–39.
- Bliss, T. V. & Lomo, T. (1973). Long-lasting potentiation of synaptic transmission in the dentate area of the anaesthetized rabbit following stimulation of the perforant path. *The Journal of physiology*, 232, 331–56.
- Bloom, D. E., Cafiero, E., Jané-Llopis, E., Abrahams-Gessel, S., Reddy Bloom, L., Fathima, S., B. Feigl, A., Gaziano, T., Hamandi, A., Mowafi, M., O'Farrell, D., Ozaltin, E., Pandya, A., Prettner, K., Rosenberg, L., Seligman, B., Stein, A. Z., Weinstein, C., & Weiss, J. (2011). The Global Economic Burden of Noncommunicable Diseases. *World Economic Forum*, 184, 1–46.
- Bogerts, B., Meertz, E., & Schönfeldt-Bausch, R. (1985). Basal Ganglia and Limbic System Pathology in Schizophrenia: A Morphometric Study of Brain Volume and Shrinkage. *Archives of General Psychiatry*, 42, 784.
- Boyer, P., Phillips, J. L., Rousseau, F. L., & Ilivitsky, S. (2007). Hippocampal abnormalities and memory deficits: new evidence of a strong pathophysiological link in schizophrenia. *Brain research reviews*, 54, 92–112.
- Brandon, M. P., Bogaard, A. R., Libby, C. P., Connerney, M. A., Gupta, K., & Hasselmo, M. E. (2011). Reduction of Theta Rhythm Dissociates Grid Cell Spatial Periodicity from Directional Tuning. *Science*, 332, 595–599.
- Breese, C. R., Hampson, R. E., & Deadwyler, S. A. (1989). Hippocampal place cells: stereotypy and plasticity. *J Neurosci*, 9, 1097–1111.
- Burgess, N., Maguire, E. a., & O'Keefe, J. (2002). The human hippocampus and spatial and episodic memory. *Neuron*, 35, 625–41.
- Bush, D., Barry, C., & Burgess, N. (2014). What do grid cells contribute to place cell firing? *Trends in Neurosciences*, 37, 136–145.
- Butcher, N. J., Chow, E. W., Costain, G., Karas, D., Ho, A., & Bassett, A. S. (2012). Functional outcomes of adults with 22q11.2 deletion syndrome. *Genet Med*, 14, 836–843.
- Buzsaki, G. (2015). Hippocampal sharp wave-ripple: A cognitive biomarker for episodic memory and planning. *Hippocampus*, 25, 1073–1188.
- Buzsáki, G. & Moser, E. I. (2013). Memory, navigation and theta rhythm in the hippocampal-entorhinal system. *Nature Neuroscience*, 16, 130–138.
- Cacucci, F., Wills, T. J., Lever, C., Giese, K. P., & O'Keefe, J. (2007). Experience-dependent increase in CA1 place cell spatial information, but not spatial reproducibility, is dependent on the autophosphorylation of the alpha-isoform of the calcium/calmodulin-dependent protein kinase II. *J Neurosci*, 27, 7854–7859.
- Cannon, T. D., Chung, Y., He, G., Sun, D., Jacobson, A., van Erp, T. G., McEwen, S., Addington, J., Bearden, C. E., Cadenhead, K., Cornblatt, B., Mathalon, D. H., McGlashan, T., Perkins, D., Jeffries, C., Seidman, L. J., Tsuang, M., Walker, E., Woods, S. W., & Heinssen, R. (2015). Progressive Reduction in Cortical Thickness as Psychosis Develops: A Multisite Longitudinal Neuroimaging Study of Youth at Elevated Clinical Risk. *Biological Psychiatry*, 77, 147–157.

- Cannon, T. D., Glahn, D. C., Kim, J., Van Erp, T. G. M., Karlsgodt, K., Cohen, M. S., Nuechterlein, K. H., Bava, S., & Shirinyan, D. (2005). Dorsolateral Prefrontal Cortex Activity During Maintenance and Manipulation of Information in Working Memory in Patients With Schizophrenia. *Archives of General Psychiatry*, 62, 1071.
- Carlsson, A. & Lindqvist, M. (1963). Effect of Chlorpromazine or Haloperidol on Formation of 3-Methoxytyramine and Normetanephrine in Mouse Brain. *Acta pharmacologica et toxicologica*, 20, 140–4.
- Chamberland, S. & Topolnik, L. (2012). Inhibitory control of hippocampal inhibitory neurons. *Frontiers in Neuroscience*, 6, 1–13.
- Chen, T.-W., Wardill, T. J., Sun, Y., Pulver, S. R., Renninger, S. L., Baohan, A., Schreiter, E. R., Kerr, R. a., Orger, M. B., Jayaraman, V., Looger, L. L., Svoboda, K., & Kim, D. S. (2013). Ultrasensitive fluorescent proteins for imaging neuronal activity. *Nature*, 499, 295–300.
- Chow, E. W. C., Watson, M., Young, D. a., & Bassett, A. S. (2006). Neurocognitive profile in 22q11 deletion syndrome and schizophrenia. *Schizophrenia research*, 87, 270–8.
- Cloutier, M., Sanon Aigbogun, M., Guerin, A., Nitulescu, R., Ramanakumar, A. V., Kamat, S. A., DeLucia, M., Duffy, R., Legacy, S. N., Henderson, C., Francois, C., & Wu, E. (2016). The economic burden of schizophrenia in the United States in 2013. *The Journal of clinical psychiatry*, 2012, 764–771.
- Cohen, J. D., Barch, D. M., Carter, C., & Servan-Schreiber, D. (1999). Context-processing deficits in schizophrenia: converging evidence from three theoretically motivated cognitive tasks. *Journal of abnormal psychology*, 108, 120–33.
- Colgin, L. L., Moser, E. I., & Moser, M.-B. (2008). Understanding memory through hippocampal remapping. *Trends in Neurosciences*, 31, 469–477.
- Collin, G., Hulshoff Pol, H. E., Hajjma, S. V., Cahn, W., Kahn, R. S., & van den Heuvel, M. P. (2011). Impaired cerebellar functional connectivity in schizophrenia patients and their healthy siblings. *Front Psychiatry*, 2, 73.
- Collingridge, B. Y. G. L., Kehl, S. J., & McLennan, H. (1983). Excitatory amino acids in synaptic transmission in the schaffer collateral-commissural pathway of the rat hippocampus. *Journal of Physiology*, 334, 33–46.
- Corkin, S. (2002). What's new with the amnesic patient H.M.? *Nature reviews Neuroscience*, 3, 153–160.
- Coyle, J. T. (2006). Glutamate and schizophrenia: beyond the dopamine hypothesis. *Cellular and molecular neurobiology*, 26, 365–84.
- Coyle, J. T. (2012). NMDA receptor and schizophrenia: a brief history. *Schizophr Bull*, 38, 920–926.
- Crabtree, G. W. & Gogos, J. A. (2014). Synaptic plasticity, neural circuits, and the emerging role of altered short-term information processing in schizophrenia. *Front Synaptic Neurosci*, 6, 28.
- Crabtree, G. W., Park, A. J., Gordon, J. A., & Gogos, J. A. (2016). Cytosolic Accumulation of L-Proline Disrupts GABA-Ergic Transmission through GAD Blockade. *Cell Reports*, 17, 570–582.

- Crider, A. (1997). Perseveration in schizophrenia. *Schizophr Bull*, 23, 63–74.
- Cross, A. J., Crow, T. J., & Owen, F. (1981). 3H-Flupenthixol binding in post-mortem brains of schizophrenics: evidence for a selective increase in dopamine D2 receptors. *Psychopharmacology*, 74, 122–4.
- Danielson, N. B., Kaifosh, P., Zaremba, J. D., Lovett-Barron, M., Tsai, J., Denny, C. A., Balough, E. M., Goldberg, A. R., Drew, L. J., Hen, R., Losonczy, A., & Kheirbek, M. A. (2016a). Distinct Contribution of Adult-Born Hippocampal Granule Cells to Context Encoding. *Neuron*, 90, 101–112.
- Danielson, N. B., Turi, G. F., Ladow, M., Chavlis, S., Petrantonakis, P. C., Poirazi, P., & Losonczy, A. (2017). In Vivo Imaging of Dentate Gyrus Mossy Cells in Behaving Mice. *Neuron*, 93, 552–559.e4.
- Danielson, N. B., Zaremba, J. D., Kaifosh, P., Bowler, J., Ladow, M., & Losonczy, A. (2016b). Sublayer-Specific Coding Dynamics during Spatial Navigation and Learning in Hippocampal Area CA1. *Neuron*, 91, 652–665.
- Davis, K. L., Kahn, R. S., Ko, G., & Davidson, M. (1991). Dopamine in schizophrenia: a review and reconceptualization. *The American journal of psychiatry*, 148, 1474–86.
- de Lavilleon, G., Lacroix, M. M., Rondi-Reig, L., & Benchenane, K. (2015). Explicit memory creation during sleep demonstrates a causal role of place cells in navigation. *Nat Neurosci*, 18, 493–495.
- de Nó, R. L. (1934). Studies on the Structure of the Cerebral Cortex: Continuation of the study of the ammonic system. II. (Johann Ambrosius Barth).
- de Vignemont, F., Zalla, T., Posada, A., Louvegnez, A., Koenig, O., Georgieff, N., & Franck, N. (2006). Mental rotation in schizophrenia. *Conscious Cogn*, 15, 295–309.
- Debbané, M., Glaser, B., & Eliez, S. (2008). Encoding and retrieval processes in velo-cardio-facial syndrome (VCFS). *Neuropsychology*, 22, 226–234.
- Debbané, M., Schaer, M., Farhoumand, R., Glaser, B., & Eliez, S. (2006). Hippocampal volume reduction in 22q11.2 deletion syndrome. *Neuropsychologia*, 44, 2360–2365.
- Deguchi, Y., Donato, F., Galimberti, I., Cabuy, E., & Caroni, P. (2011). Temporally matched subpopulations of selectively interconnected principal neurons in the hippocampus. *Nature neuroscience*, 14, 495–504.
- Delay, J., Deniker, P., & Harl, J. M. (1952). Therapeutic use in psychiatry of phenothiazine of central elective action (4560 RP). *Annales medico-psychologiques*, 110, 112–7.
- Deng, W., Aimone, J. B., & Gage, F. H. (2010). New neurons and new memories: how does adult hippocampal neurogenesis affect learning and memory? *Nature reviews. Neuroscience*, 11, 339–50.
- Denk, W., Strickler, J., & Webb, W. (1990). Two-photon laser scanning fluorescence microscopy. *Science*, 248, 73–76.
- Dere, E., Pause, B. M., & Pietrowsky, R. (2010). Emotion and episodic memory in neuropsychiatric disorders. *Behav Brain Res*, 215, 162–171.

- Deshmukh, S. S. & Knierim, J. J. (2013). Influence of local objects on hippocampal representations: Landmark vectors and memory. *Hippocampus*, 23, 253–267.
- Diba, K. & Buzsaki, G. (2007). Forward and reverse hippocampal place-cell sequences during ripples. *Nat Neurosci*, 10, 1241–1242.
- Dickerson, B. C. & Eichenbaum, H. (2010). The episodic memory system: neurocircuitry and disorders. *Neuropsychopharmacology*, 35, 86–104.
- Dombeck, D. a., Harvey, C. D., Tian, L., Looger, L. L., & Tank, D. W. (2010). Functional imaging of hippocampal place cells at cellular resolution during virtual navigation. *Nature neuroscience*, 13, 1433–40.
- Dombeck, D. a., Khabbaz, A. N., Collman, F., Adelman, T. L., & Tank, D. W. (2007). Imaging large-scale neural activity with cellular resolution in awake, mobile mice. *Neuron*, 56, 43–57.
- Donato, F., Rompani, S. B., & Caroni, P. (2013). Parvalbumin-expressing basket-cell network plasticity induced by experience regulates adult learning. *Nature*, 504, 272–276.
- Drew, L. J., Stark, K. L., Fénelon, K., Karayiorgou, M., MacDermott, A. B., & Gogos, J. a. (2011). Evidence for altered hippocampal function in a mouse model of the human 22q11.2 microdeletion. *Molecular and Cellular Neuroscience*, 47, 293–305.
- Duncan, K., Ketz, N., Inati, S. J., & Davachi, L. (2012). Evidence for area CA1 as a match/mismatch detector: a high-resolution fMRI study of the human hippocampus. *Hippocampus*, 22, 389–398.
- Dupret, D., O'Neill, J., & Csicsvari, J. (2013). Dynamic Reconfiguration of Hippocampal Interneuron Circuits during Spatial Learning. *Neuron*, 78, 166–180.
- Dupret, D., O'Neill, J., Pleydell-Bouverie, B., & Csicsvari, J. (2010a). The reorganization and reactivation of hippocampal maps predict spatial memory performance. *Nature neuroscience*, 13, 995–1002.
- Dupret, D., Pleydell-Bouverie, B., & Csicsvari, J. (2010b). Rate remapping: when the code goes beyond space. *Neuron*, 68, 1015–1016.
- Eichenbaum, H. (2000). A cortical-hippocampal system for declarative memory. *Nature reviews. Neuroscience*, 1, 41–50.
- Eichenbaum, H. (2017). Memory: Organization and Control. *Annu Rev Psychol*, 68, 19–45.
- Eichenbaum, H. & Cohen, N. J. (2014). Can we reconcile the declarative memory and spatial navigation views on hippocampal function? *Neuron*, 83, 764–770.
- Eichenbaum, H., Sauvage, M., Fortin, N., Komorowski, R., & Lipton, P. (2012). Towards a functional organization of episodic memory in the medial temporal lobe. *Neuroscience & Biobehavioral Reviews*, 36, 1597–1608.
- Etienne, A. S. & Jeffery, K. J. (2004). Path integration in mammals. *Hippocampus*, 14, 180–192.
- Fanselow, M. S. & Dong, H.-W. (2010). Are the dorsal and ventral hippocampus functionally distinct structures? *Neuron*, 65, 7–19.

- Fenelon, K., Mukai, J., Xu, B., Hsu, P.-K., Drew, L. J., Karayiorgou, M., Fischbach, G. D., MacDermott, A. B., & Gogos, J. A. (2011). Deficiency of Dgcr8, a gene disrupted by the 22q11.2 microdeletion, results in altered short-term plasticity in the prefrontal cortex. *Proceedings of the National Academy of Sciences*, 108, 4447–4452.
- Fenelon, K., Xu, B., Lai, C. S., Mukai, J., Markx, S., Stark, K. L., Hsu, P.-K., Gan, W.-B., Fischbach, G. D., MacDermott, A. B., Karayiorgou, M., & Gogos, J. A. (2013). The Pattern of Cortical Dysfunction in a Mouse Model of a Schizophrenia-Related Microdeletion. *Journal of Neuroscience*, 33, 14825–14839.
- Fenton, A. A., Kao, H.-y., Neymotin, S. A., Olypher, A., Vayntrub, Y., Lytton, W. W., & Ludvig, N. (2008). Unmasking the CA1 ensemble place code by exposures to small and large environments: more place cells and multiple, irregularly arranged, and expanded place fields in the larger space. *The Journal of neuroscience : the official journal of the Society for Neuroscience*, 28, 11250–62.
- Flahault, A., Schaer, M., Ottet, M.-C., Debbané, M., & Eliez, S. (2012). Hippocampal volume reduction in chromosome 22q11.2 deletion syndrome (22q11.2DS): A longitudinal study of morphometry and symptomatology. *Psychiatry Research: Neuroimaging*, 203, 1–5.
- Floresco, S. B., Block, A. E., & Tse, M. T. (2008). Inactivation of the medial prefrontal cortex of the rat impairs strategy set-shifting, but not reversal learning, using a novel, automated procedure. *Behav Brain Res*, 190, 85–96.
- Folsom, D. P., Hawthorne, W., Lindamer, L., Gilmer, T., Bailey, A., Golshan, S., Garcia, P., Unutzer, J., Hough, R., & Jeste, D. V. (2005). Prevalence and risk factors for homelessness and utilization of mental health services among 10,340 patients with serious mental illness in a large public mental health system. *American Journal of Psychiatry*, 162, 370–376.
- Foote, S. L., Bloom, F. E., & Aston-Jones, G. (1983). Nucleus locus ceruleus: new evidence of anatomical and physiological specificity. *Physiological reviews*, 63, 844–914.
- Foster, D. J. & Wilson, M. a. (2006). Reverse replay of behavioural sequences in hippocampal place cells during the awake state. *Nature*, 440, 680–3.
- Frank, L. M., Brown, E. N., & Wilson, M. (2000). Trajectory encoding in the hippocampus and entorhinal cortex. *Neuron*, 27, 169–178.
- Frank, L. M., Stanley, G. B., & Brown, E. N. (2004). Hippocampal plasticity across multiple days of exposure to novel environments. *The Journal of neuroscience : the official journal of the Society for Neuroscience*, 24, 7681–9.
- Freund, T. F. & Antal, M. (1988). GABA-containing neurons in the septum control inhibitory interneurons in the hippocampus. *Nature*, 336, 170–3.
- Freund, T. F. & Buzsáki, G. (1996). Interneurons of the hippocampus. *Hippocampus*, 6, 347–470.
- Frey, U., Krug, M., Reymann, K. G., & Matthies, H. (1988). Anisomycin, an inhibitor of protein synthesis, blocks late phases of LTP phenomena in the hippocampal CA1 region in vitro. *Brain Research*, 452, 57–65.
- Fusar-Poli, P., Smieskova, R., Kempton, M., Ho, B., Andreasen, N., & Borgwardt, S. (2013). Progressive brain changes in schizophrenia related to antipsychotic treatment? A meta-analysis of longitudinal MRI studies. *Neuroscience & Biobehavioral Reviews*, 37, 1680–1691.

- Fyhn, M., Molden, S., Hollup, S., Moser, M.-B., & Moser, E. (2002). Hippocampal neurons responding to first-time dislocation of a target object. *Neuron*, 35, 555–66.
- Gasbarri, a., Sulli, a., & Packard, M. G. (1997). The dopaminergic mesencephalic projections to the hippocampal formation in the rat. *Progress in neuro-psychopharmacology & biological psychiatry*, 21, 1–22.
- Gerwig, M., Kolb, F. P., & Timmann, D. (2007). The involvement of the human cerebellum in eyeblink conditioning. *The Cerebellum*, 6, 38–57.
- Gilman, S. R., Chang, J., Xu, B., Bawa, T. S., Gogos, J. a., Karayiorgou, M., & Vitkup, D. (2012). Diverse types of genetic variation converge on functional gene networks involved in schizophrenia. *Nature Neuroscience*, 15, 1723–1728.
- Glausier, J. & Lewis, D. (2013). Dendritic spine pathology in schizophrenia. *Neuroscience*, 251, 90–107.
- Glessner, J. T., Reilly, M. P., Kim, C. E., Takahashi, N., Albano, A., Hou, C., Bradfield, J. P., Zhang, H., Sleiman, P. M. A., Flory, J. H., Imielinski, M., Frackelton, E. C., Chiavacci, R., Thomas, K. A., Garris, M., Otieno, F. G., Davidson, M., Weiser, M., Reichenberg, A., Davis, K. L., Friedman, J. I., Cappola, T. P., Margulies, K. B., Rader, D. J., Grant, S. F. A., Buxbaum, J. D., Gur, R. E., & Hakonarson, H. (2010). Strong synaptic transmission impact by copy number variations in schizophrenia. *Proceedings of the National Academy of Sciences*, 107, 10584–10589.
- Gold, J. M., Hahn, B., Zhang, W. W., Robinson, B. M., Kappenman, E. S., Beck, V. M., & Luck, S. J. (2010). Reduced capacity but spared precision and maintenance of working memory representations in schizophrenia. *Archives of general psychiatry*, 67, 570–7.
- Gold, J. M., Randolph, C., Carpenter, C. J., Goldberg, T. E., & Weinberger, D. R. (1992). Forms of memory failure in schizophrenia. *Journal of abnormal psychology*, 101, 487–94.
- Goldenberg, P. C., Calkins, M. E., Richard, J., McDonald-McGinn, D., Zackai, E., Mitra, N., Emanuel, B., Devoto, M., Borgmann-Winter, K., Kohler, C., Conroy, C. G., Gur, R. C., & Gur, R. E. (2012). Computerized neurocognitive profile in young people with 22q11.2 deletion syndrome compared to youths with schizophrenia and at-risk for psychosis. *Am J Med Genet B Neuropsychiatr Genet*, 159B, 87–93.
- Gothard, K. M., Skaggs, W. E., & McNaughton, B. L. (1996). Dynamics of mismatch correction in the hippocampal ensemble code for space: interaction between path integration and environmental cues. *J Neurosci*, 16, 8027–8040.
- Green, M. F. (1996). What are the functional consequences of neurocognitive deficits in schizophrenia? *The American journal of psychiatry*, 153, 321–30.
- Green, M. F., Kern, R. S., & Heaton, R. K. (2004). Longitudinal studies of cognition and functional outcome in schizophrenia: implications for MATRICS. *Schizophr Res*, 72, 41–51.
- Grunze, H. C. R., Rainnie, D. G., Hasselmo, M. E., Barkai, E., Hearn, E. F., McCarley, R. W., & Greene, R. W. (1996). NMDA-Dependent Modulation of CA1 Local Circuit Inhibition. *The Journal of Neuroscience*, 76, 2034–2043.

- Gulyas, A. I., Megias, M., Emri, Z., & Freund, T. F. (1999). Total number and ratio of excitatory and inhibitory synapses converging onto single interneurons of different types in the CA1 area of the rat hippocampus. *J Neurosci*, 19, 10082–10097.
- Hafting, T., Fyhn, M., Molden, S., Moser, M., & Moser, E. I. (2005). Microstructure of a spatial map in the entorhinal cortex. *Nature*, 436, 801–806.
- Hamm, J. P., Peterka, D. S., Gogos, J. A., & Yuste, R. (2017). Altered Cortical Ensembles in Mouse Models of Schizophrenia. *Neuron*, 94, 153–167.e8.
- Hanlon, F. M., Weisend, M. P., Hamilton, D. a., Jones, A. P., Thoma, R. J., Huang, M., Martin, K., Yeo, R. a., Miller, G. a., & Cañive, J. M. (2006). Impairment on the hippocampal-dependent virtual Morris water task in schizophrenia. *Schizophrenia Research*, 87, 67–80.
- Hargreaves, E. L., Rao, G., Lee, I., & Knierim, J. J. (2005). Major dissociation between medial and lateral entorhinal input to dorsal hippocampus. *Science (New York, N.Y.)*, 308, 1792–4.
- Harrison, G., Hopper, K., Craig, T., Laska, E., Siegel, C., Wanderling, J., Dube, K. C., Ganev, K., Giel, R., an der Heiden, W., Holmberg, S. K., Janca, a., Lee, P. W., León, C. a., Malhotra, S., Marsella, a. J., Nakane, Y., Sartorius, N., Shen, Y., Skoda, C., Thara, R., Tsirkin, S. J., Varma, V. K., Walsh, D., & Wiersma, D. (2001). Recovery from psychotic illness: a 15- and 25-year international follow-up study. *The British journal of psychiatry : the journal of mental science*, 178, 506–17.
- Hartley, T., Lever, C., Burgess, N., & O'Keefe, J. (2014). Space in the brain: how the hippocampal formation supports spatial cognition. *Philos Trans R Soc Lond B Biol Sci*, 369, 20120510.
- Hartley, T., Maguire, E. A., Spiers, H. J., & Burgess, N. (2003). The Well-Worn Route and the Path Less Traveled. *Neuron*, 37, 877–888.
- Hastie, T., R., T., & Friedman, J. (2009). *The Elements of Statistical Learning: Data Mining, Inference, and Prediction*. Springer-Verlag.
- Hayashi, Y., Sawa, A., & Hikida, T. (2015). Impaired hippocampal activity at the goal zone on the place preference task in a DISC1 mouse model. *Neuroscience research*, pp. 1–4.
- Hebb, D. O. (1949). *The Organization of Behavior: a Neuropsychological Theory*. (Wiley).
- Heckers, S. & Konradi, C. (2010). Hippocampal pathology in schizophrenia. *Curr Top Behav Neurosci*, 4, 529–553.
- Hernandez, P. J. & Abel, T. (2008). The role of protein synthesis in memory consolidation: Progress amid decades of debate. *Neurobiology of Learning and Memory*, 89, 293–311.
- Hill, A. J. (1978). First occurrence of hippocampal spatial firing in a new environment. *Exp Neurol*, 62, 282–297.
- Hitti, F. L. & Siegelbaum, S. a. (2014). The hippocampal CA2 region is essential for social memory. *Nature*, 508, 88–92.
- Ho, N. F., Iglesias, J. E., Sum, M. Y., Kuswanto, C. N., Sitoh, Y. Y., De Souza, J., Hong, Z., Fischl, B., Roffman, J. L., Zhou, J., Sim, K., & Holt, D. J. (2017). Progression from selective to general involvement of hippocampal subfields in schizophrenia. *Molecular Psychiatry*, 22, 142–152.

- Hok, V., Lenck-Santini, P.-P., Roux, S., Save, E., Muller, R. U., & Poucet, B. (2007). Goal-related activity in hippocampal place cells. *The Journal of neuroscience : the official journal of the Society for Neuroscience*, 27, 472–82.
- Hollup, S. A., Kjelstrup, K. G., Hoff, J., Moser, M. B., & Moser, E. I. (2001a). Impaired recognition of the goal location during spatial navigation in rats with hippocampal lesions. *J Neurosci*, 21, 4505–4513.
- Hollup, S. a., Molden, S., Donnett, J. G., Moser, M. B., & Moser, E. I. (2001b). Accumulation of hippocampal place fields at the goal location in an annular watermaze task. *The Journal of neuroscience*, 21, 1635–1644.
- Holtmaat, A. & Caroni, P. (2016). Functional and structural underpinnings of neuronal assembly formation in learning. *Nat Neurosci*, 19, 1553–1562.
- Howes, O. D. & Kapur, S. (2009). The Dopamine Hypothesis of Schizophrenia: Version III—The Final Common Pathway. *Schizophrenia Bulletin*, 35, 549–562.
- Howes, O. D., Montgomery, A. J., Asselin, M.-C., Murray, R. M., Grasby, P. M., & McGuire, P. K. (2007). Molecular imaging studies of the striatal dopaminergic system in psychosis and predictions for the prodromal phase of psychosis. *The British journal of psychiatry. Supplement*, 51, s13–8.
- Huang, Y. Y. & Kandel, E. R. (1995). D1/D5 receptor agonists induce a protein synthesis-dependent late potentiation in the CA1 region of the hippocampus. *Proceedings of the National Academy of Sciences of the United States of America*, 92, 2446–50.
- Hussaini, S. a., Kempadoo, K. a., Thuault, S. J., Siegelbaum, S. a., & Kandel, E. R. (2011). Increased Size and Stability of CA1 and CA3 Place Fields in HCN1 Knockout Mice. *Neuron*, 72, 643–653.
- Hutcheson, N. L., Sreenivasan, K. R., Deshpande, G., Reid, M. A., Hadley, J., White, D. M., Ver Hoef, L., & Lahti, A. C. (2015). Effective connectivity during episodic memory retrieval in schizophrenia participants before and after antipsychotic medication. *Hum Brain Mapp*, 36, 1442–1457.
- Hyman, S. E. & Fenton, W. S. (2003). What Are the Right Targets for Psychopharmacology? *Science*, 299, 350–351.
- Ibrahim, H. M. & Tamminga, C. A. (2011). Schizophrenia: treatment targets beyond monoamine systems. *Annu Rev Pharmacol Toxicol*, 51, 189–209.
- Igarashi, K. M., Ito, H. T., Moser, E. I., & Moser, M.-B. (2014). Functional diversity along the transverse axis of hippocampal area CA1. *FEBS Letters*, 588, 2470–2476.
- Insel, T., Cuthbert, B., Garvey, M., Heinssen, R., Pine, D. S., Quinn, K., Sanislow, C., & Wang, P. (2010). Research Domain Criteria (RDoC): Toward a New Classification Framework for Research on Mental Disorders. *American Journal of Psychiatry*, 167, 748–751.
- Insel, T. R. (2010). Rethinking schizophrenia. *Nature*, 468, 187–93.
- Inta, D., Monyer, H., Sprengel, R., Meyer-Lindenberg, A., & Gass, P. (2010). Mice with genetically altered glutamate receptors as models of schizophrenia: a comprehensive review. *Neuroscience and biobehavioral reviews*, 34, 285–94.

- Jacobson, L. & Sapolsky, R. (1991). The role of the hippocampus in feedback regulation of the hypothalamic-pituitary-adrenocortical axis.
- Jadhav, S. P., Kemere, C., German, P. W., & Frank, L. M. (2012). Awake hippocampal sharp-wave ripples support spatial memory. *Science* (New York, N.Y.), 336, 1454–8.
- Jadhav, S. P., Rothschild, G., Roumis, D. K., & Frank, L. M. (2016). Coordinated Excitation and Inhibition of Prefrontal Ensembles during Awake Hippocampal Sharp-Wave Ripple Events. *Neuron*, 90, 113–127.
- Jakob, H. & Beckmann, H. (1986). Prenatal developmental disturbances in the limbic allocortex in schizophrenics. *Journal of neural transmission*, 65, 303–26.
- Javitt, C. (1991). Recent advances in the phencyclidine model of schizophrenia. *American Journal of Psychiatry*, 148, 1301–1308.
- Jeewajee, a., Lever, C., Burton, S., O’Keefe, J., & Burgess, N. (2008). Environmental novelty is signaled by reduction of the hippocampal theta frequency. *Hippocampus*, 18, 340–8.
- Jeffery, K. J. (2011). Place cells, grid cells, attractors, and remapping. *Neural Plasticity*, 2011.
- Jeffery, K. J. (2015). Distorting the metric fabric of the cognitive map. *Trends in Cognitive Sciences*, 19, 300–301.
- Jezek, K., Henriksen, E. J., Treves, A., Moser, E. I., & Moser, M.-B. (2011). Theta-paced flickering between place-cell maps in the hippocampus. *Nature*, 478, 246–9.
- Jia, H., Rochefort, N. L., Chen, X., & Konnerth, A. (2011). In vivo two-photon imaging of sensory-evoked dendritic calcium signals in cortical neurons. *Nature protocols*, 6, 28–35.
- Jones, E., Oliphant, T., Peterson, P., & Others (2001). {SciPy}: Open source scientific tools for {Python}.
- Jones, M. W. & Wilson, M. A. (2005). Theta rhythms coordinate hippocampal-prefrontal interactions in a spatial memory task. *PLoS Biol*, 3, e402.
- Käenmäki, M., Tammimäki, A., Myöhänen, T., Pakarinen, K., Amberg, C., Karayiorgou, M., Gogos, J. a., & Männistö, P. T. (2010). Quantitative role of COMT in dopamine clearance in the prefrontal cortex of freely moving mice. *Journal of neurochemistry*, 114, 1745–55.
- Kahn, R. S. & Keefe, R. S. (2013). Schizophrenia is a cognitive illness: time for a change in focus. *JAMA Psychiatry*, 70, 1107–1112.
- Kaifosh, P., Lovett-Barron, M., Turi, G. F., Reardon, T. R., & Losonczy, A. (2013). Septo-hippocampal GABAergic signaling across multiple modalities in awake mice. *Nature Neuroscience*, 16, 1182–1184.
- Kaifosh, P., Zaremba, J. D., Danielson, N. B., & Losonczy, A. (2014). SIMA: Python software for analysis of dynamic fluorescence imaging data. *Frontiers in neuroinformatics*, 8, 80.
- Kandel, E. R. (2001). The Molecular Biology of Memory Storage: A Dialogue Between Genes and Synapses. *Science*, 294, 1030–1038.

- Kapur, S. (2003). Psychosis as a State of Aberrant Salience: A Framework Linking Biology, Phenomenology, and Pharmacology in Schizophrenia. *American Journal of Psychiatry*, 160, 13–23.
- Kapur, S. & Mamo, D. (2003). Half a century of antipsychotics and still a central role for dopamine D2 receptors. *Progress in neuro-psychopharmacology & biological psychiatry*, 27, 1081–90.
- Karayiorgou, M., Morris, M. a., Morrow, B., Shprintzen, R. J., Goldberg, R., Borrow, J., Gos, a., Nestadt, G., Wolyniec, P. S., & Lasseter, V. K. (1995). Schizophrenia susceptibility associated with interstitial deletions of chromosome 22q11. *Proceedings of the National Academy of Sciences of the United States of America*, 92, 7612–6.
- Karayiorgou, M., Simon, T. J., & Gogos, J. a. (2010). 22q11.2 microdeletions: linking DNA structural variation to brain dysfunction and schizophrenia. *Nature Reviews Neuroscience*, 11, 402–416.
- Karlsson, M. P. & Frank, L. M. (2008). Network dynamics underlying the formation of sparse, informative representations in the hippocampus. *J Neurosci*, 28, 14271–14281.
- Kay, S. R., Fiszbein, A., & Opler, L. A. (1987). The Positive and Negative Syndrome Scale (PANSS) for Schizophrenia. *Schizophrenia Bulletin*, 13.
- Keefe, R. S. (2007). Cognitive deficits in patients with schizophrenia: effects and treatment. *J Clin Psychiatry*, 68 Suppl 1, 8–13.
- Kellendonk, C., Simpson, E. H., Polan, H. J., Malleret, G., Vronskaya, S., Winiger, V., Moore, H., & Kandel, E. R. (2006). Transient and selective overexpression of dopamine D2 receptors in the striatum causes persistent abnormalities in prefrontal cortex functioning. *Neuron*, 49, 603–615.
- Kentros, C., Hargreaves, E., Hawkins, R. D., Kandel, E. R., Shapiro, M., & Muller, R. V. (1998). Abolition of long-term stability of new hippocampal place cell maps by NMDA receptor blockade. *Science (New York, N.Y.)*, 280, 2121–6.
- Kentros, C. G., Agnihotri, N. T., Streater, S., Hawkins, R. D., & Kandel, E. R. (2004). Increased attention to spatial context increases both place field stability and spatial memory. *Neuron*, 42, 283–95.
- Kerr, J. N. D. & Denk, W. (2008). Imaging in vivo: watching the brain in action. *Nature reviews. Neuroscience*, 9, 195–205.
- Kesner, R. P., Farnsworth, G., & Kametani, H. (1991). Role of parietal cortex and hippocampus in representing spatial information. *Cerebral Cortex*, 1, 367–73.
- Kessler, R. C., Birnbaum, H., Demler, O., Falloon, I. R., Gagnon, E., Guyer, M., Howes, M. J., Kendler, K. S., Shi, L., Walters, E., & Wu, E. Q. (2005). The Prevalence and Correlates of Nonaffective Psychosis in the National Comorbidity Survey Replication (NCS-R). *Biological Psychiatry*, 58, 668–676.
- Kjelstrup, K. B., Solstad, T., Brun, V. H., Hafting, T., Leutgeb, S., Witter, M. P., Moser, E. I., & Moser, M.-B. (2008). Finite scale of spatial representation in the hippocampus. *Science (New York, NY)*, 321, 140–143.

- Klausberger, T., Magill, P. J., Marton, L. F., Roberts, J. D., Cobden, P. M., Buzsaki, G., & Somogyi, P. (2003). Brain-state- and cell-type-specific firing of hippocampal interneurons in vivo. *Nature*, 421, 844–848.
- Klausberger, T. & Somogyi, P. (2008). Neuronal diversity and temporal dynamics: the unity of hippocampal circuit operations. *Science* (New York, N.Y.), 321, 53–7.
- Knable, M. B., Barci, B. M., Webster, M. J., Meador-Woodruff, J., & Torrey, E. F. (2004). Molecular abnormalities of the hippocampus in severe psychiatric illness: postmortem findings from the Stanley Neuropathology Consortium. *Molecular Psychiatry*, 9, 544,609–620.
- Knierim, J. J. & Hamilton, D. A. (2011). Framing spatial cognition: neural representations of proximal and distal frames of reference and their roles in navigation. *Physiol Rev*, 91, 1245–1279.
- Knierim, J. J., Kudrimoti, H. S., & McNaughton, B. L. (1998). Interactions between idiothetic cues and external landmarks in the control of place cells and head direction cells. *J Neurophysiol*, 80, 425–446.
- Knierim, J. J. & Neunuebel, J. P. (2016). Tracking the flow of hippocampal computation: Pattern separation, pattern completion, and attractor dynamics. *Neurobiology of Learning and Memory*, 129, 38–49.
- Knierim, J. J. & Rao, G. (2003). Distal landmarks and hippocampal place cells: effects of relative translation versus rotation. *Hippocampus*, 13, 604–617.
- Knöpfel, T. (2012). Genetically encoded optical indicators for the analysis of neuronal circuits. *Nature reviews. Neuroscience*, 13, 687–700.
- Knowlton, B. J., Mangels, J. A., & Squire, L. R. (1996). A neostriatal habit learning system in humans. *Science* (New York, N.Y.), 273, 1399–1402.
- Kobayashi, T., Nishijo, H., Fukuda, M., Bures, J., & Ono, T. (1997). Task-dependent representations in rat hippocampal place neurons. *J Neurophysiol*, 78, 597–613.
- Koch, M. (1996). The septohippocampal system is involved in prepulse inhibition of the acoustic startle response in rats. *Behavioral neuroscience*, 110, 468–77.
- Koenig, J., Linder, A. N., Leutgeb, J. K., & Leutgeb, S. (2011). The Spatial Periodicity of Grid Cells Is Not Sustained During Reduced Theta Oscillations. *Science*, 332, 592–595.
- Komiyama, T., Sato, T. R., O'Connor, D. H., Zhang, Y.-X., Huber, D., Hooks, B. M., Gabitto, M., Svoboda, K., T, K., TR, S., DH, O., YX, Z., D, H., BM, H., M, G., & K, S. (2010). Learning-related fine-scale specificity imaged in motor cortex circuits of behaving mice. *Nature*, 464, 1182–1186.
- Konradi, C., Yang, C. K., Zimmerman, E. I., Lohmann, K. M., Gresch, P., Pantazopoulos, H., Berretta, S., & Heckers, S. (2011). Hippocampal interneurons are abnormal in schizophrenia. *Schizophrenia Research*, 131, 165–173.
- Korotkova, T., Fuchs, E. C., Ponomarenko, A., von Engelhardt, J., & Monyer, H. (2010). NMDA receptor ablation on parvalbumin-positive interneurons impairs hippocampal synchrony, spatial representations, and working memory. *Neuron*, 68, 557–69.

- Krabbe, S., Duda, J., Schiemann, J., Poetschke, C., Schneider, G., Kandel, E. R., Liss, B., Roeper, J., & Simpson, E. H. (2015). Increased dopamine D2 receptor activity in the striatum alters the firing pattern of dopamine neurons in the ventral tegmental area. *Proceedings of the National Academy of Sciences*, p. 201500450.
- Krupic, J., Bauza, M., Burton, S., Barry, C., & O'Keefe, J. (2015). Grid cell symmetry is shaped by environmental geometry. *Nature*, 518, 232–235.
- Krystal, J. H., Karper, L. P., Seibyl, J. P., Freeman, G. K., Delaney, R., Bremner, J. D., Heninger, G. R., Bowers, M. B., & Charney, D. S. (1994). Subanesthetic effects of the noncompetitive NMDA antagonist, ketamine, in humans. Psychotomimetic, perceptual, cognitive, and neuroendocrine responses. *Archives of general psychiatry*, 51, 199–214.
- Kudrimoti, H. S., Barnes, C. A., & McNaughton, B. L. (1999). Reactivation of hippocampal cell assemblies: effects of behavioral state, experience, and EEG dynamics. *J Neurosci*, 19, 4090–4101.
- Landgraf, S., Amado, I., Purkhart, R., Ries, J., Olie, J. P., & van der Meer, E. (2011). Visuo-spatial cognition in schizophrenia: confirmation of a preference for local information processing. *Schizophr Res*, 127, 163–170.
- Langston, R. F., Ainge, J. a., Couey, J. J., Canto, C. B., Bjerknes, T. L., Witter, M. P., Moser, E. I., & Moser, M.-B. (2010). Development of the spatial representation system in the rat. *Science* (New York, N.Y.), 328, 1576–80.
- Lapray, D., Lasztoczi, B., Lagler, M., Viney, T. J., Katona, L., Valenti, O., Hartwich, K., Borhegyi, Z., Somogyi, P., & Klausberger, T. (2012). Behavior-dependent specialization of identified hippocampal interneurons. *Nature Neuroscience*, 15, 1265–1271.
- Larkin, M. C., Lykken, C., Tye, L. D., Wickelgren, J. G., & Frank, L. M. (2014). Hippocampal output area CA1 broadcasts a generalized novelty signal during an object-place recognition task. *Hippocampus*, 24, 773–783.
- Larson, M. K., Walker, E. F., & Compton, M. T. (2010). Early signs, diagnosis and therapeutics of the prodromal phase of schizophrenia and related psychotic disorders. *Expert Rev Neurother*, 10, 1347–1359.
- Lashley, K. (1929). *Brain Mechanisms and Intelligence: a Quantitative Study of Injuries to the Brain*. (University of Chicago Press).
- Leavitt, V. M. & Goldberg, T. E. (2009). Episodic memory in schizophrenia. *Neuropsychol Rev*, 19, 312–323.
- LeDoux, J. E. (2000). Emotion Circuits in the Brain. *Annual Review of Neuroscience*, 23, 155–184.
- Lee, A. K., Manns, I. D., Sakmann, B., & Brecht, M. (2006a). Whole-cell recordings in freely moving rats. *Neuron*, 51, 399–407.
- Lee, I., Griffin, A. L., Zilli, E. A., Eichenbaum, H., & Hasselmo, M. E. (2006b). Gradual Translocation of Spatial Correlates of Neuronal Firing in the Hippocampus toward Prospective Reward Locations. *Neuron*, 51, 639–650.
- Lee, I. & Knierim, J. J. (2007). The relationship between the field-shifting phenomenon and representational coherence of place cells in CA1 and CA3 in a cue-altered environment. *Learn Mem*, 14, 807–815.

- Leeson, V. C., Robbins, T. W., Matheson, E., Hutton, S. B., Ron, M. A., Barnes, T. R., & Joyce, E. M. (2009). Discrimination learning, reversal, and set-shifting in first-episode schizophrenia: stability over six years and specific associations with medication type and disorganization syndrome. *Biol Psychiatry*, 66, 586–593.
- Leutgeb, J. K., Leutgeb, S., Moser, M.-B., & Moser, E. I. (2007). Pattern separation in the dentate gyrus and CA3 of the hippocampus. *Science (New York, N.Y.)*, 315, 961–6.
- Leutgeb, J. K., Leutgeb, S., Treves, A., Meyer, R., Barnes, C. a., McNaughton, B. L., Moser, M.-B., & Moser, E. I. (2005a). Progressive transformation of hippocampal neuronal representations in "morphed" environments. *Neuron*, 48, 345–58.
- Leutgeb, S., Leutgeb, J. K., Barnes, C. A., Moser, E. I., McNaughton, B. L., & Moser, M.-B. (2005b). Independent codes for spatial and episodic memory in hippocampal neuronal ensembles. *Science (New York, N.Y.)*, 309, 619–23.
- Leutgeb, S., Leutgeb, J. K., Moser, M. B., & Moser, E. I. (2005c). Place cells, spatial maps and the population code for memory. *Curr Opin Neurobiol*, 15, 738–746.
- Leutgeb, S., Leutgeb, J. K., Treves, A., Moser, M.-B., & Moser, E. I. (2004). Distinct ensemble codes in hippocampal areas CA3 and CA1. *Science (New York, N.Y.)*, 305, 1295–8.
- Lever, C., Burgess, N., Cacucci, F., Hartley, T., & O'Keefe, J. (2002a). What can the hippocampal representation of environmental geometry tell us about Hebbian learning? *Biological Cybernetics*, 87, 356–372.
- Lever, C., Wills, T., Cacucci, F., Burgess, N., & O'Keefe, J. (2002b). Long-term plasticity in hippocampal place-cell representation of environmental geometry. *Nature*, 416, 90–94.
- Lewis, D. a., Hashimoto, T., & Volk, D. W. (2005). Cortical inhibitory neurons and schizophrenia. *Nature reviews. Neuroscience*, 6, 312–24.
- Lewis, D. a. & Levitt, P. (2002). Schizophrenia as a disorder of neurodevelopment. *Annual review of neuroscience*, 25, 409–32.
- Li, S., Cullen, W. K., Anwyl, R., & Rowan, M. J. (2003). Dopamine-dependent facilitation of LTP induction in hippocampal CA1 by exposure to spatial novelty. *Nature neuroscience*, 6, 526–31.
- Lichtenstein, P., Yip, B. H., Björk, C., Pawitan, Y., Cannon, T. D., Sullivan, P. F., & Hultman, C. M. (2009). Common genetic determinants of schizophrenia and bipolar disorder in Swedish families: a population-based study. *The Lancet*, 373, 234–239.
- Lieberman, J. A., Kane, J. M., & Alvir, J. (1987). Provocative tests with psychostimulant drugs in schizophrenia. *Psychopharmacology*, 91, 415–33.
- Lieberman, J. A., Stroup, T. S., McEvoy, J. P., Swartz, M. S., Rosenheck, R. A., Perkins, D. O., Keefe, R. S. E., Davis, S. M., Davis, C. E., Lebowitz, B. D., Severe, J., & Hsiao, J. K. (2005). Effectiveness of antipsychotic drugs in patients with chronic schizophrenia. *The New England journal of medicine*, 353, 1209–23.
- Lisman, J. (2012). Excitation, inhibition, local oscillations, or large-scale loops: what causes the symptoms of schizophrenia? *Current Opinion in Neurobiology*, 22, 537–544.

- Lisman, J. E. & Otmakhova, N. A. (2001). Storage, recall, and novelty detection of sequences by the hippocampus: Elaborating on the SOCRATIC model to account for normal and aberrant effects of dopamine. *Hippocampus*, 11, 551–568.
- Liu, H., Heath, S. C., Sabin, C., Roos, J. L., Galke, B. L., Blundell, M. L., Lenane, M., Robertson, B., Wijsman, E. M., Rapoport, J. L., Gogos, J. A., & Karayiorgou, M. (2002). Genetic variation at the 22q11 PRODH2/DGCR6 locus presents an unusual pattern and increases susceptibility to schizophrenia. *Proceedings of the National Academy of Sciences of the United States of America*, 99, 3717–22.
- Looger, L. L. & Griesbeck, O. (2012). Genetically encoded neural activity indicators. *Current Opinion in Neurobiology*, 22, 18–23.
- Lovett-Barron, M., Kaifosh, P., Kheirbek, M. a., Danielson, N., Zaremba, J. D., Reardon, T. R., Turi, G. F., Hen, R., Zemelman, B. V., & Losonczy, A. (2014). Dendritic inhibition in the hippocampus supports fear learning. *Science (New York, N.Y.)*, 343, 857–63.
- Lovett-Barron, M., Turi, G. F., Kaifosh, P., Lee, P. H., Bolze, F., Sun, X.-H., Nicoud, J.-F., Zemelman, B. V., Sternson, S. M., & Losonczy, A. (2012). Regulation of neuronal input transformations by tunable dendritic inhibition. *Nature Neuroscience*, 15, 423–430.
- Lu, L., Leutgeb, J. K., Tsao, A., Henriksen, E. J., Leutgeb, S., Barnes, C. a., Witter, M. P., Moser, M.-B., & Moser, E. I. (2013). Impaired hippocampal rate coding after lesions of the lateral entorhinal cortex. *Nature neuroscience*, 16, 1085–93.
- Ma, J., Tai, S. K., & Leung, L. S. (2012). Septohippocampal GABAergic neurons mediate the altered behaviors induced by n-methyl-D-aspartate receptor antagonists. *Hippocampus*, 000.
- Maguire, E. A., Frackowiak, R. S., & Frith, C. D. (1997). Recalling routes around london: activation of the right hippocampus in taxi drivers. *The Journal of neuroscience : the official journal of the Society for Neuroscience*, 17, 7103–7110.
- Mala, H., Andersen, L. G., Christensen, R. F., Felbinger, A., Hagstrom, J., Meder, D., Pearce, H., & Mogensen, J. (2015). Prefrontal cortex and hippocampus in behavioural flexibility and posttraumatic functional recovery: reversal learning and set-shifting in rats. *Brain Res Bull*, 116, 34–44.
- Mankin, E. A., Diehl, G. W., Sparks, F. T., Leutgeb, S., & Leutgeb, J. K. (2015). Hippocampal CA2 Activity Patterns Change over Time to a Larger Extent than between Spatial Contexts. *Neuron*, 85, 190–201.
- Mankin, E. A., Sparks, F. T., Slayyeh, B., Sutherland, R. J., Leutgeb, S., & Leutgeb, J. K. (2012). Neuronal code for extended time in the hippocampus. *Proceedings of the National Academy of Sciences*, 109, 19462–19467.
- Manns, J. R. & Eichenbaum, H. (2006). Evolution of declarative memory. *Hippocampus*, 16, 795–808.
- Maren, S., Phan, K. L., & Liberzon, I. (2013). The contextual brain: implications for fear conditioning, extinction and psychopathology. *Nat Rev Neurosci*, 14, 417–428.
- Marín, O. (2012). Interneuron dysfunction in psychiatric disorders. *Nature reviews. Neuroscience*, 13, 107–20.

Markus, E. J., Barnes, C. a., McNaughton, B. L., Gladden, V. L., & Skaggs, W. E. (1994). Spatial information content and reliability of hippocampal CA1 neurons: effects of visual input. *Hippocampus*, 4, 410–21.

Markus, E. J., Qin, Y. L., Leonard, B., Skaggs, W. E., McNaughton, B. L., & Barnes, C. A. (1995). Interactions between location and task affect the spatial and directional firing of hippocampal neurons. *The Journal of neuroscience : the official journal of the Society for Neuroscience*, 15, 7079–94.

Marr, D. (1971). Simple Memory: A Theory for Archicortex. *Philosophical Transactions of the Royal Society B: Biological Sciences*, 262, 23–81.

Marshall, C. R., Howrigan, D. P., Merico, D., Thiruvahindrapuram, B., Wu, W., Greer, D. S., Antaki, D., Shetty, A., Holmans, P. A., Pinto, D., Gujral, M., Bandler, W. M., Malhotra, D., Wang, Z., Fajarado, K. V. F., Maile, M. S., Ripke, S., Agartz, I., Albus, M., Alexander, M., Amin, F., Atkins, J., Bacanu, S. A., Belliveau, R. A., Bergen, S. E., Bertalan, M., Bevilacqua, E., Bigdely, T. B., Black, D. W., Bruggeman, R., Buccola, N. G., Buckner, R. L., Bulik-Sullivan, B., Byerley, W., Cahn, W., Cai, G., Cairns, M. J., Campion, D., Cantor, R. M., Carr, V. J., Carrera, N., Catts, S. V., Chambert, K. D., Cheng, W., Cloninger, C. R., Cohen, D., Cormican, P., Craddock, N., Crespo-Facorro, B., Crowley, J. J., Curtis, D., Davidson, M., Davis, K. L., Degenhardt, F., Del Favero, J., DeLisi, L. E., Dikeos, D., Dinan, T., Djurovic, S., Donohoe, G., Drapeau, E., Duan, J., Dudbridge, F., Eichhammer, P., Eriksson, J., Escott-Price, V., Essioux, L., Fanous, A. H., Farh, K.-H., Farrell, M. S., Frank, J., Franke, L., Freedman, R., Freimer, N. B., Friedman, J. I., Forstner, A. J., Fromer, M., Genovese, G., Georgieva, L., Gershon, E. S., Giegling, I., Giusti-Rodríguez, P., Godard, S., Goldstein, J. I., Gratten, J., de Haan, L., Hamshere, M. L., Hansen, M., Hansen, T., Haroutunian, V., Hartmann, A. M., Henskens, F. A., Herms, S., Hirschhorn, J. N., Hoffmann, P., Hofman, A., Huang, H., Ikeda, M., Joa, I., Kähler, A. K., Kahn, R. S., Kalaydjieva, L., Karjalainen, J., Kavanagh, D., Keller, M. C., Kelly, B. J., Kennedy, J. L., Kim, Y., Knowles, J. A., Konte, B., Laurent, C., Lee, P., Lee, S. H., Legge, S. E., Lerer, B., Levy, D. L., Liang, K.-Y., Lieberman, J., Lönnqvist, J., Loughland, C. M., Magnusson, P. K. E., Maher, B. S., Maier, W., Mallet, J., Mattheisen, M., Mattingdal, M., McCarley, R. W., McDonald, C., McIntosh, A. M., Meier, S., Meijer, C. J., Melle, I., Mesholam-Gately, R. I., Metspalu, A., Michie, P. T., Milani, L., Milanova, V., Mokrab, Y., Morris, D. W., Müller-Myhsok, B., Murphy, K. C., Murray, R. M., Myin-Germeys, I., Nenadic, I., Nertney, D. A., Nestadt, G., Nicodemus, K. K., Nisenbaum, L., Nordin, A., O'Callaghan, E., O'Dushlaine, C., Oh, S.-Y., Olincy, A., Olsen, L., O'Neill, F. A., Van Os, J., Pantelis, C., Papadimitriou, G. N., Parkhomenko, E., Pato, M. T., Paunio, T., Perkins, D. O., Pers, T. H., Pietiläinen, O., Pimm, J., Pocklington, A. J., Powell, J., Price, A., Pulver, A. E., Purcell, S. M., Quested, D., Rasmussen, H. B., Reichenberg, A., Reimers, M. A., Richards, A. L., Roffman, J. L., Roussos, P., Ruderfer, D. M., Salomaa, V., Sanders, A. R., Savitz, A., Schall, U., Schulze, T. G., Schwab, S. G., Scolnick, E. M., Scott, R. J., Seidman, L. J., Shi, J., Silverman, J. M., Smoller, J. W., Söderman, E., Spencer, C. C. A., Stahl, E. A., Strengman, E., Strohmaier, J., Stroup, T. S., Suvisaari, J., Svarkic, D. M., Szatkiewicz, J. P., Thirumalai, S., Toone, P. A., Veijola, J., Visscher, P. M., Waddington, J., Walsh, D., Webb, B. T., Weiser, M., Wildenauer, D. B., Williams, N. M., Williams, S., Witt, S. H., Wolen, A. R., Wormley, B. K., Wray, N. R., Wu, J. Q., Zai, C. C., Adolfsson, R., Andreassen, O. A., Blackwood, D. H. R., Bramon, E., Buxbaum, J. D., Cichon, S., Collier, D. A., Corvin, A., Daly, M. J., Darvasi, A., Domenici, E., Esko, T., Gejman, P. V., Gill, M., Gurling, H., Hultman, C. M., Iwata, N., Jablensky, A. V., Jönsson, E. G., Kendler, K. S., Kirov, G., Knight, J., Levinson, D. F., Li, Q. S., McCarroll, S. A.,

- McQuillin, A., Moran, J. L., Mowry, B. J., Nöthen, M. M., Ophoff, R. A., Owen, M. J., Palotie, A., Pato, C. N., Petryshen, T. L., Posthuma, D., Rietschel, M., Riley, B. P., Rujescu, D., Sklar, P., St Clair, D., Walters, J. T. R., Werge, T., Sullivan, P. F., O'Donovan, M. C., Scherer, S. W., Neale, B. M., & Sebat, J. (2016). Contribution of copy number variants to schizophrenia from a genome-wide study of 41,321 subjects. *Nature Genetics*, 49, 27–35.
- Masurkar, A. V., Srinivas, K. V., Brann, D. H., Warren, R., Lowes, D. C., & Siegelbaum, S. A. (2017). Medial and Lateral Entorhinal Cortex Differentially Excite Deep versus Superficial CA1 Pyramidal Neurons. *Cell Reports*, 18, 148–160.
- Matosin, N., Fernandez-Enright, F., Lum, J. S., Engel, M., Andrews, J. L., Gassen, N. C., Wagner, K. V., Schmidt, M. V., & Newell, K. A. (2016). Molecular evidence of synaptic pathology in the CA1 region in schizophrenia. *NPJ schizophrenia*, 2, 16022.
- Matthysse, S. (1973). Antipsychotic drug actions: a clue to the neuropathology of schizophrenia? *Federation proceedings*, 32, 200–5.
- McCabe, K., Rich, D., Loughland, C. M., Schall, U., & Campbell, L. E. (2011). Visual scanpath abnormalities in 22q11.2 deletion syndrome: is this a face specific deficit? *Psychiatry Res*, 189, 292–298.
- McGrath, J., Saha, S., Chant, D., & Welham, J. (2008). Schizophrenia: A Concise Overview of Incidence, Prevalence, and Mortality. *Epidemiologic Reviews*, 30, 67–76.
- McHugh, T. J., Blum, K. I., Tsien, J. Z., Tonegawa, S., & Wilson, M. a. (1996). Impaired hippocampal representation of space in CA1-specific NMDAR1 knockout mice. *Cell*, 87, 1339–49.
- McHugh, T. J., Jones, M. W., Quinn, J. J., Balthasar, N., Coppari, R., Elmquist, J. K., Lowell, B. B., Fanselow, M. S., Wilson, M. A., & Tonegawa, S. (2007). Dentate Gyrus NMDA Receptors Mediate Rapid Pattern Separation in the Hippocampal Network. *Science*, 317, 94–99.
- Mehta, M. R., Barnes, C. a., & McNaughton, B. L. (1997). Experience-dependent, asymmetric expansion of hippocampal place fields. *Proceedings of the National Academy of Sciences of the United States of America*, 94, 8918–21.
- Melzer, S., Michael, M., Caputi, A., Eliava, M., Fuchs, E. C., Whittington, M. A., & Monyer, H. (2012). Long-RangeProjecting GABAergic Neurons Modulate Inhibition in Hippocampus and Entorhinal Cortex. *Science*, 335, 1506–1510.
- Meyer-Lindenberg, A. S., Olsen, R. K., Kohn, P. D., Brown, T., Egan, M. F., Weinberger, D. R., & Berman, K. F. (2005). Regionally specific disturbance of dorsolateral prefrontal-hippocampal functional connectivity in schizophrenia. *Arch Gen Psychiatry*, 62, 379–386.
- Millan, M. J., Andrieux, A., Bartzokis, G., Cadenhead, K., Dazzan, P., Fusar-Poli, P., Gallinat, J., Giedd, J., Grayson, D. R., Heinrichs, M., Kahn, R., Krebs, M.-O., Leboyer, M., Lewis, D., Marin, O., Marin, P., Meyer-Lindenberg, A., McGorry, P., McGuire, P., Owen, M. J., Patterson, P., Sawa, A., Spedding, M., Uhlhaas, P., Vaccarino, F., Wahlestedt, C., & Weinberger, D. (2016). Altering the course of schizophrenia: progress and perspectives. *Nature reviews. Drug discovery*, 15, 485–515.
- Miller, E. K. & Cohen, J. D. (2001). An integrative theory of prefrontal cortex function. *Annu Rev Neurosci*, 24, 167–202.

- Milner, B., Corkin, S., & Teuber, H.-L. (1968). Further analysis of the hippocampal amnesia syndrome: 14-year follow-up study of H.M. *Neuropsychologia*, 6, 215–234.
- Mizuseki, K., Diba, K., Pastalkova, E., & Buzsáki, G. (2011). Hippocampal CA1 pyramidal cells form functionally distinct sublayers. *Nature neuroscience*, 14, 1174–.
- Moita, M. a. P., Rosis, S., Zhou, Y., LeDoux, J. E., & Blair, H. T. (2004). Putting fear in its place: remapping of hippocampal place cells during fear conditioning. *The Journal of neuroscience : the official journal of the Society for Neuroscience*, 24, 7015–23.
- Monaco, J. D., Rao, G., Roth, E. D., & Knierim, J. J. (2014). Attentive scanning behavior drives one-trial potentiation of hippocampal place fields. *Nat Neurosci*, 17, 725–731.
- Morgan, C. J. a., Dodds, C. M., Furby, H., Pepper, F., Fam, J., Freeman, T. P., Hughes, E., Doeller, C., King, J., Howes, O., & Stone, J. M. (2014). Long-Term Heavy Ketamine Use is Associated with Spatial Memory Impairment and Altered Hippocampal Activation. *Frontiers in psychiatry*, 5, 149.
- Morice, R. (1990). Cognitive inflexibility and pre-frontal dysfunction in schizophrenia and mania. *Br J Psychiatry*, 157, 50–54.
- Moriyoshi, K., Masu, M., Ishii, T., Shigemoto, R., Mizuno, N., & Nakanishi, S. (1991). Molecular cloning and characterization of the rat NMDA receptor. *Nature*, 354, 31–37.
- Morris, R. (1984). Developments of a water-maze procedure for studying spatial learning in the rat. *Journal of Neuroscience Methods*, 11, 47–60.
- Morris, R. G. M. (2013). NMDA receptors and memory encoding. *Neuropharmacology*, 74, 32–40.
- Morris, R. G. M., Anderson, E., Lynch, G. S., & Baudry, M. (1986). Selective impairment of learning and blockade of long-term potentiation by an N-methyl-D-aspartate receptor antagonist, AP5. *Nature*, 319, 774–776.
- Morris, R. G. M., Garrud, P., Rawlins, J. N. P., & O'Keefe, J. (1982). Place navigation impaired in rats with hippocampal lesions. *Nature*, 297, 681–683.
- Moser, E. I., Krobert, K. A., Moser, M. B., & Morris, R. G. (1998). Impaired spatial learning after saturation of long-term potentiation. *Science (New York, N.Y.)*, 281, 2038–42.
- Moser, E. I., Kropff, E., & Moser, M.-B. (2008). Place cells, grid cells, and the brain's spatial representation system. *Annual review of neuroscience*, 31, 69–89.
- Moser, E. I., Roudi, Y., Witter, M. P., Kentros, C., Bonhoeffer, T., & Moser, M.-B. (2014). Grid cells and cortical representation. *Nature Reviews Neuroscience*, 15, 466–481.
- Moser, M. B. & Moser, E. I. (1998). Functional differentiation in the hippocampus.
- Moser, M. B., Moser, E. I., Forrest, E., Andersen, P., & Morris, R. G. (1995). Spatial learning with a minislab in the dorsal hippocampus. *Proceedings of the National Academy of Sciences of the United States of America*, 92, 9697–701.
- Moser, M.-B., Rowland, D. C., & Moser, E. I. (2015). Place Cells, Grid Cells, and Memory. *Cold Spring Harbor Perspectives in Biology*, 7, a021808.

- Mukai, J., Dhilla, A., Drew, L. J., Stark, K. L., Cao, L., MacDermott, A. B., Karayiorgou, M., & Gogos, J. a. (2008). Palmitoylation-dependent neurodevelopmental deficits in a mouse model of 22q11 microdeletion. *Nature neuroscience*, 11, 1302–10.
- Mukai, J., Tamura, M., Fénelon, K., Rosen, A. M., Spellman, T. J., Kang, R., MacDermott, A. B., Karayiorgou, M., Gordon, J. A., & Gogos, J. A. (2015). Molecular Substrates of Altered Axonal Growth and Brain Connectivity in a Mouse Model of Schizophrenia. *Neuron*, 86, 680–696.
- Muller, R. U. & Kubie, J. L. (1987a). The effects of changes in the environment on the spatial firing of hippocampal complex-spike cells. *The Journal of neuroscience : the official journal of the Society for Neuroscience*, 7, 1951–68.
- Muller, R. U. & Kubie, J. L. (1987b). The effects of changes in the environment on the spatial firing of hippocampal complex-spike cells. *The Journal of neuroscience : the official journal of the Society for Neuroscience*, 7, 1951–68.
- Murphy, K. C., Jones, L. A., & Owen, M. J. (1999). High Rates of Schizophrenia in Adults With Velo-Cardio-Facial Syndrome. *Archives of General Psychiatry*, 56, 940.
- Murray, A. J., Sauer, J.-F., Riedel, G., McClure, C., Ansel, L., Cheyne, L., Bartos, M., Wisden, W., & Wulff, P. (2011). Parvalbumin-positive CA1 interneurons are required for spatial working but not for reference memory. *Nature neuroscience*, 14, 297–9.
- Muzzio, I. a., Kentros, C., & Kandel, E. (2009). What is remembered? Role of attention on the encoding and retrieval of hippocampal representations. *The Journal of Physiology*, 587, 2837–2854.
- Nakazawa, K., McHugh, T. J., Wilson, M. a., & Tonegawa, S. (2004). NMDA receptors, place cells and hippocampal spatial memory. *Nature reviews. Neuroscience*, 5, 361–72.
- Nakazawa, K., Quirk, M. C., Chitwood, R. A., Watanabe, M., Yeckel, M. F., Sun, L. D., Kato, A., Carr, C. A., Johnston, D., Wilson, M. A., & nakazawa.science.297.2002.211 Tonegawa, S. L. B. (2002). Requirement for Hippocampal CA3 NMDA Receptors in Associative Memory Recall. *Science*, 297, 211.
- Narr, K. L., Thompson, P. M., Szeszko, P., Robinson, D., Jang, S., Woods, R. P., Kim, S., Hayashi, K. M., Asunction, D., Toga, A. W., & Bilder, R. M. (2004). Regional specificity of hippocampal volume reductions in first-episode schizophrenia. *Neuroimage*, 21, 1563–1575.
- Navawongse, R. & Eichenbaum, H. (2013). Distinct pathways for rule-based retrieval and spatial mapping of memory representations in hippocampal neurons. *J Neurosci*, 33, 1002–1013.
- Navratilova, Z., Hoang, L. T., Schwindel, C. D., Tatsuno, M., & McNaughton, B. L. (2012). Experience-dependent firing rate remapping generates directional selectivity in hippocampal place cells. *Front Neural Circuits*, 6, 6.
- Nelson, M. D., Saykin, A. J., Flashman, L. A., & Riordan, H. J. (1998). Hippocampal Volume Reduction in Schizophrenia as Assessed by Magnetic Resonance Imaging: A Meta-analytic Study. *Archives of General Psychiatry*, 55, 433–440.
- Neunuebel, J. P. & Knierim, J. J. (2014). CA3 Retrieves Coherent Representations from Degraded Input: Direct Evidence for CA3 Pattern Completion and Dentate Gyrus Pattern Separation. *Neuron*, 81, 416–427.

Nielsen, J. V., Blom, J. B., Noraberg, J., & Jensen, N. A. (2010). Zbtb20-Induced CA1 pyramidal neuron development and area enlargement in the cerebral midline cortex of mice. *Cerebral Cortex*, 20, 1904–1914.

Nitz, D. & McNaughton, B. (2004). Differential modulation of CA1 and dentate gyrus interneurons during exploration of novel environments. *J Neurophysiol*, 91, 863–872.

O'Carroll, R. (2000). Cognitive impairment in schizophrenia. *Advances in Psychiatric Treatment*, 6, 161–168.

O'Connor, D. H., Clack, N. G., Huber, D., Komiyama, T., Myers, E. W., & Svoboda, K. (2010). Vibrissa-Based Object Localization in Head-Fixed Mice. *Journal of Neuroscience*, 30, 1947–1967.

O'Dushlaine, C., Rossin, L., Lee, P. H., Duncan, L., Parikhshak, N. N., Newhouse, S., Ripke, S., Neale, B. M., Purcell, S. M., Posthuma, D., Nurnberger, J. I., Lee, S. H., Faraone, S. V., Perlis, R. H., Mowry, B. J., Thapar, A., Goddard, M. E., Witte, J. S., Absher, D., Agartz, I., Akil, H., Amin, F., Andreassen, O. A., Anjorin, A., Anney, R., Anttila, V., Arking, D. E., Asherson, P., Azevedo, M. H., Backlund, L., Badner, J. A., Bailey, A. J., Banaschewski, T., Barchas, J. D., Barnes, M. R., Barrett, T. B., Bass, N., Battaglia, A., Bauer, M., Bayés, M., Bellivier, F., Bergen, S. E., Berrettini, W., Betancur, C., Bettecken, T., Biederman, J., Binder, E. B., Black, D. W., Blackwood, D. H. R., Bloss, C. S., Boehnke, M., Boomsma, D. I., Breuer, R., Bruggeman, R., Cormican, P., Buccola, N. G., Buitelaar, J. K., Bunney, W. E., Buxbaum, J. D., Byerley, W. F., Byrne, E. M., Caesar, S., Cahn, W., Cantor, R. M., Casas, M., Chakravarti, A., Chambert, K., Choudhury, K., Cichon, S., Mattheisen, M., Cloninger, C. R., Collier, D. A., Cook, E. H., Coon, H., Cormand, B., Corvin, A., Coryell, W. H., Craig, D. W., Craig, I. W., Crosbie, J., Cuccaro, M. L., Curtis, D., Czamara, D., Datta, S., Dawson, G., Day, R., De Geus, E. J., Degenhardt, F., Djurovic, S., Donohoe, G. J., Doyle, A. E., Duan, J., Dudbridge, F., Duketis, E., Ebstein, R. P., Edenberg, H. J., Elia, J., Ennis, S., Etain, B., Fanous, A., Farmer, A. E., Ferrier, I. N., Flickinger, M., Fombonne, E., Foroud, T., Frank, J., Franke, B., Fraser, C., Freedman, R., Freimer, N. B., Freitag, C. M., Friedl, M., Frisén, L., Gallagher, L., Gejman, P. V., Georgieva, L., Gershon, E. S., Giegling, I., Gill, M., Gordon, S. D., Gordon-Smith, K., Green, E. K., Greenwood, T. A., Grice, D. E., Gross, M., Grozeva, D., Guan, W., Gurling, H., De Haan, L., Haines, J. L., Hakonarson, H., Hallmayer, J., Hamilton, S. P., Hamshire, M. L., Hansen, T. F., Hartmann, A. M., Hautzinger, M., Heath, A. C., Henders, A. K., Herms, S., Hickie, I. B., Hipolito, M., Hoefels, S., Holsboer, F., Hoogendoijk, W. J., Hottenga, J.-J., Hultman, C. M., Hus, V., Ingason, A., Ising, M., Jamain, S., Jones, E. G., Jones, I., Jones, L., Tzeng, J.-Y., Kähler, A. K., Kahn, R. S., Kandaswamy, R., Keller, M. C., Kennedy, J. L., Kenny, E., Kent, L., Kim, Y., Kirov, G. K., Klauck, S. M., Klei, L., Knowles, J. A., Kohli, M. A., Koller, D. L., Konte, B., Korszun, A., Krabbendam, L., Krasucki, R., Kuntsi, J., Kwan, P., Landén, M., Längström, N., Lathrop, M., Lawrence, J., Lawson, W. B., Leboyer, M., Ledbetter, D. H., Lencz, T., Lesch, K.-P., Levinson, D. F., Lewis, C. M., Li, J., Lichtenstein, P., Lieberman, J. A., Lin, D.-Y., Linszen, D. H., Liu, C., Lohoff, F. W., Loo, S. K., Lord, C., Lowe, J. K., Lucae, S., MacIntyre, D. J., Madden, P. A. F., Maestrini, E., Magnusson, P. K. E., Mahon, P. B., Maier, W., Malhotra, A. K., Mane, S. M., Martin, C. L., Martin, N. G., Matthews, K., Mattingsdal, M., McCarroll, S. A., McGhee, K. A., McGough, J. J., McGrath, P. J., McGuffin, P., McInnis, M. G., McIntosh, A., McKinney, R., McLean, A. W., McMahon, F. J., McMahon, W. M., McQuillin, A., Medeiros, H., Medland, S. E., Meier, S., Melle, I., Meng, F., Meyer, J., Middeldorp, C. M., Middleton, L., Milanova, V., Miranda, A., Monaco, A. P., Montgomery, G. W., Moran, J. L., Moreno-De-Luca, D., Morken, G., Morris, D. W., Morrow, E. M., Moskvina, V., Muglia, P.,

Mühleisen, T. W., Muir, W. J., Müller-Myhsok, B., Murtha, M., Myers, R. M., Myin-Germeys, I., Neale, M. C., Nelson, S. F., Nievergelt, C. M., Nikolov, I., Nimagaonkar, V., Nolen, W. A., Nöthen, M. M., Nwulia, E. A., Nyholt, D. R., Oades, R. D., Olincy, A., Oliveira, G., Olsen, L., Ophoff, R. A., Osby, U., Owen, M. J., Palotie, A., Parr, J. R., Paterson, A. D., Pato, C. N., Pato, M. T., Penninx, B. W., Pergadia, M. L., Pericak-Vance, M. A., Pickard, B. S., Pimm, J., Piven, J., Potash, J. B., Poustka, F., Propping, P., Puri, V., Quested, D. J., Quinn, E. M., Ramos-Quiroga, J. A., Rasmussen, H. B., Raychaudhuri, S., Rehnström, K., Reif, A., Ribasés, M., Rice, J. P., Rietschel, M., Roeder, K., Roeyers, H., Rothenberger, A., Rouleau, G., Ruderfer, D., Rujescu, D., Sanders, A. R., Sanders, S. J., Santangelo, S. L., Sergeant, J. A., Schachar, R., Schalling, M., Schatzberg, A. F., Scheftner, W. A., Schellenberg, G. D., Scherer, S. W., Schork, N. J., Schulze, T. G., Schumacher, J., Schwarz, M., Scolnick, E., Scott, L. J., Shi, J., Shilling, P. D., Shyn, S. I., Silverman, J. M., Slager, S. L., Smalley, S. L., Smit, J. H., Smith, E. N., Sonuga-Barke, E. J. S., Clair, D. S., State, M., Steffens, M., Steinhausen, H.-C., Strauss, J. S., Strohmaier, J., Stroup, T. S., Sutcliffe, J. S., Szatmari, P., Szelinger, S., Thirumalai, S., Thompson, R. C., Todorov, A. A., Tozzi, F., Treutlein, J., Uhr, M., van den Oord, E. J. C. G., Van Grootheest, G., Van Os, J., Vicente, A. M., Vieland, V. J., Vincent, J. B., Visscher, P. M., Walsh, C. A., Wassink, T. H., Watson, S. J., Weissman, M. M., Werger, T., Wienker, T. F., Wijsman, E. M., Willemse, G., Williams, N., Willsey, A. J., Witt, S. H., Xu, W., Young, A. H., Yu, T. W., Zammit, S., Zandi, P. P., Zhang, P., Zitman, F. G., Zöllner, S., Devlin, B., Kelsoe, J. R., Sklar, P., Daly, M. J., O'Donovan, M. C., Craddock, N., Kendler, K. S., A Weiss, L., Wray, N. R., Zhao, Z., Geschwind, D. H., Sullivan, P. F., Smoller, J. W., Holmans, P. A., & Breen, G. (2015). Psychiatric genome-wide association study analyses implicate neuronal, immune and histone pathways. *Nature Neuroscience*, 18, 199–209.

O'Keefe, J. & Dostrovsky, J. (1971). The hippocampus as a spatial map . Preliminary evidence from unit activity in the freely-moving rat. *Brain research*, 34, 171–175.

O'Keefe, J. & Nadel, L. (1978). The Hippocampus as a cognitive map. Clarendon, Oxford, UK.

Okuyama, T., Kitamura, T., Roy, D. S., Itohara, S., & Tonegawa, S. (2016). Ventral CA1 neurons store social memory. *Science*, 353, 1536–1541.

Oliphant, T. E. (2007). Python for Scientific Computing. *Computing in Science & Engineering*, 9, 10–20.

Olton, D. S. & Paras, B. C. (1979). Spatial memory and hippocampal function. *Neuropsychologia*, 17, 669–682.

Papp, O. I., Karlocai, M. R., Toth, I. E., Freund, T. F., & Hajos, N. (2013). Different input and output properties characterize parvalbumin-positive basket and Axo-axonic cells in the hippocampal CA3 subfield. *Hippocampus*, 23, 903–918.

Parent, M. B. & Baxter, M. G. (2004). Septohippocampal acetylcholine: involved in but not necessary for learning and memory? *Learning & memory (Cold Spring Harbor, N.Y.)*, 11, 9–20.

Park, E., Dvorak, D., & Fenton, A. A. (2011). Ensemble place codes in hippocampus: CA1, CA3, and dentate gyrus place cells have multiple place fields in large environments. *PLoS ONE*, 6, 1–9.

Pastalkova, E., Itskov, V., Amarasingham, A., & Buzsáki, G. (2008). Internally generated cell assembly sequences in the rat hippocampus. *Science (New York, N.Y.)*, 321, 1322–7.

- Paterlini, M., Zakharenko, S. S., Lai, W.-S., Qin, J., Zhang, H., Mukai, J., Westphal, K. G. C., Olivier, B., Sulzer, D., Pavlidis, P., Siegelbaum, S. a., Karayiorgou, M., & Gogos, J. a. (2005). Transcriptional and behavioral interaction between 22q11.2 orthologs modulates schizophrenia-related phenotypes in mice. *Nature neuroscience*, 8, 1586–94.
- Peyrache, A., Battaglia, F. P., & Destexhe, A. (2011). Inhibition recruitment in prefrontal cortex during sleep spindles and gating of hippocampal inputs. *Proc Natl Acad Sci U S A*, 108, 17207–17212.
- Piskorowski, R. A., Nasrallah, K., Diamantopoulou, A., Mukai, J., Hassan, S. I., Siegelbaum, S. A., Gogos, J. A., & Chevaleyre, V. (2016). Age-Dependent Specific Changes in Area CA2 of the Hippocampus and Social Memory Deficit in a Mouse Model of the 22q11.2 Deletion Syndrome. *Neuron*, 89, 163–176.
- Piskulic, D., Olver, J. S., Norman, T. R., & Maruff, P. (2007). Behavioural studies of spatial working memory dysfunction in schizophrenia: a quantitative literature review. *Psychiatry Res*, 150, 111–121.
- Place, R., Farovik, A., Brockmann, M., & Eichenbaum, H. (2016). Bidirectional prefrontal-hippocampal interactions support context-guided memory. *Nat Neurosci*, 19, 992–994.
- Preston, A. R. & Eichenbaum, H. (2013). Interplay of hippocampus and prefrontal cortex in memory. *Curr Biol*, 23, R764–73.
- Ragozzino, M. E., Detrick, S., & Kesner, R. P. (1999a). Involvement of the prelimbic-infralimbic areas of the rodent prefrontal cortex in behavioral flexibility for place and response learning. *J Neurosci*, 19, 4585–4594.
- Ragozzino, M. E., Wilcox, C., Raso, M., & Kesner, R. P. (1999b). Involvement of rodent prefrontal cortex subregions in strategy switching. *Behav Neurosci*, 113, 32–41.
- Rajasethupathy, P., Sankaran, S., Marshel, J. H., Kim, C. K., Ferenczi, E., Lee, S. Y., Berndt, A., Ramakrishnan, C., Jaffe, A., Lo, M., Liston, C., & Deisseroth, K. (2015). Projections from neocortex mediate top-down control of memory retrieval. *Nature*, 526, 653–9.
- Ranganath, C., Minzenberg, M. J., & Ragland, J. D. (2008). The Cognitive Neuroscience of Memory Function and Dysfunction in Schizophrenia. *Biological Psychiatry*, 64, 18–25.
- Reichenberg, A. (2010). The assessment of neuropsychological functioning in schizophrenia. *Dialogues Clin Neurosci*, 12, 383–392.
- Rich, E. L. & Shapiro, M. L. (2007). Prelimbic/infralimbic inactivation impairs memory for multiple task switches, but not flexible selection of familiar tasks. *J Neurosci*, 27, 4747–4755.
- Rich, P. D., Liaw, H.-p., & Lee, A. K. (2014). Large environments reveal the statistical structure governing hippocampal representations. *Science*, 345, 814–817.
- Ripke, S., Neale, B. M., Corvin, A., Walters, J. T. R., Farh, K.-H., Holmans, P. A., Lee, P., Bulik-Sullivan, B., Collier, D. A., Huang, H., Pers, T. H., Agartz, I., Agerbo, E., Albus, M., Alexander, M., Amin, F., Bacanu, S. A., Begemann, M., Belliveau Jr, R. A., Bene, J., Bergen, S. E., Bevilacqua, E., Bigdely, T. B., Black, D. W., Bruggeman, R., Buccola, N. G., Buckner, R. L., Byerley, W., Cahn, W., Cai, G., Campion, D., Cantor, R. M., Carr, V. J., Carrera,

N., Catts, S. V., Chambert, K. D., Chan, R. C. K., Chen, R. Y. L., Chen, E. Y. H., Cheng, W., Cheung, E. F. C., Ann Chong, S., Robert Cloninger, C., Cohen, D., Cohen, N., Cormican, P., Craddock, N., Crowley, J. J., Curtis, D., Davidson, M., Davis, K. L., Degenhardt, F., Del Favero, J., Demontis, D., Dikeos, D., Dinan, T., Djurovic, S., Donohoe, G., Drapeau, E., Duan, J., Dudbridge, F., Durmishi, N., Eichhammer, P., Eriksson, J., Escott-Price, V., Essioux, L., Fanous, A. H., Farrell, M. S., Frank, J., Franke, L., Freedman, R., Freimer, N. B., Friedl, M., Friedman, J. I., Fromer, M., Genovese, G., Georgieva, L., Giegling, I., Giusti-Rodríguez, P., Godard, S., Goldstein, J. I., Golimbet, V., Gopal, S., Gratten, J., de Haan, L., Hammer, C., Hamshere, M. L., Hansen, M., Hansen, T., Haroutunian, V., Hartmann, A. M., Henskens, F. A., Herms, S., Hirschhorn, J. N., Hoffmann, P., Hofman, A., Hollegaard, M. V., Hougaard, D. M., Ikeda, M., Joa, I., Julià, A., Kahn, R. S., Kalaydjieva, L., Karachanak-Yankova, S., Karjalainen, J., Kavanagh, D., Keller, M. C., Kennedy, J. L., Khrunin, A., Kim, Y., Klovins, J., Knowles, J. A., Konte, B., Kucinskas, V., Ausrele Kucinskiene, Z., Kuzelova-Ptackova, H., Kähler, A. K., Laurent, C., Lee Chee Keong, J., Hong Lee, S., Legge, S. E., Lerer, B., Li, M., Li, T., Liang, K.-Y., Lieberman, J., Limborska, S., Loughland, C. M., Lubinski, J., Lönnqvist, J., Macek Jr, M., Magnusson, P. K. E., Maher, B. S., Maier, W., Mallet, J., Marsal, S., Mattheisen, M., Mattingsdal, M., McCarley, R. W., McDonald, C., McIntosh, A. M., Meier, S., Meijer, C. J., Melega, B., Melle, I., Mesholam-Gately, R. I., Metspalu, A., Michie, P. T., Milani, L., Milanova, V., Mokrab, Y., Morris, D. W., Mors, O., Murphy, K. C., Murray, R. M., Myint-Germeys, I., Müller-Myhsok, B., Nelis, M., Nenadic, I., Nertney, D. A., Nestadt, G., Nicodemus, K. K., Nikitina-Zake, L., Nisenbaum, L., Nordin, A., O'Callaghan, E., O'Dushlaine, C., O'Neill, F. A., Oh, S.-Y., Olincy, A., Olsen, L., Van Os, J., Endophenotypes International Consortium, P., Pantelis, C., Papadimitriou, G. N., Papiol, S., Parkhomenko, E., Pato, M. T., Paunio, T., Pejovic-Milovancevic, M., Perkins, D. O., Pietiläinen, O., Pimm, J., Pocklington, A. J., Powell, J., Price, A., Pulver, A. E., Purcell, S. M., Quested, D., Rasmussen, H. B., Reichenberg, A., Reimers, M. A., Richards, A. L., Roffman, J. L., Roussos, P., Ruderfer, D. M., Salomaa, V., Sanders, A. R., Schall, U., Schubert, C. R., Schulze, T. G., Schwab, S. G., Scolnick, E. M., Scott, R. J., Seidman, L. J., Shi, J., Sigurdsson, E., Silagadze, T., Silverman, J. M., Sim, K., Slominsky, P., Smoller, J. W., So, H.-C., Spencer, C. A., Stahl, E. A., Stefansson, H., Steinberg, S., Stogmann, E., Straub, R. E., Strengman, E., Strohmaier, J., Scott Stroup, T., Subramaniam, M., Suvisaari, J., Svrakic, D. M., Szatkiewicz, J. P., Söderman, E., Thirumalai, S., Toncheva, D., Tosato, S., Veijola, J., Waddington, J., Walsh, D., Wang, D., Wang, Q., Webb, B. T., Weiser, M., Wildenauer, D. B., Williams, N. M., Williams, S., Witt, S. H., Wolen, A. R., Wong, E. H. M., Wormley, B. K., Simon Xi, H., Zai, C. C., Zheng, X., Zimprich, F., Wray, N. R., Stefansson, K., Visscher, P. M., Trust Case-Control Consortium, W., Adolfsson, R., Andreassen, O. A., Blackwood, D. H. R., Bramon, E., Buxbaum, J. D., Børglum, A. D., Cichon, S., Darvasi, A., Domenici, E., Ehrenreich, H., Esko, T., Gejman, P. V., Gill, M., Gurling, H., Hultman, C. M., Iwata, N., Jablensky, A. V., Jönsson, E. G., Kendler, K. S., Kirov, G., Knight, J., Lencz, T., Levinson, D. F., Li, Q. S., Liu, J., Malhotra, A. K., McCarroll, S. A., McQuillin, A., Moran, J. L., Mortensen, P. B., Mowry, B. J., Nöthen, M. M., Ophoff, R. A., Owen, M. J., Palotie, A., Pato, C. N., Petryshen, T. L., Posthuma, D., Rietschel, M., Riley, B. P., Rujescu, D., Sham, P. C., Sklar, P., St Clair, D., Weinberger, D. R., Wendland, J. R., Werger, T., Daly, M. J., Sullivan, P. F., & O'Donovan, M. C. (2014). Biological insights from 108 schizophrenia-associated genetic loci. *Nature*, 511, 421–427.

Ripke, S., Sanders, A. R., Kendler, K. S., Levinson, D. F., Sklar, P., Holmans, P. A., Lin, D.-Y., Duan, J., Ophoff, R. A., Andreassen, O. A., Scolnick, E., Cichon, S., St Clair, D., Corvin, A., Gurling, H., Werger, T., Rujescu, D., Blackwood, D. H. R., Pato, C. N., Malhotra, A. K., Purcell,

S., Dudbridge, F., Neale, B. M., Rossin, L., Visscher, P. M., Posthuma, D., Ruderfer, D. M., Fanous, A., Stefansson, H., Steinberg, S., Mowry, B. J., Golimbet, V., De Hert, M., Jönsson, E. G., Bitter, I., Pietiläinen, O. P. H., Collier, D. A., Tosato, S., Agartz, I., Albus, M., Alexander, M., Amdur, R. L., Amin, F., Bass, N., Bergen, S. E., Black, D. W., Børglum, A. D., Brown, M. A., Bruggeman, R., Buccola, N. G., Byerley, W. F., Cahn, W., Cantor, R. M., Carr, V. J., Catts, S. V., Choudhury, K., Cloninger, C. R., Cormican, P., Craddock, N., Danoy, P. A., Datta, S., de Haan, L., Demontis, D., Dikeos, D., Djurovic, S., Donnelly, P., Donohoe, G., Duong, L., Dwyer, S., Fink-Jensen, A., Freedman, R., Freimer, N. B., Friedl, M., Georgieva, L., Giegling, I., Gill, M., Glenthøj, B., Godard, S., Hamshere, M., Hansen, M., Hansen, T., Hartmann, A. M., Henskens, F. A., Hougaard, D. M., Hultman, C. M., Ingason, A., Jablensky, A. V., Jakobsen, K. D., Jay, M., Jürgens, G., Kahn, R. S., Keller, M. C., Kenis, G., Kenny, E., Kim, Y., Kirov, G. K., Konnerth, H., Konte, B., Krabbendam, L., Krasucki, R., Lasseter, V. K., Laurent, C., Lawrence, J., Lencz, T., Lerer, F. B., Liang, K.-Y., Lichtenstein, P., Lieberman, J. A., Linszen, D. H., Lönnqvist, J., Loughland, C. M., Maclean, A. W., Maher, B. S., Maier, W., Mallet, J., Malloy, P., Mattheisen, M., Mattingsdal, M., McGhee, K. A., McGrath, J. J., McIntosh, A., McLean, D. E., McQuillin, A., Melle, I., Michie, P. T., Milanova, V., Morris, D. W., Mors, O., Mortensen, P. B., Moskvina, V., Muglia, P., Myin-Germeys, I., Nertney, D. A., Nestadt, G., Nielsen, J., Nikolov, I., Nordentoft, M., Norton, N., Nöthen, M. M., O'Dushlaine, C. T., Olincy, A., Olsen, L., O'Neill, F. A., Orntoft, T. F., Owen, M. J., Pantelis, C., Papadimitriou, G., Pato, M. T., Peltonen, L., Petursson, H., Pickard, B., Pimm, J., Pulver, A. E., Puri, V., Quested, D., Quinn, E. M., Rasmussen, H. B., Réthelyi, J. M., Ribble, R., Rietschel, M., Riley, B. P., Ruggeri, M., Schall, U., Schulze, T. G., Schwab, S. G., Scott, R. J., Shi, J., Sigurdsson, E., Silverman, J. M., Spencer, C. C. A., Stefansson, K., Strange, A., Strengman, E., Stroup, T. S., Suvisaari, J., Terenius, L., Thirumalai, S., Thygesen, J. H., Timm, S., Toncheva, D., van den Oord, E., Van Os, J., Van Winkel, R., Veldink, J., Walsh, D., Wang, A. G., Wiersma, D., Wildenauer, D. B., Williams, H. J., Williams, N. M., Wormley, B., Zammit, S., Sullivan, P. F., O'Donovan, M. C., Daly, M. J., Gejman, P. V., & Consortium, S. P. G.-W. A. S. G. (2011). Genome-wide association study identifies five new schizophrenia loci. *Nature Genetics*, 43, 969–976.

Rodriguez-Murillo, L., Gogos, J. A., & Karayiorgou, M. (2012). The genetic architecture of schizophrenia: new mutations and emerging paradigms. *Annu Rev Med*, 63, 63–80.

Rosenheck, R., Leslie, D., Keefe, R., McEvoy, J., Swartz, M., Perkins, D., Stroup, S., Hsiao, J. K., Lieberman, J., & Group, C. S. I. (2006). Barriers to employment for people with schizophrenia. *Am J Psychiatry*, 163, 411–417.

Roth, E. D., Yu, X., Rao, G., & Knierim, J. J. (2012). Functional differences in the backward shifts of ca1 and ca3 place fields in novel and familiar environments. *PLoS ONE*, 7, 1–10.

Royer, S., Zemelman, B. V., Losonczy, A., Kim, J., Chance, F., Magee, J. C., & Buzsáki, G. (2012). Control of timing, rate and bursts of hippocampal place cells by dendritic and somatic inhibition. *Nature Neuroscience*, 15, 769–775.

Sanders, H., Rennó-Costa, C., Idiart, M., & Lisman, J. E. (2015). Grid cells and place cells: an integrated view of their navigational/memory function. *Trends in Neurosciences*, xx, 1–13.

Scariati, E., Schaer, M., Karahanoglu, I., Schneider, M., Richiardi, J., Debbané, M., Van De Ville, D., & Eliez, S. (2016). Large-scale functional network reorganization in 22q11.2 deletion syndrome revealed by modularity analysis. *Cortex*, 82, 86–99.

- Schaefer, J., Giangrande, E., Weinberger, D. R., & Dickinson, D. (2013). The global cognitive impairment in schizophrenia: consistent over decades and around the world. *Schizophr Res*, 150, 42–50.
- Schlessinger, A. R., Cowan, W. M., & Swanson, L. W. (1978). The time of origin of neurons in Ammon's horn and the associated retrohippocampal fields. *Anatomy and embryology*, 154, 153–173.
- Schmitt, J. E., Vandekar, S., Yi, J., Calkins, M. E., Ruparel, K., Roalf, D. R., Whinna, D., Souders, M. C., Satterthwaite, T. D., Prabhakaran, K., McDonald-McGinn, D. M., Zackai, E. H., Gur, R. C., Emanuel, B. S., & Gur, R. E. (2015). Aberrant Cortical Morphometry in the 22q11.2 Deletion Syndrome. *Biological Psychiatry*, 78, 135–143.
- Schmitt, J. E., Yi, J., Calkins, M. E., Ruparel, K., Roalf, D. R., Cassidy, A., Souders, M. C., Satterthwaite, T. D., McDonald-McGinn, D. M., Zackai, E. H., Gur, R. C., Emanuel, B. S., & Gur, R. E. (2016). Disrupted anatomic networks in the 22q11.2 deletion syndrome. *NeuroImage: Clinical*, 12, 420–428.
- Schneider, C. a., Rasband, W. S., & Eliceiri, K. W. (2012). NIH Image to ImageJ: 25 years of image analysis. *Nature Methods*, 9, 671–675.
- Schneider, M., Debbané, M., Bassett, A. S., Chow, E. W., Fung, W. L. A., van den Bree, M. B., Owen, M., Murphy, K. C., Niarchou, M., Kates, W. R., Antshel, K. M., Fremont, W., McDonald-McGinn, D. M., Gur, R. E., Zackai, E. H., Vorstman, J., Duijff, S. N., Klaassen, P. W., Swillen, A., Gothelf, D., Green, T., Weizman, A., Van Amelsvoort, T., Evers, L., Boot, E., Shashi, V., Hooper, S. R., Bearden, C. E., Jalbrzikowski, M., Armando, M., Vicari, S., Murphy, D. G., Ousley, O., Campbell, L. E., Simon, T. J., & Eliez, S. (2014). Psychiatric Disorders From Childhood to Adulthood in 22q11.2 Deletion Syndrome: Results From the International Consortium on Brain and Behavior in 22q11.2 Deletion Syndrome. *American Journal of Psychiatry*, 171, 627–639.
- Schobel, S. A., Chaudhury, N. H., Khan, U. A., Paniagua, B., Styner, M. A., Asllani, I., Inbar, B. P., Corcoran, C. M., Lieberman, J. A., Moore, H., & Small, S. A. (2013). Imaging patients with psychosis and a mouse model establishes a spreading pattern of hippocampal dysfunction and implicates glutamate as a driver. *Neuron*, 78, 81–93.
- Schobel, S. A., Lewandowski, N. M., Corcoran, C. M., Moore, H., Brown, T., Malaspina, D., & Small, S. A. (2009). Differential targeting of the CA1 subfield of the hippocampal formation by schizophrenia and related psychotic disorders. *Archives of general psychiatry*, 66, 938–46.
- Scoville, W. B. & Milner, B. (1957). Loss of recent memory after bilateral hippocampal lesions. *Journal of neurology, neurosurgery, and psychiatry*, 20, 11–21.
- Seidman, L. J., Giuliano, A. J., Meyer, E. C., Addington, J., Cadenhead, K. S., Cannon, T. D., McGlashan, T. H., Perkins, D. O., Tsuang, M. T., Walker, E. F., Woods, S. W., Bearden, C. E., Christensen, B. K., Hawkins, K., Heaton, R., Keefe, R. S., Heinssen, R., Cornblatt, B. A., & North American Prodrome Longitudinal Study, G. (2010). Neuropsychology of the prodrome to psychosis in the NAPLS consortium: relationship to family history and conversion to psychosis. *Arch Gen Psychiatry*, 67, 578–588.
- Sheffield, J. M., Williams, L. E., Cohen, N., & Heckers, S. (2012). Relational memory in psychotic bipolar disorder. *Bipolar Disord*, 14, 537–546.

- Shepherd, A. M., Laurens, K. R., Matheson, S. L., Carr, V. J., & Green, M. J. (2012). Systematic meta-review and quality assessment of the structural brain alterations in schizophrenia. *Neuroscience & Biobehavioral Reviews*, 36, 1342–1356.
- Shi, J. & Malik, J. (2000). Normalized cuts and image segmentation. *IEEE Transactions on Pattern Analysis and Machine Intelligence*, 22, 888–905.
- Siapas, A. G., Lubenov, E. V., & Wilson, M. A. (2005). Prefrontal phase locking to hippocampal theta oscillations. *Neuron*, 46, 141–151.
- Sigurdsson, T. & Duvarci, S. (2015). Hippocampal-Prefrontal Interactions in Cognition, Behavior and Psychiatric Disease. *Front Syst Neurosci*, 9, 190.
- Sigurdsson, T., Stark, K. L., Karayiorgou, M., Gogos, J. a., & Gordon, J. a. (2010). Impaired hippocampalprefrontal synchrony in a genetic mouse model of schizophrenia. *Nature*, 464, 763–767.
- Simons, J. S. & Spiers, H. J. (2003). Prefrontal and medial temporal lobe interactions in long-term memory. *Nat Rev Neurosci*, 4, 637–648.
- Simpson, E. H., Kellendonk, C., & Kandel, E. (2010). A Possible Role for the Striatum in the Pathogenesis of the Cognitive Symptoms of Schizophrenia. *Neuron*, 65, 585–596.
- Singer, A. C. & Frank, L. M. (2009). Rewarded Outcomes Enhance Reactivation of Experience in the Hippocampus. *Neuron*, 64, 910–921.
- Singh, T., Kurki, M. I., Curtis, D., Purcell, S. M., Crooks, L., McRae, J., Suvisaari, J., Chheda, H., Blackwood, D., Breen, G., Pietiläinen, O., Gerety, S. S., Ayub, M., Blyth, M., Cole, T., Collier, D., Coomber, E. L., Craddock, N., Daly, M. J., Danesh, J., DiForti, M., Foster, A., Freimer, N. B., Geschwind, D., Johnstone, M., Joss, S., Kirov, G., Körkkö, J., Kuismin, O., Holmans, P., Hultman, C. M., Iyegbe, C., Lönnqvist, J., Männikkö, M., McCarroll, S. A., McGuffin, P., McIntosh, A. M., McQuillin, A., Moilanen, J. S., Moore, C., Murray, R. M., Newbury-Ecob, R., Ouwehand, W., Paunio, T., Prigmore, E., Rees, E., Roberts, D., Sambrook, J., Sklar, P., Clair, D. S., Veijola, J., Walters, J. T. R., Williams, H., Sullivan, P. F., Hurles, M. E., O'Donovan, M. C., Palotie, A., Owen, M. J., & Barrett, J. C. (2016). Rare loss-of-function variants in SETD1A are associated with schizophrenia and developmental disorders. *Nature neuroscience*, 19, 571–577.
- Skaggs, W. E. & McNaughton, B. L. (1998). Spatial firing properties of hippocampal CA1 populations in an environment containing two visually identical regions. *The Journal of neuroscience : the official journal of the Society for Neuroscience*, 18, 8455–66.
- Skaggs, W. E., McNaughton, B. L., Gothard, K. M., & Markus, E. J. (1993). An Information-Theoretic Approach to Deciphering the Hippocampal Code. In NIPS, pp. 1030–1037. (Morgan Kaufmann).
- Slomianka, L. (1992). Neurons of origin of zinc-containing pathways and the distribution of zinc-containing boutons in the hippocampal region of the rat. *Neuroscience*, 48, 325–352.
- Slomianka, L., Amrein, I., Knuesel, I., Sørensen, J. C., & Wolfer, D. P. (2011). Hippocampal pyramidal cells: the reemergence of cortical lamination. *Brain Structure and Function*, 216, 301–317.

- Sloviter, R. S. (1989). Calcium-Binding Protein ( Calbindin-DZgk ) and Parvalbumin Immuno-cytochemistry : Localization in the Rat Hippocampus With Specific Reference to the Selective Vulnerability of Hippocampal Neurons to Seizure Activity. *Neurology*, 196.
- Smith, D. M. & Mizumori, S. J. (2006). Hippocampal place cells, context, and episodic memory. *Hippocampus*, 16, 716–729.
- Sokal, R. & Michener, C. (1958). A statistical method for evaluating systematic relationships. *University of Kansas Science Bulletin*, 38, 269.
- Solstad, T., Solstad, T., Boccara, C. N., Boccara, C. N., Kropff, E., Kropff, E., Moser, M.-B., Moser, M.-B., Moser, E. I., & Moser, E. I. (2008). Representation of geometric borders in the entorhinal cortex. *Science*, 322, 1865–1868.
- Sørensen, J. C., Slomianka, L., Christensen, J., & Zimmer, J. (1995). Zinc-containing telencephalic connections to the rat striatum: a combined Fluoro-Gold tracing and histochemical study. *Experimental brain research*, 105, 370–382.
- Sørensen, J. C., Tønder, N., & Slomianka, L. (1993). Zinc-positive afferents to the rat septum originate from distinct subpopulations of zinc-containing neurons in the hippocampal areas and layers. A combined fluoro-gold tracing and histochemical study. *Anatomy and embryology*, 188, 107–15.
- Spellman, T., Rigotti, M., Ahmari, S. E., Fusi, S., Gogos, J. a., & Gordon, J. a. (2015). Hippocampalprefrontal input supports spatial encoding in working memory. *Nature*.
- Spencer, K. M., Nestor, P. G., Perlmutter, R., Niznikiewicz, M. A., Klump, M. C., Frumin, M., Shenton, M. E., & McCarley, R. W. (2004). Neural synchrony indexes disordered perception and cognition in schizophrenia. *Proceedings of the National Academy of Sciences*, 101, 17288–17293.
- Spieker, E. A., Astur, R. S., West, J. T., Griego, J. A., & Rowland, L. M. (2012). Spatial memory deficits in a virtual reality eight-arm radial maze in schizophrenia. *Schizophrenia Research*, 135, 84–89.
- Squire, L. R. (2009). The Legacy of Patient H.M. for Neuroscience. *Neuron*, 61, 6–9.
- Stark, K. L., Xu, B., Bagchi, A., Lai, W.-S., Liu, H., Hsu, R., Wan, X., Pavlidis, P., Mills, A. a., Karayiorgou, M., & Gogos, J. a. (2008). Altered brain microRNA biogenesis contributes to phenotypic deficits in a 22q11-deletion mouse model. *Nature Genetics*, 40, 751–760.
- Stensola, T., Stensola, H., Moser, M.-B., & Moser, E. I. (2015). Shearing-induced asymmetry in entorhinal grid cells. *Nature*, 518, 207–212.
- Stone, M., Gabrieli, J. D., Stebbins, G. T., & Sullivan, E. V. (1998). Working and strategic memory deficits in schizophrenia. *Neuropsychology*, 12, 278–88.
- Strange, B. A., Witter, M. P., Lein, E. S., & Moser, E. I. (2014). Functional organization of the hippocampal longitudinal axis. *Nature Reviews Neuroscience*, 15, 655–669.
- Suh, J., Foster, D. J., Davoudi, H., Wilson, M. A., & Tonegawa, S. (2013). Impaired Hippocampal Ripple-Associated Replay in a Mouse Model of Schizophrenia. *Neuron*, 80, 484–493.
- Swerdlow, N. R., M., G., & D., B. (2001). Neural circuit regulation of prepulse inhibition of startle in the rat: current knowledge and future challenges. *Psychopharmacology*, 156, 194–215.

- Tamminga, C. A., Stan, A. D., & Wagner, A. D. (2010). The Hippocampal Formation in Schizophrenia. *American Journal of Psychiatry*, 167, 1178–1193.
- Tamura, M., Mukai, J., Gordon, J. A., & Gogos, J. A. (2016). Developmental Inhibition of Gsk3 Rescues Behavioral and Neurophysiological Deficits in a Mouse Model of Schizophrenia Predisposition. *Neuron*, 89, 1100–1109.
- Tandon, R., Keshavan, M., & Nasrallah, H. (2008). Schizophrenia, Just the Facts What we know in 2008. 2. Epidemiology and etiology. *Schizophrenia Research*, 102, 1–18.
- Taube, J. S. (2007). The head direction signal: origins and sensory-motor integration. *Annual review of neuroscience*, 30, 181–207.
- Thompson, L. T. & Best, P. J. (1990). Long-term stability of the place-field activity of single units recorded from the dorsal hippocampus of freely behaving rats. *Brain research*, 509, 299–308.
- Tiihonen, J., Lönnqvist, J., Wahlbeck, K., Klaukka, T., Niskanen, L., Tanskanen, A., & Haukka, J. (2009). 11-year follow-up of mortality in patients with schizophrenia: a population-based cohort study (FIN11 study). *The Lancet*, 374, 620–627.
- Tognin, S., Pettersson-Yeo, W., Valli, I., Hutton, C., Woolley, J., Allen, P., McGuire, P., & Mechelli, A. (2014). Using Structural Neuroimaging to Make Quantitative Predictions of Symptom Progression in Individuals at Ultra-High Risk for Psychosis. *Frontiers in Psychiatry*, 4, 1–9.
- Toro, C. & Deakin, J. (2007). Adult neurogenesis and schizophrenia: A window on abnormal early brain development? *Schizophrenia Research*, 90, 1–14.
- Treves, A. & Rolls, E. T. (1992). Computational constraints suggest the need for two distinct input systems to the hippocampal CA3 network. *Hippocampus*, 2, 189–199.
- Treves, A. & Rolls, E. T. (1994). Computational analysis of the role of the hippocampus in memory. *Hippocampus*, 4, 374–391.
- Tsai, G. (1995). Abnormal Excitatory Neurotransmitter Metabolism in Schizophrenic Brains. *Archives of General Psychiatry*, 52, 829.
- Tsai, G., Yang, P., Chung, L. C., Lange, N., & Coyle, J. T. (1998). D-serine added to antipsychotics for the treatment of schizophrenia. *Biological psychiatry*, 44, 1081–9.
- Tsien, J. Z., Huerta, P. T., & Tonegawa, S. (1996). The Essential Role of Hippocampal CA1 NMDA ReceptorDependent Synaptic Plasticity in Spatial Memory. *Cell*, 87, 1327–1338.
- Tulving, E. (1972). Episodic and semantic memory. In *Organization of memory*, vol. 1. pp. 381–403.
- Uhlhaas, P. J. & Singer, W. (2010). Abnormal neural oscillations and synchrony in schizophrenia. *Nature reviews. Neuroscience*, 11, 100–13.
- Uhlhaas, P. J. & Singer, W. (2012). Neuronal dynamics and neuropsychiatric disorders: toward a translational paradigm for dysfunctional large-scale networks. *Neuron*, 75, 963–80.
- van Os, J. & Kapur, S. (2009). Schizophrenia. *Lancet*, 374, 635–45.
- Varga, C., Golshani, P., & Soltesz, I. (2012). Frequency-invariant temporal ordering of interneuronal discharges during hippocampal oscillations in awake mice. *Proceedings of the National Academy of Sciences of the United States of America*, 109, E2726–34.

- Varga, V., Losonczy, A., Zemelman, B. V., Borhegyi, Z., Nyiri, G., Domonkos, A., Hangya, B., Holderith, N., Magee, J. C., & Freund, T. F. (2009). Fast synaptic subcortical control of hippocampal circuits. *Science* (New York, N.Y.), 326, 449–53.
- Vinogradova, O. S. (2001). Hippocampus as comparator: role of the two input and two output systems of the hippocampus in selection and registration of information. *Hippocampus*, 11, 578–598.
- Vita, A., De Peri, L., Silenzi, C., & Dieci, M. (2006). Brain morphology in first-episode schizophrenia: a meta-analysis of quantitative magnetic resonance imaging studies. *Schizophr Res*, 82, 75–88.
- Vorstman, J. A., Breetvelt, E. J., Duijff, S. N., Eliez, S., Schneider, M., Jalbrzikowski, M., Armando, M., Vicari, S., Shashi, V., Hooper, S. R., Chow, E. W., Fung, W. L., Butcher, N. J., Young, D. A., McDonald-McGinn, D. M., Vogels, A., van Amelsvoort, T., Gothelf, D., Weinberger, R., Weizman, A., Klaassen, P. W., Koops, S., Kates, W. R., Antshel, K. M., Simon, T. J., Ousley, O. Y., Swillen, A., Gur, R. E., Bearden, C. E., Kahn, R. S., Bassett, A. S., International Consortium on, B., & Behavior in 22q11.2 Deletion, S. (2015). Cognitive decline preceding the onset of psychosis in patients with 22q11.2 deletion syndrome. *JAMA Psychiatry*, 72, 377–385.
- Walsh, T., McClellan, J. M., McCarthy, S. E., Addington, A. M., Pierce, S. B., Cooper, G. M., Nord, A. S., Kusenda, M., Malhotra, D., Bhandari, A., Stray, S. M., Rippey, C. F., Rocanova, P., Makarov, V., Lakshmi, B., Findling, R. L., Sikich, L., Stromberg, T., Merriman, B., Gogtay, N., Butler, P., Eckstrand, K., Noory, L., Gochman, P., Long, R., Chen, Z., Davis, S., Baker, C., Eichler, E. E., Meltzer, P. S., Nelson, S. F., Singleton, A. B., Lee, M. K., Rapoport, J. L., King, M.-C., & Sebat, J. (2008). Rare Structural Variants Disrupt Multiple Genes in Neurodevelopmental Pathways in Schizophrenia. *Science*, 320, 539–543.
- Wang, Y. W. & Wahba, G. (1995). Bootstrap confidence intervals for smoothing splines and their comparison to bayesian confidence intervals. *Journal of Statistical Computation and Simulation*, 51.
- Watson, J. B. (1913). Psychology as the behaviorist views it. *Psychological Review*, 20, 158–177.
- Weinberger, D. R., Berman, K. F., & Zec, R. F. (1986). Physiologic dysfunction of dorsolateral prefrontal cortex in schizophrenia. I. Regional cerebral blood flow evidence. *Archives of general psychiatry*, 43, 114–24.
- Weinberger, R., Yi, J., Calkins, M., Guri, Y., McDonald-McGinn, D. M., Emanuel, B. S., Zackai, E. H., Ruparel, K., Carmel, M., Michaelovsky, E., Weizman, A., Gur, R. C., Gur, R. E., & Gothelf, D. (2016). Neurocognitive profile in psychotic versus nonpsychotic individuals with 22q11.2 deletion syndrome. *European Neuropsychopharmacology*, 26, 1610–1618.
- Welham, J., Isohanni, M., Jones, P., & McGrath, J. (2009). The Antecedents of Schizophrenia: A Review of Birth Cohort Studies. *Schizophrenia Bulletin*, 35, 603–623.
- Weniger, G. & Irle, E. (2008). Allocentric memory impaired and egocentric memory intact as assessed by virtual reality in recent-onset schizophrenia. *Schizophr Res*, 101, 201–209.
- Wersinger, S. R., Ginns, E. I., O'Carroll, A.-M., Lolait, S. J., & Young, W. S. (2002). Vasopressin V1b receptor knockout reduces aggressive behavior in male mice. *Molecular psychiatry*, 7, 975–984.

- Wierzynski, C. M., Lubenov, E. V., Gu, M., & Siapas, A. G. (2009). State-dependent spike-timing relationships between hippocampal and prefrontal circuits during sleep. *Neuron*, 61, 587–596.
- Wilkins, L. K., Girard, T. a., Konishi, K., King, M., Herdman, K. a., King, J., Christensen, B., & Bohbot, V. D. (2013). Selective deficit in spatial memory strategies contrast to intact response strategies in patients with schizophrenia spectrum disorders tested in a virtual navigation task. *Hippocampus*, 23, 1015–1024.
- Wills, T. J., Cacucci, F., Burgess, N., & O'Keefe, J. (2010). Development of the Hippocampal Cognitive Map in Preweanling Rats. *Science*, 328, 1573–1576.
- Wills, T. J., Lever, C., Cacucci, F., Burgess, N., & O'Keefe, J. (2005). Attractor dynamics in the hippocampal representation of the local environment. *Science* (New York, N.Y.), 308, 873–6.
- Wilson, M. a. & McNaughton, B. L. (1993). Dynamics of the hippocampal ensemble code for space. *Science* (New York, N.Y.), 261, 1055–8.
- Wilson, M. A. & McNaughton, B. L. (1994). Reactivation of hippocampal ensemble memories during sleep. *Science*, 265, 676–679.
- Witthaus, H., Mendes, U., Brune, M., Ozgurdal, S., Bohner, G., Gudlowski, Y., Kalus, P., Andreasen, N., Heinz, A., Klingebiel, R., & Juckel, G. (2010). Hippocampal subdivision and amygdalar volumes in patients in an at-risk mental state for schizophrenia. *J Psychiatry Neurosci*, 35, 33–40.
- Wood, E. R., Dudchenko, P. A., & Eichenbaum, H. (1999). The global record of memory in hippocampal neuronal activity. *Nature*, 397, 613–616.
- Xu, B., Hsu, P.-K., Stark, K. L., Karayiorgou, M., & Gogos, J. a. (2013). Derepression of a neuronal inhibitor due to miRNA dysregulation in a schizophrenia-related microdeletion. *Cell*, 152, 262–75.
- Xu, B., Roos, J. L., Dexheimer, P., Boone, B., Plummer, B., Levy, S., Gogos, J. A., & Karayiorgou, M. (2011). Exome sequencing supports a de novo mutational paradigm for schizophrenia. *Nature Genetics*, 43, 864–868.
- Xu, B., Roos, J. L., Levy, S., van Rensburg, E. J., Gogos, J. A., & Karayiorgou, M. (2008). Strong association of de novo copy number mutations with sporadic schizophrenia. *Nat Genet*, 40, 880–885.
- Yizhar, O., Fenno, L. E., Prigge, M., Schneider, F., Davidson, T. J., O'Shea, D. J., Sohal, V. S., Goshen, I., Finkelstein, J., Paz, J. T., Stehfest, K., Fudim, R., Ramakrishnan, C., Huguenard, J. R., Hegemann, P., & Deisseroth, K. (2011). Neocortical excitation/inhibition balance in information processing and social dysfunction. *Nature*, 477, 171–8.
- Zaremba, J. D., Diamantopoulou, A., Danielson, N. B., Grosmark, A. D., Kaifosh, P. W., Bowler, J. C., Liao, Z., Sparks, F. T., Gogos, J. A., & Losonczy, A. (2017a). Data from: Impaired hippocampal place cell dynamics in a mouse model of the 22q11.2 deletion. Dryad Digital Repository. <http://dx.doi.org/10.5061/dryad.rq560>.
- Zaremba, J. D., Diamantopoulou, A., Danielson, N. B., Grosmark, A. D., Kaifosh, P. W., Bowler, J. C., Liao, Z., Sparks, F. T., Gogos, J. A., & Losonczy, A. (2017b). Impaired hippocampal place cell dynamics in a mouse model of the 22q11.2 deletion. *Nature Neuroscience*, AOP, 1–19.

- Zeng, H., Chattarji, S., Barbarosie, M., Rondi-Reig, L., Philpot, B. D., Miyakawa, T., Bear, M. F., & Tonegawa, S. (2001). Forebrain-specific calcineurin knockout selectively impairs bidirectional synaptic plasticity and working/episodic-like memory. *Cell*, 107, 617–29.
- Zhang, S.-J., Ye, J., Miao, C., Tsao, A., Cerniauskas, I., Ledergerber, D., Moser, M.-B., & Moser, E. I. (2013). Optogenetic Dissection of Entorhinal-Hippocampal Functional Connectivity. *Science*, 340, 1232627–1232627.
- Zhang, Z. J. & Reynolds, G. P. (2002). A selective decrease in the relative density of parvalbumin-immunoreactive neurons in the hippocampus in schizophrenia. *Schizophrenia research*, 55, 1–10.
- Zhou, Y., Shu, N., Liu, Y., Song, M., Hao, Y., Liu, H., Yu, C., Liu, Z., & Jiang, T. (2008). Altered resting-state functional connectivity and anatomical connectivity of hippocampus in schizophrenia. *Schizophr Res*, 100, 120–132.
- Zierhut, K. C., Graßmann, R., Kaufmann, J., Steiner, J., Bogerts, B., & Schiltz, K. (2013). Hippocampal CA1 deformity is related to symptom severity and antipsychotic dosage in schizophrenia. *Brain*, 136, 804–814.
- Ziv, Y., Burns, L. D., Cocker, E. D., Hamel, E. O., Ghosh, K. K., Kitch, L. J., Gamal, A. E., & Schnitzer, M. J. (2013). Long-term dynamics of CA1 hippocampal place codes. *Nature Neuroscience*, 16, 264–266.